The biogeochemistry of bioactive trace elements cadmium and cobalt in the Southern Ocean, Atlantic sector

VALIDATING A SIMULTANEOUS ICP-MS QUANTIFICATION TECHNIQUE

by
Jean Christian Loock

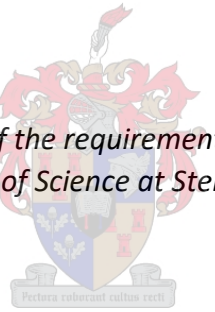

Thesis presented in fulfilment of the requirements for the degree of Master of Science in the Faculty of Science at Stellenbosch University

Supervisor: Prof. Alakendra N. Roychoudhury

March 2017

Declaration

By submitting this thesis electronically, I declare that the entirety of the work contained therein is my own, original work, that I am the sole author thereof (save to the extent explicitly otherwise stated), that the reproduction and publication thereof by Stellenbosch University will not infringe any third-party rights and that I have not previously in its entirety or in part submitted it for obtaining any qualification.

Full Name: Jean Christian Loock

March 2017

Signed……..

Acknowledgements

It is with the sincerest gratitude that I extend my thanks to my research supervisor Prof Alakendra Roychoudhury for your unceasing patience, guidance and fantastic open door policy, and who had the faith to involve me in a project that was undeniably abundant in both the challenges and opportunities it has afforded me. The admiration and respect I hold for you, drives a resolute effort to present research of admirable quality. The responsibilities you have entrusted to me have allowed me to garner immense experience in leadership, project management and scientific expertise – a true privilege. I look forward to the continued development of this project under your guidance.

To Susanne Fietz, your support and mentorship in my undergraduate and postgraduate studies, as well as your remarkable attention to detail ensuring the cruise was ultimately successful, I extend my thanks. To Dr, T Mtshali – who was our chief scientist and team leader during the voyage – it is a pleasure working in tandem with you and I thank you for your efforts in enabling a successful project. To Riana Russouw, a scientific undertaking always contains many unforeseen events that necessitate flexibility; for all your efforts in adjusting to our time schedules and setting up the ICP-MS at the drop of a hat, I express my gratitude. George Olivier, I cannot thank you enough for helping us over the past 3 years in all things procurement related and other.

I'd like to thank the National Research Foundation (NRF) for graciously awarding me with a Master Innovation and Scarce skills bursary. Without this funding I would not have been able to continue this remarkable journey. Some huge thanks goes to all those involved in the cruise, especially the "Iron Team" members Raissa Philibert, Gillian Trollope and Mari Scott. Leigh-Anne Palmer, your data enabled a lot of the work herein to come to fruition and I thank you for that. Thank you to Natasha van Horsten and Johan Viljoen for the physiological data required to make sense of a large portion of this work.

To perhaps the most important person involved in this project together with me, Ryan Cloete, you have put in a large amount of work this year and thank you for that, your friendship, and humour – without you this would not have been possible.

To my mother, Emlitia Loock, who started me on this path a very long time ago, I express my utmost gratitude. Your guidance, support and caring nature has been abundant – even from halfway across the world. Determination and dedication is something I would not have had without your influence.

Finally, I would like to thank my parents Carl and Lesley Loock for affording me the opportunity to qualify myself. Your support, friendship and patience in my relentless pursuit of further education has been immense and I only hope that I have made you as proud of me, as I am of you.

Table of Contents

Abstract

The biogeochemical cycling of the bio-active dissolved trace metals cadmium (DCd) and cobalt (DCo), are reported on a meridional transect of the Southern Atlantic, spanning 36°S to 68°S. Seawater samples were collected using an adaptation of the GEOTRACES clean sampling method concurrent to the austral mid-summer (2015). A multi-element inductively coupled plasma mass spectrometry (ICP-MS) technique, coupled with the commercially available sea*FAST* pre-concentration module was set up and validated for 8 trace elements (Mn, Fe, Co, Ni, Cu, Zn, Cd, Pb). The method proved highly precise (≤10%RSD) in the repeated analysis of an in-house control (TM4A), and accurate in the analysis of the SAFe (D2) international natural seawater reference material. Iron (Fe) quantification proved precise (≤5%RSD) and accurate under repeat analysis. Furthermore, two GEOTRACES standards, GSP and GSC, were analysed for contributing to the determination of their consensus values. DCo concentrations within the oligotrophic sub-surface waters (500m) of the Sub-Tropical Zone (STZ) are heavily depleted (12.57 pmol/kg) owing to strong bio-utilization. Conversely, sub-surface Antarctic Intermediate Waters (AAIW) near the Sub-Antarctic Front (SAF) were elevated (36.1 pmol/kg). Concentrations subsequently decline meridionally through the Antarctic Circumpolar Current (ACC) steadying within the Weddell Gyre (20.3 pmol/kg). STZ DCd sub-surface concentrations are notably depleted (74.1 pmol/kg). However, sub-surface concentrations increase within the ACC at the SAF (450 pmol/kg), continuing into the Weddell Gyre (700.8 pmol/kg). DCd exhibits a typical nutrient-like profile, with bio-utilization in the surface (MLD), followed by regeneration and conservation. The nutrient like behaviour of bio-utilized DCd was exemplified by an excellent Cd/P sub-surface correlation in the ACC, waning somewhat in the sub-optimal productivity of the Weddell Gyre. However, abiotic factors may have contributed to DCd concentrations. The complete water column concentrations ranged from 8.4 ± 0.05 pmol/kg to 902 ± 22.71 pmol/kg. Conversely, DCo demonstrated a typical hybrid-type vertical distribution – nutrient uptake and remineralization in the surface succeeded by scavenging controlled by heterogeneous oxidising bacteria. The complete water column concentrations ranged from 4.1 ± 0.02 pmol/kg to 38.9 ± 0.3 pmol/kg. Elevated DCo concentrations in the sub-surface and a poor but significant DCo/Salinity correlation, suggest DCo flux in the expanse surrounding 46°S and 68°S.

Keywords: Biogeochemical cycling, Dissolved Co and Cd, GEOTRACES, ICP-MS, Iron (Fe), sea*FAST,* Southern Atlantic.

Opsomming

Die biogeochemiese sirkulering van die bio-aktiewe opgelosde spoor metale kadmium (DCd) en kobalt (DCo), word berig op 'n meridionale transeksie van die Suider-Atlantiese Oseaan, wat van 36 °S tot 68 °S strek. Seewater monsters was ingesamel met behulp van 'n aanpassing van die GEOTRACES skoon steekproefmetode tydens die middel van die suidelike somer (2015). 'N Multi-element induktiefgekoppelde plasma massaspektrometrie (ICP-MS) tegnologie, tesame met die kommersieel beskikbare seaFAST pre-konsentrasie module is opgestel en bekragtig vir 8 spoorelemente (Mn, Fe, Co, Ni, Cu, Zn, Cd, Pb). Die metode bewys hoogs akkuraat (≤10% RSD) in die herhaalde analise van 'n in-huis beheer (TM4A), en akkuraat in die ontleding van die SAFe (D2) internasionale natuurlike seewater verwysingsmateriaal. Yster (Fe) kwantifisering bewys presies (≤5% RSD) en akkuraat onder herhaalende analise. Verder, twee GEOTRACES standaarde, GSP en GSC, is ontleed om by te dra tot die bepaling van hul konsensus waardes. DCo konsentrasies binne die oligotrofiese sub-oppervlak water (500m) van die Subtropiese Sone (STZ) is swaar uitgeput (12,57 pmol/kg) as gevolg van 'n sterk bio-benutting. Aan die ander kant was Sub-Antarktiese Front (SAF) sub-oppervlak water (AAIW) verhef (36.1 pmol/kg). Konsentrasies daal daarna meridionally deur die Antarktiese Circumpolaire Huideging (ACC) en bedaar binne die Weddell Gyre (20.3 pmol/kg). STZ DCd sub-oppervlak konsentrasies was veral arm (74,1 pmol / kg). Maar, sub-oppervlak konsentrasies verhoog binne die ACC naby die SAF (450 pmol / kg), voortgesette in die Weddell Gyre (700,8 pmol/kg). DCd toon 'n tipiese voedingstof-agtige profiel, met bio-benutting in die oppervlak (MLD), gevolg deur die wedergeboorte en bewaring. Die voedingstowwe soos gedrag van bio-gebruik DCd is vergestalt deur 'n uitstekende Cd/P sub-oppervlak korrelasie in die ACC, besig om te kwyn ietwat in die sub-optimale produktiwiteit van die Weddell Gyre. Dit kan egter wees dat abiotiese faktore bygedra het tot DCd konsentrasies. Die volledige waterkolom konsentrasies het gewissel van 8.4 ± 0.05 pmol/kg tot 902 ± 22,71 pmol/kg. Aan die ander kant, demonstreer DCo 'n tipiese baster-tipe vertikale verspreiding - voedingsopname en remineralisatie in die oppervlak, opgevolg deur aas beheer tekoms heterogene oksideer- bakterieë. Die volledige waterkolom konsentrasies het gewissel van 4.1 ± 0,02 pmol/kg tot 38,9 ± 0,3 pmol/kg. Verhoogde DCo konsentrasies in die sub-oppervlak en 'n arm, maar beduidende DCo/Zoutgehalte korrelasie, raai DCo vloed in die uitspansel rondom 46 °S en 68 °S.

Sleutelwoorde: biogeochemiese sirkulering, opgelosde Co en Cd, GEOTRACES, induktiefgekoppelde plasma massaspektrometrie (ICP-MS), yster (Fe), sea*FAST*, Suider-Atlantiese Oseaan.

CHAPTER 1

An Examination of Trace Metal Research

1. Introduction

The coordinated resolve exemplified by marine scientists studying trace metals the world over, has been the vanguard for the venerable progression refining our understanding of oceanic biogeochemical cycling and oceanic productivity. Given the vastness of the Southern Ocean – ≈ 14% of the surface of the earth – it undeniably demands greater insight concerning its potential as a significant carbon (C) sink (Abouchami *et al.*, 2014). Nonetheless, fundamental elements concerning the distribution and controls of trace elements in the Southern Ocean biogeochemical cycle, remain largely presumptive; albeit iron (Fe) has been better constrained recently (Sañudo-Wilhelmy *et al.*, 2002; Klunder *et al.*, 2011; Boye *et al.*, 2012). Furthermore, pending recent advances, exceptionally low concentrations of trace metals (< 0.05 µmol/kg), compounded by countless contamination risks and a complex seawater matrix, have traditionally inhibited the accurate measurements of trace metals and thereby stunted efforts to constrain bioactive trace metals (Biller and Bruland, 2012). The role ascribed to trace metals in marine phytoplankton productivity means that the elucidation of the factors controlling biogeochemical cycling are integral to proficient ocean-atmosphere carbon flux predictions.

The Southern Ocean is characterised by an unusual phenomena that sees low chlorophyll conditions subsist south of the Polar Front (PF), albeit in the presence of high concentrations of the macronutrients nitrate (NO_3), silicic acid (SiO_4) and phosphate (PO_4) (Sunda, 1991; Frew *et al.*, 2001). This phenomenon is recognized as the Southern Ocean Paradox: the unusual circumstance where High Nutrient Low Chlorophyll (HNLC) waters subsist. It is postulated that this limitation is caused by a scarcity of micronutrients (trace elements), specifically those essential in the metabolic function of marine phytoplankton species such as Cyanobacteria, Coccolithophorids, Diatoms and Dinoflagellates (Sunda and Huntsman, 1995; Moffett and Ho, 1996; Frew *et al.*, 2001). Consequently, sub-optimal macronutrient bio-utilisation characterises the region south of the Sub-Antarctic zone (Wefer and Fischer, 1991; Frew *et al.*, 2001). Should physiological growth of marine phytoplankton not experience limitations grounded on micronutrient availability, the sequestration of inorganic carbon and its conversion to organic carbon by photosynthetic processes, would result in measurably increased drawdown of C into the oceans.

Several studies have confirmed that the factor constraining growth is the limited availability of bioactive trace elements, primarily Fe (Bruland, Donat and Hutchins, 1991; Frew *et al.*, 2001; Saito and

Moffett, 2002; Klunder *et al.*, 2011). Similarly, studies have shown that Cobalt (Co) and Cadmium (Cd), along with Zinc (Zn), Nickel (Ni) and Copper (Cu), are micronutrients essential to phytoplankton growth, while others, such as lead (Pb), silver (Ag), and mercury (Hg), may be considered biological inhibitors wanting of known metabolic functions (Bruland, Donat and Hutchins, 1991; Sunda, 1991; Boye *et al.*, 2012). However, Co and Cd are micronutrients whose role in the biogeochemical cycle is poorly constrained (Sunda, 2012). The notion of Fe – considering an abundance of $3.5*10^4$ ppm in the upper continental crust (Eby, 2004) – being a limiting trace element seems as counterintuitive as the HNLC paradox. However, it is the availability, or rather lack thereof, that limits Fe uptake by planktonic species – resulting in an estimated 27-36% limitation on productivity of primary producers (Biller and Bruland, 2012). In view of the much lower, relative to Fe, upper crustal abundance of 69ppm and 10ppm for Co and Cd respectively (Eby, 2004), bioavailability is likewise limited.

Commonly, oceanic trace metals input mechanisms are ascribed to coastal fluxes, wind-blown dust, hydrothermal vents and glacially entrained sediments (Klunder et al. 2011). Moreover, trace metal distribution characteristics allow categorization whereby cycling via bio-utilization and regeneration is termed "nutrient type"; whereas cycling via particle adsorption is termed "scavenged type" (Saito and Moffett, 2002). Literature suggests that Southern Ocean dissolved Co (DCo) and Cd (DCd) concentrations remain poorly constrained with limited studies reporting concentrations in the pico-molar range (4-120 pmol kg^{-1}) (Saito and Moffett, 2001, 2002; Ellwood, 2008)**.** The primary controls recognised in the cycling of DCd are: vertical mixing, removal by physical adsorption, and biological uptake and regeneration, with atmospheric deposition of DCd in the ocean's surface waters deemed insignificant (Baars *et al.*, 2014). The correlation between DCd and the macronutrient PO_4, exemplifies the behaviour befitting nutrient type classification (Sunda and Huntsman, 2000). Sources for DCo stem from poorly constrained atmospheric inputs, continental margin inputs and glacially entrained sediments in addition to remineralization (Bown *et al.*, 2011). The bio-utilzation of DCo in the euphotic zone may see classification as nutrient type in certain oceanographic regions (Saito *et al.*, 2010). However, DCo may also exemplify scavenged type elemental behaviour – prominent below the remineralized zone (Bown *et al.*, 2011). It follows that DCo is classified as a hybrid type element, that is: an element that exhibits both nutrient and scavenged type behaviour.

Ultimately, the curiosity commanding improved constraining of the biogeochemical cycle is related to the role of the oceans in the mitigation of climate change. The oceans regulation of the earth's climate patterns is unparalleled; crucially, by way of carbon fixation, the oceans are the main protagonists in the mitigation of increasing levels of the greenhouse gas carbon dioxide (CO_2). The coupling of ocean and atmosphere is emphasized by a 60 times larger dissolved inorganic carbon (DIC) fraction within the oceans; as opposed to terrestrial sequestration (Peng *et al.*, 1987; Reid *et al.*, 2009).

Moreover, it is estimated that 40% of anthropogenic CO_2 is sequestered by the oceans each year (Reid *et al.*, 2009). This disproportionality between oceanic and terrestrial CO_2 uptake exists due to an inherent reaction between CO_2 and water to form soluble species of ions (Eby, 2004). CO_2 sequestration is initiated by diffusion and dissolution into the sea surface waters – a physico-chemical process (Reid *et al.*, 2009). Sequestered C is exported to the deep ocean via the ocean "carbon pumps" – Solubility (Physical), Biological, and Carbonate (Eby, 2004).

The biological carbon pump (Figure 1) controls CO_2 sequestration through the photosynthetic productivity of marine phytoplankton – in turn governed by the availability of macro and micro nutrients. There are three distinct components, namely: carbon fixation by phytoplankton (photosynthesis) in the euphotic zone, regenerative cycling in the euphotic zone and/or fallout as marine snow, and remineralisation/decomposition of fixed carbon in deep waters that may escape sequestration into the sediments (Elderfield, Holland and Turekian, 2006). Carbon fixation by the autotrophic microorganisms (phytoplankton) is initiated upon absorption of light by the reaction centres containing chlorophyll. Inorganic carbon (CO_2) and water (H_2O) are then converted by proteins in the cells to organic carbon glucose ($C_6H_{12}O_6$) and oxygen gas (O_2) (Eby, 2004). The resultant compounds nicotinamide adenine dinucleotide phosphate (NADH) and adenosine triphosphate (ATP) are the drivers of cellular activity. Bioactive trace elements catalyse this process by serving as essential active centres or structural factors in the enzymes of the protein (Morel and Price, 2002). Regenerative cycling and remineralization reintroduce certain constituents utilized by the phytoplankton through the breakdown of organic material. In large remineralization at depth is mediated by a series of organisms and metabolic pathways (Morel and Price, 2002). However, the links to biogeochemical cycling are poorly understood and potentially fragile. Should the balance be disturbed, the mixed zone, settling of organic matter (OM), decomposition and photosynthetic efficiencies, might misfire and compound the sub-optimal CO_2 sequestration (Reid *et al.*, 2009). A biological pump, anthropogenically enhanced to function near maximum capacity, would deplete oxygen in the bottom waters due to increased organic matter degradation (Morford and Emerson, 1999). This decrease in oxygen concentration, in conjunction with increased marine snow rates, alters the redox state in the surface sediments. This is turn would affect the dissolution and remineralisation of redox sensitive trace metals in the water column, potentially varying the characteristic solubility of essential nutrients (Morford and Emerson, 1999).

The efficiency of the carbon pump in the sequestration of inorganic carbon by marine phytoplankton, is further controlled by the physiological nutrient requirement demonstrated by the resident plankton community. Elucidating the physiological bioactive trace nutrient requirement, be that absolute or substitutive, has gained the devotion of several studies in recent years (Brand, Sunda

and Guillard, 1986; Sunda and Huntsman, 1995; Saito and Moffett, 2002; Bertrand *et al.*, 2007). Marine cyanobacteria *Prochlorococcus* and *Synechococcus* demonstrate an absolute Co requirement for growth, lacking the ability to substitute Zn with Co – a condition of vitamin B_{12} requirement (Sunda and Huntsman, 1995; Saito and Moffett, 2002). Conversely, cyanobacteria have been found to exhibit high sensitivity to Cd toxicity as opposed to coccolithophores and dinoflagellates which exhibit intermediate sensitivity; whereas diatoms are least sensitive (Brand, Sunda and Guillard, 1986). To some extent the toxicity of dissolved Cd is limited by the lesser tendency of Cd to complex with organic ligands (Brand, Sunda and Guillard, 1986).

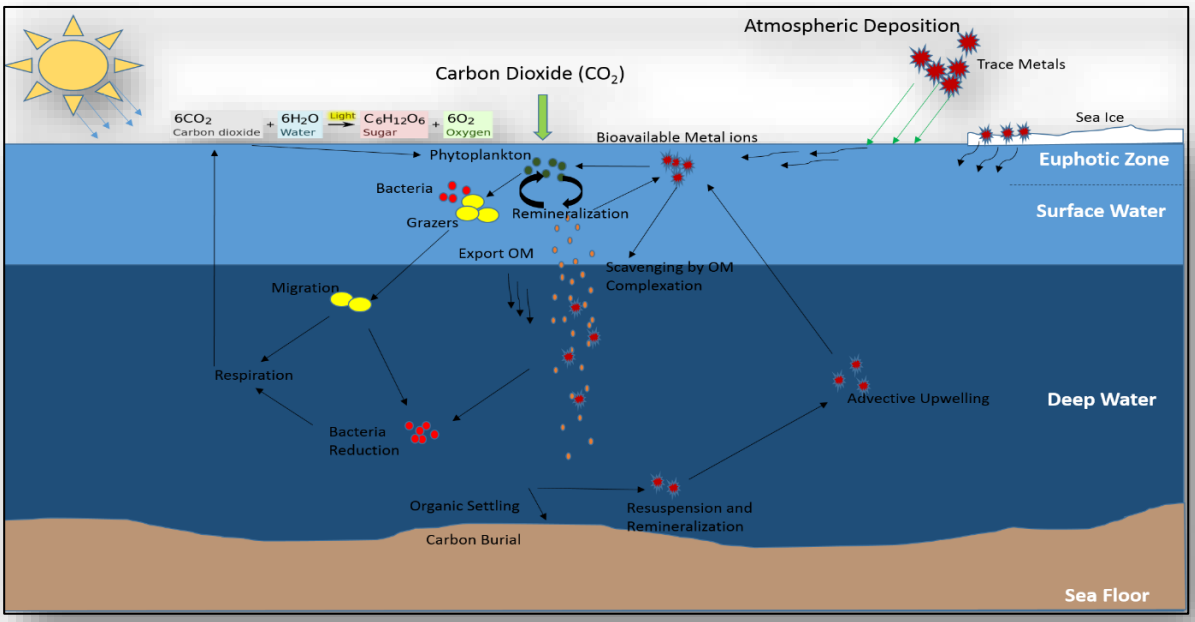

***Figure 1**-Schematic illustrating the biological pump and the cycling of micronutrients (trace metals) in the ocean. Bioactive trace metals play a crucial role in catalysing the sequestration of inorganic CO_2 by serving as essential active centres in the enzymes crucial to metabolic efficiency of the marine phytoplankton during photosynthesis. The uptake of macro and micronutrients by marine phytoplankton is reflected by the Redfield ratio.* Kuss & Kremling (1999) *report an extended Redfield ratio of: 180C:23C:1P:0.005Fe:0.0004Cd:0.0002Co for the elements concerned in this study. It should be noted that phosphorus was limiting in the case of* Kuss & Kremling (1999).

Evidence suggests that there is substitution of Zn by Cd in some carbonic anhydrase demonstrating an ability as a nutritional substitute (Sunda and Huntsman, 2000). The strain *Phaeocystis antarctica*, an efficient carbon exporter and high rate dimethylsulfoniopropionate (DMSP) producer abundant in the Ross Sea, was found to exhibit Co-Zn substitution in experiments by (Saito and Goepfert, 2008). Coccolithophores, such as *Emiliania huxleyi,* demonstrated Co-Zn substitution whereas the diatom *Chaetoceros calcitrans* lacks this genetic capability (Sunda and Huntsman, 1995; Saito and Goepfert, 2008). Evidence indicates that the physiological Zn requirement of concentric diatomic marine species (*Thalassiosira weissflogii, Thalassiosira oceanica, and Thalassiosira pseudonana*) can be replaced by Co or Cd (Sunda and Huntsman, 1995; Nodwell and Price, 2001). However, in *Thalassiosira weissflogii*

culture experiments, increasing Cd under low Zn inhibited growth – illustrating a balanced requirement (Sunda and Huntsman, 2000). Furthermore, *T. oceanica* growth rates were not affected by Zn-Cd stimulation in culture experiments by Sunda & Huntsman (2000).

Scientifically, this study at the Stellenbosch University (SU) Centre for Trace and Experimental Bio-geochemistry (TRACEx) aims to create an enlightened understanding of the factors controlling trace metal (Co and Cd) cycling, uptake and limitation in the Southern Ocean – integral to refining estimations relating to the capacity of the carbon cycle to absorb, transport, transform and ultimately store carbon. Presented in this study is a multi-element method that utilizes the sea*FAST* pico offline pre-concentration and matrix removal module coupled with modern, high resolution, inductively coupled plasma mass spectrometry (ICP-MS), as a tool in the simultaneous quantification of up to 10 trace metals. It follows that the process involving the collection, analysis and characterization of trace metals in the Southern Ocean, has been presented and discussed in its entirety.

The collection of uncontaminated trace metal samples had proven challenging for the project pending this cruise, with several past cruises returning contaminated results – notably for Fe. Thus, proving uncontaminated sample collection by way of inter-calibration and statistical validation – adhering to the guidelines delineated in the GEOTRACES cookbook (Cutter *et al.*, 2010) – would be a gateway imperative to the success of this study. Given the contaminant sensitive nature, and the analysis thereof by way of a Flow Injection Analysis (FIA) technique by inter-calibration partners at Plymouth Marine Laboratory (PML), Fe forms the foundation of the Inter-calibration and laboratory validation exercise. The results of the GEOTRACES and SAFe standards are used as reference samples to provide evidence for accurate quantification of Fe, Co and Cd.

Furthermore, the interaction between the micronutrients Co and Cd, and phytoplankton, will receive substantial discussion in this study; focusing on the spatial and temporal aspects, as well as the biogeochemical cycling of these trace elements.

2. Aims and Objectives

While the knowledge on the spatial distribution, speciation and role of bioactive trace metals in the Southern Ocean is ever increasing, too many unknowns obstruct the understanding of key biogeochemical features. This project will be centred on validating the TRACEx Laboratory trace metal collection and analysis techniques conforming to the guidelines outlined by the GEOTRACES Standards and Inter-calibration Committee (S&I). Concurrently, the controls of bioactive trace metals essential to marine phytoplankton productivity need be assessed and constrained. The objectives are as follows:

Key Objective One: Validate an improved seawater sample collection and multi elemental ICP-MS analysis procedure.

- Demonstrate that the protocol enables the collection of uncontaminated seawater samples.
- Demonstrate that ICP-MS – coupled with a pre-concentration module – is an effective and efficient multi-element method for the accurate and precise quantification of trace metals.
- Analyse for trace metals efficiently, accurately and precisely, while limiting the contamination risk and ensuring high reproducibility.
- To contribute towards consensus data as well as filling existing gaps in the database.

Key Objective Two: Understand the cycling of Cadmium (Cd) and Cobalt (Co) on a meridional transect in the Southern Ocean.

- Characterize the vertical and horizontal distribution of the dissolved fraction of the trace metals Co (DCo) and Cd (DCd) in the Southern Ocean.
    - Hypothesis 1: DCo exhibits properties of both scavenged-type and nutrient like elements
    - Hypothesis 2: DCd exhibits a typical nutrient profile
- Report on the controls and characterise the distribution of dissolved Cadmium and Cobalt in the Southern Ocean, Atlantic Sector.
    - Hypothesis: Are trace metals biologically, biogeochemically or geochemically cycled, or is it a combination.

3. Fundamental Themes and Structure

The chapter wise format of this thesis is intended to aid in the writing of stand-alone scientific papers. There are four chapters moulded around the designs delineated in the key objectives. They include: a detailed explanation of field and analytical methods; a validation and inter-calibration chapter fixated on the precision and accuracy of the analytical technique; and a chapter elucidating the controls and distribution of Cobalt and Cadmium in the Southern Ocean.

Chapter 2 details the overarching methods pertaining to the cruise, study area, sample collection and treatment, reagents and materials, analytical methods, and the reference materials. The sample collection protocols are adapted from the GEOTRACES cookbook (Cutter *et al.*, 2010).

The core element of Chapter 3 was providing statistical evidence for accurate and precise sampling techniques. While the method has seen validation, it was imperative that the Stellenbosch University laboratory follow method transfer protocols in the quest for single laboratory validation. This would prove integral to the aim of the project to contribute towards consensus database.

Chapter 4 reports the concentrations of Cadmium and Cobalt in the Southern Ocean, Atlantic Sector. Limited data is available for Cadmium on this transect and Cobalt data is entirely absent from the GEOTRACES database. The impact of these trace metals on the Southern Ocean phytoplankton communities will receive some discussion. The physical controls on the distribution of these trace metals will further help create an understanding of their biogeochemical cycling.

CHAPTER 2

Methods

1. Study Area

Trace metal samples were collected aboard the research vessel SA Augulhas II during the Austral summer (2014/2015) SANAE 54 voyage, along the Southern Ocean Good-Hope transect. Stations on the Cape Town-Antarctica transect (Figure 2) were premeditated and strategically located to coincide with known cross-over and GEOTRACES Baseline stations – references for an unproven sampling method. Trace Metal (TM#) and Deep Trace Metal (DTM#) stations enabled sampling at depths of ≈1500m (greater resolution) up to ≈4500m respectively – no fewer than 15 sample depths per locale. A conditioning station was effected in the Antarctic Zone waters prior to sampling. Reported in this study are the analytical results of DTM1-3 and TM1-4.

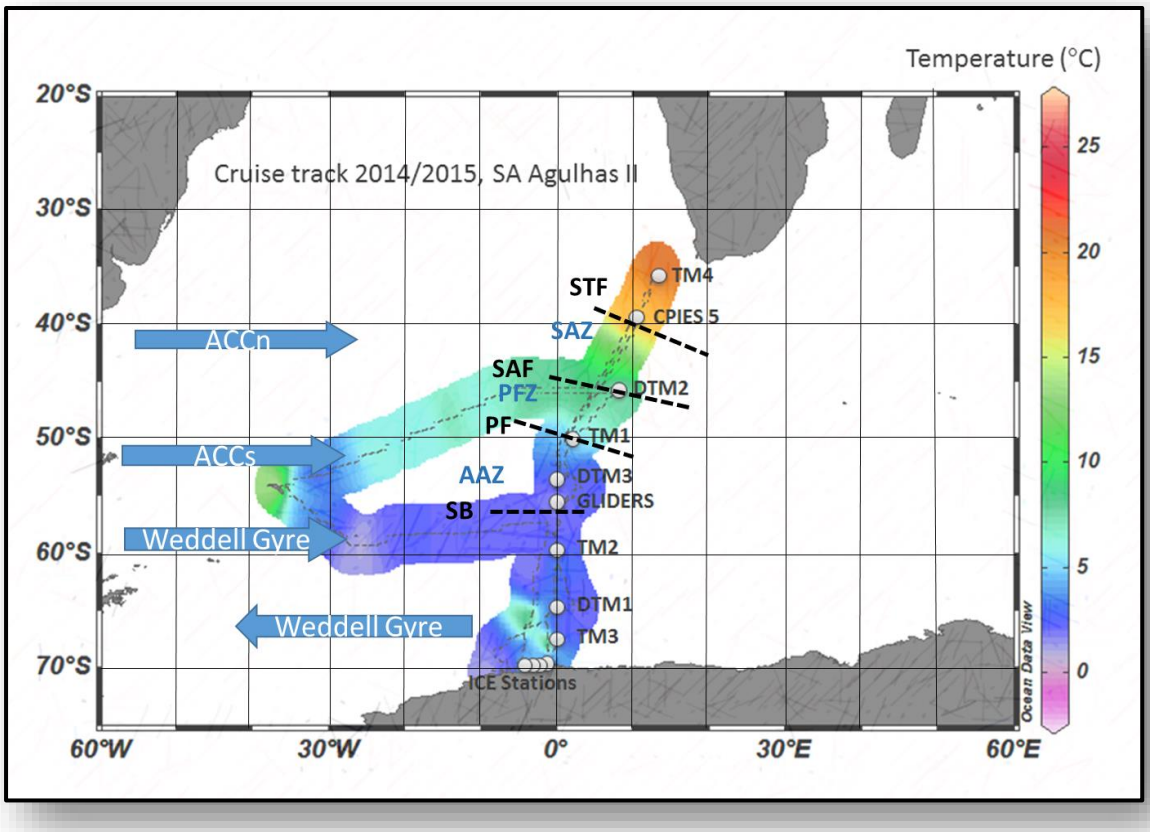

***Figure 2**-A temperature data plot (ODV) of the SANAE 54 cruise track. Stations are shown by the white circles; the dashes constrain fronts and the arrows indicate water circulation. TM denotes a trace metal station, DTM a deep trace metal station and the ICE stations are denoted as such due to their location in the within the sea ice (CPIES stations not pertinent). The Antarctic Circumpolar Current north (ACC) and the Weddell Gyre are large scale controls. The fronts and domains are as follows: Sub-tropical front (STF), Sub-antarctic Zone (SAZ), Sub-antarctic Front (SAF), Polar Frontal Zone (PFZ), Polar Front (PF), Antarctic Zone (AAZ); southern Boundary (SB).*

2. Vertical Profile Sampling

A Seabird aluminium frame carousal with the capacity for 24 Teflon-coated, acid cleaned, GO-FLO bottles (General Oceanic's Inc) was employed in vertical sampling of the water column. The rosette frame – trace metal clean and polyurethane coated – utilized a Kevlar conducting cable to systematically trigger GO-FLO bottles at depth. Weighting, provided by lead encased in epoxy, ensured a negatively buoyant system. The carousel houses a Seabird 9+ Conductivity Temperature Depth (CTD) recorder. GO-FLO's were transported from a class 100 (ISO 5) clean container to the rosette 45 minutes before each cast. Transporters wore nitrile gloves and sleeves when handling the protected GO-FLO's – shower caps top and bottom, zip-locks over the taps, and PVC liners. PVC liners were removed upon loading the rosette carousel; however, shower caps and zip-locks were only removed at the last minute. Upon retrieval, the GO-FLO's were immediately transported – mirroring the steps to guard from contamination – and placed in a class 100 (ISO 5) clean container for sub-sampling. The dissolved fraction (<0.2µm) was collected in line using a 0.2µm filter (Acropak 500 Supor Membrane) with filtered (Midisart 2000 0.20 µm) nitrogen assistance (BIP-Technology, 2 bar). Samples were acidified and stored in 125ml LDPE bottles – 3 replicates were collected. The total fraction was collected unfiltered and samples were acidified and stored in 125ml PFA bottles – only a solitary sample. All samples were acidified to a pH of 1.7 using Merck Ultrapur® HCl. Upon disembarking the cruise all samples were stored in the class-100 clean lab at Stellenbosch University. The method of sampling was adapted from the trace element collection method described in the GEOTRACES cookbook (Cutter *et al.*, 2010). The mandatory Baseline and Inter-calibration sampling station was executed at DTM3 and -sub-sampled for 23 depths (total and dissolved); 15 depths were sampled as per GEOTRACES protocols and sent to PML for inter-calibration.

3. Reagents and Materials

Deionized water (Milli-Q) purified with the Milli-Q® Advantage A10 system (Millipore) was to clean materials and prepare all solutions. Reagents employed in this study were sourced from and manufactured by Merck Millipore. The reagent grade (RG) Hydrochloric Acid 32% (HCl) used in preliminary cleaning was supplied by Merck Millipore. Trace metal grade reagents used are as follows: Suprapur® was used in cleaning and acid storage of sample bottles, seawater samples were acidified to a pH of 1.7 using Merck Millipore Ultrapur® HCl (30%). Merck, EMSURE®, Ammonium Hydroxide Solution 25% (NH4OH) diluted to 22% with Milli-Q water together with Merck EMPROVE® Acetic Acid (Glacial) 100% (CH_3COOH) was used to make the pH 6 ± 0.2 buffer solution recommended in the pre-concentration procedure. Ultrapur® Nitric Acid 60% (HNO3), Merck, functioned as the Eluent reagent

in the pre-concentration module. The sub-sampling bottle materials are perfluoroalkoxy (PFA) and low density polyethylene (LDPE). Polypropylene (PP) Falcon tubes were used in pre-concentration. An alkaline detergent (Extran) was used to rid the bottles of organic oils. Furthermore, iso-2-propanol (uniVAR) was used to clean the GO-FLO's.

Note: Cleaning protocols can be viewed in the Appendix A.

4. Sample Pre-Treatment

A major fraction of several bioactive trace metals such as Fe, Zn, Cu, Co and Cd exhibit strong complexation with organic ligands (Ellwood and Van den Berg, 2001; Lohan *et al.*, 2005). Consequently, trace metal concentrations could be underestimated. Thus, there is a need to solubilise colloidal matter, and to dissociate organometallic complexes – achieved by acidification to a pH of 1.7 with Ultrapur® 30% HCl. However, in the case of Co and Cu, acidification is not sufficient and UV-Oxidation (omitted from this study) is recommended to ensure complete dissociation (Milne *et al.*, 2010; Biller and Bruland, 2012).

Note: The omission of UV-Oxidation is rationalised in Chapter 3.

5. Analytical Methods

The difficulties in the analysis of multi-element seawater samples created the need for an improved method that would return a broad range of element concentrations reflective of the observable range in the oceans. Modern inductively coupled plasma mass spectrometers (ICP-MS), instruments with high resolution, have enabled the successful analysis of samples over a dynamic range. Presented in this study is a method in which trace metals were simultaneously extracted in an off-line pre-concentration module and analysed using ICP-MS. Chapter 3 is centred on a comprehensive discussion regarding the application of analytical methods and steps taken for single-laboratory validation.

Note: Protocols for sample handling can be viewed in the Appendix A.

5.1 Pre-concentration by Solid Phase Resin Extraction

5.1.1 SeaFAST Module

The sea*FAST*-pico SC-4 DX (Elemental Scientific Inc.) pre-concentration module is an ultra-clean, automated, low-pressure ion chromatography system capable of picogram L^{-1} detection limits. The setup consists of an S400V (S400V-1111) syringe pump containing four syringes (Rinse, Carrier, Diluent and Internal Standard), TRIO Valve Module (VM3-P6P6SSV11), 12 Port Valve (V12), 11 Port Valve

(V11), 5 Port Valve (A5e), Fluoropolymer flow paths, a seawater pre-concentration column (CF-N-0200), trace metal clean-up column and a nitrogen gas line (Figure 3).

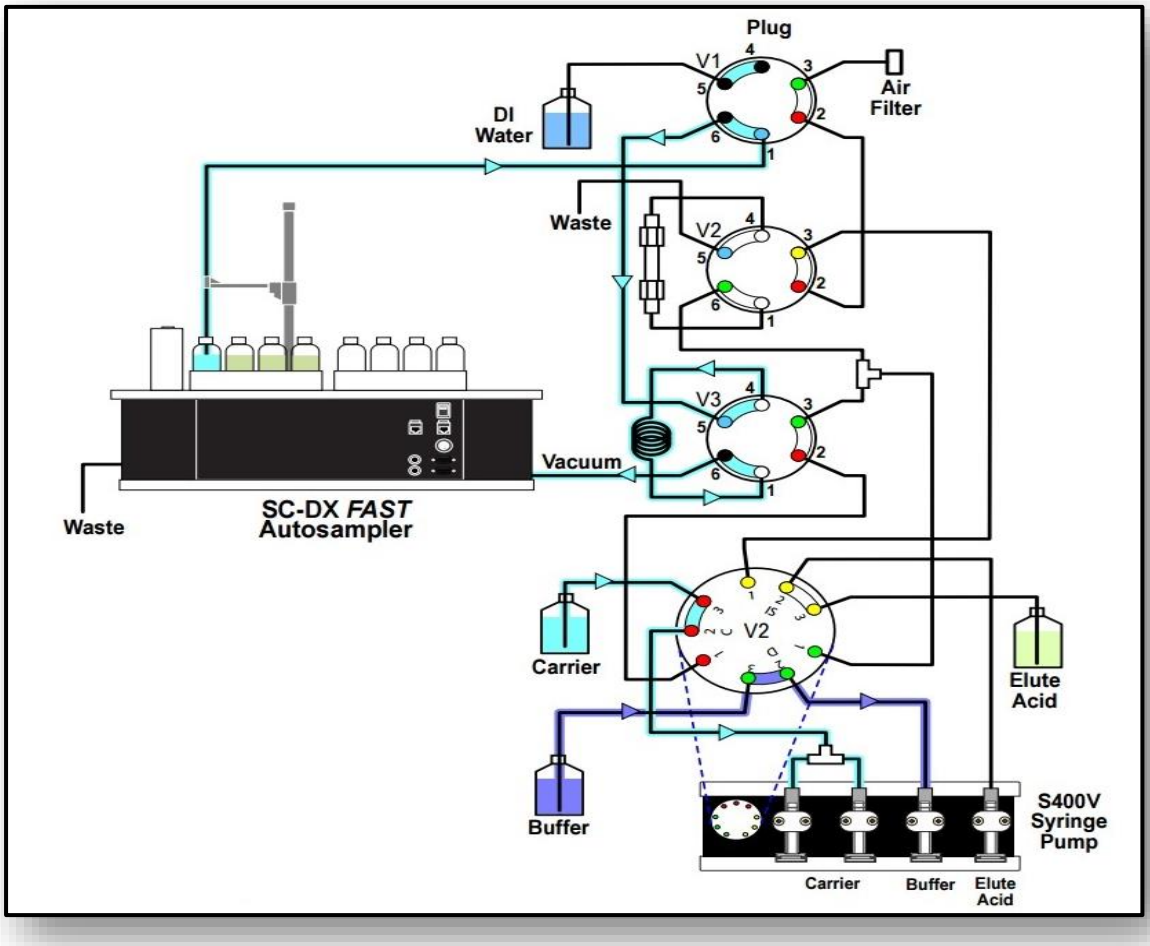

***Figure 3**-A schematic illustrating the Elemental Scientific Inc. (ESI) seaFAST SC-DX Autosampler system and outlay (Elemental Scientific Brochure). The buffer, comprising an ammonium acetate solution, must maintain a pH (6 ± 0.2) to ensure the optimal recovery for the trace metal range; the elution acid was a dilution of 53mL of trace element grade Nitric Acid (60%) to 500mL, the carrier solution was the same as the elution acid, and Ultra High Purity Deionized (DI) water was used to flush the system.*

The resin used in the sea*FAST* system column comprises an ethylenediaminetriacetic acid (EDTriA) and iminodiacetic acid (IDA) functional groups, suitable for a more than 1000 cycle lifetime. EDTriA and IDA are immobilized on the hydrophilic methacrylate polymer (60µm bead diameter), acting as high affinity metal chelators in the solid-phase extraction of trace metals. The system has a resin bed volume of 200 µL (100mg) with a column capacity of 20 µEq/column. Column materials per ESI are: PFA body and caps, polytetrafluoroethylene (PTFE) frits, and chlorotrifluoroethylene (CTFE) plugs for storage. The recommended solvents used in the pre-concentration are as follows: ammonium solution and glacial acetic acid (ammonium acetate) to prepare the sample buffer, nitric acid 2M (-8%) to elute

the column and, de-ionized (DI) water used in conjunction with ammonium acetate to recondition the column. The entire system was pressurized utilizing clean air at a pressure of 2 bar.

5.1.2 Pre-concentration Procedure

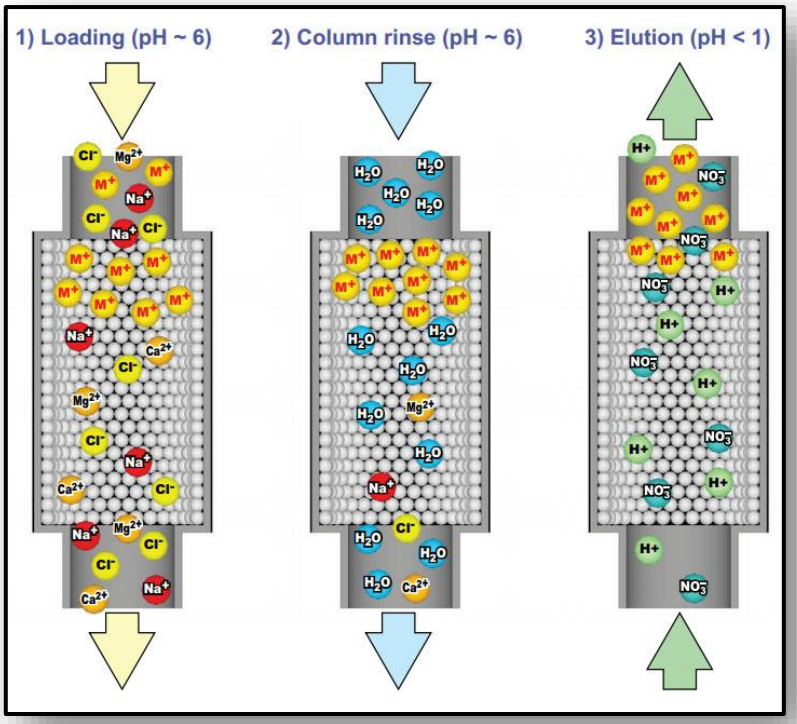

Figure 4*-A schematic illustrating the "trapping" of trace metals on the commercially available EDTriA and IDA resin (ESI), whilst the matrix constituents pass through (Elemental Scientific Brochure). Once vacuum loading has filled the sample and buffer loops, the stepwise column recovery process goes as follows: 1) loading of chelation column with the buffered solution 2) rinsing of the column with H_2O to ensure flushing the matrix elements, while retaining the metal ions 3) back elution of the trapped metals using high purity nitric acid.*

The closed system was set up in a class 100 (ISO 5) clean lab to limit potential contamination of both seawater samples and pre-concentrated samples during handling. The system was run in the off-line configuration mode whereby an automated method vacuum loads 14ml at 5.4mL/s (4mL.min^{-1}) of acidified seawater in a loop on one inert injection valve and buffers the sample. The buffered solution is loaded onto a chelating resin column attached to a second, high purity valve, where the matrix is removed and metal ions are selectively bound (Figure 4). Concentrated metal ions trapped in the column are eluted in low volumes (270 µL) to a Falcon test tube rack. A 40 times concentration ensured detection limits in the pg L^{-1}, with a 20-minute run time per sample. Prior to automated sample pre-concentration the resin columns were "primed" in compliance with the procedures in the ESI handbook. Further, at least three NaCl (3%) column conditioning blanks preceded an in-house control sample prior to commencing batch analysis. Crucially, optimal recovery for the trace metal

suite hinges on a consistent pH of 6 ± 0.2 for the ammonium acetate buffer solution (Sohrin *et al.*, 2008). The system received a minor modification in the form of a Perspex 'hood' ensuring the samples are protected from potential gravitationally afflicted atmospheric contaminants; first employed and continually used as of June, 2016.

5.2 ICP-MS Analysis

Following a 40 times pre-concentration, sample analysis was performed on an Agilent 7700 – subsequently upgraded in 2016 to the Agilent 7900 – quadrupole Inductively Coupled Plasma Mass Spectrometer (ICP-MS) at the Central Analytical Facilities (CAF) laboratory at Stellenbosch University. Agilent technologies state a doubling in sensitivity for the new instrument. The instrument was optimized for best sensitivity and low oxide ratios (< 0.3%). Samples were introduced using a low flow self-aspirating PFA nebulizer with a flow rate of ~ 0.2µl/min. Isotopes of Al^{27}, V^{51}, Mn^{55}, Fe^{56}, Co^{59}, Ni^{60}, Cu^{63}, Zn^{66}, Cd^{112} and Pb^{208} were measured using the Agilent Octopole Reaction System (ORS) in He collision mode to eliminate plasma and matrix based interferences; which were extensively reduced by using the ESI sea*FAST* system to remove the seawater matrix. Internal standards comprising Sc^{45} and Y^{89} were used to compensate for instrument drift as well as matrix differences between samples and standards. The instrument was calibrated using a multi-element standard from Inorganic Ventures Inc (Christiansburg Virginia), and the calibration verified with a multi-element standard supplied by Merck Millipore (Merck KGaA, Darmstadt, Germany). Continuous check standards were analysed throughout the run to monitor instrument drift. Data processing was performed using the Agilent ICP-MS MassHunter software.

6. Standards and In-house Controls

6.1 Inter-laboratory Reference Materials

Successful data and laboratory validation hinge on the capability of the analysts to prove precision and accuracy within the specified criteria for the employed offline pre-concentration and ICP-MS method. The study employed the community verified SAFe (D2) and commercial NASS 5 standards to evaluate the performance and concurrently provide calibrated baseline trace metal concentrations. Moreover, the GEOTRACES GSC and GSP standards were analysed with the aim to contribute towards the creation of consensus values for these standards. The seawater standards were collected by Geoffrey Smith and Ken Bruland in conjunction with the large inter-calibration effort centred on the creation of consensus data on trace metals for inter-calibration and reporting purposes. Filtered seawater was collected and homogenized during the SAFe (Sampling and Analysis of Fe) and the GEOTRACES Inter-calibration North Atlantic and North Pacific cruises. The standards used in this study

consists of 3 LDPE stored 0.5 L reference samples namely: SAFe (D2) and GEOTRACES (GSP, GSC). The GEOTRACES GSP (SAFe station) and GSC (Santa Barbara Channel) surface seawater samples were collected from ≈2 meters depth outside of ship's influence using a University of California Santa Cruz (UCSC) designed "GeoFish" towed sampling system. The SAFe D2 1000 m seawater sample was collected under multiple four-bottle casts using a Teflon™ coated, 30 L, GO-Flo sampler deployed on Kevlar™ hydroline (Bruland *et al.*, 1979).

6.2 Trace Metal 4 (TM4) In-house Control

The Trace Metal 4 (TM4) in-house control – employed to monitor precision and consistency during pre-concentration and ICP-MS analysis – saw two iterations: an unacidified batch (TM4) and a subsequent evolution to an acidified (pH 1.7) batch (TM4A). Furthermore, the evolution saw a decrease from 20L to 1L for the in-house control storage – a means to improve homogeneity. The 20L control consists of seawater collected in the sub-tropical domain at 36°S 13°E (Figure 2) – filtered as per cruise protocol for the dissolved fraction, homogenised, and stored in a 2X20L acid cleaned LDPE carboys. To improve precision through superior uniformity, a 1L sub-sample of the 20L LV control was created and used in analysis. The similarity of the in-house control with field samples made it an ideal proxy to test method precision and repeatability – denoted a 'test' run. Subsequently, a baseline concentration was established via insertion concurrent to the pre-concentration and analysis of the SAFe and GEOTRACES standards – denoted as a 'calibration' run. Moreover, the risk of further concentration by evaporation was evaluated by performing a 4hr (TM4 4hr) exposure test in the class 100 clean lab. The large sample volume enabled multiple column conditioning samples to be run; an essential step in the procedure. A trace metal standard Sodium Chloride (NaCl) solution was diluted to 3% and used to condition the resin column with a suitable matrix sample. Conditioning samples were discarded and only strategic (every 12 field samples) in-house controls were analysed.

CHAPTER 3

Validation and Inter-Calibration

Abstract

Presented in this chapter, is a comprehensive examination of the precision, accuracy and suitability of a multi-element method coupling offline pre-concentration, with inductively coupled plasma mass spectroscopy (ICP-MS). The compilation aims to provide concrete evidence in favour of accreditation by the GEOTRACES S&I Committee. The method proved accurate and precise in the simultaneous quantification of up to 8 trace metals (Mn, Fe, Co, Ni, Cu, Zn, Cd and Pb) in a seawater matrix. The commercially available sea*FAST* module was employed in the sample pre-concentration and seawater matrix removal. The module contains a high affinity metal chelating resin column (EDTriA, IDA functional groups). Seawater samples (14mL) were loaded onto the column at a pH 6.0 ± 0.02 – ammonium acetate (NH_4Ac) buffer solution and eluted via a nitric acid solution (HNO_3). A 40-times pre-concentration ensured readily detectable (ICP-MS) concentrations. An In-house Control (TM4A) was developed and used to monitor precision and recovery. Statistical evaluation of the control under repeat analysis (n=51) corroborates first-rate analytical precision (≤ 5%RSD) for several trace elements (Zn, Cu, Cd, Ni, Pb and Mn), and ≤ 10%RSD for Fe and Co. Field precision was markedly improved at ≤ 5%RSD with the difference attributed to batch variability. Analysis of the SAFe (D2) reference material substantiates "true" quantitative recovery for the range of elements – barring Co and Cu. Furthermore, the study reports concentrations for the GEOTRACES GSC and GSP (n=5) standard. The dissolved iron (DFe) concentrations are reported for a Southern Ocean Baseline and Inter-calibration station at 54°S. Inter-calibration samples analysed by Plymouth Marine Laboratory (PML) using a Flow Injection Analysis method, corroborate uncontaminated sample collection and quantification. The proficiency of the method in the quantification of Fe (≤5%RSD, Field Precision) demonstrated its suitability, in the intended replacement of Flow Injection Analysis (FIA).

Keywords: GEOTRACES S&I, GEOTRACES GSC and GSP, ICP-MS, SAFE (D2), sea*FAST*, precision, accuracy.

1. Foreword

The ongoing collaborative efforts, among marine scientists seeking to incorporate trace metal data into international consensus databases, has been the core element supplementing a greater collective understanding of biogeochemical cycling in the world's oceans. Nonetheless, seawater trace metal analytical chemistry remains notoriously intricate by way of inherently low – nmol kg^{-1} to pmol kg^{-1} – elemental concentrations of trace metals; further complicated by high concentrations of major ions (mmol kg^{-1}) in the seawater matrix. Thereby, the nature of analytical chemistry, is such that reporting commands the 'full validation' of a scientific method hinging on the concentrated evaluation – internally, and externally by collaborative trial – of laboratory techniques and analytical results; centred on precision, accuracy and reproducibility (Wood, 1999). It follows that contributions to the consensus database require, a highly sensitive, accurate method proficient in the analysis and quantification of trace metals – all the whilst heeding to validation guidelines established by the Designated Authority (DA) (Wood, 1999; Union *et al.*, 2002; Taverniers, De Loose and Van Bockstaele, 2004).

Procedural guidelines for the realization of full validation stipulate that the relevant laboratory undertake a mandatory effort to compile a comprehensive report describing the design, conduct and interpretation of a method performance study (Union *et al.*, 2002). Inclusive of such a report is a statistical investigation aimed at quantifying precision and accuracy; a powerful tool in identifying sources and forms of error that may be present. Classically, statistical errors in analytical chemistry may be encountered as: gross errors; disagreeing with experiment criteria; systematic errors; affecting accuracy; and random errors; uncontrolled variables. Concurrently, it is the role of the collaborating laboratory to corroborate the quality of the analytical quantification attained; thereby functioning to expose any bias regarding the laboratory or the performance of the method (Shah et al. 1992; Wood 1999). Significantly, it is the direct impact on the quality – thereby the integrity – of the data, that a study stands to gain, ought it undergo a rigorous validation process.

Instruments employed in the detection of trace metals have evolved through, for instance, inductively coupled plasma atomic emission spectroscopy (ICP-AES) used by Mclaren et al. (1985), to include inductively coupled plasma mass spectrometry (ICP-MS) (Biller and Bruland, 2012), graphite furnace atomic absorption spectrometry (GFAAS) (Kingston *et al.*, 1978) with lesser employed chemiluminescence, spectrophotometric colorimetry and adsorptive cathodic stripping voltammetry methods (Saito and Moffett, 2001). Further, to circumvent matrix interference and ensure quantitative detection, archetypal analytical methods involve the separation and extraction of trace

metals from the major ions and dissolved organic matter. The pre-concentration technique aids analysis by increasing the signal to blank ratio.

Selective removal of most interfering ions and pre-concentration/extraction of dissolved trace metals can be achieved utilizing several methods with numerous resin types employed – to variable success. Anodic stripping voltammetry of labile and total metals using a Beckman rotating glassy carbon electrode where pre-concentration is achieved by long depositional times (Batley and Florence, 1976), organic solvent extraction by chelation of the sample with ammonium 1-pyrrolidinedithiocarbamate and diethylammonium diethlydithiocarbamate (APDC/DDDC) with a double extraction into chloroform, and back-extraction into nitric acid (Bruland *et al.*, 1979; Sañudo-Wilhelmy *et al.*, 2002). A single extraction method, using dithiocarbamate as the complexing agent in methyl-isobutyl ketone (MIBK) organic phase with acid back extraction, has been successfully employed in matrix removal (Jan and Young, 1978; Satyanarayanan *et al.*, 2007). An ion-exchange concentration technique which uses the Chelex 100 resin to selectively bind polyvalent metal ions has proven useful when coupled with ICP-MS (Bruland *et al.*, 1979), however, it proved inadequate for determination of Cd and Pb by ICP-AES (Mclaren et al. 1985). Column or batch solid phase extraction with a suitable chelating resin was employed by Sohrin et al. (2008) and co-precipitation with magnesium hydroxide ($Mg(OH)_2$) has demonstrated some success in experiments performed by Wu & Boyle (1997).

The commercially available Toyopearl AF-Chelate-650M, with iminodiacetic acid (IDA) functional groups, has been successfully used in off-line pre-concentration in the quantification of Fe, Mn, Ni, Co, Cu, Zn, Cd and Pb (Milne *et al.*, 2010; Bown *et al.*, 2011). Nobias-chelate PA1 (Hitachi High-Technologies) is a hydrophilic methacrylate polymer resin on which both ethylenediaminetriacetic (EDTriA) and imonodiacetic acids are immobilised (Sohrin *et al.*, 2008). EDTriA, an analogue of EDTA, is a high affinity trace metal chelator with a maximum of five coordinate bonds to a metal ion the use of which in closed columns reduces the risk of contamination. Commercially available it has seen application in the simultaneous off-line extraction of trace metals (Sohrin *et al.*, 2008; Biller and Bruland, 2012). Batch extraction of trace metals Fe, Cu, Pb and Cd can be done in small volumes using Nitriloacetate (NTA)-type Superflow chelating resin beads (Lohan *et al.*, 2005; Lee *et al.*, 2011). However, the method requires isotope dilution which is not an option in the analysis of Co due to the lack of a stable isotope to use in dilution; it is possible to standardize isotope dilution by matrix-matched standard curves. Dionex MetPac CC-1 resin is a commercially available chelating column used in the concentration of cationic transition metals from high-ionic-strength matrices such as seawater. Ho et al. (2010) employed the resin in a novel online flow injection ion chromatograph (FI-IC) pre-treatment system to fully automate pre-treatment procedures for off-line trace metal analysis by ICP-

MS resulting in possible chelated elements: Al, Cd, Co, Cr, Cu, Fe, In, Mn, Ni, Pb, Th, Ti, U, V, Y, Zn and all lanthanide metals. Separation and concentration of trace metals (Mn, Cu, Ni, V, Cd and Zn) in seawater can be achieved by 50-fold adsorption on silica immobilized 8-hydroxyquinoline (8-HQ) prior to instrumental quantification (Mclaren *et al.*, 1985). The resin, which had to be synthesized from scratch, proved limited in multi-element analysis as the concentration of several trace metals are very close to the detection limit with Pb not detected altogether.

In reality, collaborative efforts have enabled progressive development of the methods proficient in multi-element quantification of trace metals in seawater; empowering the working group reporting oceanic trace metal concentrations to make commendable progress (Biller and Bruland, 2012). Significantly, replication of results across several methods has seen the reporting of accurate and precise results in consensus databases by effectively expunging the inherent limitations logically attributed to one specific method. Concurrently, this may allow improved scope in the selection of an analytical method tailored to a defined criteria – also known as the 'criteria approach' (Wood, 1999). Moreover, the emergence of commercially available resins used in the extraction/pre-concentration of trace metals in seawater have proved indispensable by expunging one or more variables in the application of a method.

This project sees an affiliation with the GEOTRACES International program; a collaborative effort among marine chemists creating a platform for the reporting, analysis and quantification of trace elements over a broad range. A novel method, employed by the SU TRACEx laboratory, couples a sea*FAST* pico offline pre-concentration and matrix removal module with modern, high resolution, magnetic sector inductively coupled plasma mass spectrometry (ICP-MS), as a tool in the simultaneous quantification of up to 10 trace metals. The accuracy and precision was evaluated by analysing the commercially available NASS-5 certified reference material (CRM), the community's SAFe and GEOTRACES inter-calibration materials, and an in-house control. It follows that the DA – those charged with validating the precision and accuracy of the data generated – be the GEOTRACES Standards and Inter-calibration (S&I) Committee. The procedural guidelines for validation are comprehensively outlined in the GEOTRACES Cookbook compiled by Cutter et al. 2010. Significantly, the analytical method employed in this study has been recognised by the DA as 'fully validated' in its application in trace metal pre-concentration, matrix removal, and ICP-MS analysis. To this extent, method-transfer procedure outlined by the DA require solely, that the TRACEx laboratory at Stellenbosch University (SU), demonstrate method competency, suitability, and proficiency in pursuit of single laboratory validation. Further, the realisation of validation is bolstered through an inter-calibration exercise whereby Plymouth Marine Laboratory (PML) analysed representative and common population samples. The PML laboratory utilized an alternative Flow Injection Analysis (FIA) method in the

analysis of the inter-calibration samples – an intentional deviation, since this study also tests the suitability of the method here-in to replace FIA in the quantification of iron. The exercise will support the effort to eliminate analyst confirmation bias, and further, enable the SU laboratory to recognize bias and imprecision resulting from operator, method and instrumentation.

To expunge ambiguity, this chapter will discuss in its entirety the analytical steps taken by the TRACEx laboratory at SU to generate the data and ensure the GEOTRACES compendium requirements are met. The validation plan purposes to test the assumptions on which the analytical method is based and evaluate the typical performance characteristics, specifically: applicability, selectivity, trueness, precision (repeatability, reproducibility), “trueness” of recovery, instrument calibration, operating range, detection limits (DL), sensitivity, and ruggedness. Hydrographic data, including macronutrients, will accompany the trace metal data for the inter-calibration exercise and Baseline station providing a comprehensive picture of the bio-geochemical process.

2. Validation Plan

Though quantum leaps in analytical techniques have permitted improved quantification of trace elements in seawater, results must be accompanied by rigorous statistical evaluation to provide evidence that a method can achieve the stated objectives. The laboratory at Stellenbosch University employed an offline pre-concentration and ICP-MS coupled method in the analysis of seawater samples. In pursuance of single laboratory validation – aided by collaborative trial – the robustness and accuracy of the method required a comprehensive validation plan and quality assurance (QA) guide. The validation plans and criteria are as follows:

Objective One: Evaluate and demonstrate the proficiency of the Stellenbosch University TRACEx laboratory in the application of a multi-element ICP-MS analytical method. Thereby, provide a comprehensive statistical report advocating single-laboratory analytical method validation adhering to the protocols and procedure outlined in the GEOTRACES Cookbook (Cutter *et al.*, 2010).

- Demonstrate that ICP-MS – coupled with a pre-concentration module – is an effective and efficient multi-element method for the accurate and precise quantification of trace metals.
- Analyse for trace metals efficiently, accurately and precisely, while limiting the contamination risk and ensuring high reproducibility - provide statistical evidence for a robust and reproducible analytical method that enables multi-element quantification.
- Demonstrate that Iron (Fe) can be accurately and precisely quantified using this method.
- Results from a Baseline station and inter-calibration exercise must be statistically evaluated to provide an indication of achieved precision and accuracy.
- Contribute towards GEOTRACES consensus data as well as filling existing gaps in the database.

Objective Two: The method must meet the following requirements for the single-laboratory validation at Stellenbosch University to be successful:

- Accuracy relative to a known certified reference material (CRM), or SAFe or GEOTRACES Consensus Inter-calibration samples – working at the 95% confidence interval (CI).
- Precision – working at the 95% CI.
    - Field replicates – repeat analysis of samples taken from a single GO-FLO.
    - Analytical replicates – repeat analysis of a single sample with a minimum of 20 data points for statistical evaluation.
- ICP-MS limits of detection (LOD) and measurable detection established – working range established adhering to the >0.99 correlation coefficient.
- The percentage relative standard deviation (%RSD) must be below 10% and ideally below 5%.

3. Methods

Note: Comprehensive methods can be studied in Chapter 2.

3.1 Analysis – A Statistical Approach

To ensure that the performance characteristics of the method employed in this study achieved true precision and accuracy several consensus standards and an in-house standard were analysed prior to sample analysis. A 'test' and subsequent 'calibration' analysis was performed prior to each extended period of sample analysis. The 'test' run – referring to the action of pre-concentration and subsequent analysis of the in-house control – served to ensure that that the method allowed simultaneous quantification of trace metals in a precise and readily replicable manner. The 'calibration' run created a baseline concentration for the Certified Reference Materials (CRM) and Reference Materials (RM) intended to certify accurate quantification of trace elements prior to sample analysis – simultaneous in-house controls were analysed to generate a 'calibrated' concentration for the control.

The in-house control – denoted TM4 Control - comprised 40L (2 X 20L carboys) of filtered (0.2µm) seawater collected during the SANAE 54 cruise. It was collected under the same protocols as the field samples with concentration ranges in-line with the nano to pico molar concentration levels expected for the bioactive elements in the samples. Hence, the in-house control is ideally suited to monitor recovery on the seaFAST resin column in addition to drift and sensitivity of the ICP-MS. A second Quality Control (QC, 1ppb IV-28) was intentionally omitted from pre-concentration and strategically inserted during ICP-MS analysis to monitor drift and sensitivity, and evaluate the performance of the Agilent 7900 ICP-MS. Furthermore, the high concentrations of the NASS 5 were used in a rudimentary evaluation of carry over on the resin column. The in-house control sample was pre-concentrated prior to, and again post NASS 5 pre-concentration on the sea*FAST* module.

3.1.1 Analytical Accuracy

Analytical chemistry demands a means to quantify the closeness of the obtained result relative to the "true" value – a qualitative concept defined as accuracy. Determining the analytical error is a crucial step in demonstrating the competent application of the method by the TRACEx Laboratory at Stellenbosch University (SU). The SU results are quantitatively compared to the GEOTRACES community consensus data utilizing the formula as follows:

$$\%\, Accuracy = 100 \times \frac{C_{obs}}{C_{consensus}}$$

Equation 1

The subsequent results are to meet the 95% Confidence Interval (CI) – corresponding to an accuracy interval of 80 – 120%. Further a probability calculation, expressed as a percentage, was performed whereby the standard deviation intervals is used to test the spread of the historic data around the mean – the likelihood that a value falls within one or two standard deviations.

The GEOTRACES arsenal comprises several consensus Reference Materials (RM) dedicated to the evaluation of analytical accuracy. This study employed the SAFe (D2) and GEOTRACES (GSP, GSC) standards collected during the SAFe, and Inter-calibration North Atlantic and Pacific cruises respectively. These standards encompass the complete range of predicted trace metals and sample concentrations. However, a limited volume was available for analyses inhibiting the replication desirable for true statistical evaluation. The NASS 5 seawater standard was also analysed to provide information regarding the measured accuracy at higher concentration; simultaneously permitting potential carry over (CO) performance evaluation on the sea*FAST* system EDTRiA resin column.

Further, determining the accuracy of the ICP-MS calibration will follow an identical statistical process with the results of two commercial check standards compared to certified values. The instrument was calibrated using a multi-element standard from Inorganic Ventures Inc (IV), and the calibration verified with a multi-element standard supplied by Merck Millipore (Merck KGaA, Darmstadt, Germany). Linearity of the calibration was ensured using the Mass Hunter Software to accomplish a linear regression based on a three-point calibration curve and determine the correlation coefficient**.**

3.1.2 Analytical Precision (TM4 In-house Control)

The precision was measured by the repeat analysis of a single homogenous sample – representative of field samples. This process serves to quantify, and thereby demonstrate, the greatest possible analytical closeness for the method and equipment based on statistical evaluation of the measurements attained for the sample analysed across multiple batches.

The reproducibility of the method was defined by determining the relative standard deviation corresponding to each trace metal in the data set (Equation 2). Protocols for the single-laboratory validation of this method see acceptance criteria permitting %RSD <10% over 30 replicates (Cutter *et al.*, 2010). It is important to note that the %RSD was calculated using the standard deviation (Std Dev), and not the CI (Equation 2).

$$\%RSD = Std\ Dev \times \frac{100}{\bar{x}}$$

Equation 2

The statistical evaluation parameters of the in-house un-acidified (TM4 Control) and later acidified (TM4A Control) control were kept identical. However, as an outcome of the notable change in the concentration post acidification an independent statistical evaluation was performed on the TM4 Control and the TM4A Control respectively. The data in excel was conditionally formatted to classify interesting cells as follows: cell values greater than one Std Dev from the mean ($\bar{x}$) were highlighted yellow; those greater than two Std Dev would be identified by small dots; and those greater than three Std Dev would be highlighted red (Appendix A, Table A1). Consequently, cells that highlighted red under the rules of the formatting were identified as outliers and omitted from the statistical calculations thereafter. The mean ($\bar{x}$), Std Dev, and the %RSD are calculated accordingly – outliers omitted. The probability intervals are calculated by determining the percentage of samples within one and two standard deviations - ignoring the outliers. Prior to the determination of the confidence levels the data was tested for any significant distributions away from the mean that may compromise the statistical evaluation. To this extent, the skewness for the in-house control – excluding outliers – was calculated applying the SKEW.P excel function. A standard error of skewness was calculated founded on equation 3.

$$Std\ Error_{Skew} = SQRT\left(\frac{6}{N}\right)$$

Equation 3

This created the framework for a 'significance of skewness' test intended to determine if the distribution of the data was 'symmetric' – an important factor for the Confidence Interval (CI) calculation. The skewness was deemed significant if the "Skew" result was greater than twice the "Std Error_Skew" – an indication of non-symmetric data distribution. The distinction allowed a more accurate calculation of the CI whereby the excel functions CONFIDENCE.NORM and CONFIDENCE.T were employed to quantify the margin of error associated for normal and non-symmetric distributions respectively. A graphical illustration of the data distribution was drawn whereby a y-coordinate value was created utilizing the NORM.DIST function in excel, to plot against the data on the x-coordinate. Furthermore, a calculation was performed to calculate the percentage likelihood that a result may be found within one or two Std Dev(s) of the mean – a type of z-score test to express the 68 and 95 percent intervals.

A run variability calculation was performed on the In-house Control as a means of quantifying the repeatability error associated with the "run effect". It was evident that the method had higher precision within each batch. This involved calculating the following: a mean for each batch or "run"; the standard deviation for the batch; and a %RSD value for the batch. Thereafter a mean intended for

a comparative effort was calculated for: the batch mean; batch standard deviation; and batch %RSD. The calculation of the Field Precision followed an identical process.

3.2 Baseline Station and Inter-calibration

The S&I Committee protocols described in the GEOTRACES Cookbook require that affiliated cruises occupy at least one Baseline Station – that is where previous affiliated cruises have reliably established the concentrations, activities and speciation of at least the key GEOTRACES trace elements and isotopes (TEI's). The Baseline and inter-calibration station selected for this cruise was located at 54°S (DTM3) in the Antarctic Zone (AAZ) – a documented crossover station (Figure 2) (Klunder *et al.*, 2011). Reoccupation must adhere to, and compile data incorporating all the ancillary parameter specified in the Cookbook (Cutter *et al.*, 2010).

The inter-calibration exercise performed in conjunction with Plymouth Marine Laboratory (PML) saw replicate samples comprising 15 depths – near surface, mid-water and deep – analysed by employing the Flow Injection Analysis (FIA) method to quantify Fe. To justify trace metal quantitative analysis, the samples were run against calibration standards (SAFe, GEOTRACES and NASS 5) further ensuring integrity and coherence. This station also served to establish the precision of replicated field samples – two or more 125 ml LDPE samples taken from a single GO-FLO. Thereby investigating variance due to sub-sampling, storage, and inherent sample variability. The guidelines state that, assuming homogenous analyte distribution, the variance of field and analytical replicates should be equal assuming sampling, storage and analysis have no effect. The field precision for the method employed in this study, has been statistically evaluated for duplicate samples (n=2) – statistically inadequate. Nonetheless, a mean %RSD calculated using duplicates from at least 15 replicated depths serves to illustrate the precision. The external validation of measurements attained by the SU TRACEx laboratory would provide significant evidence for proficient and competent application of the method in its entirety – that is field to analytical. Trace metal samples for this station are accompanied by the relevant nutrient, salinity and chlorophyll-a data aimed at assisting PML and the GEOTRACES S&I in the verification of the stated performance.

3.3 ICP-MS

The Agilent 7700 and 7900 machines at the Stellenbosch University Central Analytical Facility (CAF) were calibrated using a 4-point calibration curve constructed with the aid of: 0ppb, 1ppb, 10ppb and 20ppb calibration standards from Inorganic Ventures (IV). The solitary function of the 20ppb calibration standard was ensure consistency of calibration over a wide concentration range. The detection limits (LOD) without pre-concentration were calculated as three times the concentration of

the reagent blank. The accuracy of the calibration for the inter-calibration station was evaluated by analysing two check standards: a 0.1ppb check and a 1ppb check std. Both standards, have Fe and Zn concentrations 10 times higher at 1ppb and 10ppb respectively. To monitor instrument drift, each run was analysed in parallel with the 1ppb IV-28 Quality Control (QC) and a 2% nitric acid (HNO_3) Blank in acid cleaned Falcon tubes – analysed after every 6 samples (12 minutes) in the ICP-MS. Data processing was performed using the Agilent Mass Hunter software.

***Table 1**-The ICP-MS Agilent 7900 instrument was optimized for the analysis of each 270µL pre-concentrated sample as per the parameters outlined in the table.*

ICP-MS Experimental Parameters	
	Value
RF Power (W)	1600
Carrier gas (L/min)	0.9
Sample depth (mm)	10
Make-up gas (L/min)	0.25
He flow (ml/min)	4.5
H2 flow (ml/min)	6

4. Results

4.1 ICP-MS Performance

Note: Comprehensive precision results table available in the Appendix A.

4.1.1 Calibration Curve and Detection Limits

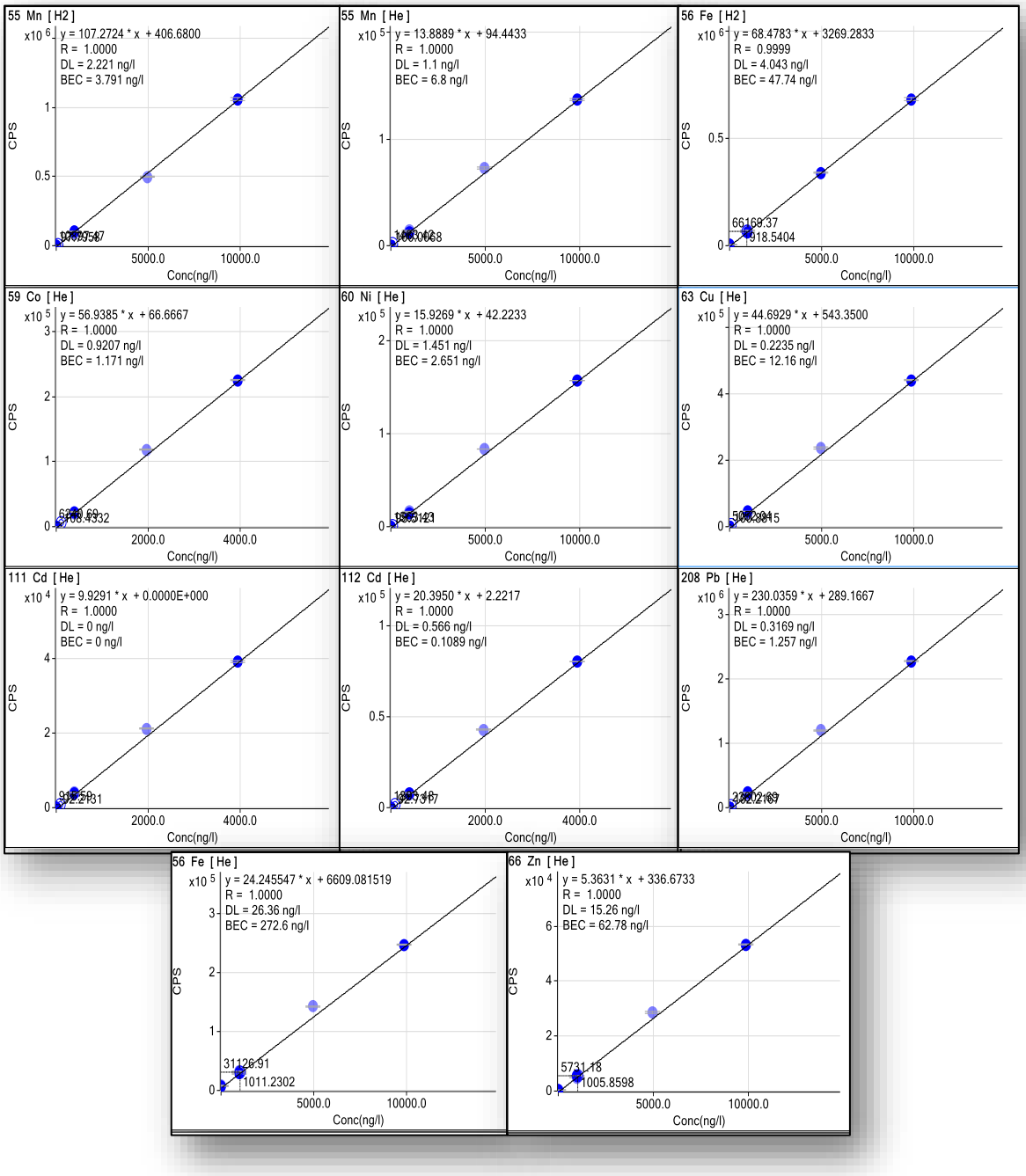

***Figure 5**-The 3-point (0ppb, 1ppb, 10ppb) calibration curve for the Baseline station at 54°S (DTM3) as per element. The linearity of the correlation coefficient was >0.99 for the collective suite of elements. Detection Limits (DL) and Background Equivalent Concentration (BEC) are given in ng/L.*

The results of the ICP-MS 3-point calibration performed for the Baseline and Inter-calibration station DTM3 at 54°S are presented in figure 5. The correlation coefficient for the 0ppb, 1ppb, 10ppb, 20 ppb calibrations standards saw linearity >0.99 for the entire suite of elements concerned. Data is also provided for the detection limits (DL) – calculated at three times standard deviation of the calibration blank – and the background equivalent concentration (BEC). Low BEC concentrations supplement the LOD data and provide further evidence for proficient recovery under low elemental signals.

The DL of the calibration are given for the Baseline station (DTM3) in table 2. The results are compared to the respective mean trace element concentrations for DTM3 and the mean open water concentrations (Sohrin *et al.*, 2008). It should be noted that a dilution factor of 0.4 was applied to the elemental concentrations which are 40-times pre-concentrated. The DL for Fe was the highest at 25.72 ng/kg for this calibration. Zn DL are similarly elevated at 14.89 ng/kg. Given the high open water Zn concentrations, DL should not see a significant impact on the accurate quantification of Zn. Conversely, Fe quantification may experience some variability given that typical concentrations are nearer the DL. Similarly, Co DL are uncomfortably close to the open water concentrations. However, the pre-concentration step serves to circumvent this limitation of ICP-MS analysis.

***Table 2**-The ICP-MS Detection Limits for the Baseline station as per the trace metal and respective isotope. The data was compared to the respective element mean field sample concentration as per the Baseline station. (r) denotes the average open water concentration is given according to those in* Sohrin et al. (2008). *(a) Denotes concentration in ng/kg.*

Detection Limits				
Trace Element	**Measured Isotope**	**SU CAF Detection Limit [a] (n=7)**	**SU DTM3 Conc. Mean [a]**	**Average Open Water Conc. [a,r]**
Mn	55	2,17	16,80	20
Fe	56	25,72	30,92	30
Co	59	0,90	1,42	1
Ni	60	1,41	358,57	500
Cu	63	0,21	119,66	200
Zn	66	14,89	376,70	300
Cd	112	0,56	80,55	70
Pb	208	0,31	1,36	2

4.1.2 Check Standards

The accuracy of the calibration was determined using two calibration check standards – "Cal check std 1 & 2" C. The results for the Baseline and Inter-calibration station can be seen in table 3. The SU results of the Cal check std 1 (0.1ppb) indicate percentage errors of < 7.3% for all the elements barring Al – a known problem for this method (Brown, Smith and Bruland, 2010). Conversely, for the Cal check std 2 (1ppb), all the elements – including Al – are within 3.5% of the certified value. It is expected that

the accuracy of the calibration would improve under the greater relative stability of the 1ppb standard.

***Table 3**-The accuracy of the ICP-MS calibration was evaluated using the "Cal check std 1/2". Cal check standard 1 was a 0.1ppb multi-element standard, Cal check std 2 was a 1ppb multi-element standard. Both standards have respective 10-times higher Fe and Zn concentrations. The value in red indicates an anomalous reading.*

ICP-MS Calibration Check Standards

	Cal check std 1		SU	Cal check std 2		SU
[µg/L]	Certified	SU CAF Analysed	%Accuracy	Certified	SU CAF Analysed	%Accuracy
Al	0,0960	0,2331	242,9	0,9670	0,9674	100,0
Mn	0,0960	0,0890	92,7	0,9670	0,9329	96,5
Fe	0,9600	0,9144	95,2	9,6700	9,7197	100,5
Co	0,0960	0,0987	102,8	0,9670	0,9515	98,4
Ni	0,0960	0,0905	94,3	0,9670	0,9621	99,5
Cu	0,0960	0,0963	100,4	0,9670	0,9653	99,8
Zn	0,9600	0,9694	101,0	9,6700	9,4304	97,5
Cd	0,0960	0,0924	96,2	0,9670	0,9485	98,1
Pb	0,0960	0,0958	99,8	0,9670	0,9875	102,1

4.1.3 Quality Control

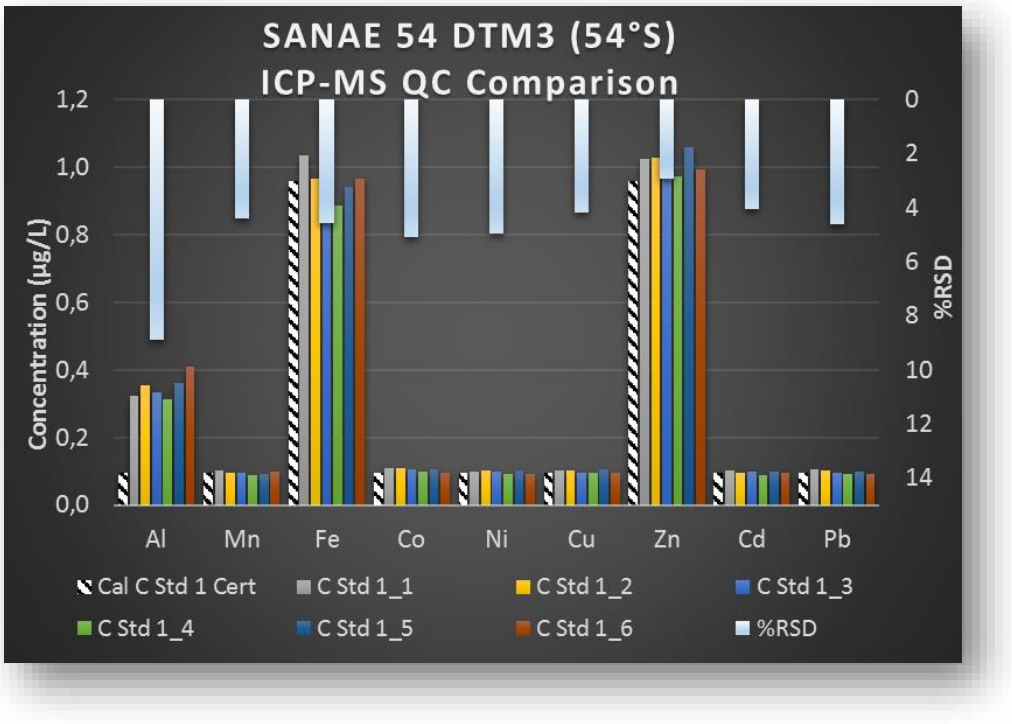

***Figure 6**-The results of a continuous quality control (QC) reference standard compared to the certified value (Cal C Std 1 Cert). The QC was used in the ICP-MS analysis of the Baseline station at 54°S, and employed to monitor drift and precision, ensuring accuracy for the duration of the run. On the secondary axis (light blue bars), the mean precision is plotted for the ICP-MS QC standard (n=6).*

The results of Quality Control (QC) standard (Check std 1) used to monitor the performance and drift of the machine during the analysis of the Baseline and Inter-calibration station are presented in Figure 6. Samples compare excellently with the certified value and demonstrate no obvious drift or decreased sensitivity. The %RSD was calculated at <4% for all the key elements – Al is higher due to method materials. This aligns admirably with the typical ICP-MS %RSD verified to be less than 5%.

4.2 Precision

4.2.1 TM4 – Pre-Acidification

The results of the Stellenbosch University (SU) TRACEx laboratory in-house TM4 Control are presented in table 4. The distribution of each trace elements data was determined with Al, Fe and Pb deemed to have significant skewness. Accordingly, the 95% CI for the trace elements were delineated as follows: Al = 3.55 ± 0.99 (nmol/kg); V = 30.55 ± 2.33 (nmol/kg); Mn = 0.19 ± 0.008 (nmol/kg); Fe = 0.13 ± 0.035 (nmol/kg); Co = 15.64 ± 0.73 (pmol/kg); Ni = 4.79 ± 0.14 (nmol/kg); Cu = 0.51 ± 0.019 (nmol/kg); Zn = 4.83 ± 0.17 (nmol/kg); Cd = 580.03 ± 17.32 (pmol/kg); Pb = 6.66 ± 0.53 (pmol/kg); and Mo = 16.68 ± 2.54 (nmol/kg).

Table 4*-The results of the Stellenbosch University (SU) statistical evaluation of the TM4 (pre-acidification) in-house control. The control was used to monitor the precision of the method and ensure quantitative recovery for the complete procedure. It was calibrated by simultaneously analysing it with the SAFe and NASS 5 reference materials. The precision is reported to the 95% Confidence Interval (CI). (a) denotes concentrations in nmol/kg, (b) denotes concentrations in pmol/kg. Note: this will not form the basis for proving precision.*

SU TM4 – Unacidified In-house Control								
	Mn[a]	**Fe[a]**	**Co[b]**	**Ni[a]**	**Cu[a]**	**Zn[a]**	**Cd[b]**	**Pb[b]**
Sample Population (n)	29	29	29	29	29	29	29	29
No. of Outliers	0	1	0	0	0	0	0	1
Mean (x̄)	0,19	0,13	15,64	4,78	0,51	4,83	580,03	6,65
Std Deviation	0,02	0,09	1,99	0,39	0,05	0,46	47,57	1,38
TM4 %RSD	11,13	67,30	12,70	8,20	10,23	9,49	8,20	20,67
TM4 4-hr Control	0.20	0.30	19.22	5.04	0.55	4.38	551.97	10.02
Skew	0,70	1,60	0,71	-0,22	-0,13	0,02	0,14	0,95
Std Error_Skew	0,45	0,46	0,45	0,45	0,45	0,45	0,45	0,46
Significant Skew (Y/N)	N	Y	N	N	N	N	N	Y
Margin of Error _Confidence (95%)	0,01	0,03	0,72	0,14	0,02	0,17	17,31	0,53
% Within one std dev	75,9	92,9	65,5	69,0	75,9	69,0	69,0	96,4
% Within two std dev	89,7	96,4	96,6	100,0	93,1	100,0	93,1	100,0

4.2.2 TM4A – Post Acidification

The results of the in-house TM4A Control are presented in the table 5 and Appendix A -Figure A1. Statistically the data for all the trace elements barring Cu demonstrated normal distribution – insignificant skewness (Table 5). Accordingly, the 95% CI for the trace elements were delineated as follows: Mn = 0.26 ± 0.003 (nmol/kg); Fe = 0.29 ± 0.009 (nmol/kg); Co = 19.64 ± 0.66 (pmol/kg); Ni =

5.91 ± 0.053 (nmol/kg); Cu = 1.63 ± 0.017 (nmol/kg); Zn = 5.79 ± 0.063 (nmol/kg); Cd = 637.78 ± 5.84 (pmol/kg); Pb = 6.62 ± 0.076 (pmol/kg). It is evident that the margin of error has improved for all the elements post acidification of the in-house control. Although concentrations increased across the elemental suite post acidification, Fe and Cu confirmed their affinity for organics by displaying marked increases. Conversely, Pb concentrations did not increase and pre-acidification levels persisted.

***Table 5**-The results of the Stellenbosch University (SU) statistical evaluation of the TM4A (post-acidification) in-house control. The control was used to monitor the precision of the method and ensure quantitative recovery for the complete procedure. It was calibrated by simultaneously analysing it with the SAFe and NASS 5 reference materials. The precision is reported to the 95% Confidence Interval (CI). (a) denotes concentrations in nmol/kg, (b) denotes concentrations in pmol/kg. This will form the basis of discussions in favour of high precision.*

SU TM4A – Acidified In-house Control								
	Mn[a]	**Fe[a]**	**Co[b]**	**Ni[a]**	**Cu[a]**	**Zn[a]**	**Cd[b]**	**Pb[b]**
Sample Population (n)	51	51	51	51	51	51	51	51
No. Outliers	2	1	0	2	1	1	1	2
Mean ($\bar{x}$)	0,26	0,29	19,64	5,91	1,63	5,79	637,78	6,62
Std Deviation	0,01	0,03	2,42	0,19	0,06	0,22	21,10	0,27
TM4A %RSD	4,17	11,18	12,32	3,18	3,81	3,82	3,31	4,09
Skew	0,39	0,14	0,34	0,56	0,42	0,74	0,61	0,08
Std Error_Skew	0,35	0,35	0,34	0,35	0,35	0,35	0,35	0,35
Significant Skew (Y/N)	N	N	N	N	N	Y	N	N
Margin or Error_Confidence (95%)	0,00	0,01	0,66	0,05	0,02	0,06	5,85	0,08
% Within one std dev	85,7	74,0	66,7	81,6	74,0	80,0	72,0	85,7
% Within two std dev	95,9	98,0	100,0	98,0	98,0	98,0	96,0	100,0

4.2.3 Field Precision and the Batch Effect

To quantify the repeatability error, the "run effect" was calculated as a mean of the precision for each batch (Figure 7). The results indicate that the precision within each batch was notably better than the analytical precision – marked improvements for Co (12.32 to 4.5 %RSD) and Fe (11.18 to 7.43 %RSD). Field precision showed similar improvement relative to analytical precision for the collective suite – barring Fe (12.21 %RSD). However, Fe is notably skewed by erroneous outliers as demonstrated by a median precision value of 4.46 %RSD –. The remaining metals in the suite largely demonstrate ≤1% variability between batches, boding well for quantitative recovery. This extract perhaps provides interesting details regarding the method – an idea elaborated upon in the discussion.

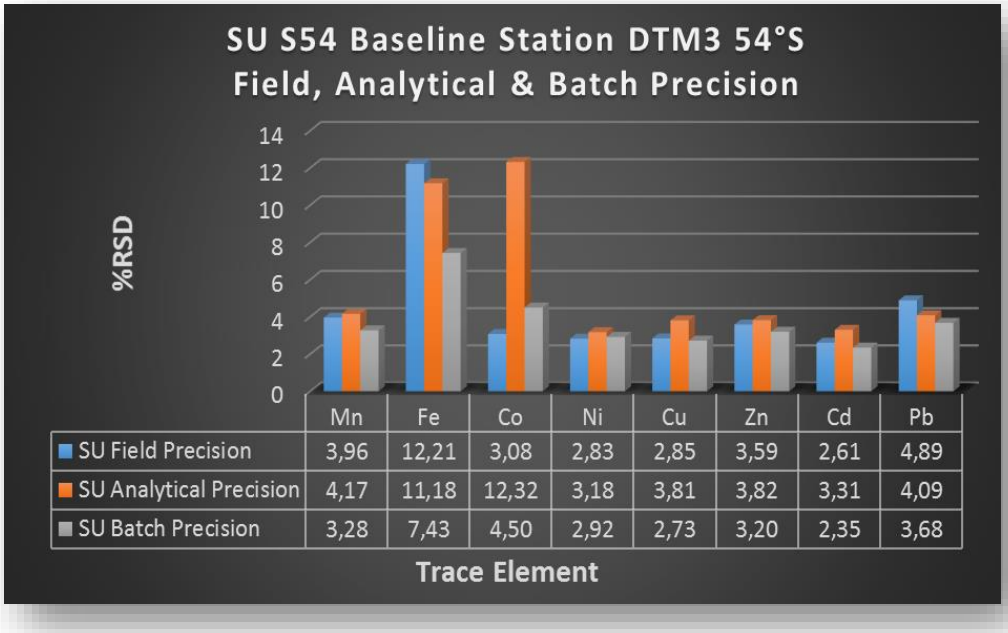

***Figure 7**-A comparison of the different means used to quantify precision presented as percentage relative standard deviation (%RSD). The Analytical and Field precision are cruicial elements for validation stipulated in the GEOTRACES Cookbook. The Field precision is a mean of the %RSD for all the depths at the Baseline station. The mean Batch precision was used to demonstrate the influence iterative ICP-MS calibrations had on the precision of certain elemements – notably Fe and Co.*

4.3 Resin Column Performance

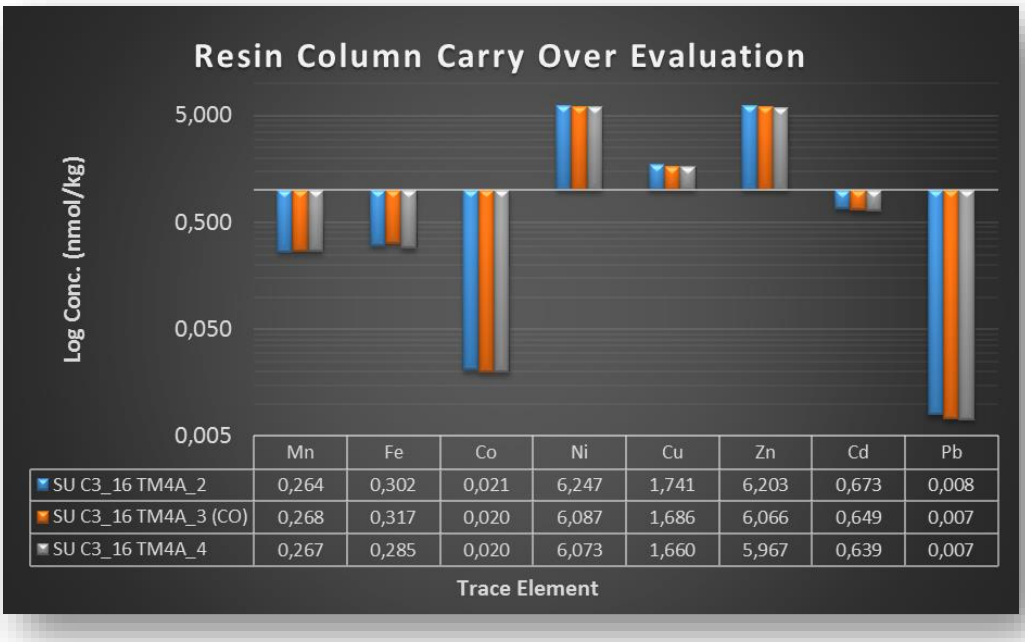

***Figure 8**-Log graph illustrating the results of a stress test evaluating the risk of trace metal carry over (CO) on the high affinity resin column used in pre-concentration. NASS 5 aliquots were pre-concentrated successively prior to the TM4A_3 CO sample. No CO was detectable even under the higher concentrations of the NASS 5 sample. The resin also demonstrated quantitative recovery under high concentrations of several trace elements by returning accurate NASS 5 results. (SU) denotes Stellenbosch University.*

The results of a rudimentary experiment quantifying the risk of trace metal carry over (CO) can be seen in figure 8. Control sample TM4A_3 (CO) – pre-concentrated directly after two NASS 5 standards – is well within the expected concentrations for all the elements with marginally higher Fe (< 8% RSD) measured. However, given the variability of Fe we would need to run this test several more times for a statistically valid carry over result. Nonetheless, several key elements are within 2%RSD suggesting excellent resin column performance over a wide range. Further, the stress of relatively high trace metal concentrations on the resin bed does not appear to decrease the sensitivity or affinity of the column.

4.4 Accuracy – Reference Materials

4.4.1 SAFe Standard (D2)

The SU analytical results for the SAFe standards D2 (1000m), alongside the achieved accuracy, can be viewed in the table 6. The results were used to quantify the potential of the analytical method for measuring "true" concentrations. Statistical calculations were performed on 5 replicates of the sample with excellent precision (<10%RSD) for all the trace elements barring Al. The results of the trace elements (nmol/kg) at the 95% CI are as follows: Al = 1.74 ± 0.28; Mn = 0.4 ± 0.03; Fe = 0.96 ± 0.02; Co = 0.03 ± 0.00; Ni = 8.05 ± 0.10; Cu = 2.04 ± 0.03; Zn = 7.23 ± 0.22; Cd = 0.96 ± 0.05; Pb = 0.03 ± 0.00 (± terms signify 95% CI). As expected, due the materials in the method Al has the worst %RSD; however, it was not deemed a criteria element (Brown, Smith and Bruland, 2010). The %RSD for Mn is near the bounding limits of the method at 9.46%.

***Table 6**-The results of the SAFe (D2) standard evaluating the accuracy of the method, alongside the available consensus values as of May 2013 (www.geotraces.org). Values are given in nmol/kg. A density of 1.025kg/L was used in conversions. SU denotes Stellenbosch University and represents the samples analysed in this project. Al must be disregarded given the materials used in analysis.*

SAFe D2								
(n=5) nmol/kg]	**SAFe_D2 Consensus**	**Std Dev**	**%RSD**	**SAFe_D2 SU**	**Std Dev**	**%RSD**	**SU %Accuracy**	**SU %Error (Accuracy)**
Al	1,03	0,09	8,74	1,74	0,32	18,4	**168,6**	**68,6**
Mn	0,35	0,05	14,29	0,4	0,039	9,68	**114,3**	**14,3**
Fe	0,933	0,023	2,47	0,96	0,025	2,65	**103**	**3**
Co	0,0457	0,0029	6,35	0,03	0,0004	1,35	**71,6**	**-28,4**
Ni	8,63	0,25	2,9	8,05	0,11	1,4	**93,3**	**-6,7**
Cu	2,28	0,15	6,58	2,04	0,03	1,6	**89,5**	**-10,5**
Zn	7,43	0,25	3,36	7,23	0,25	3,39	**97,3**	**-2,7**
Cd	0,986	0,023	2,33	0,96	0,06	6,25	**96,9**	**-3,1**
Pb	0,0277	0,0015	5,42	0,03	0,0012	4,18	**102,8**	**2,8**

4.4.2 GEOTRACES Standards (GSC and GSP)

The results of the Stellenbosch University (SU) quantification of the GEOTRACES GSP and GSC standards are presented in table 7, 8 – a single standard deviation has been reported based on a sample population of n=5. This study reports the following concentration (nmol/kg) yields for the GSP standard: Mn = 0.69 ± 0.07; Fe = 0.38 ± 0.02; Co = 0.01 ± 0.00; Ni = 2.37 ± 0.11; Cu = 0.56 ± 0.02; Zn = 0.16 ± 0.05; Cd = 0.005 ± 0.01; Pb = 0.06 ± 0.00 (± terms signify 95% CI) (Table 7). The %RSD for each trace element in the standard are well within or acceptably near the limit of the objective criteria for the method. However, Zn and Cd are on the lower limit of their anticipated concentrations and thereby the precision may reasonably be slightly exaggerated.

Table 7*-The results of the GEOTRACES GSP standard as analysed in this study. Several elements demonstrate excellent precision, while some leave room for improvement. It should be notes that those elements demonstrating poorer precision are typically skewed by one of two values of n=5. With limited sample volumes is was impossible to analyse more of the standard to gain improved statistical results. The margin of error reports the 95% Confidence Interval (CI).*

GEOTRACES GSP								
(n=5) [nmol/kg]	**Mn**	**Fe**	**Co**	**Ni**	**Cu**	**Zn**	**Cd**	**Pb**
SU GSP_Mean ($\bar{x}$)	0,69	0,38	0,01	2,37	0,56	0,16	0,005	0,06
Std Dev	0,074	0,028	0,001	0,121	0,020	0,054	0,001	0,003
%RSD	10,71	7,31	11,90	5,11	3,63	34,25	27,22	4,25
Margin of Error Confidence (95%)	0,065	0,024	0,001	0,106	0,018	0,047	0,001	0,002

The results of the GSC standard (Table 8) where n=5, describe concentrations (nmol/kg) for the trace elements as follows: Mn = 1.96 ± 0.18; Fe = 1.51 ± 0.08; Co = 0.08 ± 0.004; Ni = 3.91 ± 0.16; Cu = 1.14 ± 0.04; Zn = 1.41 ± 0.1; Cd = 0.35 ± 0.02; Pb = 0.04 ± 0.002 (± terms signify 95% CI). The %RSD for the inter-calibration standard's trace elements are excellent with only Mn near the 10% method criteria limit. This also substantiates the precision and reproducibility of the method.

Table 8*-The results of the GEOTRACES GSC standard for which no consensus values are available. The precision was very high with all the elements, barring Mn, below the 10%RSD requirement. Limited volumes were available hence the limited analysis of the standard (n=5). The margin of error reports the 95% Confidence Interval (CI). Recently published data is available for comparison* (Hawco *et al.*, 2016).

GEOTRACES GSC								
(n=5) [nmol/kg]	**Mn**	**Fe**	**Co**	**Ni**	**Cu**	**Zn**	**Cd**	**Pb**
SU GSC_Mean ($\bar{x}$)	1,96	1,51	0,08	3,91	1,14	1,41	0,35	0,04
Std Dev	0,20	0,09	0,005	0,18	0,05	0,11	0,02	0,002
%RSD	10,19	6,17	5,56	4,60	4,36	7,83	6,93	5,33
Margin of Error Confidence (95%)	0,175	0,081	0,004	0,158	0,043	0,096	0,021	0,002

4.4.3 NASS 5 Standard

The results of the commercially available NASS 5 certified standard can be viewed in table 9. Statistical calculations are based on a sample population of n=5 and concentrations (nmol/kg) present as follows: Al = 2.92 ± 0.05; Mn = 15.49 ± 0.83; Fe = 3.70 ± 0.13; Co = 0.18 ± 0.009; Ni = 3.77 ± 0.28; Cu = 4.4 ± 0.23; Zn = 1.63 ± 0.04; Cd = 0.18 ± 0.01; Pb = 0.03 ± 0.00 (± terms signify one Std Dev). The precision for the NASS 5 was excellent with all trace elements comfortably below the 10% RSD performance criteria.

***Table 9**-The SU NASS 5 (CRM) data in comparison to the certified values calculated at the 95% Confidence Interval. The accuracy is given as a percentage error.*

NASS 5							
[nmol/kg]	**NASS 5 Certified**	**Std Dev**	**%RSD**	**NASS 5 SU**	**Std Dev**	**%RSD**	**SU % Error (Accuracy)**
Mn	16,32	1,01	6,20	15,49	0,82	5,32	-5,08
Fe	3,62	0,61	16,91	3,70	0,13	3,45	2,39
Co	0,18	0,05	27,27	0,18	0,01	4,86	0,02
Ni	4,21	0,47	11,07	3,77	0,28	7,37	-10,47
Cu	4,56	0,71	15,49	4,40	0,23	5,18	-3,57
Zn	1,52	0,58	38,24	1,63	0,04	2,57	7,20
Cd	0,20	0,03	13,04	0,18	0,01	5,22	-9,52
Pb	0,04	0,02	62,50	0,03	0,00	4,49	-12,01

4.5 Baseline Station and Inter-calibration

Note: Comparisons and calculations have been drawn for corresponding depths only. Plymouth Marine Laboratory (PML) only provided Fe data (FIA) and not a full trace metal range.

***Table 10**-Dissolved iron (DFe) concentrations for the Baseline station within the AAZ (54°S) as quantified by: Inter-calibration partners Plymouth Marine Laboratory (PML) using Flow Injection Analysis (FIA) technique; Stellenbosch University (SU) using an ICP-MS technique and* Klunder et al. 2011 *using FIA. The Mixed Layer Depth (MLD) was calculated at 100m for this locale using a 0.03 kg/m density criterion. The PML and* Klunder et al. 2011 *data was converted to nmol/kg using an average density = 1.025 kg/L. PML Std Dev is based on single bottle duplicated analysis, SU Std Dev on duplicate bottle analysis. (a) denotes depth in m, (b) concentrations in nmol/kg, (*) that the value is an average, values in blue report no Std Dev, and values in red highlight anomalous disagreement.*

Plymouth Marine Laboratory (PML)				*Stellenbosch University (SU)*					*Klunder et al.2011 54°S*		
GO-FLO#	**Depth [a]**	**DFe[b]**	**Std Dev[b]**	**GO-FLO#**	**Depth [a]**	**DFe[b]**	**Std Dev[b]**	**%Error vs PML**	**Depth [a]**	**DFe[a]**	**Std Dev[b]**
				24	15	0,24	0,02		8	0,51	0
23	23	0,08	0	**23**	23	0,12	0,01	37,42	25	0,14	0
22	50	0,19	0,03	**22**	50	0,18		-0,57	51	0,25	0
21	75	0,29	0	**21**	75	0,22		-33,39	76	0,26	0,01
19	101	0,09	0,01	**19**	101	0,21	0,04	58,98	101	0,25	0,01
18	151	0,23	0,02	**18**	151	0,27	0,05	13,4	152		0,01
17	250	0,37	0,01	**17**	250	0,41	0,04	9,5	251	0,31	0,01
				16	298	1,22	0		301	0,35	0,01
									301	0,3	0,01
				15	350	1,82	0,02		350	0,46	0,01
14	398	1,02	0,03	**14**	398	0,92	0,01	-11,47	401	0,37	0,02
13	450	0,32	0,01	**13**	450	0,44	0,06	27,07	450	0,39	0,01
				12	500	0,45			500	0,51	0,02
				11	549	0,94	0,01		552	0,43	0,01
10	599	0,37	0	**10**	599	0,45	0,05	17,65	600	0,38	0
9	650	0,46	0,01	**9**	650	0,51	0,03	10,8	649	0,52	0,01
8	749	0,47	0	**8**	749	0,46	0	-1,1	750	0,35	0,01
7	1000	0,33	0,02	**7**	1000	0,39	0	15,8	999	0,66	0
6	1250	0,36	0,01	**6**	1250	0,43	0,01	16,51	1249	0,38	0
5	1502	0,43	0	**5**	1502	0,49	0,08	13,17	1499	1,17	0
				4	1749	0,48	0,01		1749	2,16	0
				3	2001	0,57	0,01		2000	1,51	0
2	2249	0,61	0	**2**	2249	0,56	0,02	-9,43	2248	1,59	0,01
1	2400	0,51	0	**1**	2400	0,59	0,01	13,7	2398	1,87	0,02
Surface (MLD)*		0,16	0,087			0,186	0,038	13,28		0,23	0,052
Sub-surface (500m)*		0,32	0,282			0,348	0,239	6,75		0,3	0,094
Deep (>500m)*		0,44	0,086			0,537	0,061	17,61		0,73	0,485

4.5.1 Plymouth Marine Laboratory DTM3 (54S)

The results of the crossover station at 54°S, as analysed by the collaborators at Plymouth Marine Laboratory (PML), are presented in table 10. The concentration of DFe in the water column ranged from a minimum of 0.08 ± 0.00 nmol/kg in the surface to a maximum of 1.02 ± 0.03 nmol/kg – due to

an 'unusual' but not unexpected (see discussion) spike in the concentration. The average surface (100m) concentration was 0.16 ± 0.09 nmol/kg increasing to 0.32 ± 0.28 nmol/kg in the sub-surface waters. Concentrations continue to incrementally increase at depths greater than 500m recording a mean of 0.44 ± 0.09 nmol/kg. The profile (Figure 12) exhibits the nutrient like shape with biological utilization in the surface (MLD), re-mineralization around the MLD and subsequent conservative behaviour – mimicking the trend reported by Klunder et al. (2011) for Fe in the Southern Ocean.

4.5.2 *Stellenbosch University Laboratory DTM3 (54S)*

The SU inter-calibration results are presented in table 10. Greater sample resolution allowed a more complete profile where DFe concentration ranged from a minimum of 0.12 ± 0.01 nmol/kg in the surface to a maximum of 1.82 ± 0.02 nmol/kg (Figure 12). A general increasing with depth trend is observed with a sharp spike observed 300-400m. The average concentrations for the corresponding depths are as follows: 0.19 ± 0.04 nmol/kg in the surface (100m); 0.35 ± 0.24 nmol/kg in the sub-surface waters (<500m) and increasing to 0.54 ± 0.06 nmol/kg at depths greater than 500m. The percentage error (Table 10) was calculated using the PML analytical data as the 'true' measurement. There is a general trend for the SU laboratory to overestimate the DFe concentration. However, the 'accuracy' improves somewhat when plotting the %Error for the concentration average in the surface (MLD), sub-surface (<500m) and depth (>500m) with percentage errors of 13.28, 6.75 and 17.61 respectively.

The SU and PML concentrations in table 10 were compared to the concentrations as measured by Klunder et al. 2011 in the same region – 54°S crossover station. The data corroborates a nutrient like profile (Figure 14) for Fe in the Southern Ocean and will form the basis of the crossover comparative effort in the discussion.

5. Discussion

5.1 ICP-MS Performance

The broad multi-point instrument calibration ensured useful detection across the entire range of anticipated analyte concentrations. The pre-concentration step was required to circumvent the likelihood that certain trace metals are characterised by concentrations below the detection limit of the machines. Simultaneously, the menacing interference frequently associated with the precipitation of seawater matrix elements on the instrument cones was successfully removed by the seaFAST module. This ensured consistent ion-transmission, and thereby sensitivity and recovery.

5.1.1 Calibration Accuracy and Detection Limits

Testing the accuracy of the calibration was a crucial step in eliminating a variable potentially attributed to this step. The calibration data substantiates a working range conforming to the requirements outlined in the GEOTRACES compendia. Further, the concentration range of the calibration analyte ensured that the machine maintained a suitable concentration interval for the projected field sample lower and upper limit, whilst maintaining the precision, accuracy and linearity. The linearity of the element calibration curve remained within the following parameters: $r > 0.999$, y-intercept within 0-5% of target concentration and the RSD of the calibration curve < 1.5-2%. The results of the Check Standards analysed during the analysis of the Baseline and Inter-calibration station provide unequivocal evidence for accurate calibration and quantification at the respective (0.1ppb and 1ppb) concentrations of the standards (Table 3). Granting the calibration for the Baseline and Inter-calibration station proved acceptable, there does appear to be variation in the calibration between batches as demonstrated by the DL (Figure 10) – a subject discussed in detail in the precision evaluation.

The analysis of pre-concentration omitted Milli-Q water in acid cleaned Falcon Tubes typically found trace element concentrations below the detection limit. Further, the detection limit for the elements Cd and Cu, may well vary slightly contingent to the isobaric – different elements whose isotopes share a common mass – interference stemming from MoO^+ and $ArNa^+/ArMg^+$ respectively (Wu and Boyle, 1997). The interfering mass can be corrected for by applying the isotope abundance ratio of the measured isotope and interfering isotope (Wu and Boyle, 1997). The relatively 'high' detection limit of Fe (25.72 ng/kg, Table 2) is a recognized feature of ICP-MS Fe analysis (Mclaren *et al.*, 1985). Batterham et al. (1997) attribute this to high background isobaric interference on ^{54}Fe and ^{57}Fe stemming from ArN and ArOH respectively. Further, they state that the fluctuations may become significant at low ppt levels of Fe, thereby affecting the precision. While Zn also demonstrates

relatively high detection limits (14.89 ng/kg), the remaining trace metals are greatly improved when compared to similar methods (Mclaren *et al.*, 1985; Batterham, Munksgaard and Parry, 1997). The average concentration of the trace metals (Table 2) at the Baseline station (54°S; DTM3) suggest that our detection limits are below the sample concentrations even when disregarding the pre-concentration.

5.1.2 Quality Control and Blanks

The QC data suggests that potential reductions in sensitivity and selectivity, due to matrix influence, were minimal and drift was readily corrected using the Agilent MASS HUNTER software (Figure 6). The 6-12 sample Blank (2% Nitric Acid) – not that used in calibration – was occasionally exposed to monitor potential atmospheric contributions for the duration of the run in the CAF ICP-MS lab. This provided crucial insights into potential contamination sources and where improvements should be made. The Blank was found to incrementally, yet somewhat randomly, gain notable amounts of atmospheric Fe and Zn, at an estimated rate of <0.33 µg/L.min and <0.125 µg/L.min respectively for the 6-sample monitoring interlude (12 minutes). This reaffirms the suspicion that contamination may be introduced at this juncture if samples were left exposed to atmospheric conditions. Consequently, samples on the ICP-MS auto-sampler were only opened at most 3 concurrently and not at all during the iterative QC and Blank analysis. It must be noted that this was retrospective upon investigation of the initial batches (DTM1 &2) whereby occasionally 5 samples were opened concurrently. The impact this phenomenon will have on sample precision is expected to be minimal bearing in mind that duplicate samples are analysed in quick succession. Nonetheless, contributions to samples may logically contribute to the %RSD and thereby randomly impact the Fe and Zn data. Ultimately, the consistency of the analytical QC and blanks inserted in parallel with the samples on ICP-MS, proved their practicality as drift and performance monitors.

5.2 Multi-Element Trace Metal Quantification

The comparison of the method used in this study with several of the methods utilizing chelating resins, in the extraction/pre-concentration of trace metals, substantiates its use herein. Similar methods (Sohrin *et al.*, 2008; Biller and Bruland, 2012) have been acknowledged as the preferred way to analyse for multiple trace metals simultaneously in seawater due to the low blanks, excellent precision and good accuracy. A major advantage of the off-line pre-concentration method utilizing the sea*FAST* module was the low sample volume (<14ml per sample) required. It could be argued that a disadvantage of the off-line pre-concentration technique was the time taken to prepare and preconcentrate samples for the analysis by ICP-MS (±24 hrs per 50 samples). An integral chunk of the

discussion that follows will be identifying and reducing the amount of uncertainty through the evaluation of the attained precision and accuracy of the method. The stipulated performance criteria demanded that the method maintain a coefficient of variation (%RSD) <10% working at the 95% Confidence Interval; all indications suggest this to be true – lest stated else. The statistical analysis further substantiates the degree of closeness of the data whereby it was found that 67-86% and 96-100% of samples are within one and two standard deviations respectively – typical for a normal distribution working at the 95% Confidence Interval (Table 5).

The rudimentary carry over (CO) experiment evaluated the prospect of residual trace elements being introduced into the subsequent sample – affecting accuracy and precision (Figure **8**). The Control TM4A_3 (CO) sample, run directly after the NASS 5 standard on the pre-concentration module, exhibited no indication that resin column CO may affect the data. The trace elements on the CO test sample were within 1% RSD of the normal control concentrations – barring increased Pb (4%) and Fe (8%). However, the values for Fe may be attributed to the normal analytical deviation of this method (%RSD ≤ 11%). Moreover, the subsequent TM4A_4 sample suggests that Fe has returned to below the Fe value prior to NASS 5 stress analysis. This suggests that if carry over does occur, it is marginal (≤ 8 %RSD, Fe) even under high concentrations.

While several resins have similar selective adsorption behaviour, those not commercially available introduce the potential for discrepancies in the recovery of trace metals through variations in batch consistency. Further, selectivity and affinity are largely dependent on the ionic strength of the resin – a pH dependant function. Though convenient, the amino-carboxylic acid-type chelate resins are problematic when associated with alkaline earth elements such as Mg and Ca; the adsorption of which, even under weakly acidic conditions, causes interference (Kagaya et al. 2009). It is possible to overcome this disadvantage by adjusting the pH, using a washing solution after the adsorption of elements. Wang et al. (2014) experimented with Ca-Mg interference on ICP-MS using an automated high pressure ion chromatography (IC) pre-treatment employing an IDA-type resin (Dionex Metpac CC-1). They found that trace metal concentrations decreased by 80% at high (4mM) Ca-Mg concentrations. Interestingly, they found minor enhancements within 0.05 mM Ca-Mg – attributed the formation of Ca- and Mg- based aerosols facilitating the transmission of trace metals to the plasma.

The simultaneous extraction of up to 10 trace metals proved a major advantage over the NTA-Type resin used by Lee et al. (2011) which requires individual measurements. Kagaya et al. (2009) prepared a new chelate resin immobilizing carboxymethylated pentaethylenehexamine (CM-PEHA) with admirable results. The Toyopearl Chelate-650 (Tosoh Biosciences) IDA used by Milne et al. (2010) was

found to be inadequate in the quantitative recovery of Mn. Further the method does not require isotope dilution to account for non-quantitative recoveries; a crucial advantage in the quantitative analysis of Co and Mn as they lack the stable isotopes needed for isotope dilution. Conversely, the idea of accurately quantifying total trace metals concentration based on the recovery of an added ionic metal spike is often ignorant of the behaviour of metals in the non-labile form (Batley and Florence, 1976). The Nobias-Chelate-PA1 resin has proved notable in its ability to remove large amounts of alkaline earth elements at pH below 7 with an optimal trace metal recovery range of pH 6.00 ± 0.05 and salinities ranging from 0 to 35 ‰ (Sohrin *et al.*, 2008; Wang, Lee and Ho, 2014; Minami *et al.*, 2015). Concurrently, a pH of 6.00 ± 0.2 was used in this study to limit the recovery of Mo ensuring minimal Cd mass interference of MoO^{+} on ICP-MS (Biller and Bruland, 2012). The same chelator was found to decrease Al retention capability below a pH of 6; reported by Minami et al. (2015) who tested the pH dependant recovery of the resin for several key elements. Moreover, in a field application test their study found that Fe was inclined to exhibit a higher %RSD (7.4%) in relation to the other trace metals – < 4% for Mn, Ni, Cu, Zn, and Cd.

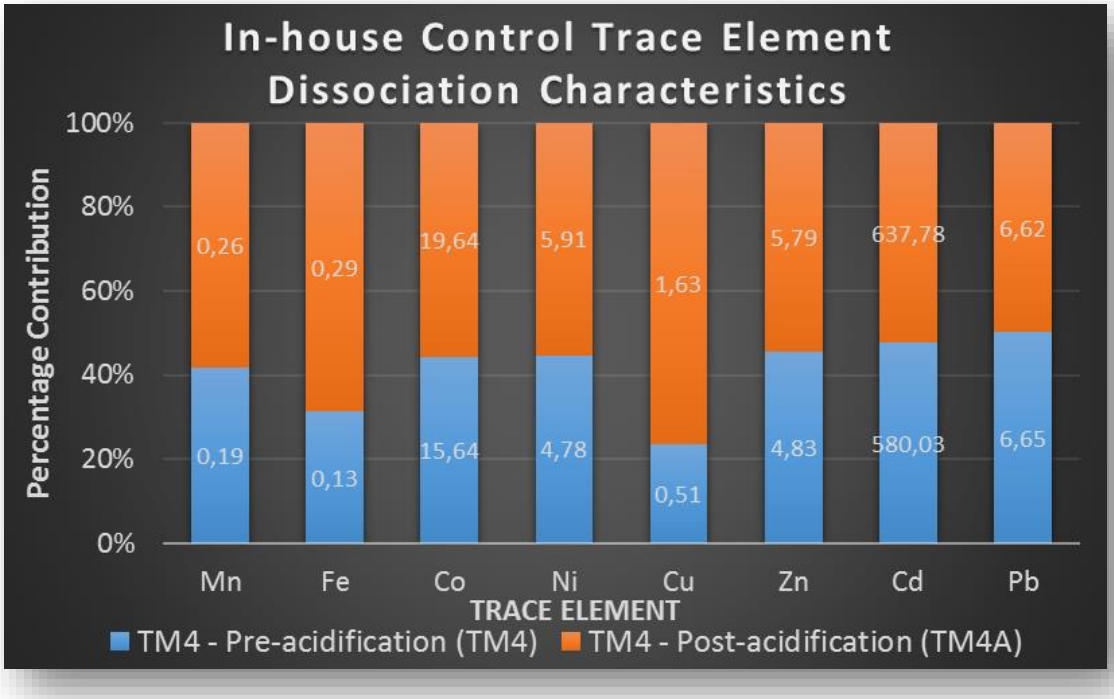

***Figure 9**-Dissociation characteristics of the TM4 in-house control sample illustrating the importance of acidification in the analysis of the total dissolved fraction. Note the increases in Fe and Cu – a consequence of their ligand associations.*

The method evolution and optimisation, involving the experimentation with an un-acidified and subsequent acidified control, enabled important insights regarding the tendency of certain trace metals – Fe, Cu and Co – to demonstrate chelation with the natural organic ligand pool. The complexation may render these elements blind to the resin used in pre-concentration and

subsequently result in an underestimation of the 'true' concentration. The results herein – substantiated by literature (Milne *et al.*, 2010; Biller and Bruland, 2012) – indicate that Fe and Cu are readily solubilised by acidification with the results signifying 118% and 222% respective improvements in recovery post acidification (Figure 10).

Typically trace metals associated with binding complexes are labile enough to allow extraction by the resin – given acidification (pH 1.7). However, certain trace metals, such as Co and Cu, may be associated with colloidal matter or organo-metallic complexes that are stronger binding agents than the even acidification is able to solubilise (Milne *et al.*, 2010). As if to demonstrate the strength of the binding agents, Co, exhibited a comparatively minor increase (25.5%) in concentration post acidification of the in-house control (Figure 10). Typically, a UV Oxidation step is required to effectively dissociate Co and Cu from their complexes'. The underestimation of Co and Cu in the analysis of the SAFe (D2) standard (Table 6), can largely be explained by differences in the analytical accuracy when UV-Oxidation is omitted. In the UV oxidation of SAFe deep-water (D2), Milne et al. (2010) found the concentration of Co increased by approximately 50% after 1 hr. There was a lack of response by some organically bound trace metals (Fe, Mn, Ni, Cd and Zn) to oxidation which is as a result of the resin being a stronger competitor for binding the metal, as opposed to the natural ligand pool, and/or kinetics favoured the labile fraction (Biller and Bruland, 2012). Biller & Bruland (2012) found that complete metal recovery required only 1 hr of UV-oxidation; which resulted in an approximately 33% increase in the dissolved Co concentration. Milne et al. (2010) also subjected the SAFe surface water sample (S1) to the process; their results indicated no significant change. It is possible that this is a consequence of the inherent metal concentration in the surface waters was sufficiently low that the detection limit was reached. Nonetheless, there is a need to UV-oxidise the samples further for 'true' quantitative recovery of Co and Cu. It is imperative that during this operation no contamination be introduced and/or no transformations of chemical species, aside from the expected release of metals from organic species (Batley and Florence, 1976; Moffett and Ho, 1996; Biller and Bruland, 2012). It follows that the lack of UV oxidation in this study may result in an approximately 20-30% underestimation of the concentration of Co and Cu in regions where complexation is prominent (Saito and Moffett, 2001; Milne *et al.*, 2010; Biller and Bruland, 2012).

5.2.1 Precision

Statistical analysis (n=29) of the results suggest that the TM4 (pre-acidification) and TM4A (post acidification) Control samples demonstrate mediocre and excellent respective precision in the simultaneous quantification of up to 8 trace elements (Table 4, 5). However, the TM4 Control samples showed insufficient consistency and were awkwardly straddling the required precision limit for several

trace elements (Table 4). The results of Fe (67%RSD) and Pb (20%RSD) presented notably poorly. However, random infrequent spikes in concentration notably influenced the standard deviation skew rather the results. These spikes indicate that although the sea*FAST* pico module was set up in a class 10 (ISO 5) clean lab, there is a risk that the contamination observed in several samples was introduced at this juncture; or more likely, in the CAF ICP-MS laboratory as proven by the continuous blank results. Nonetheless, there are only a handful of outliers (>3*Std Dev) across the 11 trace elements and this is verified by the percentage of samples within one and two standard deviations (Appendix A-Table A1). A Reference TM4 4hr Control used to assess the sensitivity of a sample to contamination and artificial concentration by evaporation, presented negligible, by way of inconsistent changes in concentration (Table 4). However, there was the potential for minor contamination of Fe and Pb after 4 hours of exposure in the ultra-clean laboratory without the sea*FAST* hood in place. The test monitored the extreme end of the spectrum and samples are typically only exposed for a maximum of 2 hours whilst the falcon tubes remain un-capped in the class 100 clean lab. Furthermore, the batch precision data suggests that the modification to the sea*FAST* module – installation of a "hood" manufactured from Perspex – successfully eradicated the potential for truly random erroneous values stemming from atmospheric contaminants.

Comparatively statistical analysis (n=51) of the TM4A Control demonstrated excellent analytical precision in the simultaneous quantification of up to 8 trace elements – minor exceptions for Fe (11.18 %RSD) and Co (12.32 %RSD) (Table 5). Cu was the only element found to have a significant skew with normal distribution dominating the suite of trace elements (Table 5). Investigation into the source of the precision errors for Fe and Co suggested two possible origins: firstly, inconsistent recovery of the elements on the EDTRiA resin, and secondly, the elements are sensitive to minute variations in the ICP-MS calibration. The possibility of inconsistent recovery was readily acquitted by evaluating the excellent batch precision for the elements – <4.5 %RSD excepting Fe at 7.43 %RSD. Moreover, SU SOSCEX III DTM3 (Appendix A) was pre-concentrated in two separate batches over two days but analysed as part of the same calibration. The results are a 2.1%RSD mean for the batch, and 4.42% and 1.89% for Fe and Co respectively; attesting to the robustness of the sea*FAST* module. This does not suggest that no variability is occurring during the pre-concentration since an error persists. The calibration error was evaluated by studying the data in Appendix A, displaying TM4A Control samples that were pre-concentrated in the same batch – SU S54 TM1. Although detection limits (Figure 10) for Fe were generally consistent there were instances where variability was high (6.06-42.1 ng/L). This may, to a certain degree, explain the %RSD associated with Fe in the repeat analysis of the in-house control. Moreover, samples S54 TM1 TM4A_5/6 were analysed after the ICP-MS was recalibrated due to an error in analysis. The trace elements Mn, Ni, Cu, Zn, Cd and Pb remain within 7% RSD for the

station. However, Fe and Co are 20% and 30% higher than their respective results on the previous calibration – the greatest variation seen. This suggests that a large portion of the Analytical precision error can be attributed to the variations in ICP-MS calibrations.

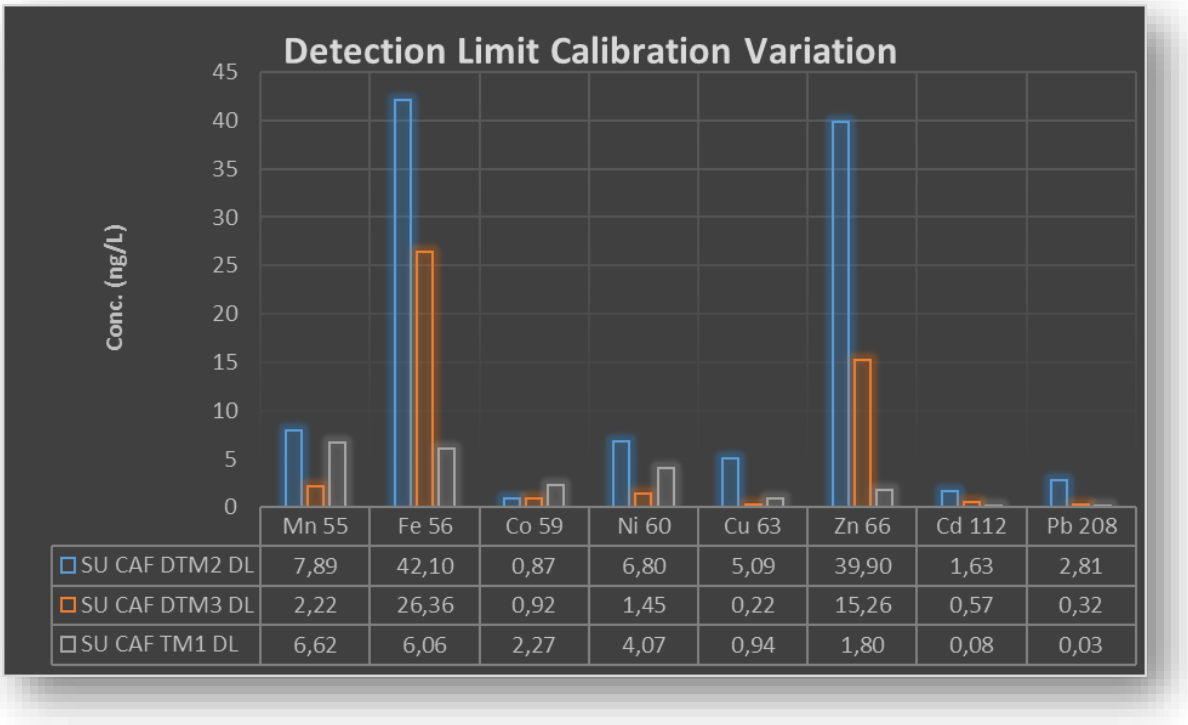

	Mn 55	Fe 56	Co 59	Ni 60	Cu 63	Zn 66	Cd 112	Pb 208
SU CAF DTM2 DL	7,89	42,10	0,87	6,80	5,09	39,90	1,63	2,81
SU CAF DTM3 DL	2,22	26,36	0,92	1,45	0,22	15,26	0,57	0,32
SU CAF TM1 DL	6,62	6,06	2,27	4,07	0,94	1,80	0,08	0,03

***Figure 10**-The ICP-MS Detection Limits (DL) of three different analysis. Small variations in calibration accuracy may be causing variation in the detection limits, which in turn contributes towards a larger precision error (%RSD).*

The results of the Field sample precision calculated for the Baseline and Inter-calibration station, further substantiate the proficiency of the method in the simultaneous quantification of trace elements (Figure 7). The precision was calculated based on a mean the respective %RSD for each duplicated sample depth. The data corroborates the hypothesis that a large portion of the historical data %RSD for Co is a result of the elements sensitivity to the quality of the calibration on ICP-MS. A variance of 9.24% was determined for the Co field error vs analytical error – 3.08 %RSD and 12.32 %RSD respectively. This calibration error, must be considered a systemic error potentially affecting the accuracy of the analytical quantification – a bias impacting positively or negatively on the result. Nonetheless, the mean Batch precision (4.5 %RSD) suggests that the elimination of the Fe and Co calibration error, would result in excellent precision for the method (<4.5 RSD) for all the elements barring Fe (<7.4 %RSD).

However, entertaining the idea that Co errors are higher in the historical data because of calibration error, it is apparent that the Fe error would not be wholly resolved by eliminating the calibration error. The precision for Fe between the Field and Analytical samples does not exhibit a

large variance – 12.21 %RSD and 11.18 %RSD respectively (Figure 7). There was a small improvement when considering the batch effect whereby mean batch precision was quantified at 7.43 %RSD. This suggests that the error is perhaps two-fold – part calibration sensitivity and part an alternate variable. Consider: Fe is highly contaminant sensitive but it may also be naturally poorly homogenised in the GO-FLO water sample. This idea essentially suggests that the duplicate sub-samples from the identical GO-FLO bottle are not entirely identical and thereby introducing a variable impacting the %RSD. This would go a long way in explaining the precision achieved by PML on the replicate DTM3 inter-calibration samples. Furthermore, it is evident from the comparisons of the TM4 un-acidified and acidified controls that decreasing the storage contained volume for the control (20L to 1L), improved homogeneity, and thereby precision. Logically, this could be tested by analysing replicates of the same Field sample bottle and comparing the precision. A short repeat run was performed on several field depths for the Baseline and Inter-calibration station. However, it was not possible to reliably separate the error stemming from calibration and homogeneity, or rather lack thereof. A rectification for the calibration error is theoretically possible if a baseline calibration curve under accurate and precise analysis was established and then used to correct for the entire analysis ICP-MS variability. Conversely, this error may be interpreted as a standard uncertainty of repeatability advocating for the ruggedness of the method. Additional experimentation by trial and error may enable the SU laboratory to identify the source of the error. However, it might be conceivably faster externally validating the TM4A Control thereby providing a comparative baseline for precision among laboratories and thus evaluate the sources of error – also validating reproducibility.

5.2.2 Accuracy

The accuracy of the method is substantiated by the closeness of the SAFe D2 data to the consensus values; all the trace elements, barring Co and perhaps Cu, within, or near, the consensus one standard deviation (Figure 11). Fe concentration for the standard was in excellent agreement with the consensus value, at 0.96 ± 0.025 nmol/kg vs the 0.93 ± 0.05 nmol/kg respectively. Since UV-Oxidation was omitted for the samples, elements with a propensity to remain organically bound will be underestimated by the method. It follows that Co and Cu concentrations are understandably lower with SU vs consensus results as follows: Co - 0.03 ± 0.0004 nmol/kg vs 0.046 ± 0.003 nmol/kg, and Cu - 2.04 ± 0.03 nmol/kg vs 2.28 ± 0.015 nmol/kg. This translates to an approximately 28.4% and 10.5% underestimation for Co and Cu respectively in this study; neatly in line with the degree of underestimation in the SAFe D2 reported in literature (Biller and Bruland, 2012). Unreliable Al concentrations are an expected consequence of the LDPE PP lids and Falcon Tubes used in the study (Brown, Smith and Bruland, 2010). Crucially, the concentrations for Cd – the other element crucial in

the study – corresponded exceptionally to the consensus value. This suggest that at these concentrations interference from MoO^+ was suitably negated.

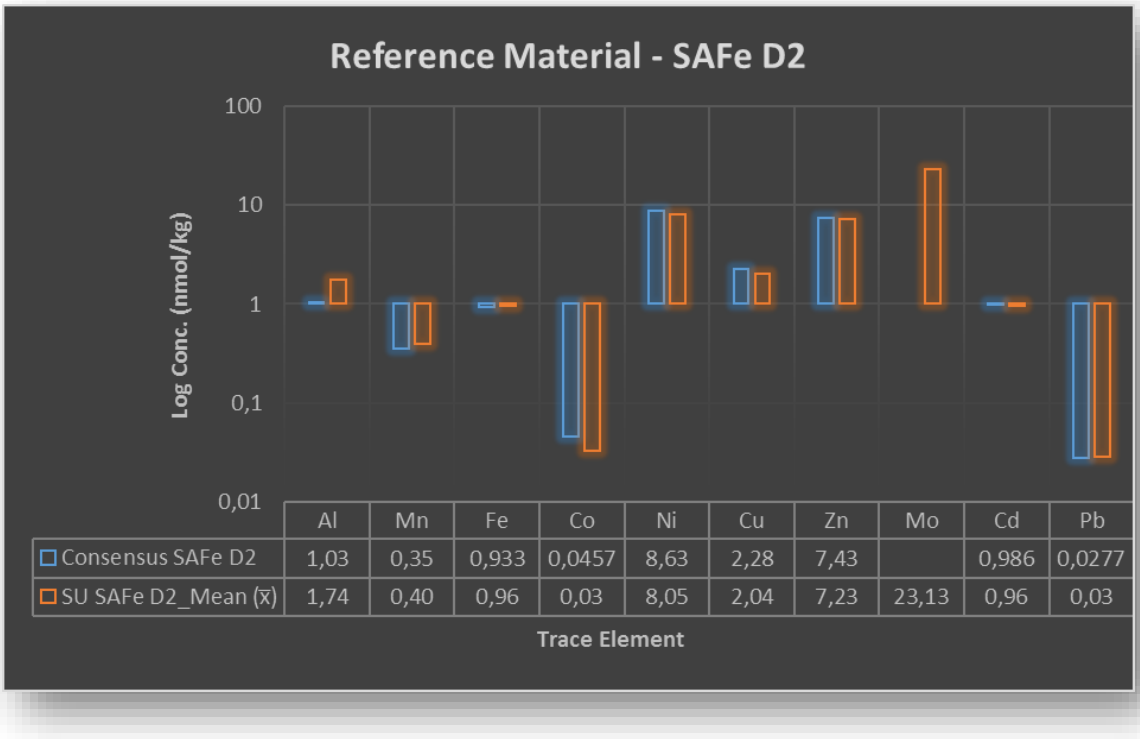

	Al	Mn	Fe	Co	Ni	Cu	Zn	Mo	Cd	Pb
Consensus SAFe D2	1,03	0,35	0,933	0,0457	8,63	2,28	7,43		0,986	0,0277
SU SAFe D2_Mean (x̄)	1,74	0,40	0,96	0,03	8,05	2,04	7,23	23,13	0,96	0,03

***Figure 11**-A visual demonstration the SU SAFe (D2) results (n=5) compared to the consensus values. The y-axis has been logged and the concentrations in the table are in nmol/kg. The accuracy was excellent barring the underestimation of Co – a consequence of omitting UV-Oxidation.*

The accuracy of the NASS 5 standard substantiates the proficiency of the method to quantify true' concentrations (Table 9). However, the concentrations of Cd, Pb and Ni were slightly underestimated (<12%). Despite the fact limited data (Hawco *et al.*, 2016) is available for comparison of the GEOTRACE GSP and GSC standards, the general precision (<10%RSD; n=5) does bode well for the reproducibility of the data (Table 7, 8). The GSP Co concentrations of 5 pmol/kg measured in this study are in excellent agreement with the consensus value of 4.9 pM given in Hawco *et al.*, 2016. However, their study reports the concentration at 2.5 pM. Conversely, while no consensus value is given for GSC, this study quantified concentrations at 82 pmol/kg, which is markedly similar to the 77.7 pM reported in Hawco *et al.*, 2016. The GSP standard Zn concentration (0.16 ± 0.054 nmol/kg) may be slightly elevated because of two potentially elevated concentrations recorded – responsible for the 34%RSD (Table 7). Similarly, Cd concentration is affected by two inconsistent concentrations causing the 27%RSD seen in the GSP. Given the excellent precision of these two elements for the in-house TM4A Control (<3.82%RSD), these values are unusual and may be attributed to random contamination issues. Further data analysis will provide a more statistically significant mean concentration for these

standards. Nonetheless, the existing data may assist in forming the initial platform for the creation of consensus values around the GSC and GSP standards.

5.3 Inter-calibration – PML Laboratory

The results of Inter-calibration exercise performed in conjunction with PML for the Baseline station located within the AAZ at 54°S – on the zero meridian – will prove integral to the successful accreditation and validation of the SU TRACEx Laboratory. Figure 13 illustrates the agreement between the PML and SU data sets for the vertical profile.

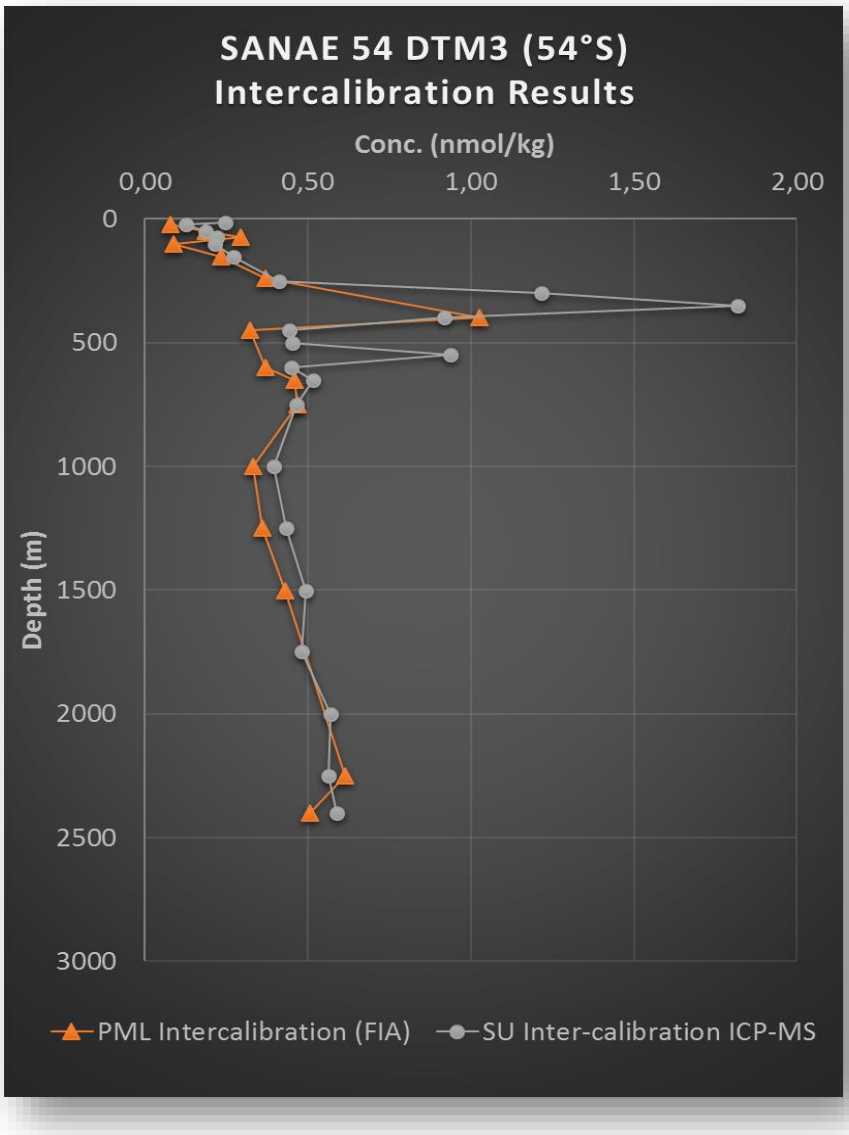

***Figure 12**-The inter-calibrated DFe concentrations for the Baseline station within the Bouvet Triple Junction (52-52°S). The spikes in DFe concentration are the result of hydrothermal activity which sees corresponding spikes in DMn (Figure 15). Profiles are in excellent agreement substantiating the quantification of DFe by a multi-elemental ICP-MS technique. The duplicate (SU) vs replicate (PML) sampling may account for small variations.*

The agreement between the SU data (23 depths) and the respective inter-calibration samples analysed by PML (15 depths), results in a first-rate correlation of profiles. PML quantified surface concentrations of 0.16 ± 0.09 nmol/kg; these correspond excellently to the 0.19 ± 0.04 nmol/kg reported herein (Table 10). Further, the concentrations in the sub-surface (500m) are very close at 0.32 ± 0.28 nmol/kg and 0.34 ± 0.24 nmol/kg for PML and SU respectively. Heading through the intermediate waters into the deep, SU results are marginally higher at 0.54 ± 0.06 nmol/kg for SU vs 0.44 ± 0.09 nmol/kg for PML. The enhanced sample resolution of the SU data (23 depths) illustrates the importance of high resolution sampling. The concentration peak observed at 400m may seem anomalous if only the PML dataset is considered. However, the collaborative datasets substantiate this "peak"; SU high-res data indicates further elevation in the 250m to 400m zone.

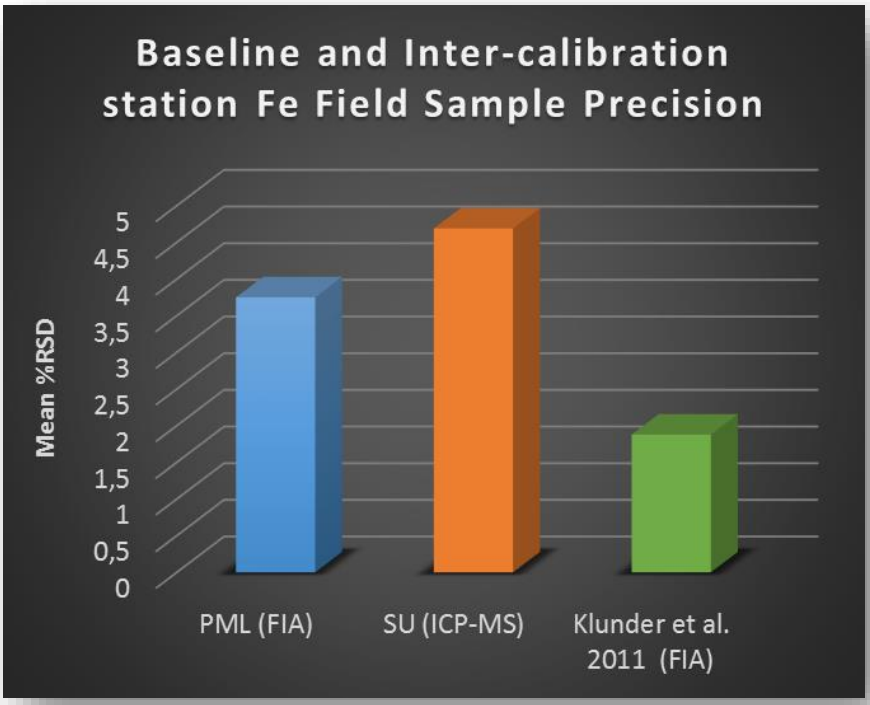

***Figure 13**-Graphical illustration of the Field precision achieved by respective laboratories and methods at the Baseline and Inter-calibration station. Precision is a mean of the %RSD at respective depths. It should be noted that the SU data shown here (n=18) has omitted %RSD values that are outliers (n=5) – hence the improvement relative to other calculations in the thesis.*

The impressive precision (≈ 3.75%) achieved by the inter-calibration partners at PML, using the FIA single aliquot technique (Figure 13), demonstrated that there is room for improvement in the method employed at SU – several readily eliminated variables have been identified. However, it should be noted that PML data was based on replicates of the same sample bottle; conversely, SU data represents duplicated LDPE bottles – introducing an additional variable in homogeneity. While the ≈ 4.7%RSD for the SU field samples at the Baseline station substantiates precise quantification, Klunder

et al. (2011) achieved a remarkable ≈ 1.9%RSD in their FIA application. The data suggest that should the variability introduced by calibration and potential minor contributions in the CAF lab be eliminated, the ICP-MS technique used herein would see ample improved precision. Nonetheless, the reproducibility between the respective FIA and ICP-MS methods substantiates competent and proficient data quantification by both, analysts and method.

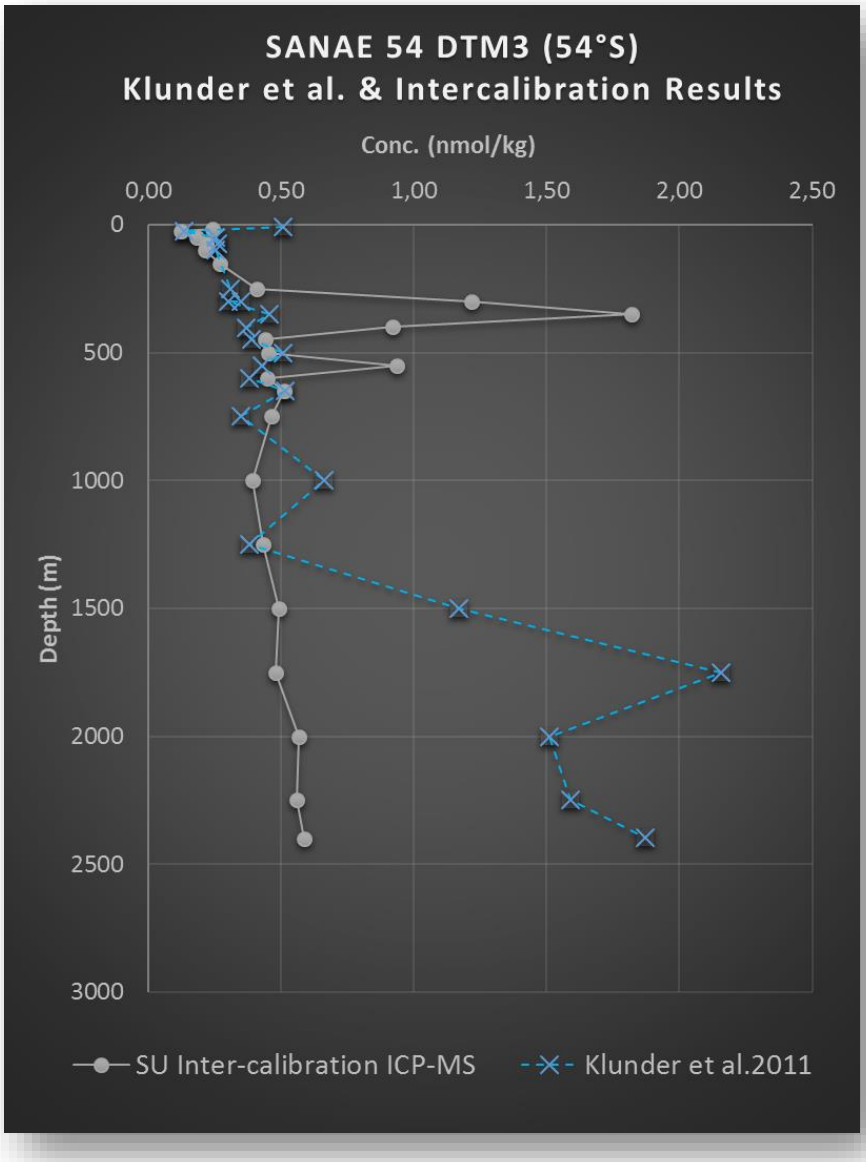

***Figure 14**-The DFe concentrations for the Baseline station within the Bouvet Triple Junction (52-52°S) as reported in this study and a study by* Klunder et al. (2011)*. The spikes in DFe concentration are the result of hydrothermal activity which sees corresponding spikes in DMn (Figure 15). The comparison of the methods substantiates the use of an ICP-MS technique in the quantification of DFe.*

The data reported by Klunder et al. (2011) suggest correspondingly elevated concentrations for the surface at 0.23 ± 0.12 nmol/kg; they attribute this to a recent deposition of aeolian dust originating in South America. This study found elevated concentrations (± 1.09 nmol/kg) in the sub-surface waters

between 250 and 400m, a consequence of the Bouvet Triple Junction (52-56°S) hydrothermal plume activity. While Klunder et al. (2011) likewise suggest that elevated DFe concentrations in the Bouvet region are characteristic of hydrothermal inputs, they only observed elevated concentrations (≤ 2.21 nmol/L) of DFe in the deep-water samples. However, in the GEOTRACES Electronic Atlas, section GIPY5_e does indeed show the localised Fe hotspot at the same location (Figure 15b). The elevated sub-surface concentrations may be a consequence of topographically induced upwelling of the hydrothermal inputs. Moreover, hydrothermal inputs of DFe coincide with elevated DMn concentrations. This study records the same phenomena with corresponding 'spikes' in the DMn (± 0.67 nmol/kg) concentrations in the zone between 150 and 400m (Figure 15a). Middag et al. (2011) report similar elevated DMn in the Bouvet region – subsequently incorporated into the GEOTRACES Electronic Atlas (Figure 15c). Constant Al concentrations are further signs that hydrothermal vents are the responsible for this behaviour. Klunder et al. (2011) demonstrate the consistency of Al in this region by calculating the Al/(Al+Fe+Mn) ratio.

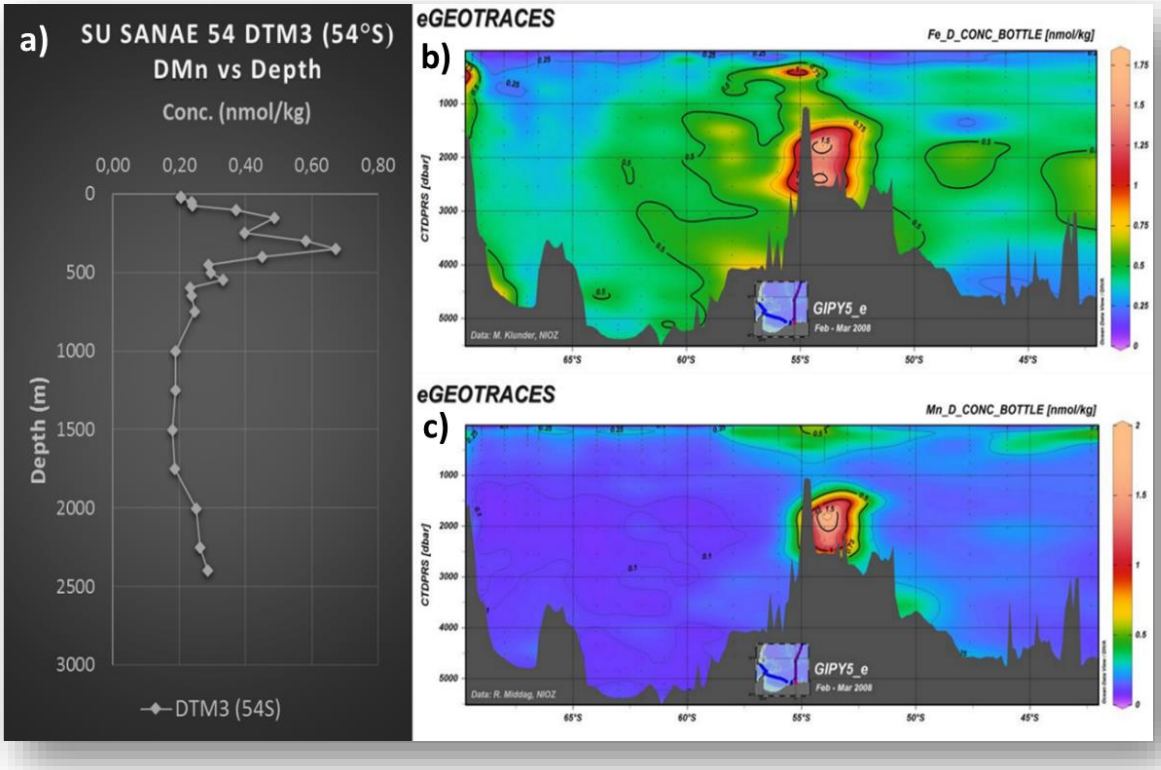

***Figure 15**-The DMn concentrations (a) for the Bouvet Triple Junction (52-56°S) as recorded in this study. The region sees known hydrothermal activity elevate the concentrations of DFe and DMn. The eGEOTRACES (www.egeotraces.org/sections) data corroborates the elevated DFe (b) and DMn (c) observed by this study for the Baseline station at 54°S. The contributions for the DFe and DMn data were made by* Klunder et al. (2011) *and* Middag et al. (2011).

Ultimately, the data suggests that hydrothermal activity plays a major role in the DFe and DMn concentrations in the Bouvet region. Consequently, concentrations may be highly variable and only provide an indication of the conditions at the time of sampling – snapshot sampling. The

concentrations reported in this study are not as elevated as those seen by Klunder et al. (2011) (Figure 14); this suggests that both atmospheric and hydrothermal activity had a lesser impact on the concentrations at the time of sampling. Nonetheless, sub-surface concentrations bear notable similarities affirming the quality of the data in this study. Significantly, the inter-calibration and crossover exercise ultimately provided the obligatory evidence to verify that the multi-element technique would allow accurate and precise quantification of DFe.

6. Conclusions

Seawater trace element analysis has seen rapid progression with the advent of modern multi-elemental quantification methods. The use of various-methods – single or multi element – has highlighted the inherent limitations attributed to a single method and thereby encouraged optimisation. The greatest benefit of multi-element methods has been the time efficiency of quantification with up to 10 trace elements quantified in a single aliquot. The Stellenbosch University TRACEx laboratory's application of a coupled pre-concentration/extraction and ICP-MS procedure, further advocates simultaneous trace metal quantification techniques moving forward. The data corroborates excellent precision over a wide dynamic range supported by high sensitivity and good detection limits. Given the combination of simultaneous multi-elemental recovery, high throughput, and accurate recovery, the seaFAST (ESI) resin column proved excellent in the quantification of trace metals in seawater. Moreover, the module proved effective in limiting the matrix interference commonly association with the ICP-MS analysis of seawater.

The samples demonstrated field and analytical precision well within the 10% RSD – typically <5%RSD – required by the protocols with confident identification of the variables impacting the limit straddling elements, Fe and Co. In the analysis of Fe, we found a few bad apples spoilt the mean precision of field samples (12.2 %RSD) – illustrated by the median value (4.46 %RSD). The results of the GEOTRACES SAFe (D2) standard support accurate quantification of trace elements in a typical seawater sample – reiterating the importance of high quality reference materials. Further, the SU results for the SAFe D2 and NASS 5 largely demonstrated improved precision over the consensus values. The GSC standard exhibited excellent <10 %RSD precision for all the elements. Conversely, the GSP standard showed average precision for Zn and Cd whilst remaining near the 10% limit for several other trace elements. This precision bodes positively for early contributions enabling the creation of a consensus database for these reference materials. Nonetheless, it remains to be seen if systematic independent evaluation proves the data accurate.

Ultimately, the determination to provide qualitative evidence pro validation, has contributed immensely to the integrity of the data. The SU TRACEx laboratory demonstrated competency in the understanding of the method-transfer procedure and application thereof, permitting the accurate and precise quantification of multiple trace elements (up to pico molar range) at the 95% Confidence Interval. Thereby, providing the project with quantitative data further constraining trace metal concentrations in the Southern Ocean. The exercise provides comprehensive evidence aimed at assisting the GEOTRACES S&I Committee in their evaluation of the SU Laboratory's application of the method.

7. Recommendations

The following suggestions are intended to improve the validity of the data in future studies.

- Employ an Internal Standard (IS) in the pre-concentration of samples to monitor the sea*FAST* module performance simultaneously improving stability.
- Improve the consistency of the ICP-MS calibration by ensuring consistency of detection limits.
- Upgrade the clean protocols and air filtration class in the CAF facility – samples exposed to contamination due to poor air filtration.
- Test the precision of replicate samples in the evaluation of variables resulting in Fe %RSD.
- Analyse method blanks utilizing a suitable matrix.

CHAPTER 4

The Meridional Distribution and Controls of Cobalt and Cadmium

Abstract

This chapter elucidates on the meridional distribution and controls of dissolved cobalt (DCo) and cadmium (DCd) for seven stations (36°S to 68°S) of a Southern Atlantic traverse. DCo exhibits meridionally decreasing concentrations in the Southern Ocean; conversely, DCd concentrations increased in the high latitudes. The depletion of both DCo and DCd in the surface indicates bio-utilization by marine phytoplankton. DCd vertical distribution exemplified a nutrient like profile correlating to the macronutrient phosphate (PO4). Surface concentrations were notably depleted for entire extent of the transect notwithstanding low Chl-a – suggestive of biotic and abiotic controls. Concentrations below the euphotic zone were dominated by remineralization and an intermediate depth peak contingent to the AAIW/UCDW advective boundary. The latitudinal shoaling of this boundary may resupply DCd to the sub-surface explaining the southerly concentration elevation. Concentrations ranged from 8.4 ± 0.05 pmol/kg to 902 ± 22.71 pmol/kg. Conversely, DCo exhibited a hybrid type profile exemplified by bio-utilization in the euphotic zone, succeeded by rapid remineralization and scavenging. The AAIW/UCDW boundary also apparently controls the scavenging onset depth and may be a prominent control in the meridional depletion of sub-surface DCo. Scavenging is typically inhibited by organic complexation of Co (II) preventing the oxidation by heterogenous bacteria. The interaction of DCo with organic ligands may limit bio-availability and phytoplankton growth – notably at 46°S. The concentrations ranged from 4.1 ± 0.02 pmol/kg to 38.9 ± 0.3 pmol/kg. Elevated DCo concentrations in the sub-surface, corresponding to a poor but significant DCo/Salinity correlation, suggest auxiliary DCo flux in the expanse surrounding 46°S and 68°S.

Keywords: AAIW/UCDW boundary, Bio-utlization, DCo, DCd, hybrid type, nutrient type, scavenging.

1. Foreword

The elucidated understanding of the role which bio-active trace elements, most notably iron (Fe), play in the growth of marine phytoplankton has enabled the biogeochemical community to make important advances pertaining to phytoplankton dynamics across the world's oceans. However, while growth limitation of Fe has been widely accepted (Coale, 1991; Klunder *et al.*, 2011), it has become clear that phytoplankton growth may be further limited, or co-limited, through the availability of trace metals such as cobalt (Co) and cadmium (Cd) (Sunda and Huntsman, 2000; Saito and Goepfert, 2008; Shelley *et al.*, 2012). Elucidating on the controls of Co and Cd on the resident plankton communities, has been stunted by a limited understanding of the distribution and controls of these elements; most notably in the High Nutrient Low Chlorophyll (HNLC) region of the Southern Ocean, Atlantic sector. While several studies have recently reported on Cd cycling in the region (Abouchami *et al.*, 2014; Baars *et al.*, 2014), Co has yet to be incorporated into the GEOTRACES consensus database.

In general, dissolved Co (DCo) distribution in the world's oceans may be characterized by a surface depletion followed by "enrichment" as remineralization ensues – nutrient like behaviour (Shelley *et al.*, 2012). However, in the Atlantic region of the Southern Ocean, DCo concentrations exhibit further scavenged type behaviour whereby concentrations decrease at controlled rates below the remineralized zone (Bown *et al.*, 2011). These are indications that distributions may be influenced by biotic, and abiotic sources and sinks – elevated surface concentrations are perhaps indicative of atmospheric dust inputs (Moffett and Ho, 1996). The euphotic zone is dominated by the nutrient like profile with rapid depletion by phytoplankton around the Chl-a max depth value (Bown *et al.*, 2011). An "enrichment" caused by regeneration then appears to happen, as concentrations increase until physical controls dominate at greater depths in the column where depletion by scavenging occurs (Saito and Moffett, 2001; Biller and Bruland, 2012). Thereby, the distribution of DCo within the Antarctic Circumpolar Current (ACC) is said to mimic a hybrid type profile (Bown *et al.*, 2011; Biller and Bruland, 2012).

Commonly, DCd vertical distribution in the ocean mimics a typical nutrient like profile with strong depletion by phytoplankton in the surface waters (Boye *et al.*, 2012). There is a correlation between Cd and phosphate (PO_4), demonstrating the removal of trace nutrients in surface waters by marine phytoplankton, commonly expressed as the Cd/P ratio (Sunda and Huntsman, 1995; Baars *et al.*, 2014). The Cd/P ratio should exhibit a linear trend in the ocean with values of between 0.50-0.58 nM/µM reported in the Weddell Sea and the Antarctic Circumpolar Current (Loscher, 1999; Sañudo-Wilhelmy *et al.*, 2002). A model developed by Boyle 1988, predicts a constant fractionation factor – that is the ratio imparted to euphotic waters due to bio-utilization – of $\alpha \approx 2.5$ (Cd/P) for the global

ocean. In the Southern Ocean a fractionation factor of α≈5 (Cd/P) emphasises the bioactive relationship of Cd in the biological process (Frew *et al.*, 2001). In the North Atlantic research has shown that for any given P concentration, Cd can be predicted to within 7% (Boyle, 1988). Generally, constant concentrations of DCd exist below chl-a max in the water column, a consequence of remineralization of particulate and marine snow ascribed to sinking planktonic matter. Distribution and reworking of Cd is controlled to some extent by the particles dominating the water column. In the Weddell Sea, where siliceous diatoms dominate, the inert silica particles inhibit reworking of suspended Cd. In the PFZ on the other hand, Cd is ascribed to easily dissolved carbon particles as coccolithophores dominate. Isotopic fractionation of Cd sees biological activity impart heavy isotope ($^{112/110}$Cd) signatures to the surface and consequently lighter isotopic fractionation of intermediate waters due to regenerations of isotopically light Cd from sinking organic matter (Abouchami *et al.*, 2014). A southwards decrease – Antarctic Circumpolar Current (ACC) to the Weddell Gyre – in the Cd isotope fractionation factor exists in the southern ocean (Abouchami *et al.*, 2014). This coupling between trace metals and macronutrients can be used as paleo-proxies in the reconstruction of past changes in ocean productivity and circulation (Boye *et al.*, 2012). One such method is based on the incorporation of Cd^{2+} into the structural lattice of marine carbonates ($CaCO_3$) in a fraction representative of the seawater concentration at the time of $CaCo_3$ formation (Wu and Boyle, 1997; Frew *et al.*, 2001). Moreover, partitioning of Cd to the particulate phase is directly correlative with the algal growth in the waters, in the same way that the Redfield ratio reflects C:N:P. Planktonic Cd concentrations are inversely related to Mn and Zn ion concentrations (Sunda and Huntsman, 1995; Ellwood, 2004). The enhanced cellular uptake of Cd is controlled by the cell's Mn uptake system other than the reduced bio-dilution associated with Mn limitation (Sunda and Huntsman, 2000).

Further the chemical speciation of bioactive trace metals governs biogeochemical cycles through a complex relationship established in the chemical interaction of metals with biomolecules on the surface and within cells (Sunda, 1991). Metal transport into the cell is determined by the interplay between the metal speciation in the medium and ligand exchange reactions at transport sites on the plasmalema (Sunda, 1991). The speciation of Cd and Co governs bioavailability to marine phytoplankton. Moreover toxicity may be controlled by the free metal ion concentration, not simply the total concentration (Bruland, Donat and Hutchins, 1991). Co is an essential micronutrient for photosynthetic cyanobacteria (Sunda and Huntsman, 1995), which in the pH and Eh ranges of natural waters can exist as Co(II) or Co(III) (Moffett and Ho, 1996). The divalent cation, Co (II), can form strong, labile organic complexes, thus impacting bioavailability. Co (III) bioavailability is affected by the inclination to form inert complexes or oxides (Moffett and Ho, 1996). Little is known about the interaction of various eukaryotic phytoplankton with metal-ligand complexes, nevertheless it may be

that they are able to synthesize and utilize Co-ligand complexes (Saito and Moffett, 2002). The adsorption and oxidation of Co, occurring on the surfaces of Mn oxides in the water column, is postulated to be a significant mechanism for Co removal (Moffett and Ho, 1996; Saito and Moffett, 2002). Mn oxidizing bacteria have been proposed to control Co (II) oxidation via a common microbial pathway (Moffett and Ho, 1996). Surface waters may see the organically bound fraction of Cd exceeding 70% (Bruland, Donat and Hutchins, 1991; Sunda and Huntsman, 2000). However, an experiment performed by Batley & Florence 1976 found organically bound Cd comprised only 18% of the total. The underestimation of DCo, due to complexation, is expected to be more pronounced within highly productive regions due to raised concentrations of naturally occurring complexing agents. The dissolved fraction of DCd – present in the +II oxidation state – bind with Cl forming the $CdCl^{+}$ ion. Experiments performed by Sunda & Huntsman, (2000) showed that cellular Cd and Co concentrations increased with increasing Cd^{2+}, Co^{2+} and with decreasing Zn^{2+} concentrations in the marine species *T. weisflogii*, *E. huxleyi* and *T. oceanica.* This could indicate uptake by a common inducible transport system regulated by cellular Zn (Sunda and Huntsman, 2000).

In this chapter, the distribution and controls of DCo and DCd in the Southern Ocean, Atlantic sector, will be discussed in their entirety in an attempt to gain insights into the biogeochemical cycling of these elements. While only DCo and DCd will be discussed, the multi-elemental ICP-MS technique provides a collective suite of elements to assist in the creation of a distinctly unique understanding of the DCo and DCd trace metal interactions.

2. Site Description

2.1 Hydrography

The Southern Ocean, Atlantic Sector, is meridionally characterised by several distinct biogeochemical provinces delineated by unique physical hydrographic domains and environmental conditions. The location of deep reaching hydrographic boundaries – known as frontal systems – have a direct influence on both the physical and biological distribution of trace metals in the Southern Ocean (Baars et al. 2014; Pollard et al. 2002). It follows that such a boundary would isolate the water masses on either side on the physical current thereby inhibiting mixing in the ocean (Graham, 2014). Sloping isopycnals expose or remove dissimilar water masses to the surface layer – an important control on stratification (Pollard et al. 2002). Concurrently, regions proximal to fronts may contain increased biomass as the nutrient stocks are replenished. The system responsible for replenishment is posited as a two-fold mechanism involving horizontal advection and subservient nutrient upwelling (Graham, 2014). Satellite imaging in the region indicates that Chl-a concentrations are elevated in the frontal zones: indicative of enhanced biological activity (Graham, 2014).

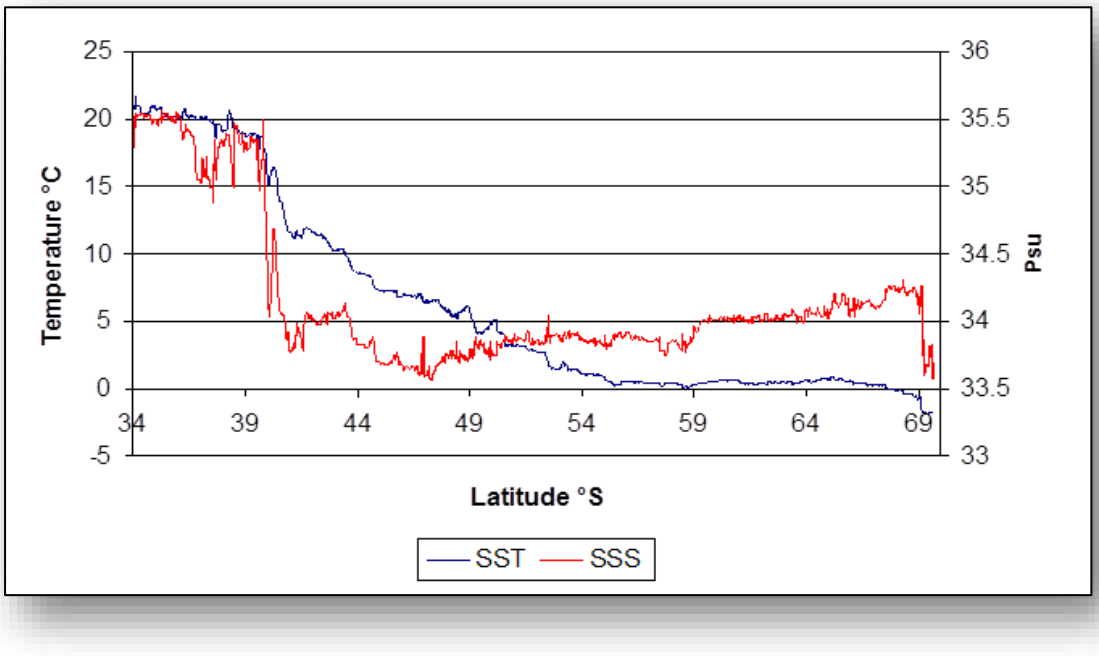

***Figure 16**-Thermosalinograph for the SANAE 54 voyage smoothed over 20 minute intervals. The northern boundary of the ACC known as the STF is marked by the sharp salinity variation at 40.5°S. Temperature controls surface stratification north of the STF (40.5°S), whereas salinity controls surface stratification in waters south of the PF (50°S).*

The meridional variation opens with the Sub-Tropical Zone (STZ) describing the region north of the Sub-Tropical Front (STF; ≈40.54°S). Advancing south the variation is primarily controlled by the Antarctic Circumpolar Current (ACC; ≈42°-55°S) driven by the Roaring Forties (Pollard, Lucas and Read, 2002; Bown *et al.*, 2011). The ACC is frequently described by apportioning it into three major fronts

incorporating two frontal zones (Pollard, Lucas and Read, 2002). Within the northern extent of the ACC (ACCn) is the Sub-Antarctic Zone (SAZ; ≈42°-46°S), the zone of ACC transport which is makes up the Polar Frontal Zone (PFZ; ≈46°-50°S), and the Antarctic Zone (AAZ; ≈50°-56°S) bounded to the south by the ACC (ACCs) (Pollard, Lucas and Read, 2002; Klunder *et al.*, 2011). The Sub-Antarctic Front (SAF; ≈46.38°S) is the boundary between the SAZ and the PFZ to the south. It follows that the Polar Front (PF; ≈50.5°S) is bound by the PFZ (north) and the AAZ (south). The Southern Boundary (SB; ≈56°S) demarcates the AAZ and the zone south of the ACC (SACCZ; ≥57°S) (Orsi, Whitworth and Nowlin, 1995; Pollard, Lucas and Read, 2002). According to Le Moigne et al. 2013 distributions are constrained by three to four distinguishable biogeochemical domains: the subtropical Atlantic, the confluence zone of the sub-tropical and Sub-Antarctic domains known as the Subtropical Front (STF) located at approximately 42°2'S (Bown *et al.*, 2011); Polar Front (PF; 50°22.4'S) in the Antarctic Circumpolar Current (ACC) which is the boundary between the AAZ to the south and the PFZ to the north; and the north-eastern branch of the Weddell Gyre.

2.2 Macronutrients in the Southern Ocean, Atlantic Sector

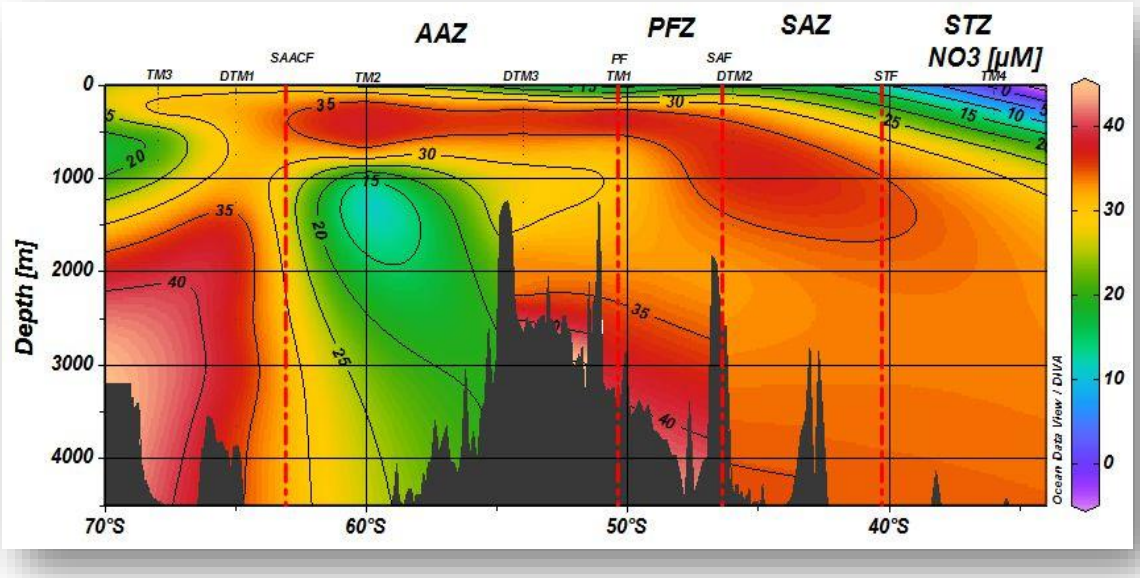

***Figure 17**-Southern Ocean Nitrate (NO3) concentrations as collected by Leigh-Ann Palmer on the SANAE 54 cruise* (Palmer, 2015) *and presented in an ODV contour plot. The frontal regions are delineated the same as this study-barring the SACCF. The SB (60°S) was used as the Weddell Gyre boundary in this study. The results were used to ascertain the likelihood of limitation by macronutrients and to further constrain the behavioural aspect of bioactive elements in the water column.*

Macronutrient (Figure 17-19) concentrations on this cruise were collected and quantified by a Leigh-Anne Palmer who collaborated on the project (Palmer, 2015)**.** The conditions in the Southern Ocean surface waters display a consistent increase south of the STF. In the STZ macronutrient concentrations exemplify the depletion seen in oligotrophic waters. Conditions in the sub-tropical

domains are characterized by these extremely low concentrations (<0.5µM) of nutrients; nitrogen, silica and phosphate (Bown *et al.*, 2011; Le Moigne *et al.*, 2013). Nitrate and phosphate recover to reasonable levels within the surface waters near the SAF (Figure 17,18). However, silicic acid concentrations are comparatively low throughout the ACC (5.4-30 µmol/L), with higher concentrations observed within the SACCZ (Figure 19). Nitrate and phosphate increase to 20 µM and 1 µM respectively in the PFZ, while silicate remains ≤10 µM (Bown *et al.*, 2011). This cruise saw higher concentrations within the PFZ (≥ 1.5 µmol/L). Results from within the PFZ indicate that this region continues to exhibit low concentrations of the macronutrient silicic acid. Silicic acid concentrations within the SACCZ are conceivably being recharged by continental sources – perhaps further leaking into the deep waters of the ACC. The primary growth limitation for the region around 36°S is credibly a function of the extremely low macronutrient concentrations. DTM2, located at 46°S, is north of the HNLC condition with surface macronutrient concentrations for phosphate (≤ 1.76 µmol/L) and nitrate (≤ 16.7 µmol/L) having increased, however silicic acid (≤ 5.33 µmol/L) remained extremely low. TM1, located at 50°S within the PF, saw similar concentrations of phosphate (≤ 1.86 µmol/L) in the surface; while nitrate showed a sharp decrease (≤ 11.75 µmol/L), and silicic acid remained low (≤ 5.33 µmol/L). The stations within ACC experience a mid-depth peak in phosphate concentrations – a characteristic feature of the region. Silicic Acid concentrations increased (≤ 30.86 µmol/L) within the surface of the AAZ at 54°S, with phosphate and nitrate remaining stable.

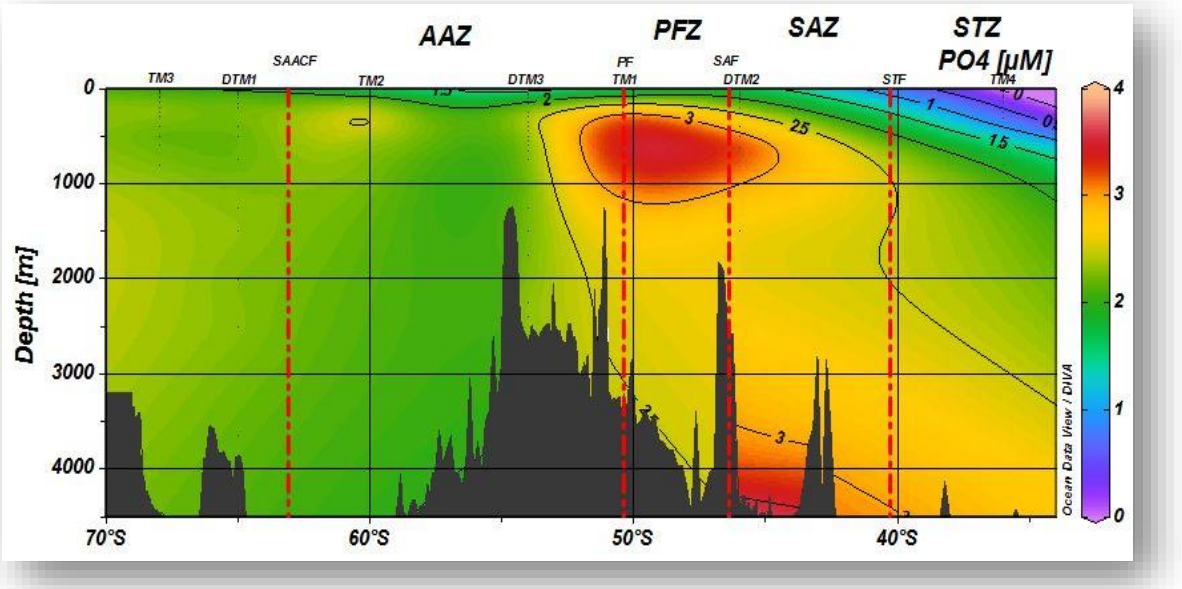

***Figure 18**-Southern Ocean Phosphate (PO4) concentrations as collected by Leigh-Ann Palmer on the SANAE 54 cruise* (Palmer, 2015) *and presented in an ODV contour plot. The frontal regions are delineated the same as this study-barring the SACCF. The SB (60°S) was used as the Weddell Gyre boundary in this study. The results were used to ascertain the likelihood of limitation by macronutrients and to further constrain the behavioural aspect of bioactive elements in the water column.*

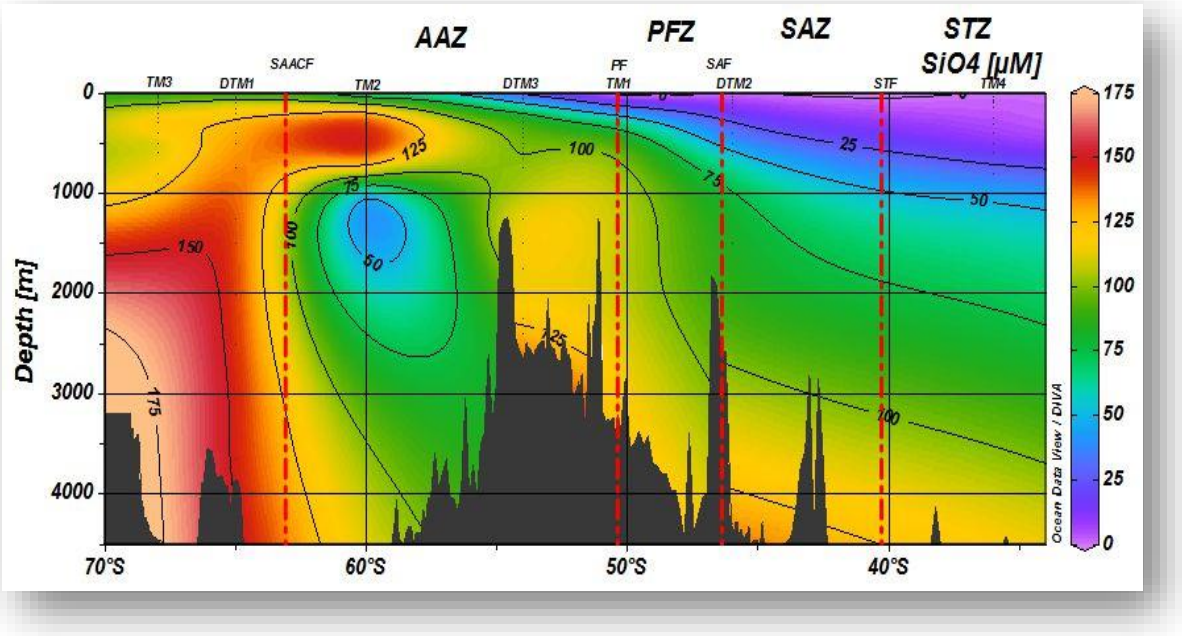

***Figure 19**-Southern Ocean Silicic Acid (SiO4) concentrations as collected by Leigh-Ann Palmer on the SANAE 54 cruise* (Palmer, 2015) *and presented in an ODV contour plot. The frontal regions are delineated the same as this study-barring the SACCF. The SB (60°S) was used as the Weddell Gyre boundary in this study. The results were used to ascertain the likelihood of limitation by macronutrients and to further constrain the behavioural aspect of bioactive elements in the water column.*

Vertical distribution sees increasing concentrations with depth, with biological utilization responsible for the depletion within the surface waters. The rate of recharge is dependent on the macronutrient and its organic association. South of the ACC, nutrient rich deep waters are transported to the surface by the upwards sloping isopycnals responsible for exposing the different water masses at frontal zones (Pollard, Lucas and Read, 2002). The nature of diapycnic mixing may allow the transfer of silicate rich water to the surface heading south along the transect. Nonetheless, within the SAZ and PFZ silicate levels may be low enough to limit the growth of siliceous marine phytoplankton (Pollard, Lucas and Read, 2002). A HNLC paradox exists in the AAZ region between the PF (≈50°30.3'S) and the SB of the ACC (≈55°54.3'S) continuing southwards, where silicate (20-70 µM) and nitrate (30 µM) concentrations increase (Bown *et al.*, 2011). Within the STZ, concentrations remain depleted up to 1000m. In the SACCZ, macronutrient concentrations exhibit conservative behaviour with depth as concentrations are replenished after approximately 100m and remain comparatively constant up to 3500m.

3. Results

Note: 1) The complete trace metal results tables can be viewed in Appendix B.

2) The results of TM2-4 may be slightly overestimated due to the Suprapur Acid used in analysis: <1pmol/kg for Cobalt and <4pmol/kg Cadmium established at low concentrations.

3.1 Hydrography and the Mixed Layer Depth

The cruise traversed several characteristic zones and frontal regions between Cape Town and Antarctica. These regions reveal important physical controls on the biogeochemical cycling of Co and Cd whereby the vertical flux of trace metals and nutrients may in large be controlled by vertical mixing through the stable density gradient region below the MLD. Parallel downwelling and upwelling waters may create shear induced turbulence (eddies) which, typically present as a concentration depth peak in the water column (Figure 27; DCd). While phytoplankton utilization may control bioactive trace element uptake in the MLD, large concentrations of bacteria may influence concentrations below the pycnocline, a consequence of the interactions with euphotic detritus (marine snow). Therefore, delineating these controls will elucidate on the cycling of the trace elements in the surface waters.

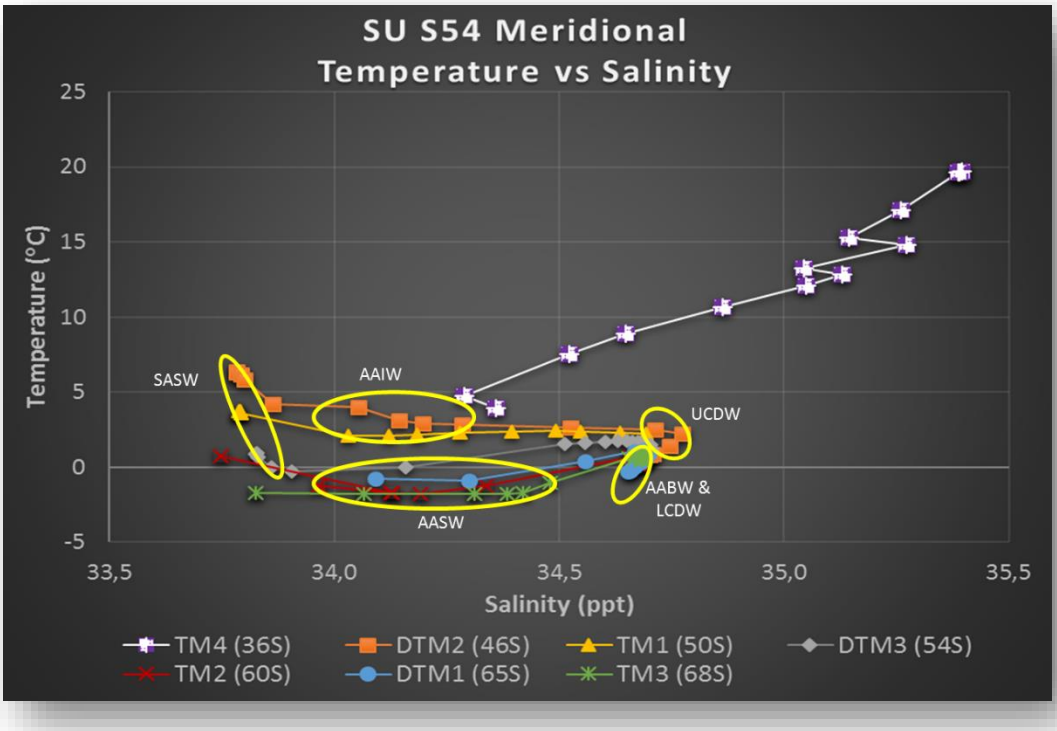

***Figure 20**-A meridional illustration of the CTD measurements for Temperature (°C) vs Salinity (ppt) in the entire water column. The segregation of the water masses delineated in the diagram is an approximation. Water masses are denoted as follows: Sub-Antarctic Surface Water (SASW), Antarctic Intermediate Water (AAIW), Antarctic Surface Water (AASW), Upper Circumpolar Deep Water (UCDW), Lower Circumpolar Deep Water (LCDW) and Antarctic Bottom Water (AABW).*

The vertical distribution of water masses commonly see appropriation into several characteristic masses including (Figure 20): northerly advecting Sub-Antarctic Surface Water (SASW) and Sub-Tropical Surface Water (STSW) that characterize the upper 50-100m north of 43°S; Sub-Antarctic Mode Water (SAMW) characterize ≈0-500m depth north of the SAF sub-ducting along the SASW to 100m upper depth and subsisting to 500m lower boundary; downwelling Antarctic Intermediate Water (AAIW) which lies below the sub-surface water at depths between 500-1000m in the SAZ's and 0-1000m in the PFZ; northerly advecting Antarctic Surface Waters (AASW) found south of the PF in the upper 300m (Loscher, 1999); Upper Circumpolar Deep Water (UCDW) at depths between 1000-1500m in the region around the Polar Front (PF) progressively upwelling to the south; the waters between 1500-3000m around the PF are classified as Lower Circumpolar Deep Water (LCDW) progressively upwelling with the UCDW towards the SB in the SACCZ; Antarctic Bottom Water (AABW) beneath the surface in the Weddell Sea region – formed from the Weddell Sea Bottom Water (WSBW) – and flowing north beneath the Lower Circumpolar Deep Water (LCDW) in the far South region near the Antarctic continental margin (Veth, Peeken and Scharek, 1997; Loscher, 1999; Le Moigne *et al.*, 2013).

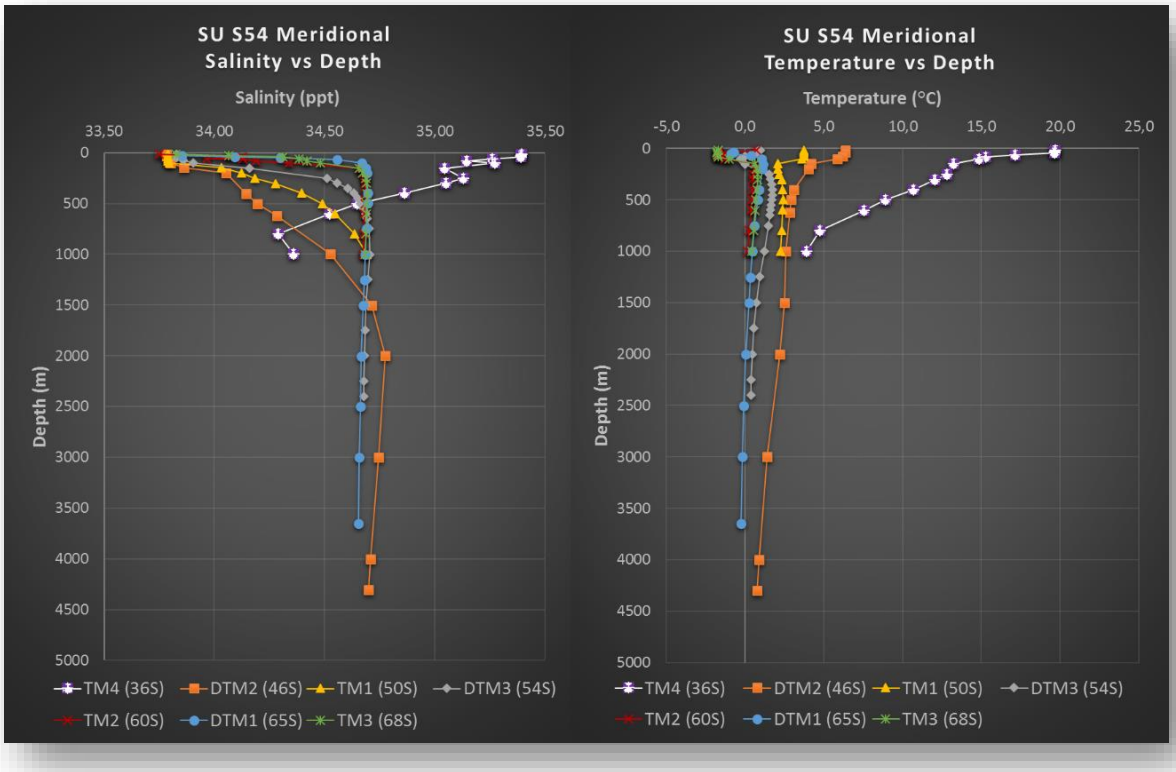

***Figure 21**-Meridional CTD measured Temperature (°C) and Salinity (ppt) data for the entire water column. This data was used to identify the water masses as well as elucidating on the physical control these water masses have on the distribution of trace metals.*

The Mixed Layer Depth (MLD) was commonly delineated by way of temperature with a fixed threshold criterion of 0.2 °C (Equation 4). However, in the case of the temperature inversions seen at

DTM3 and TM2, caused by a narrow band of cold AASW sub-ducting a rapidly dissipating warmer SASW surface layer, a density fixed threshold (0.03kg/m^3) criterion formula was used (Equation 5).

$$MLD_{DT02} = depth\ where\ (\theta = \theta_{15m} \pm 0.2\ ^{\circ}C)$$

Equation 4

OR

$$MLD_{DR003} = depth\ where\ (\sigma_0 = \sigma_{0_{15m}} \pm 0.03kg.m^{-1})$$

Equation 5

This technique, applied by de Boyer Montégut et al. (2004), has proven successful in the accurate estimation of the MLD. In this cruise the data allowed the calculations of MLD (Figure 23) as follows: 42m at TM4 within the STZ (36°S), increasing to 79m within the SAF at DTM2 (46°S); 102m at TM1 at the PF (50°S); 100m at DTM3 within the AAZ (54°S); shoaling to 50m at TM2 just south of the SB (60°S); 55m at DTM1 within the Weddell Gyre (65°S); and deepening to 86m at TM3 (68°S) near the continental mass (Figure 22).

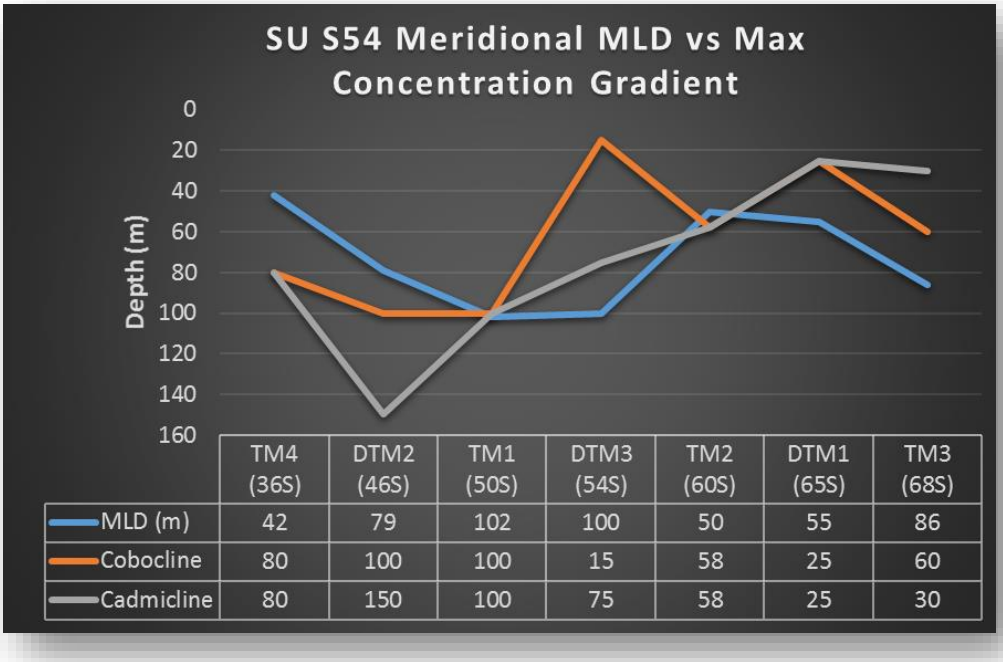

	TM4 (36S)	DTM2 (46S)	TM1 (50S)	DTM3 (54S)	TM2 (60S)	DTM1 (65S)	TM3 (68S)
MLD (m)	42	79	102	100	50	55	86
Cobocline	80	100	100	15	58	25	60
Cadmicline	80	150	100	75	58	25	30

***Figure 22**-The depth of the Mixed Layer (MLD) in comparison to the maximum concentration gradient of DCo and DCd – a type of 'Cobocline" and "Cadmicline". The Cobocline tends to be inconsistent – perhaps a consequence of weak utilization in parts combined with atmospheric inputs. The Cadmicline consistently shoals throughout the ACC into the SACCZ – coinciding with the upwelling UCDW.*

According to Le Moigne et al. (2013) the mixed layer depth (MLD) in the Sub-tropical and Sub-Antarctic domain is around 50m, increasing to 60m in the PFZ and continuing the southwards increasing trend to 90m in the Weddell Gyre (Le Moigne *et al.*, 2013). The trend presented in figure

22 is better constrained by the north-south MLD trend observed by Klunder et al. (2011). Further, in the STZ and SAZ, near surface stratification is controlled by temperature. Conversely, towards the south influxes of fresh melt-water sees salinity dominating (Figure 16) – a trend also observed by Pollard et al. (2002). However, within the AAZ and the station TM2 near the SB, a temperature inversion controls the MLD. This may be a consequence of cold, dense SASW sub-ducting the warmer surface waters in a narrow band.

3.2 Chlorophyll-a in the Southern Ocean, Atlantic Sector

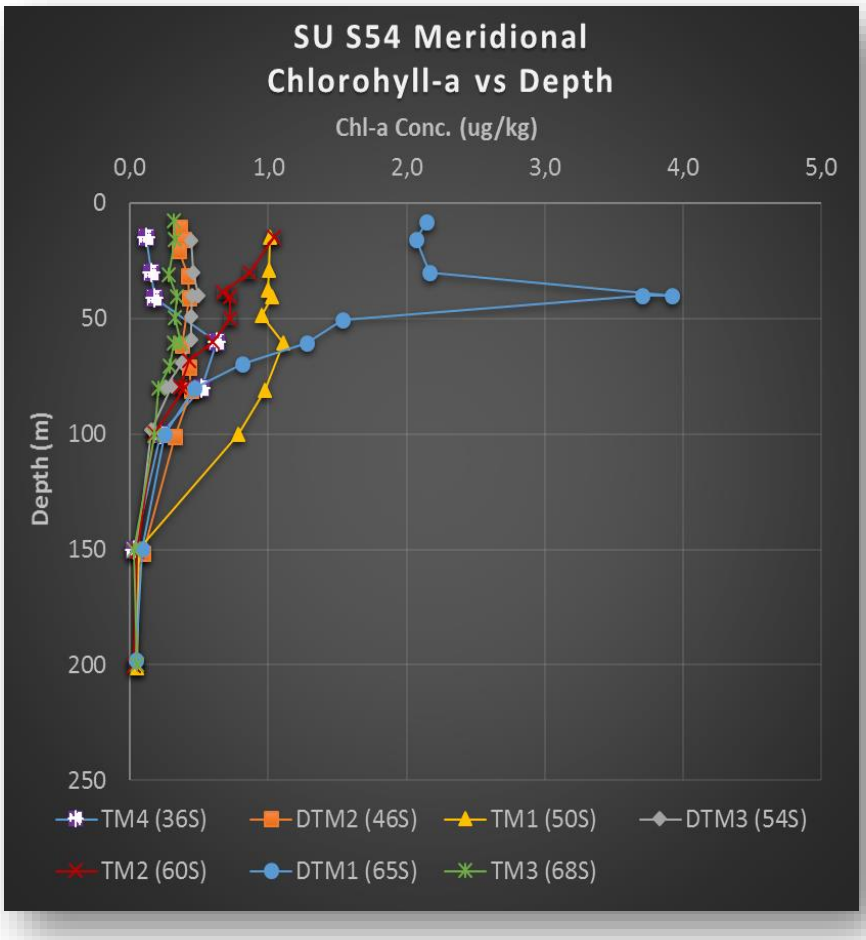

***Figure 23**-Chlorophyll-a data collected by Leigh-Ann Palmer during the SANAE 54 voyage* (Palmer, 2015). *This data was crucial to understanding the biological demand of trace elements under varying productivity levels and community structures. The impact of bioavailability may also be somewhat elucidated using the Chl-a concentrations.*

Surface Chl-a concentrations for the Good-Hope transect were reported below 0.5 µg/L by Le Moigne et al. (2013). Comparatively, average surface Chl-a concentrations on this cruise were measured at ± 0.177 µg/kg with a single region at ± 0.57 µg/kg (65°S). Furthermore, Le Moigne et al. (2013) report concentrations of 0.3 µg/L in the PFZ; markedly lower than the ± 0.7 µg/kg observed in this study. Surface Chl-a concentrations within the STZ ranged between 0.11 µg/kg and 0.59 µg/kg –

perhaps due to a macronutrient primary limitation. However, similar low Chl-a concentrations were observed for the AAZ. In the STZ region Bown et al. (2011) report a range of 0.29 µg/kg to 0.49 µg/kg – conditions typical of oligotrophic waters. Chl-a concentrations remain comparatively low within the SAF at 46°S (DTM2), with a mean of 0.4 µg/kg in the surface. However, the profile is interesting as it does not show one recorded strong peak, instead there are several peaks at 15, 41 and 81m respectively (Figure 23) – a characteristic of the diverse plankton community (Figure 28). There may be a shoaling of the Chl-maxima farther south on the transect – barring the STZ anomaly. In the south-eastern edge of the Weddell Gyre at 65°S (DTM1) a remarkably high chl-a maximum of 3.91 µg/kg was recorded in one sharp peak at 40m – observations at the time of sampling also indicate high zooplankton numbers. Total productivity for the stations was estimated at 100m by means of integration of the curves. Given the high Chl-a concentrations, results predictably indicate much higher "total" productivity at DTM1 (157 µgm/kg) in the eastern edge of the Weddell Gyre; with subordinate concentrations within the PF (97.7 µgm/kg) at 50°S, and south of the SB at 60°S (68.9 µgm/kg). Concentrations at the remaining stations were analogous and decidedly low, ranging between 32-38 µgm/kg – no single factor is apparently responsible.

3.3 Meridional and Vertical Distribution of Total Cobalt and Cadmium

The meridional and vertical profiles for the total Co (TCo) concentrations in the Southern Ocean are presented in figure 24 with the data provided in tables 11-17. The general trend inclines towards lower concentrations of TCo heading south through the ACC towards the Weddell Gyre (SACCZ) – the only trace element to exhibit this behaviour. Moreover, the highest concentrations are observed in the surface waters of the transect; thereafter concentrations decrease – scavenging being the primary control.

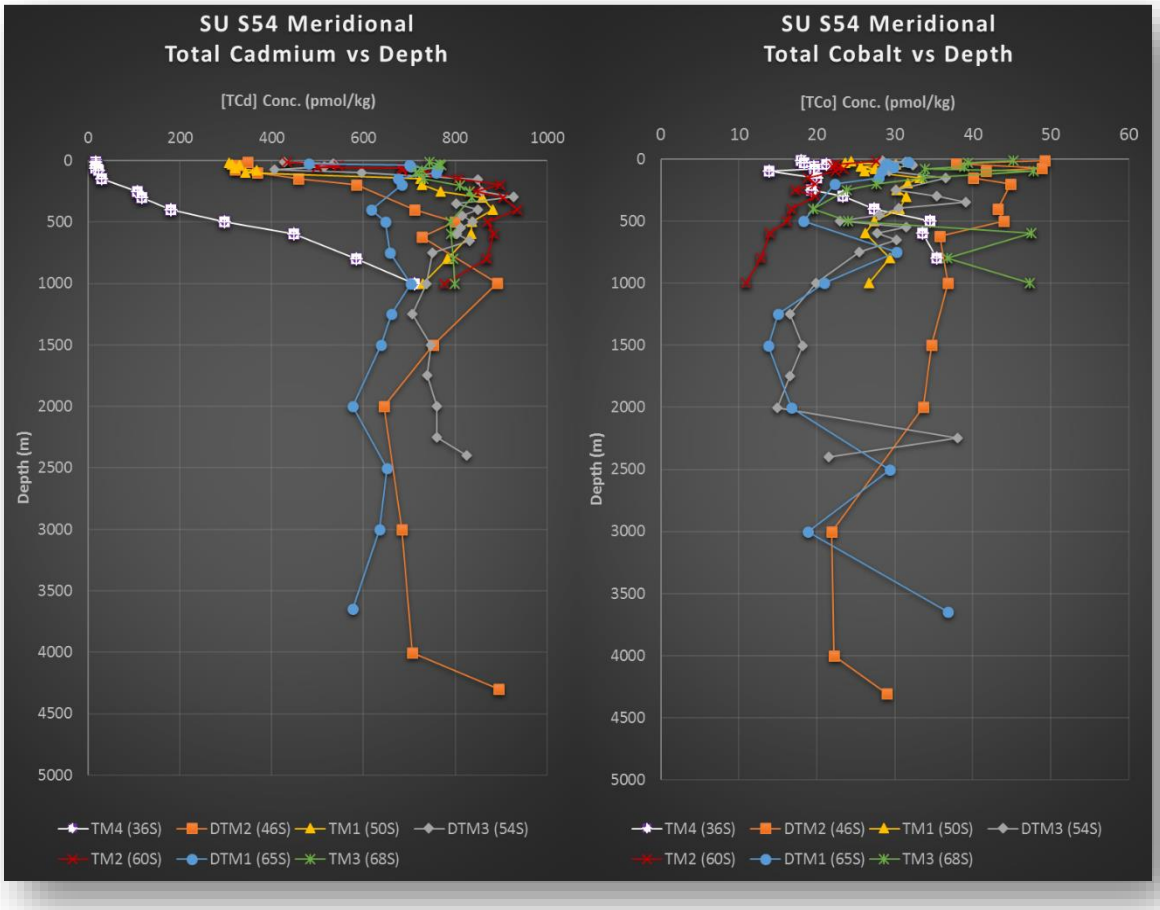

***Figure 24**-The meridional distribution of the total fractions of cadmium and cobalt (TCd and TCo) plotted against depth (m). Note the similarities between the TCd and DCd profile. Conversely, TCo behaviour is erratic relative to DCo. These concentrations were quantified based on single pre-concentrated samples and not duplicates (n=1).*

Generally, TCo concentrations in the surface (MLD) ranged from 45.3 pmol/kg (46°S) in the SASW to 24 pmol/kg (60°S) in the AASW. The trend was dodged by the stations at 36°S (STZ, TM4) and 68°S (SACCZ, TM3). At 36°S, TCo concentrations were strongly depleted at 19.18 pmol/kg in the surface (42m; STSW), and remain depleted throughout the sub-surface (SAMW) at 20.1 pmol/kg. Conversely, at 68°S the lower high latitude concentration trend was reversed and concentrations of TCo increase

in the surface (86m; AASW) to 39.34 pmol/kg reducing to 31.78 pmol/kg in the sub-surface (AADW) – given the proximity to the Antarctic land mass perhaps coastal dust and melting ice are contributing.

The meridional and vertical profiles for the total Cd (TCd) concentrations are presented in figure 24 with the data provided in table 11-17. Contrary to TCo, TCd concentrations follow the typical trace metal trend that sees concentrations increasing through the AAC into the high latitude Weddell Gyre. Moreover, the TCd profile mimics the DCd profile throughout the water column with depletion in the surface, regeneration and conservation thereafter – typical nutrient like behaviour. The concentrations in the surface (MLD) range from extremely depleted at 17.24 pmol/kg (42m; SAMW) within the STZ, to elevated concentrations of 744.58 pmol/kg at 68°S – displaying a complete lack of relative depletion proximal to the Antarctic continent (Figure 2; TM3). Sub-surface (500m) concentrations ranged from 82.45 pmol/kg within the STZ, to 775.5 pmol/kg at 68°S (TM3) within the south-eastern edge of the Weddell Gyre. Interestingly, the station at 65°S (DTM1) bucks the increasing concentration trend and exhibit comparatively lower concentrations. TCd concentration in the intermediate waters are relatively conservative and similar at ≈754.5 pmol/kg. The greatest concentration range is typically found within the first 500m of the water column at 46°S, shoaling towards the south at 65°S where it was found at 40m – coinciding with the shoaling of the UCDW. The concentrations are highly depleted in the STZ dropping as low as 17.24 pmol/kg in the surface (42m; SAMW).

3.4 Meridional and Vertical Distribution of Dissolved Cobalt and Cadmium

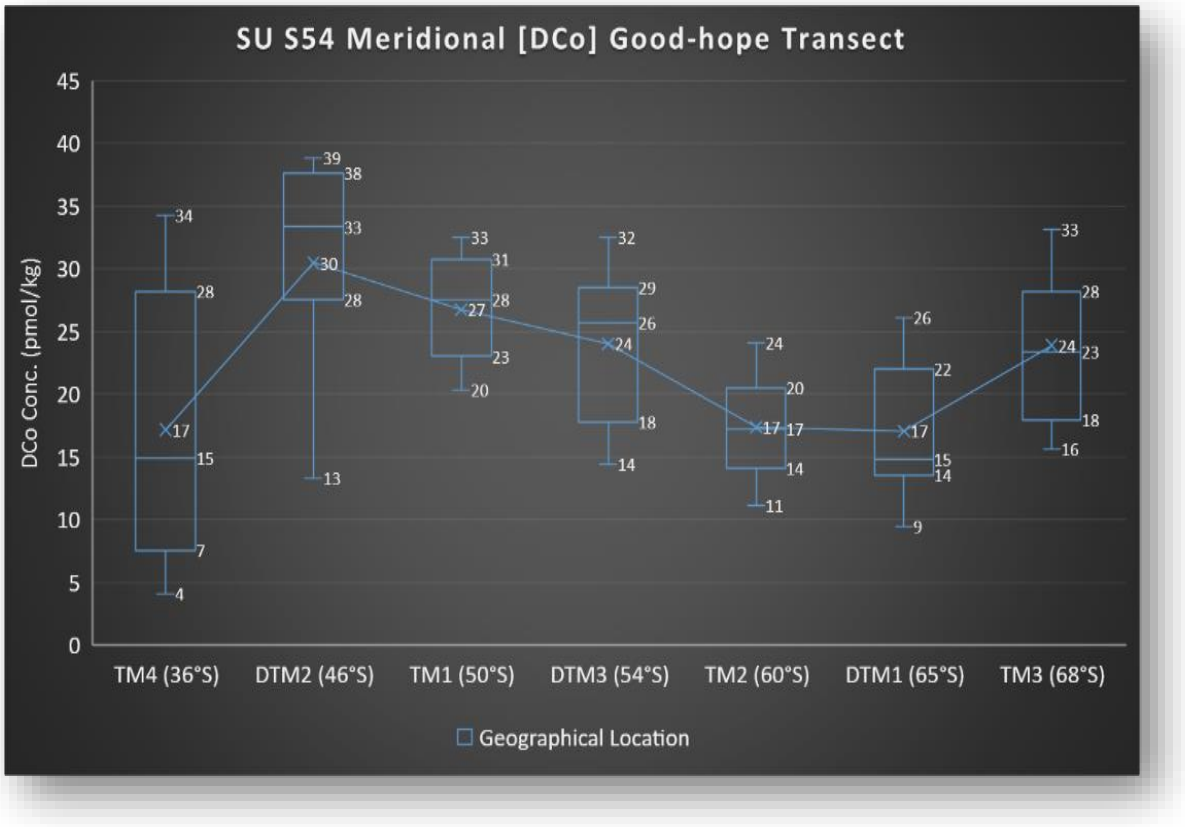

***Figure 25**-The Box and Whisker plot illustrates the North-South DCo concentration (pmol/kg) range for the entire water column. The concentrations are based on the statistical maximum and minimum, exclusive median (more accurate "outlier" identification), upper and lower quartliles, and a mean marker with trendline linking the stations. A notable feature is the decreasing concentrations with increasing latitude. While some minima occur in the surface, others occur at depth.*

The meridional concentration range of Dissolved Cobalt (DCo) for the South Atlantic is presented in figure 25 with the data provided in tables 11-17. The vertical distribution is illustrated in figure 27. DCo concentrations along the cruise transect ranged from ≈ 7 pmol/kg in the strongly depleted sub-surface waters of the STZ at 36°S, to a maximum of ≈ 39 pmol/kg within the sub-surface of the SAF at 46°S. There is an obvious north-south gradient within the ACC that reveals a decrease in DCo concentrations. The station within the STZ is anomalous due to its location within the oligotrophic waters and thus is excluded from the HNLC conditions of the ACC – a good proxy for behaviour nonetheless. The strength of bio-utilization also accounts for the large range in concentration observed at 36°S. Furthermore, the proximity of the station at 68°S to the Antarctic land mass may explain the elevation in DCo concentration observed in the south-eastern edge of the Weddell Gyre. In general concentrations were depleted in surface waters (≈MLD) followed by rapid remineralization leading to an increase to the maximum, only to start decreasing again, within the middle-lower reaches of the sub-surface water layer (≈500m). Concentrations within intermediate (≈500-1700m)

and deep (>1700m) waters are very similar with the trend established in the mid reaches of the intermediate waters keeping constant with depth until conservative behaviour in the lower reaches of the water mass. Concentrations were higher in the ACC as opposed to the Weddell Gyre. The range of concentrations at each locale was generally small – barring 36°S where bio-utilization was high.

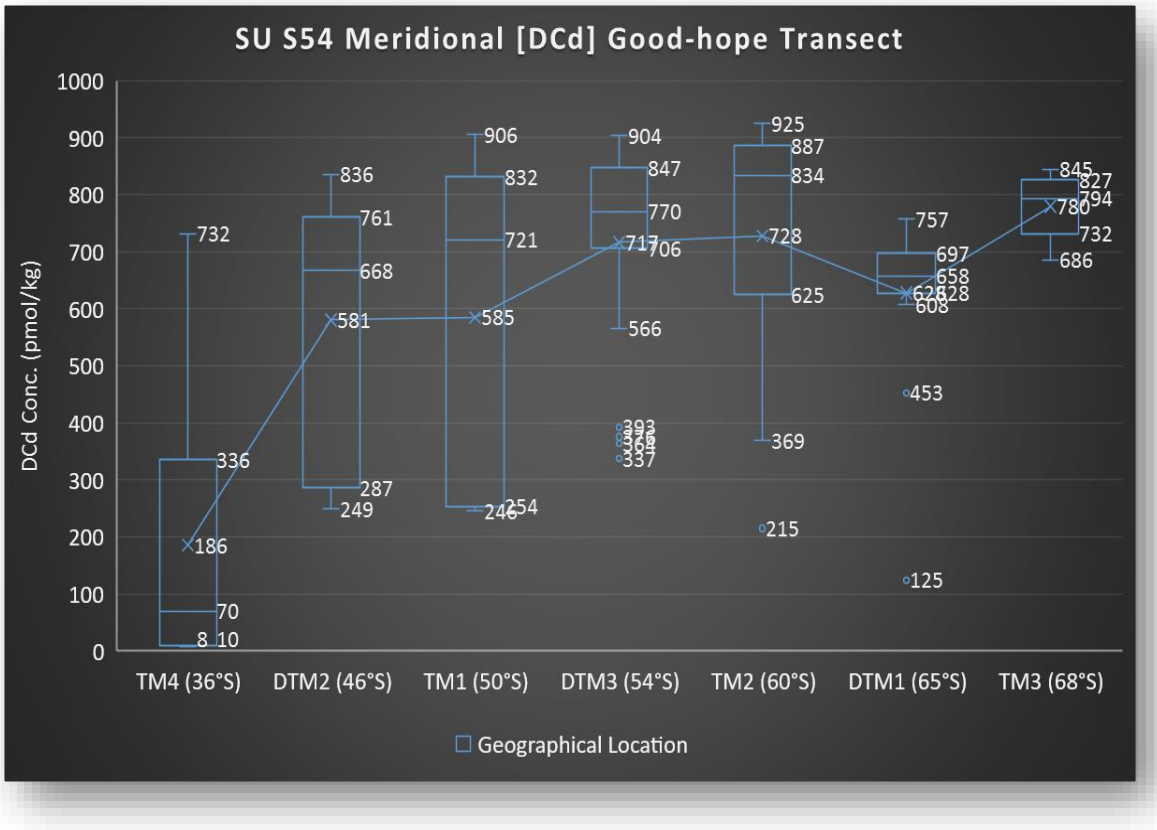

***Figure 26**-The Box and Whisker plot illustrates the North-South DCd concentration (pmol/kg) range for the entire water column. The concentrations are based on the statistical maximum and minimum, exclusive median (more accurate "outlier" identification), upper and lower quartiles, and a mean marker with trendline linking the stations. Note: the "outliers" here are viewed as such due to strong depletion in the surface. The consistency of depletion is a notable feature.*

The meridional distribution of Dissolved Cadmium (DCd) for the South Atlantic is presented in figure 26 with the data in tables 11-17. DCd concentrations exhibited a large range with concentrations of 10 pmol/kg within the heavily depleted waters of the STZ, to 925 pmol/kg south of the SB at 60°S. Moreover, the concentration ranges within each locale mimicked these large concentration ranges owing to depletion of DCd in the surface waters. The consistency of DCd depletion in the surface is a notable feature of the meridional transect – even under low Chl-a conditions. Sub-surface DCd concentrations exhibit a north-south gradient increasing gradient, comparable to that of the macronutrient phosphate corresponding to the shoaling of the UCDW. The highest concentrations of DCd were found in a mid-depth peak observed as a function of the hydrographic water mass control

(Figure 27). The mid-depth DCd peak shoaled consistently from approximately 1000m within the SAF, to 250m within the SACCZ – stabilising within the SACCZ.

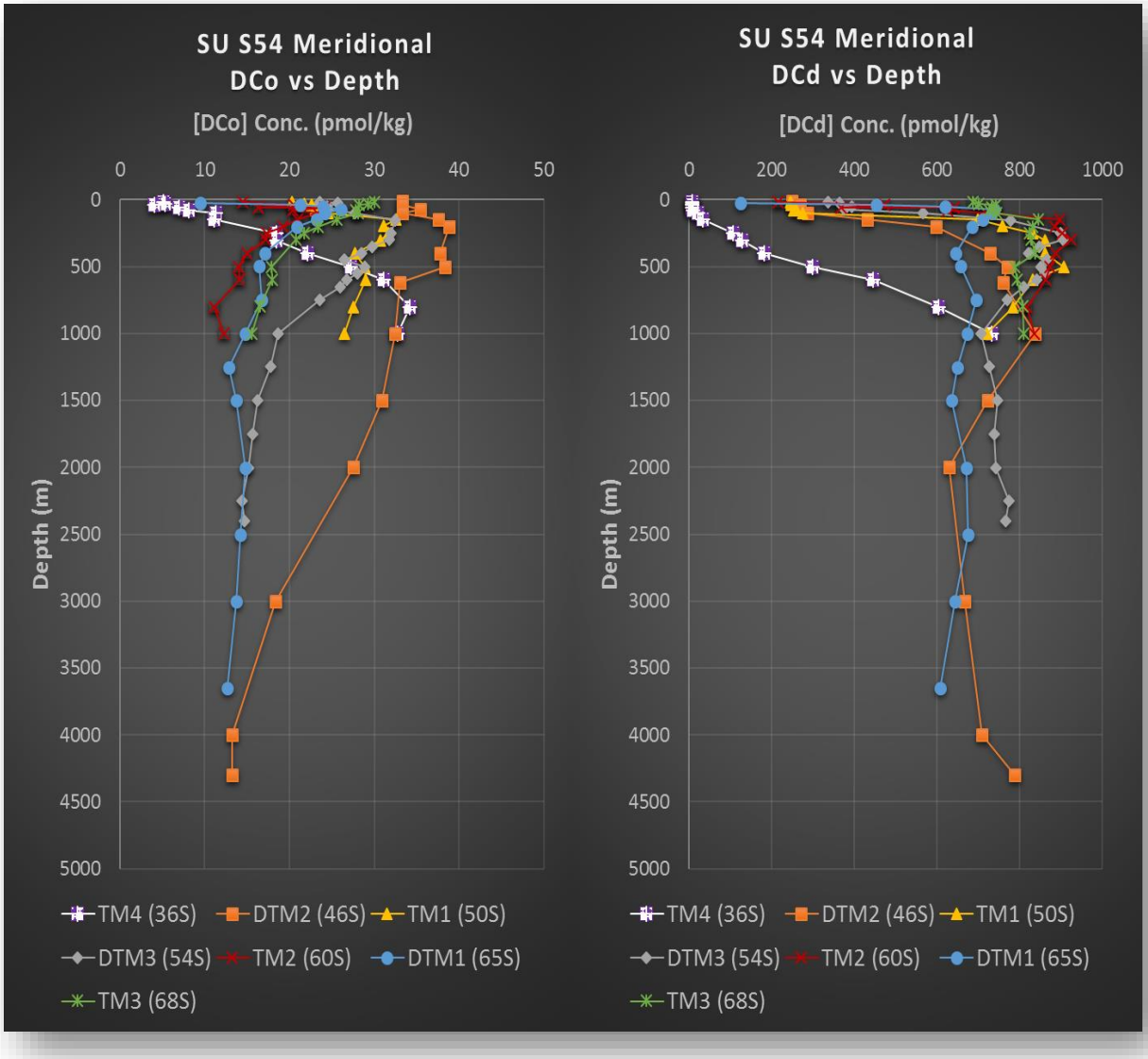

Figure 27*-The vertical and meridional distribution of DCo and DCd given in pmol/kg for the Southern Ocean, Atlantic Sector. The profiles are created as an average of duplicate samples at each respective depth. The consistency of surface depletion and the mid-depth peak are notable features of the DCd profiles. DCo surface depletion is more inconsistent, while shoaling of the scavenging depth is a prominent feature.*

3.4.1 STZ DCo and DCd (TM4; 36°S, 13°E)

***Table 11**-Sub-Tropical Zone (TM4) total (T) and dissolved (D) cadmium and cobalt concentrations corresponding to depth. Calculations omit concentrations with %RSD > 10% - values in blue. One standard deviation reported on duplicate samples, total fraction samples were collected unfiltered in PFA's, dissolved 0.2µm filtered collected in LDPE's. The (ª) represents units (pmol/kg). The (*) denotes that results are an average of respective depths.*

Domain (Station)	Latitude & Longitude	Depth (m)	TCd ª	TCo ª	DCd ª	Std Dev DCd ª	DCo ª	Std Dev DCo ª
STZ (TM4)	36˚ 00.00'S 13˚ 09.71'E	15	16,57	18,02	11,43	2,78	7,66	2,52
		30	18,60	18,35	8,68	0,09	6,69	1,40
		41	16,57	21,20	8,40	0,05	4,10	0,02
		60	17,42	19,57	8,62	0,02	7,00	0,76
		80	23,23	19,68	10,25	0,24	8,09	0,21
		100			21,47	0,38	11,33	1,30
		150	29,70	13,90	33,41	1,63	11,16	0,50
		250	107,27	20,03	106,50	2,87	18,43	0,16
		301	117,62	19,34	128,62	5,55	18,42	0,46
		400	180,52	23,32	181,83	3,21	22,15	0,11
		501	297,46	27,37	299,39	1,31	27,25	1,69
		600	448,65	34,47	445,76	6,28	31,06	0,01
		801	584,19	33,60	604,57	6,39	34,24	0,68
		1000	711,01	35,42	732,09	1,59	32,75	0,25
Maximum			711,01	35,42	732,09		34,24	
Minimum			16,57	13,90	8,40		4,10	
Surface (MLD) *			17,25	19,19	9,50		6,15	
Sub-surface (500m) *			82,49	20,08	79,71		13,10	
Inter (500-1700m) *			510,33	32,71	520,45		31,32	

The observed DCo concentrations at TM4 (36°S), located in the Sub-Tropical Zone (Figure 2), are presented in table 11**.** Concentrations range from 4.10 ± 0.02 pmol/kg – the lowest recorded for the transect - in the strongly depleted surface waters (41m; STSW), consistently increasing (≈0.04 pmol/kg m) through the SAMW to a curiously deep maximum of 34.24 ± 0.68 pmol/kg at 800m in the lower reaches of the AAIW. Mean concentrations of 6.15 pmol/kg, 13.1 pmol/kg and 31.32 pmol/kg are reported for the surface, sub-surface and intermediate depths respectively. The profile correlates exceptionally with the macronutrient profiles (Figures 17-19). The water column DCo/Salinity comparison (Figure 33) presented the only strongly significant salinity correlation with an R^2 = 0.93 and the relationship was given by the equation: [DCo] = 27.61[Salinity] + 982.85. Moreover, DCo exhibits strong nutrient like behaviour as demonstrated by the strong correlation coefficient with PO4 (R^2=0.9545), equated by: [DCo] = 14.47[PO4] +6.591 (Figure 35).

The DCd profile is similarly analogous to the macronutrients phosphate, with a predictable positive DCd concentration gradient of ≈0.74 pmol/kg m (Figure 27). Exceptionally low concentrations of 8.4 ± 0.05 pmol/kg are found in the depleted surface waters (41m; STSW), increasing consistently through the SAMW and the AAIW to reach a maximum of 732.1 ± 1.59 pmol/kg at 1000m (Table 11). The surface sees an average concentration of 9.50 pmol/kg increasing to 74 pmol/kg through the sub-

surface and 520 pmol/kg into intermediate waters. The DCd:PO4 ratio was quantified between 0 and 347 – DCd and PO4 were non-existent in the sub-surface. DCd at the locale demonstrates a strong positive liner correlation with phosphate (PO4) over the entire 1000m sampled water column; equated by [DCd] = 320.23[PO4] – 42.03 and an R^2=0.95 (Figure 32)**.** Concurrently, DCd correlated inversely – the only occurrence on the transect – with salinity; [DCd] = 600.59[Sal] + 21196 with a correlation coefficient: R^2 = 0.90.

3.4.2 SAF DCo and DCd (DTM2; 46°S, 08°E)

Table 12*-Sub-Antarctic Front (DTM2) total (T) and dissolved (D) cadmium and cobalt concentrations corresponding to depth. The data set reports concentrations – corrections for potentially contaminated samples. Data reported in text has been corrected for excessive errors (>10% RSD). One standard deviation reported on duplicate samples, values in red are deemed anomolous, values in blue indicate %RSD > 10%, total fraction samples were collected unfiltered in PFA's, 0.2 µm filtered dissolved fraction in LDPE's. The (ᵖ) represents units (pmol/kg). The (*) deontes that results are an average of respective depths.*

Domain (Station)	Latitude & Longitude	Depth (m)	TCd [a]	TCo [a]	DCd [a]	Std Dev DCd [a]	DCo [a]	Std Dev DCo [a]
SAF (DTM2)	46˚ 00.113'S 08˚ 00.002'E	14	348,07	49,22	249,01	0,57	33,34	0,94
		35	324,63	37,85	268,11	4,70	33,35	1,64
		75	321,00	48,84	269,61	13,40	35,47	2,21
		100	368,12	41,72	286,60	31,76	33,37	5,08
		150	457,45	40,02	431,72	0,84	37,59	0,59
		200	584,55	44,81	597,62	8,41	38,84	0,30
		400	711,69	43,16	727,69	30,50	37,73	1,15
		501	799,08	44,02	769,51	8,35	38,39	1,41
		622	727,83	35,76	760,55	46,08	33,05	1,55
		1000	891,60	36,79	836,17	6,13	32,42	0,36
		1501	752,50	34,68	722,64	37,87	30,87	1,90
		2000	644,25	33,68	629,05	12,17	27,52	1,14
		3000	683,01	21,90	667,70	14,40	18,34	0,79
		4002	706,93	22,24	708,84	19,89	13,29	0,73
		4302	894,34	28,95	787,23	0,87	13,27	0,46
Maximum			894,34	49,22	836,17		38,84	
Minimum			321,00	21,90	249,01		13,27	
Surface (MLD) *			331,24	45,31	262,24		34,05	
Sub-surface (500m) *			489,33	43,71	449,98		36,01	
Inter (500-1700m) *			790,64	35,74	773,12		32,11	
Deep (>1700m) *			732,13	26,69	698,20		18,10	

The analytical data for DCo at DTM2 (46°S), located within the SAF (Figure 2), quantified concentrations in the range 13.27 ± 0.46 pmol/kg to 38.4 ± 1.41 pmol/kg (Table 12). The lowest concentration was recorded in the lower reaches of AADW at 4300m. The highest concentration (38.4 ± 1.41 pmol/kg), recorded in AAIW at 200m in the regenerative zone, was also the highest

concentration recorded for the transect. Characteristically, concentrations remain consistent from the regenerative max at 200m through to 500m – suggesting comparatively delayed scavenging. The imprint indicative of the strength of depletion by marine phytoplankton sees range of 5.5 pmol/kg between the surface and regenerative max. Surface waters (79m; SASW) averaged 34.05 pmol/kg, increasing to 36.39 pmol/kg in the sub-surface waters – the respective "records" for the transect. Concentrations in the sub-surface waters (500m; SASW to AAIW), are notably conservative with regeneration seemingly strong. The depletion by plankton in surface (SASW) waters see a range between 33.3 ± 1.64 pmol/kg to 37.59 ± 0.59 pmol/kg – below peak productivity at 150m. Proceeding down the water column, concentrations decrease constantly after the maximum recorded value to the minimum. DCo versus salinity in the sub-surface waters demonstrated a poor yet, significant (*F = 0.0026, <0.05)* correlation with an $R^2 = 0.07$ and equated by: [DCo] = 31.23[Salinity] – 1021.3 (Figure 33, 37).

The profile for DCd shown in figure 27 is analogous to that of phosphate (Figure 32) mirroring the characteristic maximum concentration kink in the region at 1000m where the column progresses through the downwelling AAIW into the upwelling UCDW. Concentrations ranged from a minimum of 249 ± 0.57 pmol/kg recorded in the surface (SASW) to 836 ± 6.13 pmol/kg recorded at the 1000m "boundary". Ensuing which concentrations decline to 629 ± 12.2 pmol/kg (2000m; UCDW), only to increase again to near the maximum in the LCDW (4300m) – suggesting remineralization (Table 12). The relationship between DCd and PO4 (Cd/P) for the entire water column confirms that there is a strong relationship in the vertical profile of these two elements within the SAF (Figure 32). An average Cd/P spot ratio of 142 was recorded for the surface in the SAF. This ratio increased steadily down the water column to a maximum of 287 before steadily decreasing. Linear regression plots the relationship for the whole water column per: [DCd] = 333.56[PO4] - 281.79, with similarity demonstrated by $R^2 = 0.819$ and significance $F = 2.284E^{-06}$. The correlation is weaker in the surface waters with an $R^2 = 0.5336$ – suggesting superior utilization of DCd. It should be noted that the bottom depth at this station was precariously close to the seabed justifying the late increase in concentration.

3.4.3 PF DCo and DCd (TM1; 50°S; 00°E)

***Table 13**- Polar Frontal (TM1) total (T) and dissolved (D) cadmium and cobalt concentrations and corresponding depth. The data set reports concentrations – corrections for potentially contaminated samples. Data reported in text has been corrected for excessive errors (>10% RSD). One standard deviation reported on duplicate samples, values in red are deemed anomolous, values in blue indicate %RSD > 10%, total fraction samples were collected unfiltered in PFA's, 0.2 µm filtered dissolved fraction in LDPE's. The (ª) represents units (pmol/kg). The (*) deontes that results are an average of respective depths.*

Domain (Station)	Latitude & Longitude	Depth (m)	TCd ª	TCo ª	DCd ª	Std Dev DCd ª	DCo ª	Std Dev DCo ª
PF (TM1)	50°26,99'S 02°00.12'E	16	307,27	24,40	245,60	11,16	20,30	0,83
		31	313,74	23,63	248,25	20,44	21,69	2,63
		40	330,08	30,17	247,15	3,44	22,64	0,40
		60	320,40	25,67	257,46	16,12	23,13	0,94
		78	367,56	27,41	253,52	1,21	23,01	0,59
		100	343,06	26,07	275,90	4,30	24,55	0,24
		150	724,62	33,21	698,59	4,03	32,51	0,24
		198	728,29	31,63	758,77	10,08	31,14	0,02
		251	768,60	30,20	831,51	2,83	31,73	0,38
		303	859,34	31,46	861,58	14,65	30,73	0,11
		400	882,56	30,59	859,94	28,78	27,74	1,06
		500	836,28	27,32	905,86	25,43	28,89	0,46
		599	834,32	26,22	830,61	1,39	28,96	0,34
		800	782,81	29,38	783,03	0,96	27,56	0,29
		1002	729,21	26,67	721,36	6,89	26,51	0,34
Maximum			882,56	33,21	905,86		32,51	
Minimum			307,27	23,63	245,60		20,30	
Surface (MLD) *			330,35	26,22	254,65		22,55	
Sub-surface (500m) *			565,15	28,48	537,01		26,50	
Inter (500-1700m) *			795,65	27,40	810,22		27,98	

DCo concentrations at TM1 (50°S), located within the PF (Figure 2), are quantified in the range 20.3 ± 0.83 pmol/kg to 32.51 ± 0.24 pmol/kg (Table 13). The lowest concentrations were recorded in the surface water (SASW) – owing to biological utilization. The disparity between surface and regenerative zone concentrations sees biological DCo depletion account for 12.21 pmol/kg. The highest concentration was recorded in AAIW at 150m in the regenerative zone – subsequently scavenging commences depleting DCo to the 1000m final depth. Surface waters (100m; SASW) averaged 22.55 pmol/kg, increasing to 26.5 pmol/kg in the sub-surface waters (500m; SASW to AAIW). Proceeding down the water column (UCDW), concentrations decrease continually after the regenerative maximum to 26.51 ± 0.34 pmol/kg – the impact of scavenging.

The profile for DCd shown in figure 27 remains analogous to that of phosphate (Figure 32). The concentration kink has shoaled and is now observed at 500m – shoaling of the upwelling UCDW. Concentrations ranged from a minimum of 245 ± 11.16 pmol/kg recorded in the surface (SASW)

increases through the AAIW to 906 ± 25.43 pmol/kg recorded at the 500m "boundary" layer. Subsequent UCDW concentrations demonstrate a reduction to 721 ± 6.89 pmol/kg at the final depth (1000m). Biological depletion in the surface (SASW) is demonstrated by the preferential utilisation of DCd with a Cd/P ratio of 132 in the euphotic zone, swelling to the 282 maximum near the 200m regenerative peak (Appendix B). Linear regression plots the relationship for the whole water column per: [DCd] = 369.79[P] - 383.33, with similarity demonstrated by R^2 = 0.933 (Figure 32). The correlation is very weak in the surface waters with an R^2 = 0.174 – supporting superior utilization of DCd with respect to PO4.

3.4.4 AAZ DCo and DCd (DTM3; 54°S; 00°E)

***Table 14**-Antarctic Zone (DTM3) total (T) and dissolved (D) cadmium and cobalt concentrations corresponding to depth. Data reported in text has been corrected for excessive errors (>10% RSD) – highlighted in blue. One standard deviation reported on duplicate samples, total fraction samples were collected unfiltered in PFA's, 0.2 µm filtered dissolved fraction in LDPE's. The ([a]) represents units (pmol/kg). The (*) deontes that results are an average of respective depths.*

Domain (Station)	Latitude & Longitude	Depth (m)	TCd [a]	TCo [a]	DCd [a]	Std Dev DCd [a]	DCo [a]	Std Dev DCo [a]
AAZ (DTM3)	53°59,85'S 00°00.01'E	15	426,89	28,41	337,32	2,64	23,56	0,90
		23	533,96	31,36	364,28	2,15	25,68	0,28
		50	514,70	32,28	393,04	23,23	24,46	0,63
		75	406,89	29,60	375,99	3,22	24,43	0,79
		101	596,36	29,25	566,16	9,66	27,77	0,37
		151	848,85	36,54	778,08	11,97	32,47	0,05
		250	856,73	30,12	899,14	5,79	31,96	0,42
		298	927,65	35,36	903,99	46,65	31,77	1,20
		350	802,50	39,08	847,38	48,15	29,79	1,47
		398	848,66	30,46	822,10	1,40	28,51	0,64
		450	814,46	28,03	864,45	23,68	26,46	0,63
		500	838,34	22,98	851,31	20,41	28,87	1,10
		549	812,36	31,45	861,39	75,35	28,05	2,39
		599	804,53	27,77	840,60	15,91	26,72	1,82
		650	830,68	30,24	810,01	44,63	26,03	1,68
		749	750,70	25,48	770,50	39,06	23,60	1,37
		1000	737,72	19,87	706,04	3,04	18,67	0,07
		1250	706,47	16,55	726,00	7,38	17,76	0,19
		1502	747,26	18,21	746,40	17,36	16,26	0,40
		1749	738,59	16,55	738,15	19,53	15,64	0,41
		2001	759,42	14,90	741,19	6,08	15,14	0,31
		2249	759,42	38,08	772,87	18,66	14,42	0,34
		2400	824,51	21,52	765,49	7,81	14,69	0,25
Maximum			927,65	39,08	903,99		32,47	
Minimum			406,89	14,90	337,32		14,42	
Surface (MLD) *			495,76	30,18	407,36		25,18	
Sub-surface (500m) *			701,33	31,12	666,94		27,98	
Inter (500-1700m) *			778,51	24,07	789,03		23,25	
Deep (>1700m) *			770,48	22,76	754,42		14,97	

DCo concentrations at DTM3 (54°S), located within the AAZ (Figure 2), are quantified in the range 14.42 ± 0.34 pmol/kg to 32.47 ± 0.05 pmol/kg (Table 14). The lowest concentrations were recorded in the deep waters of the southward shoaling LCDW (Figure 27). DCo was strongly scavenged at a predictable rate (± 0.01647 pmol/kg m) between the regenerative maximum at 150m and 1000m – spanning the AAIW through to the lower region of the UCDW. Concentrations subsequently stabilised as scavenging weakened in the LCDW – conserving DCo at ± 15 pmol/kg. The disparity between surface

(AASW) and regenerative zone optimal concentrations accredits an 8.91 pmol/kg drawdown owing to biological depletion. The highest concentration was recorded in AAIW at 150m in the regenerative zone. Subsequently, scavenging depletes DCo through the AAIW and UCDW until stabilisation in the LCDW. Surface waters (100m; AASW) averaged 25.18 pmol/kg, increasing to 27.98 pmol/kg in the sub-surface waters (500m; AAIW to UCDW). Proceeding down the water column, concentrations decrease through the intermediate depths to 23.25 pmol/kg to stabilize in the deep water (LCDW).

The profile for DCd shown in figure 27 remains analogous to that of phosphate (Figure 32). The concentration kink has shoaled and is now observed at 300m – continued shoaling of the upwelling UCDW. Concentrations ranged from a minimum of 337 ± 2.64 pmol/kg recorded in the surface (AASW) increasing rapidly, through the narrow AAIW (100-150m) into the UCDW, to 904 ± 46.65 pmol/kg recorded at 300m in the "boundary" layer – near maximum for the transect. Subsequent concentrations in the UCDW decrease to 706 ± 3.04 pmol/kg at 1000m where border to the LCDW is found. Concentrations subsequently increase to 772 ± 18.66 pmol/kg at the 2400m final depth. The surface (100m; AASW) DCd/P ratio of 256 suggests sub-optimal bio-utilization of DCd in the euphotic zone (Appendix B). Linear regression plots the relationship for the whole water column per: [DCd] = 538.88[PO4] - 432.62, with the correlation demonstrated by an $R^2 = 0.9293$ (Figure 32). The correlation improves ($R^2 = 0.9416$) in the surface waters (100m, AASW).

3.4.5 South SB (SACCZ) DCo and DCd (TM2; 60°S; 00°E)

***Table 15**-Weddell Gyre (North-East) (TM2) total (T) and dissolved (D) cadmium and cobalt concentrations corresponding to depth. Data reported in text has been corrected for excessive errors (>10% RSD) – highlighted in blue. One standard deviation reported on duplicate samples, total fraction samples were collected unfiltered in PFA's, 0.2 µm filtered dissolved fraction in LDPE's. The ([a]) represents units (pmol/kg). The (*) deontes that results are an average of respective depths.*

Domain (Station)	Latitude & Longitude	Depth (m)	TCd [a]	TCo [a]	DCd [a]	Std Dev DCd [a]	DCo [a]	Std Dev DCo [a]
Weddell Gyre (TM2)	59°59,95'S 00°00.02'E	16	433,35	27,61	215,16	1,23	14,48	0,48
		41	546,35	22,36	473,32	5,55	20,48	0,20
		58	497,95	21,97	368,77	5,95	16,33	1,30
		60	684,08	34,09	641,89	5,47	24,12	0,07
		79	685,51	23,45	624,72	2,41	20,43	0,86
		100	739,67	22,36	719,12	18,61	23,27	0,50
		150	807,37	18,88	896,40	0,21	20,94	0,03
		199	897,46	19,77	884,64	25,79	19,24	0,63
		251	844,17	17,25	902,36	22,71	17,26	0,67
	(n=1)	300	904,00	19,79	924,64	6,41	17,22	!
		399	935,37	16,74	886,59	7,69	14,97	0,13
		500	869,65	16,17	872,39	2,32	14,03	0,33
		599	883,42	13,96	862,76	12,91	14,12	1,21
		800	869,04	12,83	816,70	5,08	11,09	0,38
		1001	776,73	10,89	834,42	7,32	12,32	0,66
Maximum			935,37	34,09	924,64		24,12	
Minimum			433,35	10,89	215,16		11,09	
Surface (MLD) *			489,85	24,99	344,24		17,48	
Sub-surface (500m) *			737,08	21,70	700,83		18,56	
Inter (500-1700m) *			849,71	13,46	846,57		12,89	

DCo concentrations at TM2 (60°S), located south of the SB (SACCZ) in the north-eastern domain of the Weddell Gyre (Figure 2), are quantified in the range 11.09 ± 0.38 pmol/kg to 24.12 ± 0.07 pmol/kg (Table 15). The lowest concentrations were recorded in the deep waters of the southward shoaling UCDW at the 800m LCDW depth boundary (Figure 27). Characteristically, DCo was strongly scavenged below the further shoaled (60M) regenerative maximum up to 800m in the UCDW. A single depth in the LCDW supports the hypothetical absence of scavenging in the water mass – increase to 12.32 ± 0.66 pmol/kg. The disparity between surface (AASW) and regenerative zone optimal concentrations accredits a 9.64 pmol/kg drawdown owing to biological depletion. Subsequently, scavenging depletes DCo through the UCDW until stabilisation in the LCDW. Surface waters (50m; AASW) averaged 17.48 pmol/kg, increasing to 18.56 pmol/kg in the sub-surface waters (500m; UCDW), and decreasing strongly in the intermediate waters to 12.59 pmol/kg.

DCd concentrations at 60°S range between 215 ± 1.23 pmol/kg recorded in the surface (AASW) increasing markedly to 925 ± 6.41 pmol/kg (UCDW) – the highest of the transect. The concentration

kink produced by the "boundary" layer has shoaled slightly to 250m – sustained shoaling of the upwelling UCDW. Subsequent concentrations in the UCDW decrease to 816 ± 5.08 pmol/kg at 800m where border to the LCDW is found. Concentrations subsequently increase to 834 ± 7.32 pmol/kg at the 1000m final depth. The surface (50m; AASW) DCd/P ratio of 110 suggests mediocre bio-utilization of DCd in the euphotic zone (Appendix B-Table B12). Linear regression plots the relationship for the whole water column per: [DCd] = 529.45[PO4] - 419.58, with the correlation demonstrated by a weak R^2 = 0.788 (Figure 32).

3.4.6 Eastern Weddell Gyre (SACCZ) DCo and DCd (DTM1; 65°S; 00°E)

***Table 16**-Weddell Gyre (East) (DTM1) total (T) and dissolved (D) cadmium and cobalt concentrations corresponding to depth. Data reported in text has been corrected for: excessive errors (>10% RSD) highlighted in blue, and absolute errors in red. One standard deviation reported on duplicate samples, total fraction samples were collected unfiltered in PFA's, 0.2 µm filtered dissolved fraction in LDPE's. The (ª) represents units (pmol/kg). The (*) deontes that results are an average of respective depths.*

Domain (Station)	Latitude & Longitude	Depth (m)	TCd [a]	TCo [a]	DCd [a]	Std Dev DCd [a]	DCo [a]	Std Dev DCo [a]
Weddell Gyre (DTM1)	65˚00.15'S	25	480,92	31,79	124,69	3,79	9,46	0,12
	00˚ 00.45'E	39	700,56	28,96	452,78	1,46	13,36	7,87
		51	702,95	28,75	619,91	19,97	24,01	0,95
		70	761,33	29,88	737,80	1,98	26,09	0,38
		100	758,66	28,35	731,83	26,79	24,12	0,70
		151	674,98	27,95	710,07	2,62	23,16	0,22
		200	683,25	22,31	684,35	0,48	20,87	0,16
		400	616,51	72,38	645,97	12,24	17,15	0,01
		498	647,75	18,24	657,97	3,62	16,40	0,03
	(n=1)	749	657,33	30,24	757,20		16,69	
		1001	702,53	20,97	672,09	4,82	14,84	0,45
		1251	660,92	15,06	648,19	26,14	12,84	0,37
		1501	637,99	13,82	635,51	13,40	13,76	0,18
		2002	576,54	16,76	671,69	11,44	14,77	0,50
		2501	650,61	29,33	675,45	1,86	14,24	0,54
		3001	635,00	18,85	642,59	12,42	13,75	0,41
		3650	577,32	36,83	607,83	20,31	12,66	0,61
Maximum			761,33	36,83	737,80		26,09	
Minimum			480,92	13,82	124,69		9,46	
Surface (MLD) *			628,14	29,84	399,13		16,73	
Sub-surface (500m) *			669,66	27,03	596,15		20,16	
Inter (500-1700m) *			664,69	20,02	651,93		14,53	
Deep (>1700m) *			609,87	25,44	649,39		13,85	

The vertical distribution of DCo at DTM1 (65°S), located in the south-eastern region of the Weddell Gyre (Figure 2). Concentrations range from 9.46 ± 0.12 pmol/kg in the surface water, to a maximum of 26.1 ± 0.38 pmol/kg just below the chl-a max at 70m – peak remineralization (Table 16).

Concentrations in the surface (AASW) are strongly depleted demonstrated by the 16.63 pmol/kg drawdown in the euphotic zone – the strongest uptake recorded during the cruise. This corresponds to the remarkably high chl-a concentration recorded at this station (Figure 23). Proceeding down the water column concentrations in the LCDW decrease strongly due to sorption onto marine particles until 1000m where after concentrations remain conservative around 13.8 ± 0.79 pmol/kg. The shape of the DCo and temperature profiles are notably alike in this region (Figure 21, 27). The surface (MLD) water DCo comparison made to salinity (Figure 37) indicated a strong correlation with an R^2 = 8345 and the relationship was given by the equation: [DCo] = 22.62[Salinity] – 753.42.

The DCd profile is analogous to that of phosphate and salinity which are markedly constant beneath the surface waters (Figure 21, 27, 32). Concentrations in the surface (55m; AASW) range from 124 ± 3.79 pmol/kg to 737 ± 1.98 pmol/kg below the chl-a max (40m) at 70m signifying depletion in the surface euphotic zone (Table 16). Proceeding through the water column concentrations in the LCDW decrease to 645 ± 12.24 pmol/kg before remaining constant at 656 pmol/kg. Dissolved Cd showed a moderate linear relationship with PO4 in the water column: R^2 = 0.7905, equated by: [DCd] = 647.35[P] - 777.91 (Figure 32). As anticipated the relationship was stronger in the surface R^2 = 0.9992. Depletion by phytoplankton impart a DCd/P ratio of 80 in the surface increasing to 335 below the euphotic zone – demonstrating rapid utilization of DCd relative to phosphate. The phosphate concentration at depth 24m was essential to characterisation however, the value had to be extrapolated for with the calculation based on the decreasing concentration trend observed in the surface.

3.4.7 South-Eastern Weddell Gyre (SACCZ) DCo and DCd (TM3; 68°S; 00°E)

***Table 17**-Weddell Gyre (South-East) (TM3) total (T) and dissolved (D) cadmium and cobalt concentrations corresponding to depth. Data reported in text has been corrected for excessive errors (>10% RSD) – highlighted in blue. One standard deviation reported on duplicate samples, total fraction samples were collected unfiltered in PFA's, 0.2 µm filtered dissolved fraction in LDPE's. The (ª) represents units (pmol/kg). The (*) deontes that results are an average of respective depths.*

Domain (Station)	Latitude & Longitude	Depth (m)	TCd ª	TCo ª	DCd ª	Std Dev DCd ª	DCo ª	Std Dev DCo ª
Weddell Gyre (TM3)	67°58,04'S 00°01.12'E	15	744,36	45,17	685,82	35,13	30,05	1,65
		30	766,49	39,42	701,32	15,37	29,23	1,85
		40	770,07	67,48	742,68	4,42	28,20	0,53
		60	727,42	38,89	732,23	5,30	33,13	4,32
		80	714,56	33,87	725,38	11,01	27,79	0,49
		99	730,94	47,83	744,93	10,48	28,12	0,18
		150	810,73	33,66	844,73	18,37	25,65	0,21
		201	830,66	27,62	831,88	13,74	23,35	0,18
		250	835,75	23,83	824,07	6,53	21,73	0,11
		301	788,65	65,59	826,52	5,00	20,80	0,08
		400	790,99	19,51	836,33	9,18	22,20	2,57
		501	795,23	24,05	787,07	14,89	17,91	0,12
		600	799,71	47,48	793,63	9,96	17,96	0,52
		799	820,58	36,71	807,59	18,61	16,53	0,70
		1000	812,89	47,29	809,61	0,33	15,58	0,67
Maximum			835,75	67,48	844,73		30,05	
Minimum			714,56	714,56	685,82		15,58	
Surface (MLD)			744,58	44,97	717,49		28,82	
Sub-surface (500m)			775,49	38,91	773,58		25,28	
Inter (500-1700m)			807,10	38,88	799,47		17,00	

DCo concentrations at TM3 (68°S), located south of the SB (SACCZ) in the south-eastern domain of the Weddell Gyre (Figure 2), are quantified in the range 15.58 ± 0.67 pmol/kg to 30.05 ± 1.65. pmol/kg (Table 17). The lowest concentrations were recorded in AABW at 1000m – final depth (Figure 27). Uniquely, DCo was not depleted in the surface (86m; AASW), conversely, the maximum concentration was measured at 15m – this may suggest an external source. Scavenging is the dominant control through the 1000m sampling depth – prominent after the first depth and reducing constantly towards the final depth. Chl-a concentrations were the lowest for the cruise. Surface waters (86m; AASW) averaged 28.82 pmol/kg, decreasing to 25.28 pmol/kg in the sub-surface waters (500m; LCDW and AABW), and decreasing strongly in the intermediate waters to 17.00 pmol/kg. The DCo vs Salinity correlation in the surface was slightly inverse and extremely weak (R^2=0.0001) with no apparent depletion: [DCo] = 0.090[Sal] +32.77 (Figure 37).

The profile for DCd is illustrated in figure 27 with the data in table 17. Concentrations range between 686 ± 35.13 pmol/kg recorded in the surface (AASW) increasing to 845 ± 18.73 pmol/kg

(LCDW) – the lowest surface to depth differential for the transect. The concentration kink is absent with concentrations remaining around ± 817 pmol/kg between 150m (regenerative peak) and 1000m. There is a minor decrease at the 400m boundary between the LCDW and the AABW only for a subsequent observable increase. The surface (86m; AASW) DCd/P ratio was calculated at 339 relative to a mean of 352 for the water column – supporting poor bio-utilization of DCd in the euphotic zone – correspondingly low Chl-a concentrations. Linear regression plots the relationship for the whole water column per: [DCd] = 315.14[PO4] + 81.83, with the correlation demonstrated by a weak R^2 = 0.5681 (Figure 32).

4. Discussion

4.1 Phytoplankton Community Structures

The resident phytoplankton community structures were mapped by Viljoen (2016) using a CHEMTAX approach to differentiate functional groups (Figure 28). Samples were collected through the underway system and summarise the community structures within the foremost 10m of the water column. Phytoplankton functional group composition allow crucial insights regarding the biological acquisition ratios of trace metals by correlating them to the representative group requirements. However, samples taken at 10m are typically variable relative to the representative community dominating at the Chl-a max (Viljoen, 2016)vil. Nonetheless, while the community may not be entirely representative the surface sample community does enable a breakdown of the plankton species/trace metal requirements for the region.

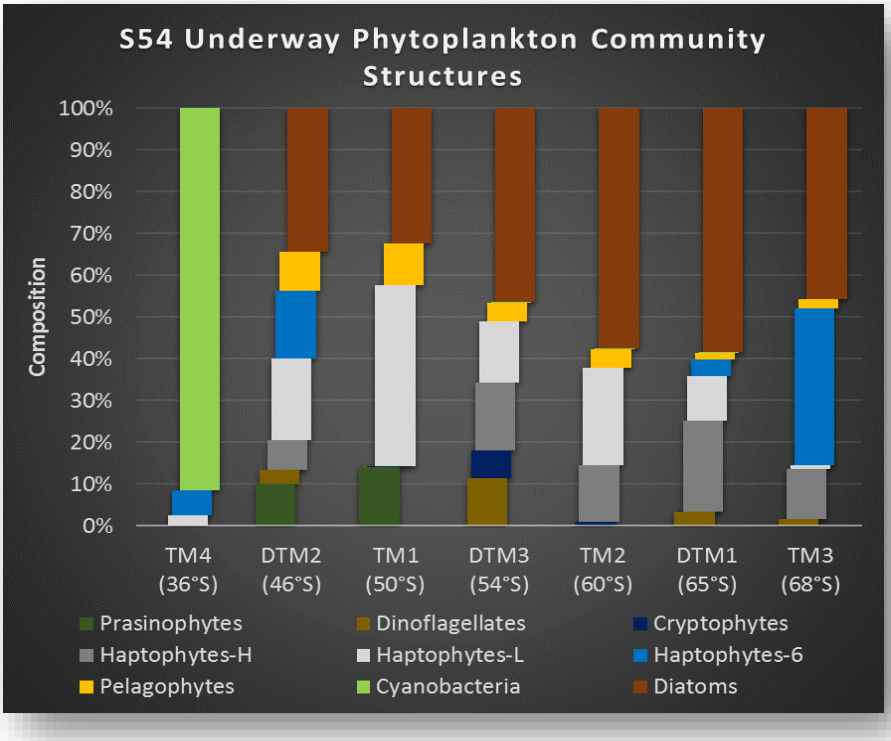

***Figure 28**-The meridional phytoplankton community structures constructed by Johann Viljoen* (Viljoen, 2016) *using underway (10m depth) samples collected during the SANAE 54 voyage. It should be noted that the community composition may not be representative of the community structure at depth.*

Furthermore, bioassay experiments were performed by Van Horsten (2015), at two locations: DTM2 (46°S) and DTM1 (65°S). The results in figure 29 demonstrate controlled growth experiments of phytoplankton under: normal conditions; median light (L2) with added Fe; median light (L2) with no added Fe; high light (L3) with added Fe; and high light (L3) with no added Fe. The results of the

experiment at DTM2 (46°S) suggest that light is a key factor limiting growth. The DCo/DFe correlation for this region supports the sub-optimal utilization of trace metals DCo and DFe through Conversely, the data at DTM1 (65°S) supports Fe limitation where the greatest growth occurs under the L2 added Fe condition. Low Fe concentrations may be limiting growth in the Haptophyte-H community (DTM1 65°S). However, low Fe cannot account for entirely for large increase in the total biomass at DTM2. It is likely that the small variation seen between light with Fe and light with no Fe at DTM2 (46°S) is a consequence of another factor resulting in co-limitation. Further, under high light conditions a resident community not adapted to this phenomenon may experience photodegradation resulting in a decline in light susceptible species biomass. The data reiterates the need for a thorough understanding of community structure and genetic adaptation when studying the surface trace metal concentrations. Moreover, the genetic adaptation of a community to region specific characteristics, may see variable behaviour of the same species in different regions. A community accustomed to light limitation may not demonstrate full utilization of increased light due to an adaptation in the chl-a reaction centres responsible for the absorption of light. It follows that phytoplankton growth may be inhibited by variable co-limitation of trace metals Co and Cd.

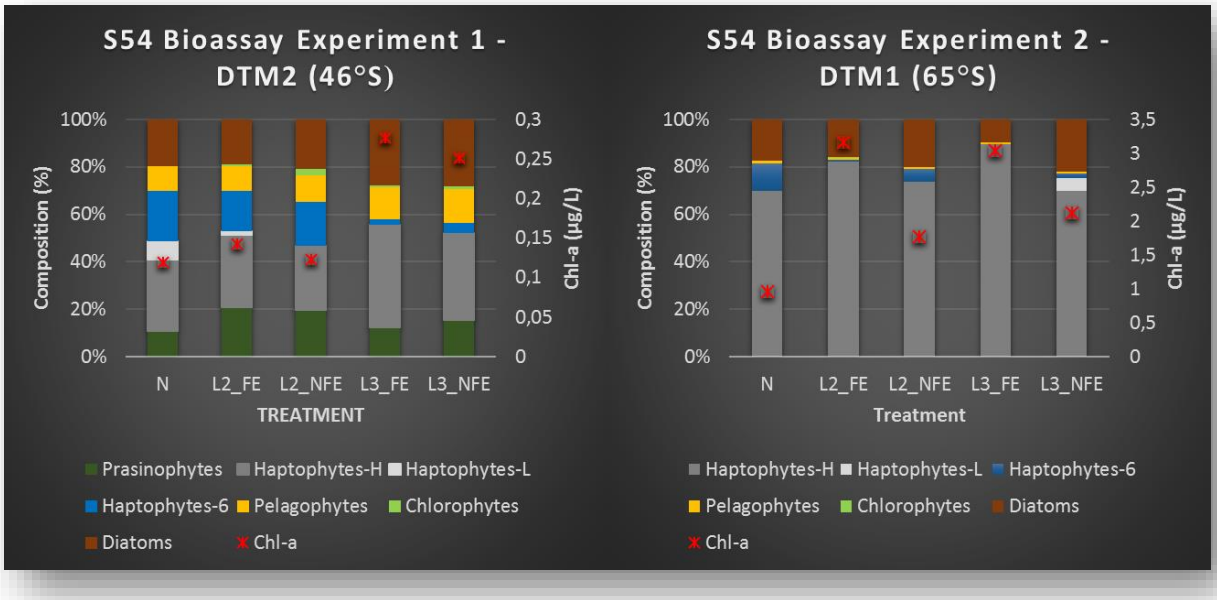

Figure 29*-The results of Bioassay incubation experiments performed at 46°S and 65°S* Van Horsten (2015) *during the SANAE 54 voyage. The experiment applied various Fe and light supplementation to the phytoplankton communities. (N) denotes control sample, (L) denotes light strength setting, (Fe) denotes Fe supplementation, (NFe) no Fe supplementation.*

4.2 Southern Ocean, Atlantic Sector Cobalt and Cadmium Distribution and Controls

The distribution and controls of Co and Cd in the Southern Ocean Atlantic Sector are still poorly reported with limited contribution to consensus data. DCo concentrations in this sector are yet to be incorporated into the GEOTRACES database, and while limited DCd concentrations have been incorporated, supplementary information may further constrain biogeochemical cycling. Moreover, the contrasting bio-geochemical provinces – controlled in part by the frontal zones and trace metal bioavailability – coupled with the seasonality impacting the structure of the phytoplankton community and blooms, reaffirms the importance of reoccupying this region. The biological utilization of DCo and DCd in the euphotic zone will typically present as a strong coupling between the DCo/DCd and PO4 cycles. However, while DCd remains strongly coupled throughout the water column, DCo cycles will likely become decoupled after remineralization – a consequence of scavenging.

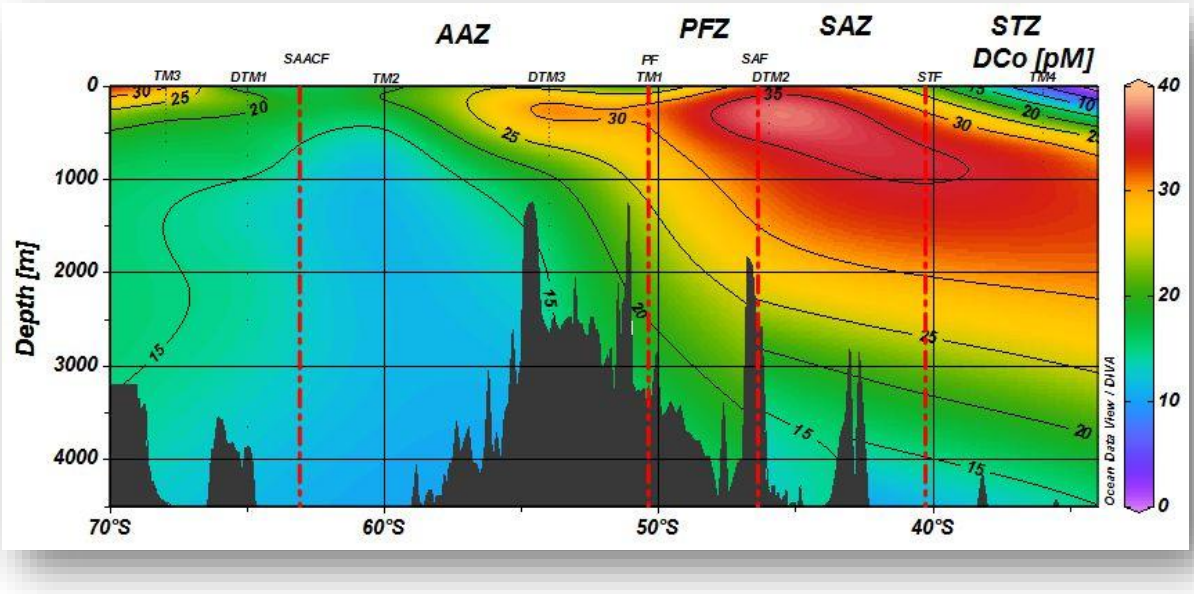

Figure 30- *Southern Ocean Dissolved Cobalt (DCo) presented in an ODV contour plot. Concentrations were quantified using a multi-elemental ICP-MS technique. The frontal regions are delineated the same as this study-barring the SACCF. The SB (60°S) was used as the Weddell Gyre boundary in this study. South of the SAF DCo concentrations decrease. The high DCo concentration at DTM2 within the SAZ may be a consequence of atmospherically supplemented DCo enriching the downwelling AAIW. Scavenging is pronounced with the UCDW.*

The concentrations of DCo exhibit a unique southerly decreasing trend (Figure 27, 30), whereas the balance of trace metals exhibit increasing concentrations towards the south. It is likely that DCo is further removed from its source region – perhaps near the SAF. Conversely, the shoaling of the scavenging depth may remove more DCo from the water towards the south. Moreover, organic ligands play a major role in the distribution of Co by preferentially binding free bioactive metal ions below the surface thereby controlling the concentration (Saito and Moffett, 2001; Bown *et al.*, 2011). The

comparative increase in other trace metals may result in increased competition for organic complexation by these elements; thereby relaxing the complexation of DCo in Co-binding ligands and producing a greater bioavailable fraction. Studies have shown that when Co-binding ligand concentrations are present in excess of the total DCo concentrations, the entire fraction of DCo was organically bound (Ellwood and Van den Berg, 2001). The phytoplankton data suggests that coccolithophores contributed to a large portion of the species composition within the SACCZ, regardless of the lower DCo concentrations– perhaps due to the greater bio-availability. Bulbous concentrations of coccolithophore species, under elevated DCo, advocate for an *E.Huxleyi* community experiencing optimal growth (Sunda and Huntsman, 1995; Saito and Moffett, 2002). Incubation studies in the Ross Sea by Bertrand et al. (2007) have shown that where bacterial and archaeal abundance was highest, the least stimulation upon B12 addition (with supplementary Fe) was seen. Conversely, regions scarce in bacteria and archaea showed the greatest stimulation under B12 supplementation in a *Phaeocystis* colony. However, they found that diatoms (*P. subcurvata*) were the primary benefactors of Fe-B12 additions, substantiating the idea that while diatoms require an external source of B12, lacking biosynthetic pathways. Moreover, under no circumstances did Bertrand et al. (2007) find that B12 alone resulted in significant stimulation – primary limitation by Fe.

Furthermore, while DCd is expected to compare well with the literature available, DCo may see a comparative underestimation when compared to studies employing a UV-Oxidation step prior to analysis – DCo in the surface oceans may present in nonreactive forms due to interactions with strong ligands. Given that the quantification of DCo is dependent on the metal affinity to the resin used in pre-concentration, an underestimation will result when the ligand is a stronger competitor for binding than the resin – as is often the case for DCo (Biller and Bruland, 2012). Samples for the dissolved fraction in this study were filtered (0.2µM), thus it is expected that the organic ligand interference potentially limiting the quantitative recovery of DCo, stem largely from the colloidal organic carbon (COC, <0.2 µM). Consequently, “true” recovery of the total dissolved fraction is said to require a UV-Oxidation step. However, herein lies the rationale behind omitting the UV-Oxidation step in this study. While some marine phytoplankton (cyanobacteria) may release “cobalophores”, akin to the siderophores responsible for Fe uptake and sequestration (Morel and Price, 2002; Saito and Moffett, 2002), certain species may lack this functionality, and no other ligands have been shown to specialize in uptake rather than detoxification (Morel and Price, 2002). Thereby, ligand bound DCo may not present in the bioavailable fraction to these communities, effectively rendering this fraction blind. Nonetheless, in the UV oxidation of SAFe (D2) deep-water reference material, Milne et al. (2010) found the concentration of Co increased by approximately 50% after 1 hr, while after 1 hr Biller & Bruland (2012) found that complete metal recovery resulted in an approximately 33% increase in the dissolved

Co concentration. Milne et al. (2010) also subjected the SAFe surface water sample (S1) to the process; their results indicated no significant change. Several organically bound trace metals (Fe, Mn, Ni, Cd and Zn) were found to exhibit no response to UV-Oxidation. Perhaps a more systematic way to quantify the total dissolved fraction concentrations, would be to perform a dual experiment with, and without UV-Oxidation; thereby, enabling the quantification of the organically bound metal ion and the free metal ion, further constraining the behaviour of bioactive trace metals. Considering all the evidence, UV-Oxidation of samples is likely a necessity where the concentrations for the total dissolved fraction (free and organically bound metal ions) are concerned.

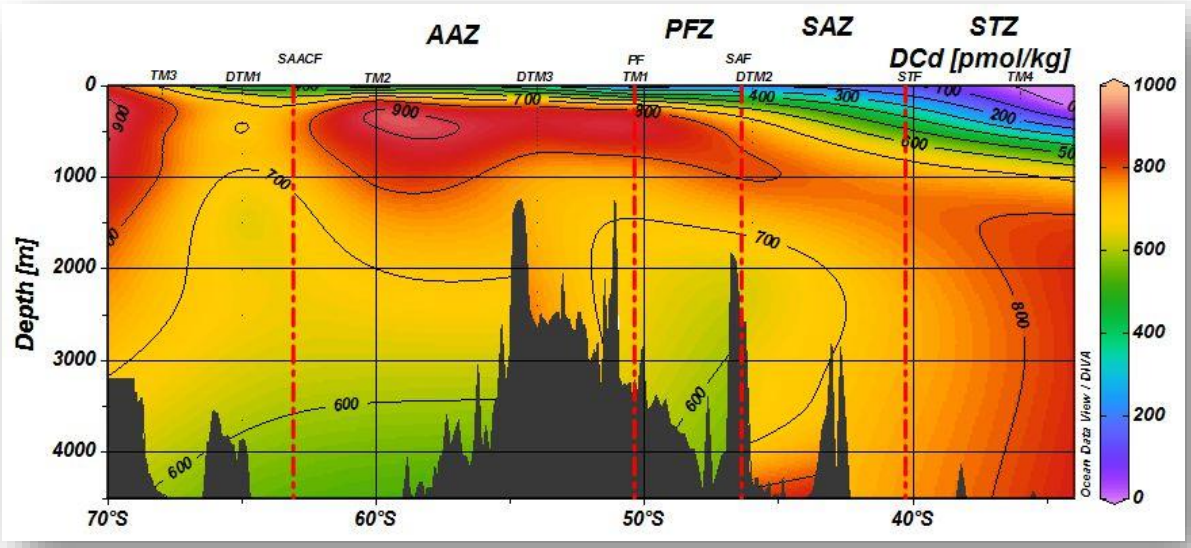

Figure 31*-Southern Ocean Dissolved Cobalt (DCo) presented in an ODV contour plot. Concentrations were quantified using a multi-elemental ICP-MS technique. The frontal regions are delineated the same as this study-barring the SACCF. The SB (60°S) was used as the Weddell Gyre boundary in this study. South of the SAF DCo concentrations decrease. The high DCo concentration at DTM2 within the SAZ may be a consequence of atmospherically supplemented DCo enriching the downwelling AAIW. Scavenging is pronounced with the UCDW.*

The meridional DCd concentrations exhibit a southerly increasing trend, akin to the trend for the balance of trace metals (Figure 27, 31). The sources for Cd are posited to be “in situ” with surface waters depleted by biotic uptake/detoxification, and resupplied by vertical mixing and remineralization. The behavioural characteristic resulting in a mid-depth peak substantiates that the source is ‘in-situ”. It is likely that DCd surface concentrations are controlled by the shoaling of the AAIW and UCDW boundary – elevating concentrations and responsible for the resupply. The concentrations of DCd reported in this study should correspond with studies reporting conditions, controls and biogeochemical regimes akin to those traversed herein. Bloom conditions are expected to cause some deviation yet, the Cd/PO4 ratio should respond accordingly. However, strong diatom blooms may preferentially utilize/detoxify Cd over PO4. The correlation further suggests that the

remineralization of these elements from organic debris, takes place at similar rates – perhaps a metabolic function for DCd. The utilization of DCd in the foremost 200m of the water column is remarkably consistent for the transect– even under low Chl-a concentrations. Evidence indicates that Cd can nutritionally substitute for Zn in certain key Zn enzymes – such as carbonic anhydrase. However, the consistency of utilization under low Chl-a indicates an alternative mechanism – such as detoxification – may also contribute to DCd depletion in the surface.

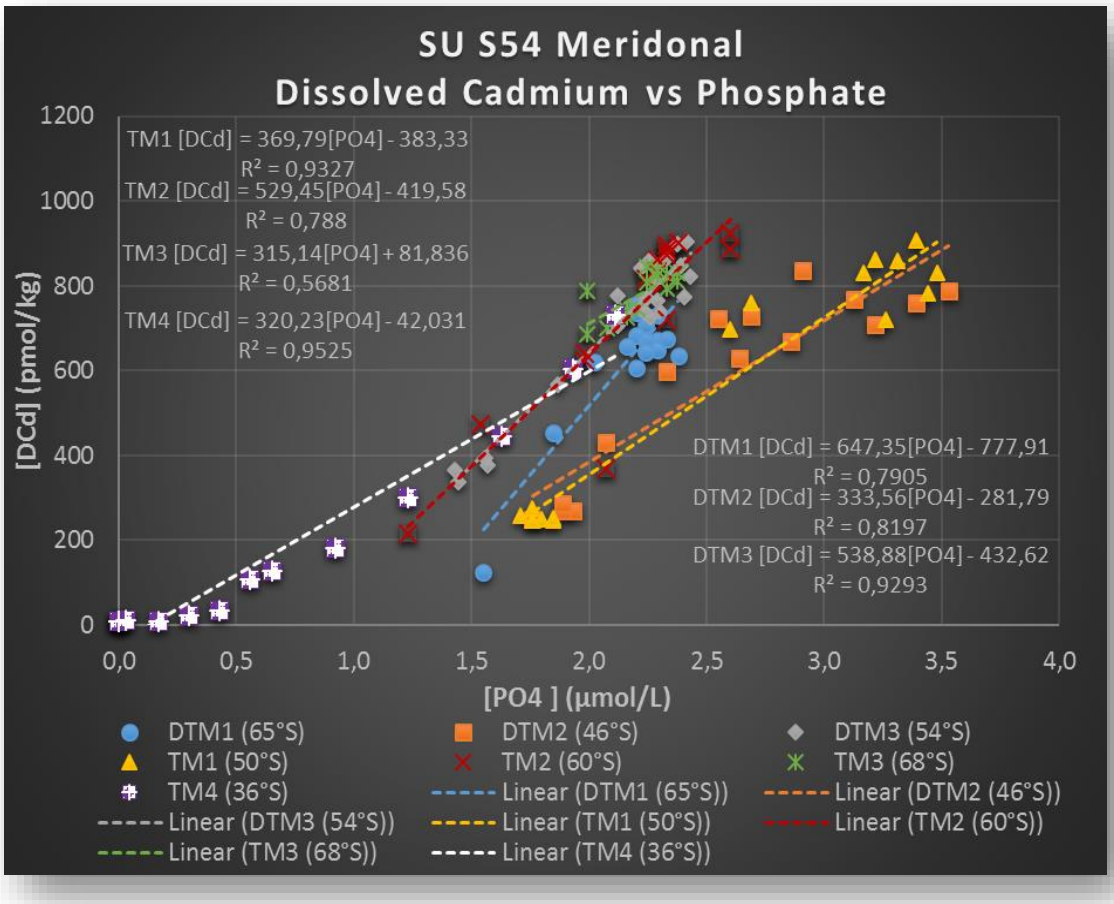

Figure 32*-The linear relationship between dissolved Cadmium and Phosphate for the whole water column. The utilization and remineralization/recycling of DCd and PO4 are uniquely similar resulting in the trend seen. Concentrations typically increase with depth. This relationship may deviate in the surface because of DCd or PO4 preferential utilization. Higher concentrations of PO4 are available within the deeper waters of the SAF (DTM2) and the PF (TM1).*

The terrestrial input sources of bioactive trace metals have not been constrained to a reasonable degree in the Southern Ocean. Largely, the origin of the elevated concentrations of DCo in the euphotic zone has been attributed to inputs from atmospheric dust (Jickells and Burton, 1988). The DCo/Salinity water column correlation was generally poor throughout the transect (Figure 33). DCo concentrations typically decrease regardless of changes in salinity below the regenerative zone – a function of scavenging. This substantiates a surface down input of DCo as opposed to inherent concentrations controlled by deep remineralization and advective upwelling. Continental source regions are thought

to include Patagonia and Australia (Jickells and Burton, 1988; Klunder *et al.*, 2011). However, HYSPLIT models run in the study suggest that air masses from the Antarctic Peninsular are prevalent over the South Atlantic – the dust flux however is uncertain (Figure 38). Further trace metals sources could stem from contact with continental margins, hydrothermal vent complexes and glacial melts rich in entrained sediments (Klunder *et al.*, 2011; Boye *et al.*, 2012). Alternatively advection and upwards mixing of deeper water masses, enriched in dissolved trace metals may play a more prominent role in supplying surface waters with essential micro and macronutrients (Boye *et al.*, 2012) – apparently, the main mechanism for DCd supply in this study. The source of DCd in deep waters is posited to be reductive dissolution within suboxic marine sediments and remineralisation of particles. The downward flux of the bio-utilized elements seems to be balanced by the heterotrophic bacteria remineralization promoting upward advective flux, resulting the in rapid remineralization seen at the surface (Morel and Price, 2002) – notably demonstrated by DCo on this transect.

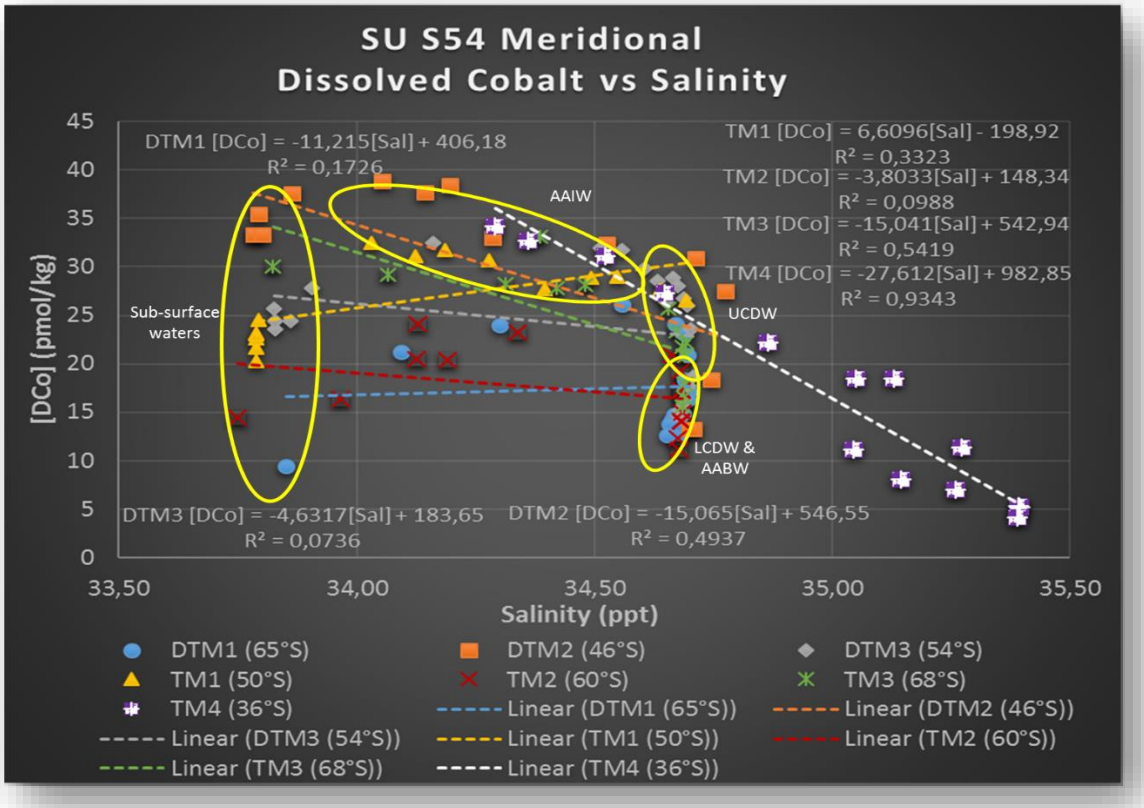

Figure 33-*The meridional relationship of DCo (pmol/kg) to salinity (ppt) for the entire water column. A poor correlation indicates a lack of salinity control on DCo due to external inputs. It may be that atmospheric deposition is a prominent source of DCo in the region near the SAF and the Antarctic Shelf at 68°S. Yellow circles denote the water masses characterising the DCo/Salinity points.*

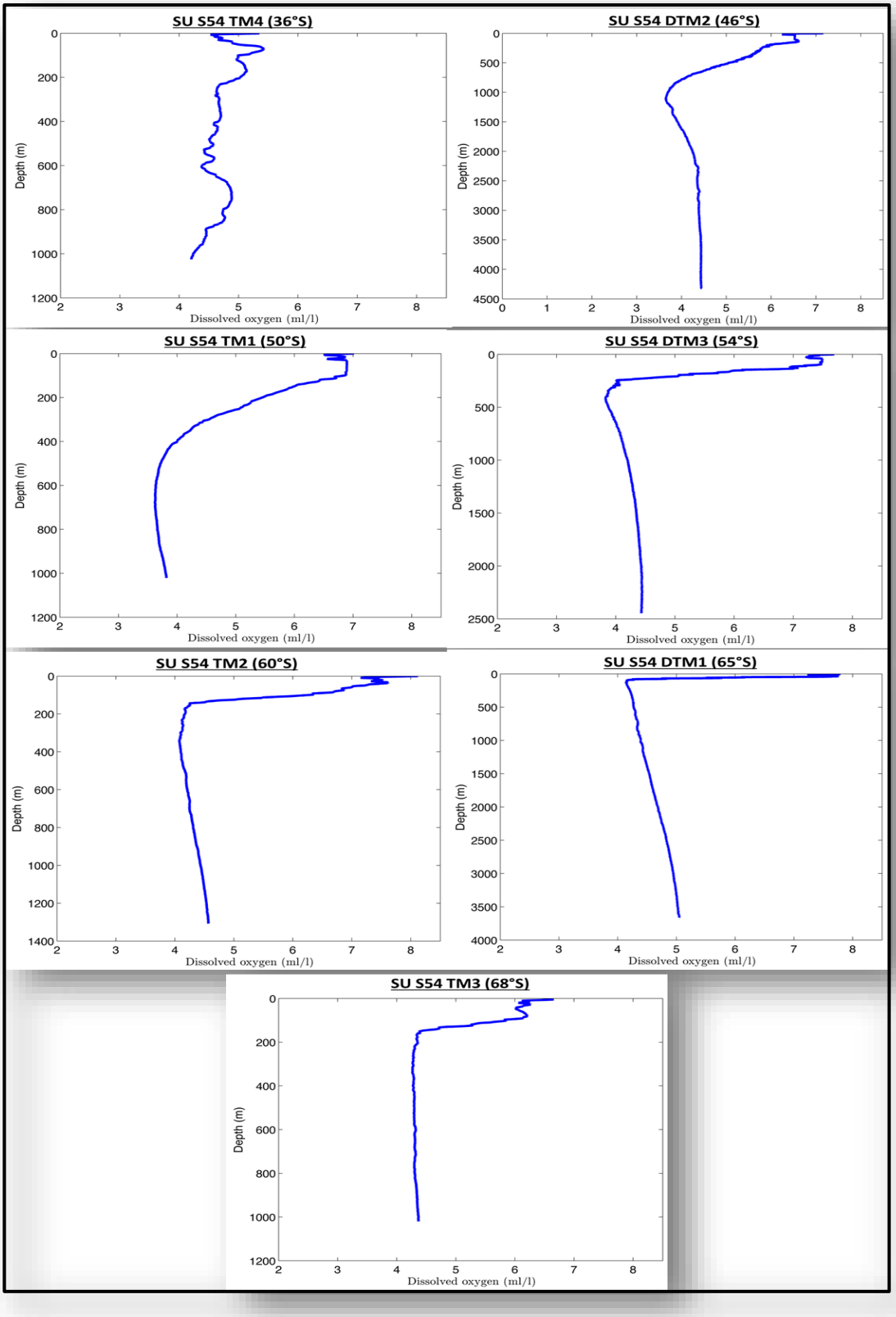

***Figure 34**-Meridional CTD Dissolved Oxygen (O_2) concentrations (ml/L) versus depth. Note: zone of rapid depletion, a consequence of heterogenous oxidising bacteria scavenging DCo and DMn. organic ligands prevent scavenging up to a certain depth by complexing Co(II). The scavenging onset depth shoals with increasing latitude-an import control on Southern Ocean DCo concentrations. Concentrations are not calibrated, nonetheless, profile shapes serve to demonstrate the control.*

The concentrations for dissolved trace metals DCd and DCo reported in this study prove soundly within the range reported by similar studies (Saito and Moffett, 2002; Sañudo-Wilhelmy *et al.*, 2002; Bown *et al.*, 2011; Boye *et al.*, 2012; Abouchami *et al.*, 2014; Baars *et al.*, 2014). Generally DCd is depleted in the surface waters, regenerating in parallel with PO4 elevating concentrations and thereafter remaining conservative. Baars et al. (2014) reported the concentration of DCd in this sector of the Atlantic Ocean with notable similarities to those observed in this study. Several studies, especially the few in the Southern Ocean, report Co as the total dissolved fraction and not just the bioavailable fraction. Hence concentrations of DCo are expected to be slightly underestimated because of the organically complexed free ion fraction not binding during pre-concentration.

4.2.1 Biogeochemical features within the STZ (TM4)

DCo concentrations within the STZ oligotrophic waters were extremely depleted (<4 pmol/kg) throughout the euphotic zone continuing into the sub-surface water column (Figure 27, 30). The distribution exhibited text book nutrient like behaviour with the lowest concentrations in the euphotic zone coinciding with the Chl-a maximum (± 0. 59 µg/kg). While the Chl-a concentrations are unremarkable, the depletion of DCo suggest strong bio-utilization by a phytoplankton community that reveal an affinity for the trace metal. DCo utilization is proportional to that of phosphate; substantiated by the strong positive correlation (R^2=0.9545) between DCo and PO4, typical for an element exhibiting nutrient like behaviour – [DCo] = 14.47[PO4] +6.591 (Figure 35). Similar observations have been made by Bown et al. (2011) and Saito & Moffett (2002). The depletion ratio was calculated at 41 pmol kg^{-1}/µM in this study – corresponding to the 44.0 µM M^{-1} reported by Bown et al. (2011). Further, the consistency of the correlation indicates that the regeneration of Co and PO4 take place at similar rates in this region – DCo remineralization is slightly faster. The DCo/Salinity correlation was strong under the intense bio-utilization in this region – an anomaly for the transect (Figure 33, 37). However, it is expected that the typical decoupling of DCo/PO4 and DCo/Salinity caused by scavenging, will materialize in the mesopelagic zone. Unusually, this mesopelagic decoupling only manifested in the region around 800m for this station (Figure 27). Nonetheless, comparable surface depletion of DCo has been reported for the sub-tropical waters of the Sargasso Sea (Shelley *et al.*, 2012) and South Pacific (Ellwood, 2008).

The strong positive correlation between DCo and PO4 (Figure 35) in conjunction with a lack of strong depletion for certain trace elements (most notably Zn), exemplified behaviour of a community that has an absolute requirement for DCo. The examination of underway phytoplankton samples by Viljoen, 2016 (Figure 28), substantiates this by suggesting a community structure dominated by cyanobacteria (≈ 90%). Studies by Saito & Moffett (2002) indicate that the cyanobacteria

Prochlorococcus and *Synechococcus* demonstrate an absolute requirement for DCo. The utilization of DCo by marine cyanobacteria lies in their requirement of the Vitamin B12 – an organometallic biomolecule with Co as an essential metal cofactor. B12 in turn is required by the enzyme methionine synthase which catalyses' the last step in the synthesis of the amino acid methionine (Bertrand *et al.*, 2007). While some marine phytoplankton (*Thalassiosira pseudonana*) may lack the B12 biosynthesis pathway, it has been found in the majority of cyanobacterial genomes (Bertrand *et al.*, 2007). The biosynthesis of B12 is limited to certain bacteria and archaea (Saito *et al.*, 2010). Thereby eukaryotic phytoplankton demonstrating a requirement for B12, rely on B12 producers, else they possess an dissimilar, B12 devoid, biochemistry (Bertrand *et al.*, 2007).

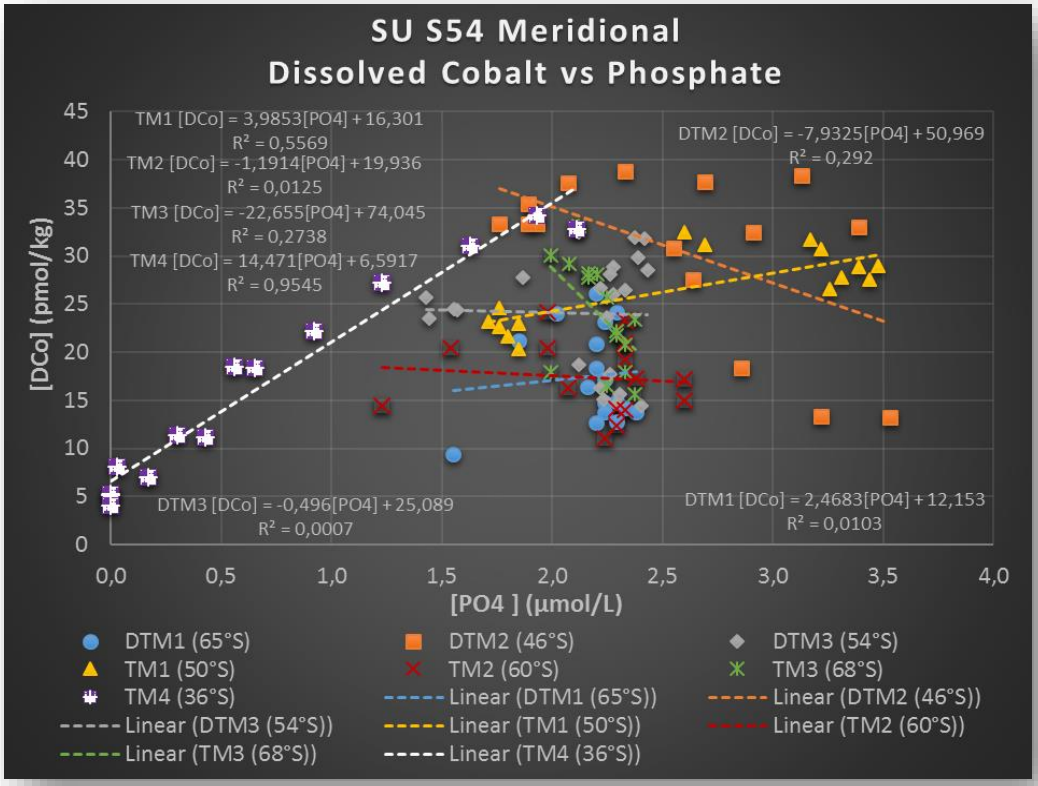

***Figure 35**-The linear correlation between DCo (pmol/kg) and PO4 (µmol/L) for the entire water column. While DCo and PO4 are expected to correlate well in the surface owing to bio-utilization by marine phytoplankton, the rapid remineralization and depletion of DCo due to scavenging in certain regions will result in a poor correlation below the remineralized zone.*

The "deep" depletion observed here may assist in gaining an improved understanding of the remineralization characteristics of cyanobacteria. Typically, diatoms release DCo rapidly during remineralization with small delay in the remineralization of DCd – conceivably a characteristic of the association to PO4. However, the rate of remineralization is similar for DCo and DCd at this station (STZ). Moreover, the respective "Cobocline" and "Cadmicline" is found well below the MLD – not unexpected given the strength of depletion (Figure 22). Interestingly, the TCd concentrations were

depleted in conjunction with the DCd concentrations, while the TCo concentration exhibited no noticeable depletion under depleted DCo (Figure 24, 27). This may suggest that while the resident community demonstrates a requirement for the dissolved fraction, the solubility of TCo prevents its transformation to the free bioavailable ion, be that biologically encouraged or due to redox.

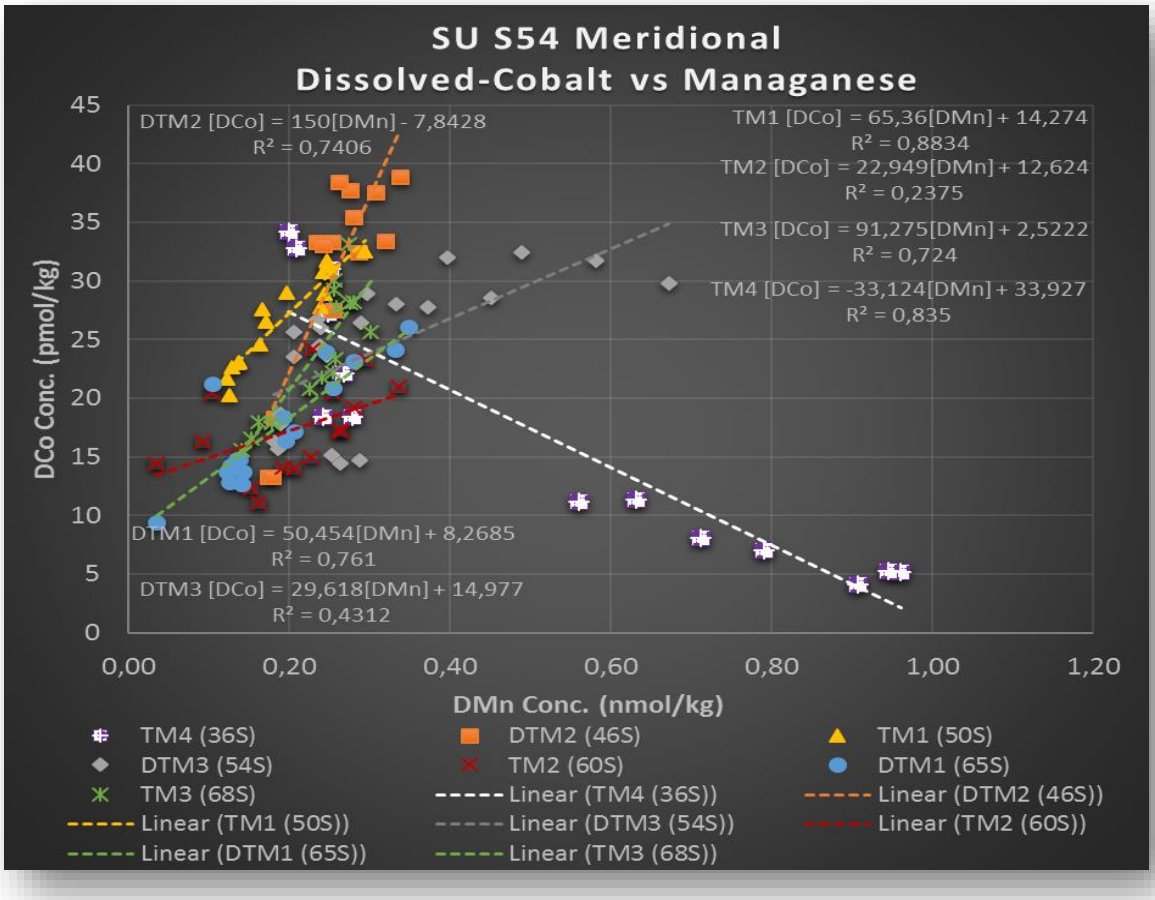

***Figure 36**-The positive linear correlation between DCo (pmol/kg) and DMn (nmol/kg) for the entire water column of the Southern Ocean, Atlantic Sector. Speciation of DMn and prominent utilization are responsible for the unusual behaviour at TM4 (36°S). While the correlation is weak in the surface owing to DCo bio-utilization, the bacterial mediation below the remineralized zone dominates both DMn and DCo scavenging – a function of similar redox chemistry.*

Furthermore, DCo concentrations typically exhibited an excellent correlation to DMn for the regions south of the STF whereby DMn scavenging is shortly followed by DCo scavenging – a product of the redox control of DCo by Mn oxidisers (Figure 36). However, DMn distribution in the surface of the STZ exhibited a unique condition whereby high concentrations subsist at the surface only to be rapidly depleted. This is explained by photochemical reduction of Mn (IV) oxides generating soluble Mn(II) – subsequently scavenged. Elevated concentrations of soluble DMn (± 1 pmol/kg; STSW) may allow Mn oxidising bacteria to flourish in this region. The significance of high concentrations of heterogenetic Mn oxidising bacteria is evident when considering the biosynthesis of the Vitamin B12 by these bacteria – Co is an essential metal cofactor in the vitamin (Moffett and Ho, 1996). This would

result in large amounts of the B12 vitamin in the surface layer and thereby assist in the growth of cyanobacteria – substantiating cyanobacteria domination in the region. However, given cyanobacterial dominance we may expect to see the utilization of DZn. Conversely, DZn concentrations in the surface are elevated and exhibit no pronounced biological utilization (Figure 39). Sunda & Huntsman (1995) state that while cyanobacteria dominate the oligotrophic gyres, they actually lack the Co-Zn substitution genetic ability; while Saito & Moffett (2002) further observed an absolute requirement for Co bu not Zn.

However, while cyanobacteria may demonstrate an absolute requirement for DCo, they exhibit high sensitivity to DCd toxicity (Brand, Sunda and Guillard, 1986) – yet DCd concentrations are similarly depleted in the STZ. Cyanobacteria (*Synechococcus*) have been shown to release strong Cu complexing agents in order to detoxify and export the metal (Brand, Sunda and Guillard, 1986), it is unclear if they do the same for DCd. Thereby, it may be that the utilization of DCd due to an alternative species of plankton is lessening the impact of DCd toxicity and thereby creating the conditions promoting a dominant cyanobacterial community. The underway data in figure 28 suggests that coccolithophores may be diversifying the community structure – a function of DCd in carbonic anhydrase (Sunda and Huntsman, 2000). Subsequently, this suggest that DCo utilization south of the STF may only occur when low concentrations of preferential (Fe, Zn) trace elements subsist; thereby creating the selection pressure driving substitution. Such a case may be present in concentric diatomic species which are capable of substituting Co or Cd, for Zn (Sunda and Huntsman, 1995; Nodwell and Price, 2001).

The cycling of DCd and DCo will be primarily dominated by the biological uptake, with regeneration and vertical mixing responsible for replenishment; consequently, these elements demonstrated a typical nutrient like profile correlating markedly with phosphate (Figure 27, 32, 35). However, growth may only be co-limited by the low DCd and DCo concentrations, given the extremely low macronutrient concentrations in this region – ≈ 0 µM in the surface (Figure 17-19). This is substantiated by the unremarkable Chl-a concentrations which only pick up below 50m and reach a maximum of <0.59 µg/kg, suggestive of production sustained by recycling.

4.2.2 Biogeochemical features within the ACC

The meridional distribution of DCo within the ACC is one of decreasing concentrations towards the southern extent, continuing into the SACCZ (Figure 27, 30). However, while concentrations decrease the profile are markedly similar – barring utilization differences. DCo concentrations were typically elevated within sub-surface waters awaiting rapid depletion near the AAIW, UCDW boundary as scavenging initiates. Scavenging removes DCo from the water column through the UCDW pending somewhat conservative behaviour in the region around the UCDW-LCDW boundary – organic ligand

stabilisation. The profiles suggest that the onset depth of scavenging be contingent on the boundary between the AAIW and the UCDW. However, the UCDW and LCDW are upwelling to the south leading to the shoaling of the boundary regions and subsequently shoaling of the scavenging onset depth. This control is mimicked by the dissolved oxygen (O_2) concentrations in the water column (Figure 34), by way of bacterially mediated O_2 depletion oxidizing Mn and Co, thereby controlling the solubility of Mn and Co.

In the pH and Eh ranges of natural waters cobalt can exist as Co(II) or Co(III) (Moffett and Ho, 1996). The formation of strong, labile organic complexes has been largely attributed to the divalent cation, Co (II). However, certain phytoplankton may demonstrate means to utilize these organic complexes resulting in a limited impact on the bioavailability. Conversely, the bacterially mediated oxidation of Co (II) to Co (III) results in the formation of inert complexes or oxides (Moffett and Ho, 1996; Saito and Moffett, 2002). Mn oxidizing bacteria have been proposed to control Co (II) oxidation via a common microbial pathway (Moffett and Ho, 1996). The manifestation of this control presents as scavenging through the adsorption and oxidation of DCo occurring on the surface of Mn oxides in the water column; this limits bioavailability and is postulated to be a significant mechanism for Co removal (Moffett and Ho, 1996; Saito and Moffett, 2002). Consequently, the DCo vertical distribution bears a remarkable resemblance to the O_2 concentrations for this transect. Under high O_2 concentrations the bacterially mediation oxidation is expected to be pronounced and thereby scavenging is correspondingly strong. However, in the deeper waters scavenging slows and dissolved O_2 concentrations stabilise. This may be a consequence of organic ligand stabilisation removing the Co (II) fraction from the water column and thereby retarding scavenging through the oxidative precipitation mediated by the Mn-oxidisers. It follows that the weak scavenging observed in the AAIW may be a consequence of high export organic ligand complexation in a downwelling water mass. Conversely, the upwelling UCDW is comparatively low in organically complexed material given its deep-water source and thereby scavenging is initiated nearer to the surface. It may be complementary to study the colloidally bound fraction of DCo to better understand the cycling of this element.

The station at 46°S within the SAF (DTM2) exhibited unusual DCo characteristics. Concentrations in the sub-surface were notably high, lacking any pronounced surface depletion (<8 pmol/kg) given the diversity of the phytoplankton community in the surface – diatoms, prasinophytes, haptophytes and pelagophytes (Figure 28). The lack of strong depletion of DCo in the surface waters, coincided with low chl-a concentrations (≤ 0.46 µg/kg) indicative of sub-optimal growth (Figure 23). However, this limitation may be caused by markedly low (≤ 5.33 µmol/L) silicic acid concentrations (Figure 19**)**. Le Moigne et al. (2013) noted similar depletion in silicic acid and attribute this condition to bio-utilization by diatoms during the early stages of the productive season. However, they suggest that growth is

further limited by low concentrations of DFe. Conversely, the results of a bioassay experiment (Figure 29) performed during the cruise by a colleague, Natasha van Horsten, suggest that at 46°S, Fe may not be a notable factor constraining growth given that high light was responsible for the greatest growth (Van Horsten, 2015). Nonetheless, strong depletion of DCd was observed – a not unusual characteristic even in the face of low chl-a concentrations. This suggests that while bio-utilization of these elements was present, Cd was favoured over Co at this station even in the diverse phytoplankton community. Thereby, under the limited growth, selection pressure is not yet great enough to see DCo fully utilized. Conversely, the surface depletion of DCo at 50°S and 54°S, indicates strong utilization by the resident community (Figure 27). Underway data indicates that diatoms, dinoflagellates and haptophytes may be prevalent in this region (Figure 28). Coccolithophores are known to be capable of Co-Zn substitutions (Saito and Goepfert, 2008). While the cellular quota of DCo may be higher for dinoflagellates, the diatom *Prochlorococcus* has been found to coincide with surface cobalt depletion (Shelley *et al.*, 2012). This substantiates the idea that while cyanobacteria (*Synechococcus*) are the primary producers of Co complexing ligands (Saito and Moffett, 2001), under declining prevalence south of the STF, organisms other than cyanobacteria have the capacity to produce Co binding ligands (Ellwood *et al.*, 2005) – perhaps a function of cobalamins. Moreover, there has been no notable shift in the community structure between 46°S and 50/54°S, reiterating that bio-availability is governing surface bio-utilization at 46°S.

The AAIW waters, prominent between approximately 150-800 at 46°S, are evidently wanting of strong scavenging behaviour. This may be a function of highly concentrated organic ligands complexing DCo in the AAIW; thereby limiting the Co (II) fraction typically associated with oxidative scavenging. Below the AAIW/UCDW boundary, sustained scavenging commences, likely driven by high concentrations of particle accumulating typical of this region. However, Ellwood et al. (2005) report that ligand concentrations within the upper reaches of PF waters (50°S) were 15-20 pmol/L higher than the concentration of total dissolved cobalt – vice versa for a station north of PFZ. This suggest that organic ligands complexing DCo were more prevalent in the UCDW than the AAIW. It may be plausible that Mn concentrations in the sub-surface waters (Figure 39) exceed the requirements of Mn oxidising bacteria which are largely responsible for DCo scavenging and/or there is an absence of Mn oxidising bacteria in the sub-surface. Additionally, should sub-surface waters see an absence of heterogenetic bacteria capable of synthesizing the vitamin B-12 it would elucidate somewhat on the lack of utilization in the surface layer while supporting co-limitation in any community that requires B12 but does not demonstrate a B12 bio-synthesis pathway.

The concentrations of DCo in the surface waters of the SAF at 46°S (DTM2), have been reported at 27.3 pmol/L (30m) to 48.2 ± 1.9 pmol/L (100m) in a study conducted in late summer (February-March)

conditions (Bown *et al.*, 2011). DCo concentration reported in this study are 33.3 ± 1.64 pmol/kg at 35m increasing to 38.5 (Std Dev not determined) pmol/kg at 100m. Both ranges illustrate the marginal uptake of DCo by marine phytoplankton in the surface waters. Bown et al. (2011) report the concentration below the surface at 46°S to exhibit conservative behaviour, and thus the concentration remains constant ranging from 40.5 ± 1.86 pmol/L (150m) to 45.5 ± 2.53 pmol/L (2050m); with a marginal increase (49.2 ± 2.01 pmol/L) observed in the region between the AAIW and UCDW. Results of this study indicate that scavenging of DCo below the sub-surface waters is responsible for a decrease from an average of 36.5 ± 2.5 pmol/kg in the sub-surface, to 32.1 ± 3.2 pmol/kg in intermediate waters, and further decreasing to 18.1 ± 5.87 pmol/kg in the deep waters at 4300m. However, Ellwood et al. (2005) reported markedly different behaviour for the total DCo concentrations within the Polar Front (PF) at 49°S and 20°E; they recorded an increasing (15-50 pmol/L) concentration with depth, suggestive of a more nutrient like behaviour, and an absence of scavenging. Further, considering the limited scope (depths 30m-2050) of the reporting by Bown et al. (2011) at this locale, a deep-water comparison to their station 1° further south (47°) within the PFZ would better constrain the range. However, Bown et al. (2011) reported a more conservative profile for 47°S, with concentrations ranging from 42.9 ± 1.8 pmol/L at 100m in the surface to 30.5 ± 0.27 pmol/L at 3980m though, there are several spikes in concentration in the mid depths reaching up to 56 ± 3.34 pmol/L at 1070m. These spikes are somewhat unusual and not observed in this study. However, the same spikes are reflected in the O_2 concentration recorded by Bown et al. (2011), leading to a possibility that it is a construct of the redox of Mn. Similarly, the conservative (sub-surface) to decreasing (lower sub-surface) concentration observed below the surface are attributed to redox processes analogous to the geochemistry of Mn leading to enhanced scavenging.

DCd is primarily controlled by biological uptake, regeneration and vertical mixing; consequently, DCd demonstrated a typical nutrient like profile correlating markedly with phosphate (Figure 32). Concentrations were relatively depleted in the sub-surface water column with DCd demonstrating an affinity for the biogenic particles at this location. Surface macronutrient concentrations for phosphate and nitrate mimic the sluggish depletion observed for DCd in the surface nevertheless concentrations increased significantly from those reported for the sub-tropical region (Klunder *et al.*, 2011; Le Moigne *et al.*, 2013). However, silicic acid concentrations remain severely depleted in the surface owing to the resident diatom community. Moreover, the restriction saw SEM imagining of samples from the cruise – performed by Palmer (2015) – reveal a large contribution by coccolithophore at the time of sampling. This supports the suspected shifts in planktonic community in response to variable biogeochemistry of the surface. The nutrient-like profile correlating into the deep waters further supports more effective reworking of Cd ascribed to easily dissolved carbon particles (coccolithophores). According

to Baars et al. (2014) concentrations range from 152-254 pmol/L for DCd with phosphate concentrations of 1.24-1.39 µmol/L in the near sub-surface waters of the SAF (46°S, 5°54 E). These values are marginally lower than those reported for the surface average (262 pmol/kg) in this study within the PFZ (DTM2; 46°S, 8°E). These concentrations correspond to the 255 pmol/kg DCd reported by Abouchami et al. (2014) in the surface around 47°S. This study quantified surface concentrations in the PF between 215-473 pmol/kg – an unusual range given the relatively higher Chl-a concentrations (1 µg/kg). While Baars et al. (2014) reported lower concentrations ranging from 152-254 pmol/kg in the surface of the PFZ. Nonetheless, they report a similar Cd/PO4 ratio of 122-182 versus the 220 herein – indicating stronger utilization of Cd during their observations. The concentrations of DCd measured in this study at 54°S (DTM3) – within the AAZ – ranged between 337-393 pmol/kg in the surface whereas Abouchami et al. (2014) report concentrations of 554-568 pmol/kg – indicative of poor utilization. Concentrations in the intermediate and deep waters were markedly similar between the studies, ranging between 778-903 pmol/kg.

The changes in surface DCd values illustrate how the sampling results may be but a snapshot of the present conditions. The deviation could conceivably be a consequence of low chl-a (≤ 0.46 µg/kg) concentrations measured at this locality during this cruise. Evidence exists in the data of the Baars et al. (2014) study, whereby phosphate values are relatively depleted in comparison to this study, which when coupled to the lesser DCd concentrations corresponds to greater biological uptake. Theoretically such an observation should be echoed in the Cd/P ratio, which at 152 reported by Baars et al. (2014) is similar to 144 herein, confirming a weaker bloom state was observed during this cruise. Further they report values of 648-865 pmol/L from the AAIW to the UCDW; which corresponds exceptionally to the range of 698-836 pmol/kg reported herein. Their record reflects a similar decrease (UCDW-NADW) followed by an increase (NADW-AADW) in concentration, reporting 643-777 nmol/L versus the 629-787 pmol/kg range reported herein. Additionally, they report values of 648-865 pmol/L (AAIW to the UCDW) to 643-777 pmol/L in the lower AADW.

While atmospheric dust flux may explain the increased surface DCo, it does not deliver an explanation for the sub-surface-intermediate depth “peak” observed in the DCd and macronutrient profiles. Perhaps plausible would be a concept supporting atmospheric deposition as the primary source for the apparently augmented Co and Mn though, proposing water column characteristics as a further control for DCo and a primary control for DCd. Cyclonic eddies resulting from disturbances created by parallel upwelling (UCDW) and down-welling (AAIW), occurring simultaneously with laterally advecting AASW water, are responsible for the enrichment of DCd seen in the sub-surface waters (Figure 27). Marginal enrichment of Co and Mn by the upwelling UCDW seems plausible considering that the AAIW and UCDW boundary coincides with the depth up to which elevated

concentrations are observed. However, the concept is more applicable to the "peak" observed in the DCd and phosphate profiles. Cd has an affinity which sees its association with the dissolved organic carbon (DOC) component resulting in an intermediate "peak" where Cd is returned to the water column**.** It is likely that this manifests as the enrichment concentrated around the boundary between the opposite flowing AAIW and the UCDW. The boundary between the upwelling UCDW and down-welling AAIW would then also act to retard the settling and drawdown of the dominantly colloidal organic carbon (COC) ligand associated Co, leading to increased sub-surface concentrations.

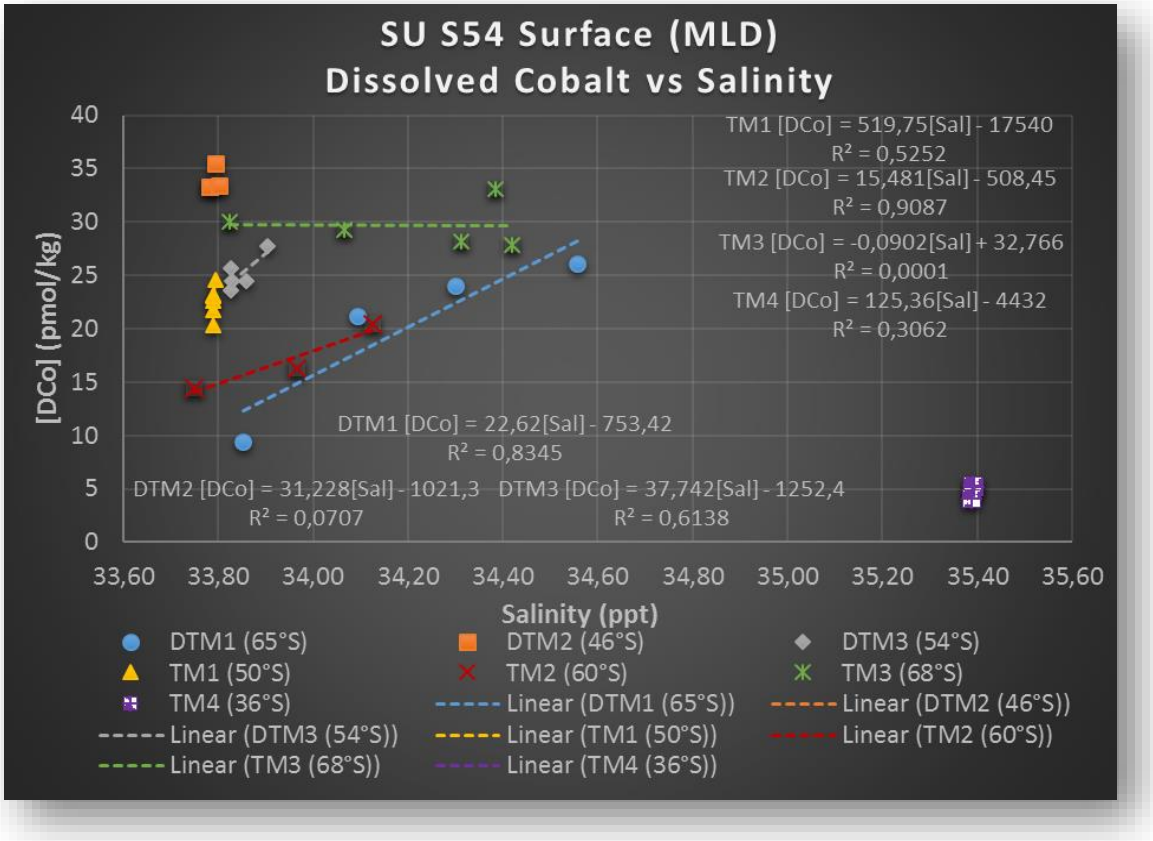

Figure 37*-The correlation between DCo (pmol/kg) and Salinity (ppt) for the surface (MLD) waters. A poor correlation may be indicating atmospherically augmented concentrations of DCo as demonstrated by the elevated concentrations for the stations at 46°S and 68°S, coinciding with poor linear regression coefficients (R^2<0.07).*

To establish the plausibility of atmospheric deposition as a source for the elevated concentrations of Co and Mn seen in the region around the SAF, the DCo/Salinity correlation was plotted for the surface waters of the transect (Figure 37). Moreover, concentrations were compared with similar studies which reiterated observations recorded herein (Bown *et al.*, 2011; Boye *et al.*, 2012). The incidence of atmospheric augmentation on the concentrations of trace metals, will reveal a poor but significant correlation with salinity. Surface DCo concentrations at 46°S displayed a poor but significant linear regression correlation with salinity (R^2≤0.0707; *F=0.0026*), substantiating augmented

concentrations by aeolian weathered material. Saito & Moffett (2001) observed a similar correlation in coastal waters, however, Boyle (1988) did not find an obvious relationship. The source region for atmospheric dust is posited to be Patagonia. A NOAA HYSPLIT (Draxler and Rolph, 2003) forward trajectory model confirms that Patagonia is a potential source region with air mass altitude proximal to the sea surface right over the station (Figure 38a). However, a backward trajectory model indicates that the air masses originate over the Antarctic Peninsula (Figure 38c). Boye et al. (2012) confirm enhanced dry deposition flux is occurring south of the ACC. However, it appears that only surface DCo concentrations are elevated with several other trace metals (Zn, Cu, Cd) remaining depleted. It may be that inputs are more perceptible as a feature of the inherently low concentrations of Co in the ocean. Baars et al. (2014) reported that atmospheric deposition of Cd in the ocean surface waters is insignificant, explaining the lack of a signal in the DCd column. This proposes that atmospheric dust sources for Co should not be overlooked. However, without soil samples from the Patagonia region it is a bit speculative to suggest that increased DCo is a consequence entirely of atmospheric dust flux. Bown et al. (2011) propose that DCo concentrations may be supplemented due to an association of the water masses injected into the eastward-flowing jet of the ACC, with the South American continental slope, prior to their injection into the ACC.

The bio-availability of atmospherically deposited Co may be limiting the utilization of DCo at 46°S. Aeolian Co has a high affinity to lithogenic particles consisting of various low solubility silicate minerals. This affinity may result in limited bio-availability of the recent dust deposited DCo due to complexation which would subsequently result in delayed scavenging. The vertical profiles for the stations at 50°S and 54°S would be akin to 46°S under limited bio-utilization; however, the utilization of DCo in these regions suggests bio-availability may not be limiting. There is no definitive difference in the productivity between 46°S and 54°S (Figure 23) that may explain DCo substitutive utilization under trace metal limitation – reinforcing bio-availability limitation. Nevertheless, to accurately quantify the role of Aeolian deposition in the elevated Co concentrations, total dust deposition flux, fraction of wet deposition that is readily dissolved and the solubilisation rates of the flux material within the euphotic zone. Saito & Moffett (2002) estimated flux by dust deposition into the Sargasso Sea to be around 1600 pmol/m^2d and assumed a soluble fraction of 45% based on Mn. Their results indicate DCo supplementation by 3 pmol/L over 3 months – an idea argued by Shelley et al. (2012) – not significant to supplement DCo concentrations. However, the fractional solubility of Co (8-100%) aerosols in the Sargasso Sea were found by Shelley et al. (2012) to be significantly higher than similar estimates for Fe (0.44%). An alternative hypothesis is that strong ligand complexation is removing bio-available DCo from the water column and thereby limiting the source to phytoplankton.

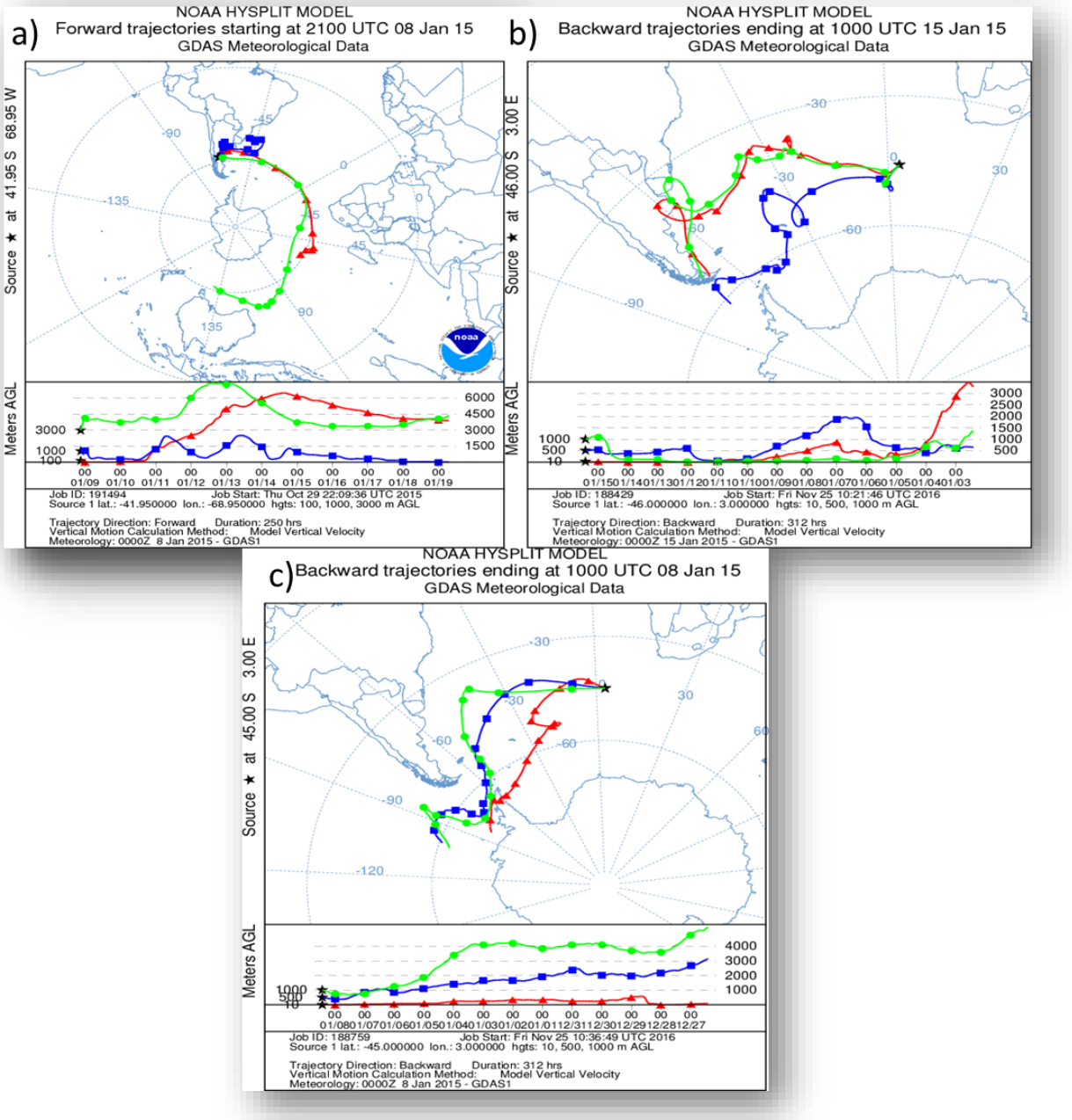

***Figure 38**-NOAA HYSPLIT models* (Draxler and Rolph, 2003) *examining potential source regions for atmospherically augmented DCo. The models are as follows: a) 10 day (250 h) forward trajectory model commencing the week of 8 January 2015 illustrates the movement of dust originating in Patagonia (41°S, 69°W) at 100m, 1000m and 3000m in the atmosphere; b) 13 day (312 h) backward trajectory model commencing the week 15 January 2015 illustrates the source of the air masses found at 10m, 500m and 1000m at the sampling location; c) 13 day (312 h) backward trajectory model, to illustrate variability, commencing the week 8 January 2015 (prior to our arrival) illustrating an Antarctic Peninsula source of the air masses found at 10m, 500m and 1000m at 46°S.*

4.2.3 Biogeochemical features within the Weddell Gyre (SACCZ)

The meridional distribution of DCo within the SACCZ sees a stabilisation of the southerly decreasing concentrations coinciding with the stabilisation of the scavenging onset depth (Figure 27). Consequently, the concentrations and the vertical profiles of the 3 stations at 60°S, 65°S and 68°S are

remarkably similar – excepting elevated surface concentrations at 68°S. The vertical profiles for the stations at 60°S and 65°S exemplify a hybrid-type distribution with nutrient-like uptake and regeneration in the surface, succeeded by scavenging – a consequence of oxidised cobalt's (Co III) affinity for adsorption onto particles – below the chl-a max. Conversely, the station at 68°S exhibited a scavenged type profile whereby DCo was constantly depleted downward from the surface with no remineralization at any stage – indicative of absent phytoplankton bio-utilization. This control may be a function of the dissolved oxygen concentrations in the water column controlling the impact of Mn oxidising bacteria and thereby the solubility of DCo. Conversely, the differences in the onset of scavenging behaviour between a phytoplankton replete and phytoplankton deplete water mass, provides pivotal evidence that a variety of phytoplankton will secrete organic ligands that bind DCo and prevent it from being scavenged. The elevated surface concentrations at 68°S are a combination of strong external inputs combined with a lack of utilization of DCo in a phytoplankton feeble water mass– conceivably compounded by the bio-availability. The DCo/Salinity correlation corroborates the incidence of atmospheric augmentation to Co concentrations by revealing a poor but significant correlation with salinity in the surface (MLD). Surface DCo concentrations at 68°S displayed a poor but significant linear regression correlation with salinity ($R^2 \leq 0.0001$), substantiating augmented concentrations by Aeolian weathered material likely released from recently melted sea ice (Figure 37).

The pronounced depletion of DCo in the surface (MLD) at 65°S, within eastern extent of the Weddell Gyre (Figure 2; DTM1), indicated that significant biological uptake was taking place in the euphotic zone; a consequence of a remarkable diatom bloom (Chl-a ≤ 3.92 µg/kg) – coinciding with the ice melt (Figure 23). It is likely that melting sea ice was responsible for a large auxiliary trace metal pulse into the surface fashioning conditions ideal for phytoplankton to bloom. DCo concentrations below the remineralized zone are subsequently depleted by oxidative induced particle adsorption whilst oxygenated sub-surface waters persist; thereafter dissolution and stabilization in the low oxygenated lower reaches of the LCDW (Bown *et al.*, 2011). Again, the bacterially mediated scavenging of DCo are attributed to redox processes analogous to the geochemistry of Mn (Figure 36, 39). The biological uptake observed in the surface supports the suggestion by Saito et al. (2010) that enzymes and other proteins vital for phytoplankton cell metabolism contain Co as a co-factor. It is possible that the strong depletion of micronutrients during bloom conditions creates the selection pressure which sees flexibility of the absolute Zn requirement relaxing to allow Co utilization (Figure 39). The co-limitation of phytoplankton growth by iron and vitamin B-12 – a cobalt containing biomolecule – observed by Saito et al. (2010) in the Ross Sea, is not however apparent under the existing circumstances at this station. This suggests that biosynthesis of vitamin B-12 by the bacterial

community is not only taking place but it is sufficient to fulfil requirements to supply a phytoplankton community which is under Fe stressed (±0.14 nmol/kg**)** conditions.

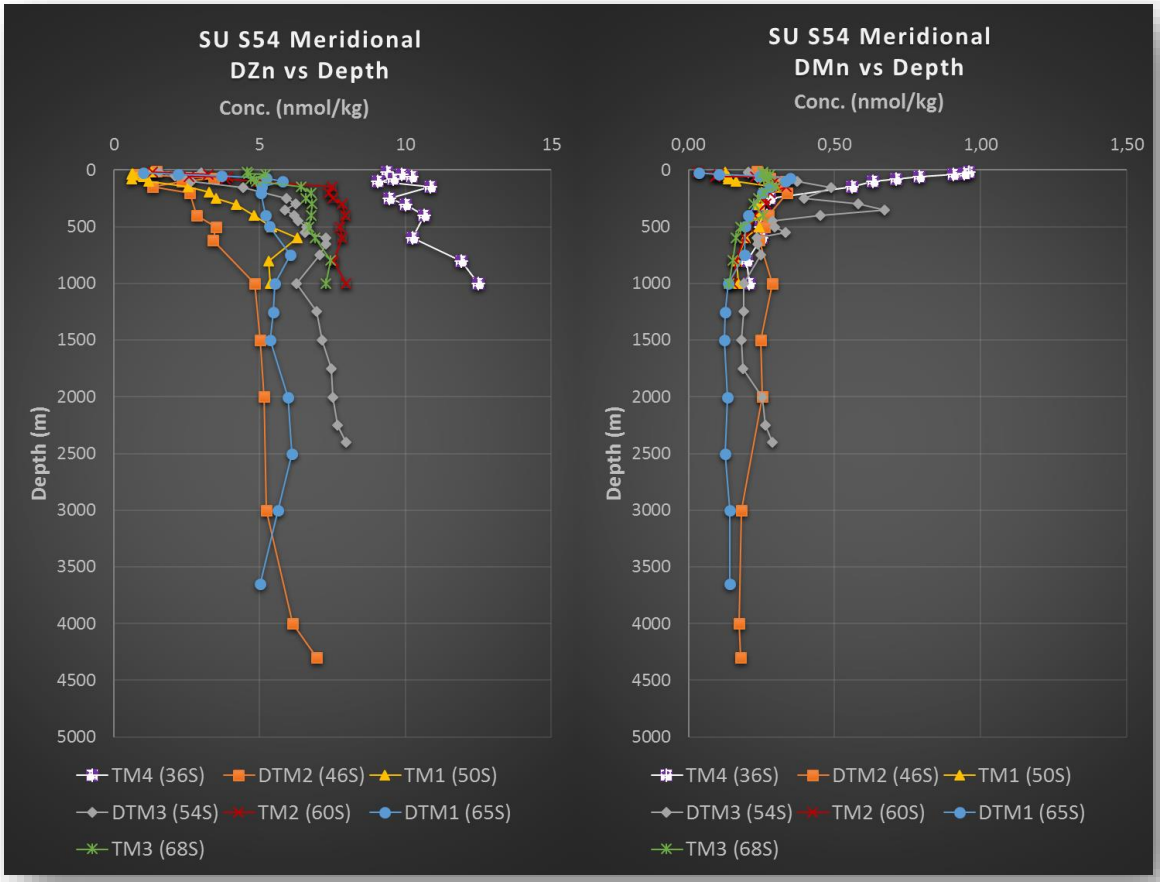

Figure 39*-The meridional water column profiles for DZn and DMn in nmol/kg. The scavenging of DCo due to a particle adsorption affinity when oxidised is mediated by DMn loving oxidising bacteria. This conrtol plays a major role in the distribution of DCo in the water column – vertically and meridionally. The depletion of DZn under certain conditions and communities might create the selection pressure initiating the increased utilization of DCo.*

In the Ross Sea *Bertrand et al. (2007)* found that diatoms *Fragilariospsis cylindrus and Chaetoceros spp.* – common components of the Antarctic ice pack – benefited markedly from Fe supplementation yet showed no further growth under Fe and vitamin B12 (Fe-B12) supplementation. This suggests that while the community is apparently Fe limited it may not utilize DCo – an idea reinforced by the lack of DCo utilization at 68°S (TM3). Further, it may be that the bacterial and archaeal cells, responsible for vitamin B12 production, may be largely inhibited or somewhat absent in this region. Consequently, the resident community has developed an adaptation to vitamin B12 limitation. Bertrand et al. (2007) found that variation in the bacterial community is consistent with the spatial Fe-B12 colimitation and the extent of B12 stimulation is negatively related to bacterial abundance. This study found an exceptionally strong bloom condition in the region around 65°S (DTM1) suggesting that light limitation ought not result in relative inhibition when considering growth for station at 68°S (TM3). Considering

all the macronutrient, micronutrient, temperature and salinity data available a single factor stands dissimilar between the two station – DCo utilization is absent at 68°S. Concurrently, DMn utilization is similarly poor. This may suggest limitation related to B12, however, it may also suggest that under the low growth conditions (68°S), the condition for DCo utilization has not yet been reached – suggesting a substitutive requirement for DCo in this region. Saito & Goepfert (2008) report that the Zn-Co biochemical substitution seen in Phaeocystis is conceivably the result of evolutionary pressure for maintaining growth rates in high export environments in which rapid depletion of Zn, Co and carbon occur simultaneously.

Concentrations of DCo reported in the western region of the Weddell Sea by Sañudo-Wilhelmy et al. (2002) are notably higher than those herein at 53 ± 16.7 pmol/L. However, the elevated concentrations relative to this study were posited to be a consequence of the proximity to the continental shelf (Sañudo-Wilhelmy *et al.*, 2002). Concentrations reported near the Fletcher Shelf (72°S, 40°W) in the Weddell Sea range between 19-33 pmol/L (Westerlund and Ohman, 1991) and demonstrate improved constraining of the lower concentrations observed in this study. The station at 60°S was compared to the values reported by Bown et al. (2011) farther north (58°S) in the Weddell Gyre along the Good-hope line. They report the surface concentration at 36.7 ± 0.49 pmol/L, while the concentrations remain conservative through the water column. Conversely, this study saw strong depletion in the euphotic zone resulting in concentrations as low as 14.5 ± 0.48 pmol/kg increasing to a maximum of 24.1 ± 0.07 pmol/kg after remineralization. It is anticipated that the degree of underestimation relative to Bown et al. (2011) was a consequence of the UV-Oxidation performed in that stduy. Samples for the dissolved fraction were filtered (0.2µM); thus, it is expected that the organic ligand interference – limiting quantitative recovery of total DCo – stem largely from the colloidal organic carbon (COC, <0.2 µM). Given that this study aimed to quantify the free metal ion, this not an unanticipated result. While no comparison is available for the stations at 65°S, the behaviour is akin to that of the station at 60°S. Concentrations reported herein range from 9.46 ± 0.12 pmol/kg to 26.1 ± 0.38 pmol/kg which can be directly correlated to the biological uptake and increased organic matter. The surface max of 26.1 pmol/kg decreased rapidly in the scavenging zone to 12.8 ± 0.37 pmol/kg and remains conservative thereafter owing to organic complexation and the slowing of bacterially mediated oxidation. The slowing of scavenging in the deeper reaches of the UCDW (800m-1000M within the SACCZ) may be attributed to decreased oxygen levels. This inhibits the oxidation of Co(II) to Co(III) and thereby prevents removal due to adsorption onto particulate within the water column (Bown *et al.*, 2011). Therefore, as the UCDW shoals so does the depth to which scavenging is occurring – removal in oxygenated sub-surface waters, and dissolution and stabilisation in the low oxygenated UCDW.

The primary controls in the cycling of DCd in the Weddell Gyre stem from biological uptake/detoxification, remineralization and vertical mixing. The shoaling of the intermediate depth peak controlled by the AAIW/UCDW boundary in the ACC and now the AASW/UCDW boundary, has augmented the surface concentrations of DCd. Nonetheless, the surface depletion range has remained markedly similar – barring poor utilization at 68°S. DCd demonstrates a good correlation with the nutrient profiles: depleted in the surface, regeneration concentrated around 300m at 60°S shoaling to 80m at 65°S, and conservative behaviour thereafter. The behaviour of DCd indicates an affinity to the particulate fraction. However, DCd exhibits a very poor correlation with PO4 at 68°S perhaps caused by a combination of weak utilization and inputs from the proximal margin. While the macronutrient concentrations are no longer expected to limit the growth of marine phytoplankton, it is expected that the continued depletion of inherent low concentration bioactive trace metals, coupled with decreasing light, will inhibit growth. The absence of DCo utilization at 68°S, whilst limited DCd utilization is present, may be a genetic adaptation of ice loving algae deficient of a B12 biosynthetic pathway. However, it may suggest that the utilization of DCd is preferential to DCo in this region as marine diatoms are known to release *phytochelatin*-Cd complexes (Morel and Price, 2002) – hence a lack of DCo depletion.

Surface DCd in the Weddell Gyre has been reported in the range 170-670 pmol/L (Sañudo-Wilhelmy *et al.*, 2002). In this study concentrations ranged from 124 pmol/kg at 65°S to 924 pmol/kg at 60°S. Concentration in the Weddell Gyre are confirmed to increase in the AABW – 799 pmol/L (Baars *et al.*, 2014). However, Baars et al. (2014) report surface concentrations in the range 409-599 pmol/L. The concentrations reported herein vary markedly at 124-732 pmol/kg for the surface and 622 pmol/kg in the AABW at 65°S. The exceptional diatom bloom state observed, is posited to explain contrasting ranges as increased uptake depletes DCd, and consequently increases regeneration of particulate organic matter below the MLD. Surface phosphate concentration ranges reflect similar results with 1.55-2.02 µmol/L in this study versus 1.65-1.88 µmol/L seen by Baars et al. (2014). Recorded Cd/P ratio for the surface range from 77-335 whereas they record 235-337, reflective of the smaller range and expected weaker Chl-a. The low end of the Cd/P range (77) observed in the surface stresses the nature of Cd depletion under strong bloom conditions exceeding nutrient depletion, suggesting that DCd is attaining concentrations depleted enough to start limiting growth (Ellwood, 2008). It may be likely that DCd was already substituting for another essential element with extremely low dissolved concentrations. Iron, with reported concentration of 0.14 nmol/kg (Klunder *et al.*, 2011), may be one such element whereby phytoplankton have demonstrated increased Cd uptake under low concentrations (Sunda and Huntsman, 2000). The Fe data for this station confirms low DFe (0.11 nmol/kg). Concurrently DZn – for which DCd can substitute in marine diatoms – concentrations are

depleted. Sunda & Huntsman (2000) demonstrated that there are two transport systems for Cd in diatomic phytoplankton, one under low DZn concentrations and the other a Mn uptake system. The concentrations for free ionic Mn are strongly depleted at this station; thus, increased Cd uptake via Mn transporters may be occurring.

5. Conclusion

The study reports an elucidated understanding of the meridional distribution and bio-geochemical cycling of cobalt and cadmium for seven stations in the Southern Ocean, Atlantic Sector. The observations made further consent to a biological role for both cobalt and cadmium in the euphotic zone. However, DCd concentrations may further be controlled by abiotic factors. Cobalt was revealed as typifying the hybrid-type distribution; with both nutrient like uptake and scavenging observed – signifying biological and biogeochemical controls. Dissolved Cadmium demonstrated a typical nutrient-like profile being utilized in the surface and remineralization correlated to the macronutrient phosphate. The vertical gradients exemplifying the distribution of bioavailable DCo and DCd appear to correspond to the frontal regime connecting the biogeochemical region traversed – suggesting strong physical controls. Concurrently, the controls are unique to: the behaviour of the plankton community, trace metal sources and regeneration, and remineralization of the locale. Moreover, the communities, in turn, may control the concentrations and speciation of bioactive trace metals in the surface waters through preferential uptake of bioavailable micronutrients. Marine phytoplankton experiencing an exceptional bloom state in the Weddell Gyre section around 65°S, exemplify the biological requirement, controls and cycling of DCd and DCo where a diatom dominated phytoplankton community – able to substitute both Co and Cd under low Zn – is present. Conversely, the cyanobacterial dominance in the STZ illustrate the absolute DCo requirement of the species, with depleted DCd attributed to a combination of uptake and detoxification. DCo distribution in the water column appears to correspond with the biogeochemical cycles of the trace metals Zn, Mn and Cd with the depletion of cobalt demonstrating its ability, along with Zn and Cd, to substitute in the active site of two important marine anhydrase metallo-enzymes while enzymatic activity remains unaffected (Saito *et al.*, 2010).

Conditions within the SAF and the region proximal to the Antarctic land mass (68°S), experience elevated concentrations of DCo attributed to atmospheric dust flux; in turn this may limit bio-availability as indicated by the low Chl-a concentrations. Moreover, at 46°S limited bio-availability results in subjugation by a coccolithophore community with a subordinate diatom community. The notably depleted silicic acid concentrations are fundamentally responsible for the subordinate diatom community nevertheless, it could further be responsible for the relatively low chlorophyll-a concentrations recorded; consequentially the uptake of DCd and DCo appears to be weak. However, the DCd profile strongly mimics that of the macronutrient phosphate which exhibits a slowly increasing with depth trend in the sub-surface waters. Conversely DCo concentrations lack traits typifying strong biological utilization and remain elevated; posited to be a consequence of

atmospheric dust flux originating in Patagonia. Biologically conditions at this station may indicate that marine diatoms demonstrate a greater requirement for DCo and DCd whereas the requirements of coccolithophores are satisfied by DCo; should Zn concentrations be low enough. Ultimately, under the right conditions, cobalt and cadmium are potentially substituting for essential bioactive trace elements such as zinc and iron, thereby advocating the potential co-limitation of marine phytoplankton productivity by depleted concentrations of dissolved cadmium and cobalt.

The shoaling of the scavenging onset depth is a function of the southerly upwelling AAIW/UCDW boundary. This may be a dominant physical control in the meridional decrease of DCo concentrations. The bacterial oxidation of Mn is posited as an important control of Co distribution in the scavenging zone, yet the understanding of the interaction is poorly understood (Moffett and Ho, 1996). Perhaps the selectivity of the catalytic site is more varied and not entirely discriminatory as has been postulated (Moffett and Ho, 1996). Thus, there subsists the premise of substitution of Mn by Co in the microbial uptake pathways. Frequently the impact of selectivity is not expected to affect the organism itself but rather the geochemistry of the element. Conversely, DCd concentrations are concentrated in the upper fragment of this boundary layer and consequently Southern Ocean DCd concentrations are elevated with the shoaling of the mid-depth peak. The consistent depletion of Cd observed throughout the transect, may substantiate the presence of a Cd-based version of carbonic anhydrase in certain diatoms – discussed by Abouchami et al. (2014) – a function of homeostatic metabolic functioning. Conversely, the surface depletion could be attributed to a strong Cd complexing agent released by prokaryotic and eukaryotic phytoplankton (Morel and Price, 2002). This suggests that the apparent bio-utilization of this element is exaggerated and that sub-surface depletion ratios are due to the complexation (detoxification) of Cd and not its utilization. Perhaps, a combination of utilization and complexation may better explain the depletion. This reiterates the lack of understanding of the role of Cd in bio-geochemical cycling. Nonetheless, comparisons with several studies confirmed that DCd concentrations are highly dependent on the strength of phytoplankton growth. Periodically the surface distribution was controlled by the strength of biological uptake, with apparent preferential DCd depletion in the absence of limitation induced growth stress.

The dataset presented herein has laid the groundwork permitting the elucidation of Co and Cd bio-geochemical cycling. Moreover, it has provided clear indicators as to which factors still inhibit further understanding, such as; chemical speciation in the region, the importance of atmospheric dust in the input of Co, the solubility of Cd, the role of the Vitamin B12, and the extent to which DCo cycling is dictated by the bacterial community. This data will form the framework for future endeavours and thereby allow this study to provide a more coherent understanding of the factors inhibiting phytoplankton growth in the Southern Ocean. The successful collection and quantification of trace

metals in the Southern Ocean demonstrates a noteworthy leap on the road to establishing the project as the centre for marine biogeochemistry in Africa.

References

Abouchami, W., Galer, S. J. G., De Baar, H. J. W., Middag, R., Vance, D., Zhao, Y., Klunder, M., Mezger, K., Feldmann, H. and Andreae, M. O. (2014) 'Biogeochemical cycling of cadmium isotopes in the Southern Ocean along the Zero Meridian', *Geochimica et Cosmochimica Acta*. Elsevier Ltd, 127, pp. 348–367. doi: 10.1016/j.gca.2013.10.022.

Baars, O., Abouchami, W., Galer, S. J. G., Boye, M. and Croot, P. L. (2014) 'Dissolved cadmium in the Southern Ocean: Distribution, speciation, and relation to phosphate', *Limnology and Oceanography*, 59(2), pp. 385–399. doi: 10.4319/lo.2014.59.2.0385.

Batley, G. E. and Florence, T. M. (1976) 'Determination of the chemical forms of dissolved cadmium, lead and copper in seawater', *Marine Chemistry*, 4(4), pp. 347–363. doi: 10.1016/0304-4203(76)90020-7.

Batterham, G. J., Munksgaard, N. C. and Parry, D. L. (1997) 'Determination of Trace Metals in Sea-water by Inductively Coupled Plasma Mass Spectrometry After Off-line Dithiocarbamate Solvent Extraction', *Instrumentation*, 12(November), pp. 1277–1280.

Bertrand, E. M., Saito, M. a., Rose, J. M., Riesselman, C. R., Lohan, M. C., Noble, A. E., Lee, P. a. and DiTullio, G. R. (2007) 'Vitamin B12 and iron colimitation of phytoplankton growth in the Ross Sea', *Limnology and Oceanography*, 52(3), pp. 1079–1093. doi: 10.4319/lo.2007.52.3.1079.

Biller, D. V. and Bruland, K. W. (2012) 'Analysis of Mn, Fe, Co, Ni, Cu, Zn, Cd, and Pb in seawater using the Nobias-chelate PA1 resin and magnetic sector inductively coupled plasma mass spectrometry (ICP-MS)', *Marine Chemistry*. Elsevier B.V., 130–131, pp. 12–20. doi: 10.1016/j.marchem.2011.12.001.

Bown, J., Boye, M., Baker, A., Duvieilbourg, E., Lacan, F., Le Moigne, F., Planchon, F., Speich, S. and Nelson, D. M. (2011) 'The biogeochemical cycle of dissolved cobalt in the Atlantic and the Southern Ocean south off the coast of South Africa', *Marine Chemistry*. Elsevier B.V., 126(1–4), pp. 193–206. doi: http://dx.doi.org/10.1016/j.marchem.2011.03.008.

Boye, M., Wake, B. D., Lopez Garcia, P., Bown, J., Baker, a. R. and Achterberg, E. P. (2012) 'Distributions of dissolved trace metals (Cd, Cu, Mn, Pb, Ag) in the southeastern Atlantic and the Southern Ocean', *Biogeosciences*, 9(8), pp. 3231–3246. doi: 10.5194/bg-9-3231-2012.

de Boyer Montégut, C., Madec, G., Fischer, A. S., Lazar, A. and Iudicone, D. (2004) 'Mixed layer depth over the global ocean: An examination of profile data and a profile-based climatology', *Journal of Geophysical Research C: Oceans*, 109(12), pp. 1–20. doi: 10.1029/2004JC002378.

Boyle, E. a. (1988) 'E. Boyle-Cd, chemical tracer of deepwate paleoceanography.pdf'. Massachusetts: Paleoceanogaphy, pp. 471–489.

Brand, L. E., Sunda, W. G. and Guillard, R. R. L. (1986) 'Reduction of marine phytoplankton reproduction rates by copper and cadmium', *Journal of Experimental Marine Biology and Ecology*, 96(3), pp. 225–250. doi: 10.1016/0022-0981(86)90205-4.

Brown, M. T., Smith, G. J. and Bruland, K. W. (2010) 'Cautionary Note on the analysis of seawater for Aluminum'.

Bruland, K. W., Donat, J. R. and Hutchins, D. a. (1991) 'Interactive influences of bioactive trace metals on biological production in oceanic waters', *Limnology and Oceanography*, 36(8), pp. 1555–1577. doi: 10.4319/lo.1991.36.8.1555.

Bruland, K. W., Franks, R. P., Knauer, G. a. and Martin, J. H. (1979) 'Sampling and analytical methods for the determination of copper, cadmium, zinc, and nickel at the nanogram per liter level in sea

water', *Analytica Chimica Acta*, Vol. 105, pp. 233–245. doi: 10.1016/S0003-2670(01)83754-5.

Coale, K. H. (1991) 'Effects of iron, manganese, copper, and zinc enrichments on productivity and biomass in the subarctic Pacific', *Limonology And Oceanography*, 36(8), pp. 1851–1864. doi: 10.4319/lo.1991.36.8.1851.

Cutter, G., Andersson, P., Codispoti, L., Croot, P., Francois, R., Lohan, M., Obata, H. and Rutgers, M. (2010) 'Sampling and Sample-handling Protocols for GEOTRACES cruises', (December), pp. 1–238. Available at: https://www.google.com.au/search?q=geotraces+cutter+et+al+2010&ie=utf-8&oe=utf-8&gws_rd=cr&ei=Wmi1VeygOYX5mAXon6W4DA.

Draxler, R. and Rolph, G. (2003) 'HYSPLIT (Hybrid single-particle Lagrangian integrated trajectory) model access via NOAA ARL READY. NOAA Air Resources Laboratory, Silver Spring', *Dostupno na: http://ready. arl. noaa. gov/HYSPLIT. php …*. Available at: https://scholar.google.co.za/scholar?hl=en&q=Draxler%2C+R.R.%2CRolph%2CG.D.%2C2003.HYSPLIT%28HYbridSingle-ParticleLagrangian+Integrated+Trajectory%29modelaccessviaNOAAARLREADY.NOAAAirResources+Laboratory%2C+SilverSpring%2CMD.Availablefrom%3A+%2Fhttp%3A%2F (Accessed: 10 November 2015).

Eby, G. N. (2004) *Principles of Environmental Geochemistry*. Edited by K. Dodson. Massachusetts: Brooks/Cole Publishing Company.

Elderfield, H., Holland, H. D. and Turekian, K. K. (2006) *The Oceans and Marine Geochemistry*. Elsevier. Available at: https://books.google.com/books?hl=en&lr=&id=BnZ77tb18UEC&pgis=1 (Accessed: 15 October 2015).

Ellwood, M. J. (2004) 'Zinc and cadmium speciation in subantarctic waters east of New Zealand', *Marine Chemistry*, 87(1–2), pp. 37–58. doi: 10.1016/j.marchem.2004.01.005.

Ellwood, M. J. (2008) 'Wintertime trace metal (Zn, Cu, Ni, Cd, Pb and Co) and nutrient distributions in the Subantarctic Zone between 40-52??S; 155-160??E', *Marine Chemistry*. Elsevier B.V., 112(1–2), pp. 107–117. doi: 10.1016/j.marchem.2008.07.008.

Ellwood, M. J. and Van den Berg, C. M. G. (2001) 'Determination of organic complexation of cobalt in seawater by cathodic stripping voltammetry', *Marine Chemistry*, 75(1–2), pp. 33–47. doi: 10.1016/S0304-4203(01)00024-X.

Ellwood, M. J., Van den Berg, C. M. G., Boye, M., Veldhuis, M., De, J. J. T. M., De, B. H. J. W., Croot, P. L. and Kattner, G. (2005) 'Organic complexation of cobalt across the Antarctic Polar Front in the Southern Ocean', *Mar. Freshwater Res.*, 56, pp. 1069–1075. doi: 10.1071/mf05097.

Frew, R., Bowie, a., Croot, P. and Pickmere, S. (2001) 'Macronutrient and trace-metal geochemistry of an in situ iron-induced Southern Ocean bloom', *Deep-Sea Research Part II: Topical Studies in Oceanography*, 48, pp. 2467–2481. doi: 10.1016/S0967-0645(01)00004-2.

Graham, R. (2014) *The role of Southern Ocean fronts in the global climate system*. Available at: http://www.diva-portal.org/smash/record.jsf?pid=diva2:760289.

Hawco, N. J., Ohnemus, D. C., Resing, J. A., Twining, B. S. and Saito, M. A. (2016) 'A dissolved cobalt plume in the oxygen minimum zone of the eastern tropical South Pacific', *Biogeosciences*, 13(20), pp. 5697–5717. doi: 10.5194/bg-13-5697-2016.

Ho, T.-Y., Chien, C.-T., Wang, B.-N. and Siriraks, A. (2010) 'Determination of trace metals in seawater by an automated flow injection ion chromatograph pretreatment system with ICPMS', *Talanta*. Elsevier B.V., 82(4), pp. 1478–1484. doi: 10.1016/j.talanta.2010.07.022.

Van Horsten, N. (2015) *Photosynthetic response of Southern Ocean phytoplankton under Iron and light limitations: Bioassay experiments*. Stellenbosch Univesity.

Jan, T. K. and Young, D. R. (1978) 'Determination of Microgram Amounts of Some Transition Metals in Seawater by Methyl Isobutyl Ketone-Nitric Acid Successive Extraction and Flameless Atomic Absorption Spectrophotometry', 50(9), pp. 1250–1253.

Jickells, T. D. and Burton, J. D. (1988) 'Sampling Samples were collected from two stations in the Sargasso Sea . One , Station filtered so the data presented are for total dissolvable trace metals . Analysis Manganese was preconcentrated forty-fold and separated from the bulk (Yeats and Bewers', *Marine Chemistry*, 23, pp. 131–144.

Kagaya, S., Maeba, E., Inoue, Y., Kamichatani, W., Kajiwara, T., Yanai, H., Saito, M. and Tohda, K. (2009) 'A solid phase extraction using a chelate resin immobilizing carboxymethylated pentaethylenehexamine for separation and preconcentration of trace elements in water samples', *Talanta*, 79(2), pp. 146–152. doi: 10.1016/j.talanta.2009.03.016.

Kingston, H. M., Barnes, I. L., Brady, T. J., Rains, T. C. and Champ, M. a. (1978) 'Separation of eight transition elements from alkali and alkaline earth elements in estuarine and seawater with chelating resin and their determination by graphite furnace atomic absorption spectrometry', *Analytical Chemistry*, 50(14), pp. 2064–2070. doi: 10.1021/ac50036a031.

Klunder, M. B., Laan, P., Middag, R., De Baar, H. J. W. and van Ooijen, J. C. (2011) 'Dissolved iron in the Southern Ocean (Atlantic sector)', *Deep Sea Research Part II: Topical Studies in Oceanography*. Elsevier, 58(25–26), pp. 2678–2694. doi: 10.1016/j.dsr2.2010.10.042.

Kuss, J. and Kremling, K. (1999) 'Spatial variability of particle associated trace elements in near-surface waters of the North Atlantic (30 degrees N/60 degrees W to 60 degrees N/2 degrees W), derived by large-volume sampling', *Marine Chemistry*, 68(1–2), pp. 71–86. doi: Doi 10.1016/S0304-4203(99)00066-3.

Lee, J.-M., Boyle, E. a., Echegoyen-Sanz, Y., Fitzsimmons, J. N., Zhang, R. and Kayser, R. a. (2011) 'Analysis of trace metals (Cu, Cd, Pb, and Fe) in seawater using single batch nitrilotriacetate resin extraction and isotope dilution inductively coupled plasma mass spectrometry', *Analytica Chimica Acta*. Elsevier B.V., 686(1–2), pp. 93–101. doi: 10.1016/j.aca.2010.11.052.

Lohan, M. C., Aguilar-Islas, A. M., Franks, R. P. and Bruland, K. W. (2005) 'Determination of iron and copper in seawater at pH 1.7 with a new commercially available chelating resin, NTA Superflow', *Analytica Chimica Acta*, 530(1), pp. 121–129. doi: 10.1016/j.aca.2004.09.005.

Loscher, B. M. (1999) 'Relationships among Ni, Cu, Zn, and major nutrients in the Southern Ocean', *Marine Chemistry*, 67(1–2), pp. 67–102. doi: Doi 10.1016/S0304-4203(99)00050-X.

Mclaren, J. W., Mykytiuk, a P., Willie, S. N. and Berman, S. S. (1985) 'Determination of Trace Metals in Seawater by Inductively Coupled Plasma Mass Spectrometry with Preconcentration on', *Analytical Chemistry*, (57), pp. 2907–2911. doi: 10.1021/ac00291a037.

Middag, R., De Baar, H. J. W., Laan, P., Cai, P. H. and Van Ooijen, J. C. (2011) 'Dissolved manganese in the Atlantic sector of the Southern Ocean', *Deep Sea Research Part II: Topical Studies in Oceanography*. Elsevier, 58(25–26), pp. 2661–2677. doi: 10.1016/S0967-0645(96)00064-1.

Milne, A., Landing, W., Bizimis, M. and Morton, P. (2010) 'Determination of Mn, Fe, Co, Ni, Cu, Zn, Cd and Pb in seawater using high resolution magnetic sector inductively coupled mass spectrometry (HR-ICP-MS)', *Analytica Chimica Acta*. Elsevier B.V., 665(2), pp. 200–207. doi: 10.1016/j.aca.2010.03.027.

Minami, T., Konagaya, W., Zheng, L., Takano, S., Sasaki, M., Murata, R., Nakaguchi, Y. and Sohrin, Y.

(2015) 'An off-line automated preconcentration system with ethylenediaminetriacetate chelating resin for the determination of trace metals in seawater by high-resolution inductively coupled plasma mass spectrometry', *Analytica Chimica Acta*. Elsevier B.V., 854, pp. 183–190. doi: 10.1016/j.aca.2014.11.016.

Moffett, J. W. and Ho, J. (1996) 'Oxidation of cobalt and manganese in seawater via a common microbially catalyzed pathway', *Geochimica et Cosmochimica Acta*, 60(18), pp. 3415–3424. doi: 10.1016/0016-7037(96)00176-7.

Le Moigne, F. a C., Boye, M., Masson, a., Corvaisier, R., Grossteffan, E., Guéneugues, a. and Pondaven, P. (2013) 'Description of the biogeochemical features of the subtropical southeastern Atlantic and the Southern Ocean south of South Africa during the austral summer of the International Polar Year', *Biogeosciences*, 10, pp. 281–295. doi: 10.5194/bg-10-281-2013.

Morel, F. M. M. and Price, N. M. (2002) 'The Biogeochemical Cycles of Trace Metals in the Oceans'.

Morford, J. L. and Emerson, S. (1999) 'The geochemistry of redox sensitive trace metals in sediments', *Geochimica et Cosmochimica Acta*, 63(11–12), pp. 1735–1750. doi: 10.1016/S0016-7037(99)00126-X.

Nodwell, L. M. and Price, N. M. (2001) 'Direct use of inorganic colloidal iron by marine mixotrophic phytoplankton', *Limnology and Oceanography*, 46(4), pp. 765–777. doi: 10.4319/lo.2001.46.4.0765.

Orsi, A. H., Whitworth, T. and Nowlin, W. D. (1995) 'On the meridional extent and fronts of the Antarctic Circumpolar Current', *Deep-Sea Research Part I*, 42(5), pp. 641–673. doi: 10.1016/0967-0637(95)00021-W.

Palmer, L. (2015) *Nutrient Availability for Primary Production in the Southern Ocean.* Stellenbosch University.

Peng, T.-H., Takahashi, T., Broecker, W. S. and Olafsson, J. (1987) 'Seasonal variability of carbon dioxide, nutrients and oxygen in the northern North Atlantic surface water: observations and a model*', *Tellus B*, 39B(5), pp. 439–458. doi: 10.1111/j.1600-0889.1987.tb00205.x.

Pollard, R. ., Lucas, M. . and Read, J. . (2002) 'Physical controls on biogeochemical zonation in the Southern Ocean', *Deep Sea Research Part II: Topical Studies in Oceanography*, 49(16), pp. 3289–3305. doi: 10.1016/S0967-0645(02)00084-X.

Reid, P. C., Fischer, A. C., Lewis-Brown, E., Meredith, M. P., Sparrow, M., Andersson, A. J., Antia, A., Bates, N. R., Bathmann, U., Beaugrand, G., Brix, H., Dye, S., Edwards, M., Furevik, T., Gangstø, R., Hátún, H., Hopcroft, R. R., Kendall, M., Kasten, S., Keeling, R., Le Quéré, C., Mackenzie, F. T., Malin, G., Mauritzen, C., Ólafsson, J., Paull, C., Rignot, E., Shimada, K., Vogt, M., Wallace, C., Wang, Z. and Washington, R. (2009) *Impacts of the oceans on climate change*, *Advances in Marine Biology*. doi: 10.1016/S0065-2881(09)56001-4.

Saito, M. a. and Goepfert, T. J. (2008) 'Zinc-cobalt colimitation of Phaeocystis antarctica', *Limnology and Oceanography*, 53(1), pp. 266–275. doi: 10.4319/lo.2008.53.1.0266.

Saito, M. a., Goepfert, T. J., Noble, a. E., Bertrand, E. M., Sedwick, P. N. and Ditullio, G. R. (2010) 'A seasonal study of dissolved cobalt in the Ross Sea, Antarctica: Micronutrient behavior, absence of scavenging, and relationships with Zn, Cd, and P', *Biogeosciences*, 7(12), pp. 4059–4082. doi: 10.5194/bg-7-4059-2010.

Saito, M. a. and Moffett, J. W. (2001) 'Complexation of cobalt by natural organic ligands in the Sargasso sea as determined by a new high-sensitivity electrochemical cobalt speciation method suitable for open ocean work', *Marine Chemistry*, 75(1–2), pp. 49–68. doi: 10.1016/S0304-4203(01)00025-1.

Saito, M. a. and Moffett, J. W. (2002) 'Temporal and spatial variability of cobalt in the Atlantic Ocean', *Geochimica et Cosmochimica Acta*, 66(11), pp. 1943–1953. doi: 10.1016/S0016-7037(02)00829-3.

Sañudo-Wilhelmy, S. a., Olsen, K. a., Scelfo, J. M., Foster, T. D. and Flegal, a. R. (2002) 'Trace metal distributions off the antarctic peninsula in the weddell sea', *Marine Chemistry*, 77(2–3), pp. 157–170. doi: 10.1016/S0304-4203(01)00084-6.

Satyanarayanan, M., Balaram, V., Rao, T. G., Dasaram, B., Ramesh, S. L., Mathur, R. and Drolia, R. K. (2007) 'Determination of trace metals in seawater by ICP-MS after preconcentration and matrix separation by dithiocarbamate complexes', *Indian Journal of Marine Sciences*, 36(1), pp. 71–75.

SHAH, V., MIDHA, K., DIGNE, S. and MCGILVERAY, I. (1992) 'Analytical Methods Validation: Bioavailability, Bioquivalence, and Pharmacokinetic Studies', *Journal of Pharmaceutical Sciences*, 3(81), pp. 309–312.

Shelley, R. U., Sedwick, P. N., Bibby, T. S., Cabedo-Sanz, P., Church, T. M., Johnson, R. J., MacEy, A. I., Marsay, C. M., Sholkovitz, E. R., Ussher, S. J., Worsfold, P. J. and Lohan, M. C. (2012) 'Controls on dissolved cobalt in surface waters of the Sargasso Sea: Comparisons with iron and aluminum', *Global Biogeochemical Cycles*, 26(2), pp. 1–16. doi: 10.1029/2011GB004155.

Sohrin, Y., Urushihara, S., Nakatsuka, S., Kono, T., Higo, E., Minami, T., Norisuye, K. and Umetani, S. (2008) 'Multielemental determination of GEOTRACES key trace metals in seawater by ICPMS after preconcentration using an ethylenediaminetriacetic acid chelating resin', *Analytical Chemistry*, 80(16), pp. 6267–6273. doi: 10.1021/ac800500f.

Sunda, W. (1991) 'Trace metal interactions with marine phytoplankton', *Biological Oceanography*, 6(June 2015), pp. 411–442. doi: 10.1080/01965581.1988.10749543.

Sunda, W. G. (2012) 'Feedback Interactions between Trace Metal Nutrients and Phytoplankton in the Ocean', *Frontiers in Microbiology*, 3(June), pp. 1–22. doi: 10.3389/fmicb.2012.00204.

Sunda, W. G. and Huntsman, S. a. (1995) 'Iron uptake and growth limitation in oceanic and coastal phytoplankton', *Marine Chemistry*, 50(1–4), pp. 189–206. doi: 10.1016/0304-4203(95)00035-P.

Sunda, W. G. and Huntsman, S. a. (2000) 'Effect of Zn, Mn, and Fe on Cd accumulation in phytoplankton: Implications for oceanic Cd cycling', *Limnology and Oceanography*, 45(7), pp. 1501–1516. doi: 10.4319/lo.2000.45.7.1501.

Taverniers, I., De Loose, M. and Van Bockstaele, E. (2004) 'Trends in quality in the analytical laboratory. II. Analytical method validation and quality assurance', *TrAC - Trends in Analytical Chemistry*, 23(8), pp. 535–552. doi: 10.1016/j.trac.2004.04.001.

Union, I., Pure, O. F., Chemistry, A., Divisions, P. C., Working, I., For, P., Of, H., Assurance, Q., For, S., Laboratories, A., Thompson, M., Ellison, S. L. R. and Wood, R. (2002) 'QUALITY ASSURANCE SCHEMES FOR ANALYTICAL LABORATORIES * HARMONIZED GUIDELINES FOR SINGLE- LABORATORY VALIDATION OF METHODS OF ANALYSIS (IUPAC Technical Report) Harmonized guidelines for single-laboratory', 74(5), pp. 835–855.

Veth, C., Peeken, I. and Scharek, R. (1997) 'Physical anatomy of fronts and surface waters in the ACC near the 6??W meridian during austral spring 1992', *Deep-Sea Research Part II: Topical Studies in Oceanography*, 44(1–2), pp. 23–49. doi: 10.1016/S0967-0645(96)00062-8.

Vichi, M., Allen, J. I., Masina, S. and Hardman-Mountford, N. J. (2011) 'The emergence of ocean biogeochemical provinces: A quantitative assessment and a diagnostic for model evaluation', *Global Biogeochemical Cycles*, 25(2), pp. 1–17. doi: 10.1029/2010GB003867.

Viljoen, J. . (2016) *Phytoplankton Pigment Analysis and CHEMTAX determination of phytoplankton community structure in the Southern Ocean*. Stellenbosch University.

Wang, B.-S., Lee, C.-P. and Ho, T.-Y. (2014) 'Trace metal determination in natural waters by automated solid phase extraction system and ICP-MS: the influence of low level Mg and Ca.', *Talanta*. Elsevier, 128, pp. 337–44. doi: 10.1016/j.talanta.2014.04.077.

Wefer, G. and Fischer, G. (1991) 'Annual primary production and export flux in the Southern Ocean from sediment trap data', *Marine Chemistry*. Elsevier Science Publishers B.V., 35(1–4), pp. 597–613. doi: 10.1016/S0304-4203(09)90045-7.

Westerlund, S. and Ohman, P. (1991) 'Cadmium, Copper, Cobalt, Nickel, Lead, and Zinc in the Water Column of the Weddell Sea, Antarctica', *Geochimica Et Cosmochimica Acta*, 55(8), pp. 2127–2146. doi: 10.1016/0016-7037(91)90092-j.

Wood, R. (1999) 'How to validate analytical methods', *TrAC - Trends in Analytical Chemistry*, 18(9–10), pp. 624–632. doi: 10.1016/S0165-9936(99)00150-8.

Wu, J. and Boyle, E. a. (1997) 'Low blank preconcentration technique for the determination of lead, copper, and cadmium in small-volume seawater samples by isotope dilution ICPMS', *Analytical chemistry*, 69(13), pp. 2464–70. doi: 10.1021/ac961204u.

Appendix A

1. Figures and Tables

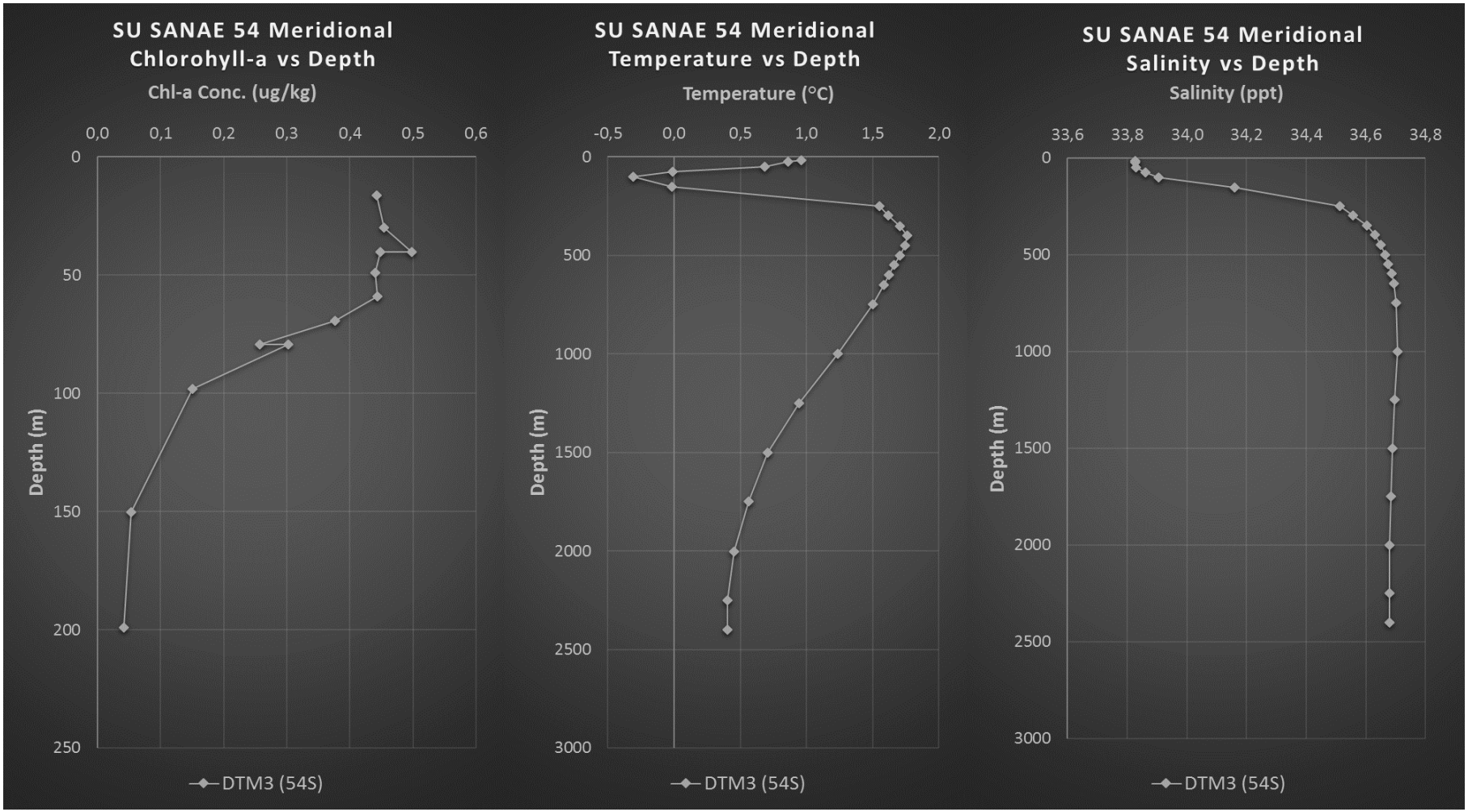

***Figure A1**-Ancillary Chlorophyll-a (µg/kg), CTD temperature (°C) and CTD salinity for the SANAE 54 Baseline and Inter-calibration station at 54°S.*

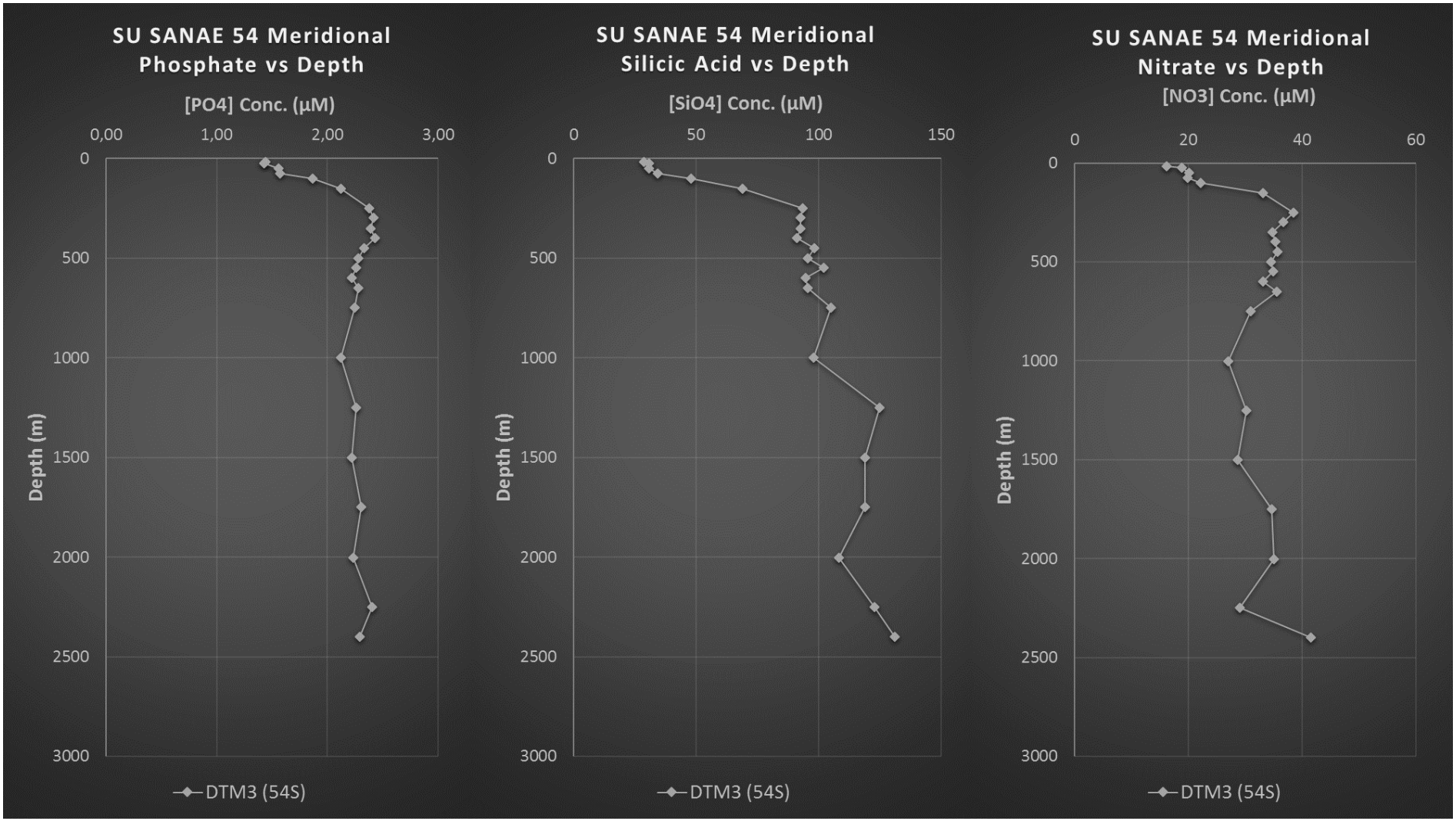

***Figure A2**-Ancillary macronutrient concentrations for the SANAE 54 Baseline and Inter-calibration station at 54°S. Phosphate (PO4), Nitrate (NO3) and Silicic Acid (SiO4) (µM) was collected and analysed by* Palmer (2015).

***Table A1**-A compilation (n=51) of the TM4A In-house control samples used in the evaluation of the method precision. Cells are conditionally formatted as follows: Yellow represents one standard deviation (Std Dev) above or below, spots in the cells indicate two Std Dev, red cells indicate three Std Dev and are subsequently deemed outliers and excluded from calculation.*

TM4 Large Volume Acidified Control (pH 1.7)			Mn	Fe	Co	Ni	Cu	Zn	Cd	Pb
Description	Date Analysed	TM4A Control	[nmol/kg]	[nmol/kg]	[pmol/kg]	[nmol/kg]	[nmol/kg]	[nmol/kg]	[pmol/kg]	[pmol/kg]
Calibration 2-2016 (2)	09_06_2016	**SU C2_16 TM4A_1**	0,271	0,329	18,556	5,970	1,617	5,933	644,344	6,892
		SU C2_16 TM4A_2	0,265	0,329	18,391	5,894	1,599	5,847	625,536	6,967
		SU C2_16 TM4A_3	0,259	0,336	18,134	5,884	1,602	5,905	636,025	6,817
		SU C2_16 TM4A_4	0,264	0,315	17,583	5,734	1,548	5,753	627,767	6,567
		SU C2_16 TM4A_5	0,257	0,329	19,382	5,843	1,583	5,914	639,754	6,751
		SU C2_16 TM4A_6	0,288	0,424	19,235	5,771	1,553	5,812	622,853	6,915
		SU C2_16 TM4A_7	0,255	0,331	18,754	5,727	1,551	5,795	615,833	6,773
		SU C2_16 TM4A_8	0,261	0,343	16,978	5,828	1,597	5,821	624,434	6,893
		SU C2_16 TM4A_9	0,263	0,314	17,441	5,571	1,505	5,737	603,503	6,575
		SU C2_16 TM4A_10	0,252	0,373	17,810	5,748	1,537	5,755	610,712	6,677
S54 DTM3 Re-Run	05_07_2016	**S54 DTM3 TM4A_1R(1)**	0,274	0,343	19,698	6,488	1,734	6,379	690,756	8,046
		S54 DTM3 TM4A_1R(2)	0,287	0,321	20,268	6,704	1,828	6,354	699,712	7,308
		S54 DTM3 TM4A_2R	0,253	0,235	17,402	5,973	1,645	5,676	635,783	6,659
S54 DTM3 Soluble Control	05_07_2016	**S54 DTM3S TM4A_3**	0,265	0,231	18,276	5,911	1,670	5,723	644,746	6,660
		S54 DTM3S TM4A_4	0,264	0,280	17,805	6,105	1,734	5,935	674,222	6,745
		S54 DTM3S TM4A_5	0,255	0,271	16,996	5,741	1,647	5,742	635,788	6,419
		S54 DTM3S TM4A_6	0,262	0,290	17,504	6,057	1,695	5,921	652,083	6,494
SOSCEX III DTM2	05_08_2016	**SOSCEX III DTM2 TM4A_1**	0,255	0,293	22,663	5,939	1,611	5,784	624,526	6,366
		SOSCEX III DTM2 TM4A_2	0,244	0,287	23,623	5,933	1,648	5,617	616,923	6,267
		SOSCEX III DTM2 TM4A_3	0,261	0,300	23,325	6,335	1,764	5,987	667,357	6,761
		SOSCEX III DTM2 TM4A_4	0,246	0,327	21,239	5,865	1,625	5,573	625,871	6,342
		SOSCEX III DTM2 TM4A_5	0,237	0,295	21,173	5,651	1,578	5,468	608,357	6,069
S54 DTM1 Soluble Control	06_07_2016	**S54 DTM1S TM4A_1**	0,259	0,255	17,534	6,115	1,645	5,675	651,558	6,488
		S54 DTM1S TM4A_2	0,263	0,270	18,595	5,913	1,684	5,825	661,105	6,771
		S54 DTM1S TM4A_3	0,254	0,234	16,741	5,685	1,617	5,519	639,397	6,469
		S54 DTM1S TM4A_4	0,250	0,248	16,380	5,638	1,652	5,624	633,623	6,715
S54 DTM2 Soluble Control	06_07_2016	**S54 DTM2S TM4A_5**	0,253	0,240	16,224	5,845	1,618	5,460	631,489	6,321
		S54 DTM2S TM4A_6	0,270	0,290	17,703	6,202	1,692	5,803	652,750	6,652
		S54 DTM2S TM4A_7	0,248	0,278	15,955	5,771	1,589	5,397	629,991	6,380

Table A1 (Continued)

TM4 Large Volume Acidified Control (pH 1.7)			Mn	Fe	Co	Ni	Cu	Zn	Cd	Pb
Description	Date Analysed	TM4A Control	[nmol/kg]	[nmol/kg]	[pmol/kg]	[nmol/kg]	[nmol/kg]	[nmol/kg]	[pmol/kg]	[pmol/kg]
S54 TM1 Controls	12_07_2016	**S54 TM1 TM4A_1**	0,234	0,280	16,769	5,708	1,567	7,029	603,101	6,890
		S54 TM1 TM4A_2	0,251	0,254	16,848	5,616	1,530	5,439	598,767	6,665
		S54 TM1 TM4A_3	0,240	0,258	17,683	5,724	1,571	5,532	607,412	6,241
		S54 TM1 TM4A_4	0,260	0,272	16,448	5,809	1,558	5,648	621,576	6,398
		S54 TM1 TM4A_5	0,211	0,319	22,585	5,815	1,685	5,781	624,918	5,973
		S54 TM1 TM4A_6	0,212	0,324	21,789	5,965	1,643	5,648	631,723	6,088
SOSCEX III TM1	04_08_2016	**SOSCEX III TM1 TM4A_1**	0,265	0,277	24,345	6,040	1,669	6,076	663,138	6,919
		SOSCEX III TM1 TM4A_2	0,248	0,267	23,229	6,057	1,662	5,858	626,564	6,652
		SOSCEX III TM1 TM4A_3	0,258	0,304	22,801	5,988	1,649	6,058	650,865	6,569
		SOSCEX III TM1 TM4A_4	0,262	0,310	22,754	6,058	1,711	6,090	653,180	7,833
	Pause									
	12_08_2016	**SOSCEX III TM1 TM4A_5**	0,269	0,309	23,513	6,094	1,692	6,141	662,438	6,828
		SOSCEX III TM1 TM4A_6	0,270	0,309	22,483	6,066	1,650	5,941	665,854	6,711
		SOSCEX III TM1 TM4A_7	0,281	0,339	24,232	6,796	1,852	6,349	710,811	7,325
		SOSCEX III TM1 TM4A_8	0,254	0,298	22,229	5,902	1,587	5,682	625,400	6,333
SOSCEX III DTM3	07_07_2016	**SOSCEX III DTM3 TM4A_1**	0,259	0,293	20,652	6,104	1,640	5,859	637,465	6,708
		SOSCEX III DTM3 TM4A_2	0,256	0,262	20,489	6,051	1,639	5,625	638,796	6,599
		SOSCEX III DTM3 TM4A_3	0,250	0,267	19,884	5,834	1,639	5,568	629,666	6,524
		SOSCEX III DTM3 TM4A_4	0,264	0,279	20,463	5,957	1,682	5,795	649,514	6,680
		SOSCEX III DTM3 TM4A_5	0,263	0,286	20,807	6,188	1,672	5,852	650,031	6,807
		SOSCEX III DTM3 TM4A_6	0,255	0,271	20,643	6,051	1,659	5,682	645,767	6,599
		SOSCEX III DTM3 TM4A_7	0,258	0,272	19,983	5,867	1,665	5,682	645,453	6,604
		SOSCEX III DTM3 TM4A_8	0,260	0,253	19,699	5,652	1,598	5,657	630,480	6,422
		Population Size	51	51	51	51	51	51	51	51
		No. Outlier Cells	2	1	0	2	1	1	1	2
		Mean (x̄)	0,26	0,29	19,64	5,91	1,63	5,79	637,78	6,62
		Std Deviation	0,01	0,03	2,42	0,19	0,06	0,22	21,10	0,27
		TM4A %RSD	4,17	11,18	12,32	3,18	3,81	3,82	3,31	4,09
		Skew	0,39	0,14	0,34	0,56	0,42	0,74	0,61	0,08
		Std Error_Skew	0,35	0,35	0,34	0,35	0,35	0,35	0,35	0,35
		Significant Skew (Y/N)	N	N	N	N	N	Y	N	N
		Margin or Error_Confidence (95%)	0,00	0,01	0,66	0,05	0,02	0,06	5,85	0,08
		% Within one std dev	85,7	74,0	66,7	81,6	74,0	80,0	72,0	85,7
		% Within two std dev	95,9	98,0	100,0	98,0	98,0	98,0	96,0	100,0

2. Method Development

2.1 Cleaning Procedures

LDPE and PFA Sampling Bottles

Pre-cruise cleaning performed stepwise adapted from GEOTRACES cookbook.

- Rinse bottles with methanol or iso-2-propanol.
- Place bottles in alkaline detergent- 1 week
- Rinse (7X) thoroughly with ultra-high purity water (UHPW such as Milli-Q).
- Fill bottles with 6M HCl reagent grade (RG) and place bottles in 2M acid bath RG HCl-3 weeks to 1 month.
- Rinse (7X) thoroughly with ultra-high purity water (UHPW such as Milli-Q).
- Fill bottles with 0.1M high grade HCl (Suprapur®) for storage (double bag).

Note: The GEOTRACES protocols for PFA's does not require such an extensive process but PFA's and LDPE's were cleaned according to same method on this cruise.

GO-FLO Cleaning Protocol

Before listing the cleaning protocol for the Go-Flo bottles the following must be noted.

- The O-rings on the inside of the Go-Flo bottles were replaced with Viton O-rings.
- Stainless steel bands were replaced by heavy duty cable ties on several GO-FLO's.

Cleaning protocol:

- Fill Go-Flo bottle with a mixture of 500ml iso-2-propanol to 10L Milli-Q water. Allow 6 hours for iso-2-propanol to leach the organic oils from the inside of the Go-Flo bottles – 10 hours (Minimum)
- Rinse Go-Flo bottles thoroughly 3X with Milli-Q.
- Fill Go-Flo with a 0.3M mixture of 10.2M HCl and Milli-Q and allowed to stand so that HCl can leach any iron inside the Go-Flo bottle – 1 day (Minimum)

Suprapur® Storage Acid Step

- Decant 6M HCl contents into chemical waste bin taking care not to make contact between waste bin and bottle
- Rinse bottle 3 times with Milli-Q taking time to rinse the lid and neck of the bottle. Fill roughly half bottle with Milli-Q
- Pipette 4ml of Suprapur® (9.45M) into bottle for a final concentration of 0.1M
- Fill remaining volume of bottle with Mill-Q
- Double zip lock bag the bottle (one person drops bottle into the first zip-lock bag held by second person).

Notes:

- Care must be taken to clean the syringe/pipette tip of the pipette before use.
    1. Rinse 3 times with acid (HCl).
    2. Rinse 3 times with Milli-Q 1.
    3. Rinse 3 times with Milli-Q 2.

Filtration (TFe)

Go-Flo bottle exteriors should be rinsed with Milli-Q prior to subsampling paying particular attention to the taps.

Responsibilities: Dirty Hand (DH), Trace Metal Sampler (TMS), Acidifier (AF)

- DH takes double zip-locked 125 ml PFA bottles from black plastic bag, removes the outer zip-lock bag and places it in the fume hood. (DH doesn't touch the inner zip-lock)
- The AF opens the inner zip-lock bag and TMS takes the bottle out. (AF doesn't touch the bottle)
- TMS empties the storage acid from the PFA bottle into the drain in the Go-Flo container.
- TMS proceeds to fill the PFA sample bottle with roughly 25ml for rinsing. A 30 cm PTFE tube is inserted into the tap of the Go-Flo and sampling is done through this tube. Repeat 3X making sure the lid and neck of the bottle is thoroughly rinsed.
- Once rinsing is complete fill the sample bottle to the neck (125ml) close lid tightly and place in the fume hood.
- AF places the bottle into its inner zip-lock bag and seals
- AF then places the zip-lock bag into the outer zip-lock bag which is held by the DH.
- The DH applies the pre-written label to the outer zip-lock bag

Filtration (DFe)

The protocol for sampling DFe is the same as for TFe except for the following additional parameters:

- Acropak 0.2µm filter with particulate shield around the tap is used to filter the samples. This attaches to the 30 cm tubing from the Go-Flo's tap.
- The AF spikes the sample with 200 µL/100 ml of Merck Ultrapur® to attain a pH of 1.8.
- Nitrogen assisted filtration. The pressure increases flow rate of seawater through the filter and ultimately speeds up the sampling process.

Notes:

1) Take care to avoid outside contamination from falling particles by making sure the sample bottle opening is under the filter shield during filtering.
2) Whenever sampling from a new Go-Flo bottle, let water run for at least 30 seconds through the Acropak (0.2µM) filter with nitrogen assistance to flush the seawater from the previous Go-Flo bottles through the filter and condition the filter. In addition to this, rinse the inside of the filters shield by holding the filter upright and allowing a small volume of water to collect in it. Swoosh it around a few times and discard. Repeat this 3 times.

2.2 Pre-Concentration Method

Falcon Tube Cleaning (adapted from LDPE and PFA)

- Place opened Falcon tubes and caps, into a 2M bath of 32% reagent grade (RG) HCl – 3 weeks
- Rinse 3 X with UHPW (Milli-Q).
- Fill 14ml Falcon tube with 1M Suprapur HCl and cap.
- Place into 0.1M Suprapur (30%) HCl bath – leave for 2 weeks.
- Vials can remain filled with 0.1M Suprarpur (30%) HCl until needed.

Notes:

1) In future, the method should follow ship protocol for cleaning of sampling bottles.
2) All sampling beakers, containers, vials, probes and the rinse station should be cleaned according to protocols prior to sample handling.

Sample Decant

- Acid filled, 0.1M, Falcon tube (14ml) is rinsed 10 times with Milli-Q, capped loosely and placed in vial rack to dry.
- Sample decanter prepares to decant 125ml bottle (PFA x 1 Total, LDPE x 2 Dissolved) under laminar flow hood.
- Sample decanter decants approximately 3ml of sample into Falcon tube held by sample receiver.
- Sample receiver caps Falcon tube and thoroughly shakes the contents to “condition” the vile.
- Sample receiver discards contents and falcon tube is filled to 12.5ml with sample.
- Falcon tube is capped tightly by sample receiver who places it in the correct origin location in the sampling vial rack.

TM4 Control Protocol

- Each batch of samples included several samples with TM4 – large volume available – contents as a control.
- Prepare according to same procedure as Field Sample.

Run Procedure

- Falcon tubes are filled with required samples (see decant procedure).
- Each tube is assigned an origin and destination number on the sampling rack.
- 6 x Sample filled Falcon tubes are opened (If lids are kept make sure it is in numerical order else cross contamination can occur should the samples need to be closed, new clean lids are also an option).
- Change gloves.
- 6 x Destination, empty, Falcon tubes are opened (keep lids in zip-lock bag). It is essential to ensure each vile is dry, else dilution and possibly contamination will occur.

Capping of Pre-concentrated Samples

- Put on clean gloves.
- Seal Falcon tube with lid (labelling can be done now or earlier). Repeat for six falcon tubes.

Notes:

1) It is essential to balance practicality and sample handling else this process is time consuming (20min per sample). Only six Falcon tubes were opened at any time during pre-concentration within the clean laboratory. This was done to minimise contamination risk and ensure that evaporation of concentrated samples did not concentrate the samples further.

Appendix B

1. Tables

***Table B1**-The multi-element, single sample aliquot, concentrations from the STZ (TM4) for the total (T) fraction. The data set reports concentrations with corrections for potentially contaminated samples. Data in red is considered anomalous. No std deviation is reported. The samples were collected unfiltered in PFA bottles. The ([a]) denotes units pmol/kg and ([b]) units in nmol/kg. The (*) denotes that results are an average of respective depths.*

Date: 05 February 2015

Domain (Station)	Latitude & Longitude	Depth (m)	TMn[b]	TFe[b]	TCo[a]	TNi[b]	TCu[b]	TZn[b]	TCd[a]	TPb[a]
STZ (TM4)	36˚ 00.00' S 13˚ 09.71' E	15	1,005	0,259	18,020	2,458	0,536	9,363	16,569	17,604
		30	1,038	0,223	18,354	2,443	0,550	10,335	18,600	19,636
		41	1,027	0,286	21,196	2,457	0,532	9,316	16,569	18,317
		60	0,854	0,386	19,574	2,445	0,502	9,492	17,416	16,919
		80	0,797	0,337	19,683	2,699	0,456	9,712	23,231	16,306
		150	0,583	0,323	13,895	2,742	0,458	8,557	29,701	15,294
		250	0,409	1,183	20,031	3,344	0,600	8,611	107,267	20,068
		301	0,354	1,329	19,335	3,406	0,591	8,445	117,616	20,096
		400	0,408	1,103	23,318	3,815	0,642	9,313	180,515	18,067
		501	0,370	1,123	27,369	4,375	0,739	8,573	297,456	15,637
		600	0,379	2,041	34,471	5,219	0,876	9,800	448,651	16,112
		801	0,280	1,349	33,599	5,446	1,001	10,036	584,192	14,730
		1000	0,313	1,643	35,420	6,178	1,271	11,531	711,006	13,584
Maximum			1,04	1,64	35,42	6,18	1,27	11,53	711,01	20,10
Minimum			0,28	0,22	13,90	2,44	0,46	8,44	16,57	13,58
Surface (MLD)*			0,98	0,29	19,29	2,45	0,53	9,63	17,29	18,12
Sub-surface (500m)*			0,66	0,78	21,39	3,22	0,59	9,23	115,78	17,64
Inter (500-1700m)*			0,30	1,50	34,51	5,81	1,14	10,78	647,60	14,16

***Table B2**-The multi-element, single sample aliquot, concentrations from the SAF (DTM2) for the total (T) fraction. The data set reports concentrations with corrections for potentially contaminated samples. Data in red is considered anomalous. No std deviation is reported. The samples were collected unfiltered in PFA bottles. The ([a]) denotes units pmol/kg and ([b]) units in nmol/kg. The (*) denotes that results are an average of respective depths. Values Fe values in italics are anomalously high as a consequence of the GO-FLO sample being taken at a depth proximal to the seabed.*

Date: 12 January 2015

Domain (Station)	Latitude & Longitude	Depth (m)	TAl[b]	TV[b]	TMn[b]	TFe[b]	TCo[a]	TNi[b]	TCu[b]	TZn[b]	TCd[a]	TPb[a]
SAF (DTM2)	46˚ 00.11' S 08˚ 00.00' E	14	17,68	36,34	0,29	0,71	49,22	5,59	1,09	0,90	348,07	11,42
		35	5,77	33,32	0,28	0,70	37,85	5,40	0,99	0,86	324,63	12,69
		75	3,65	30,39	0,24	0,56	48,84	5,08	0,98	0,76	321,00	10,17
		100	4,36	36,08	0,34	0,66	41,72	5,90	1,12	2,59	368,12	15,65
		150	2,93	36,15	0,33	0,62	40,02	5,77	1,10	1,95	457,45	19,71
		200	4,16	36,16	0,35	1,11	44,81	5,63	1,08	2,69	584,55	14,58
		400	2,64	36,23	0,26	1,31	43,16	6,16	1,26	2,31	711,69	14,10
		501	3,28	39,95	0,31	1,19	44,02	6,35	1,43	3,81	799,08	16,89
		622	2,59	34,51	0,27	1,20	35,76	5,97	1,36	4,88	727,83	13,94
		1000	2,42	38,63	0,37	1,46	36,79	7,26	1,88	5,21	891,60	14,21
		1501	2,81	39,24	0,32	1,85	34,68	6,96	2,06	4,75	752,50	13,71
		2000	3,35	37,77	0,37	1,66	33,68	6,60	2,15	6,65	644,25	18,18
		3000	3,62	37,07	0,25	1,67	21,90	6,68	2,67	5,50	683,01	8,59
		4002	4,51	35,75	0,45	***4,32***	22,24	6,75	2,97	5,82	706,93	11,16
		4302	5,58	44,35	1,08	***11,83***	28,95	8,39	3,95	6,97	894,34	10,44
Maximum			5,77	44,35	1,08	1,85	49,22	8,39	3,95	6,97	894,34	19,71
Minimum			2,42	30,39	0,24	0,56	21,90	5,08	0,98	0,76	321,00	8,59
Surface (MLD)*			4,71	33,35	0,27	0,65	45,31	5,36	1,02	0,84	331,24	11,43
Sub-surface (500m)*			3,83	35,58	0,30	0,86	43,71	5,73	1,13	1,98	489,33	14,40
Inter (500-1700m)*			2,77	38,08	0,32	1,42	37,81	6,64	1,68	4,66	792,75	14,69
Deep (>1700m)*			4,26	38,74	0,54	4,87	26,69	7,10	2,94	6,23	732,13	12,10

***Table B3**-The multi-element, single sample aliquot, concentrations from the PF (TM1) for the total (T) fraction. The data set reports concentrations with corrections for potentially contaminated samples. Data in red is considered anomalous. No std deviation is reported. The samples were collected unfiltered in PFA bottles. The ([a]) denotes units pmol/kg and ([b]) units in nmol/kg. The (*) denotes that results are an average of respective depths.*

Date: 14 January 2015

Domain (Station)	Latitude & Longitude	Depth (m)	TMn[b]	TFe[b]	TCo[a]	TNi[b]	TCu[b]	TZn[b]	TCd[a]	TPb[a]
PF (TM1)	50°26,99' S 02°00.12' E	16	0,21	0,20	24,40	4,89	0,98	0,99	307,27	5,56
		31	0,20	0,19	23,63	5,10	1,01	0,95	313,74	5,94
		40	0,22	0,19	30,17	5,34	1,08	0,91	330,08	6,83
		60	0,22	0,17	25,67	4,94	0,98	1,08	320,40	5,71
		78	0,26	0,36	27,41	5,27	1,07	1,30	367,56	6,46
		100	0,27	0,50	26,07	5,08	1,05	1,10	343,06	6,70
		150	0,31	0,56	33,21	5,80	1,20	2,72	724,62	9,65
		198	0,28	0,48	31,63	5,56	1,21	3,15	728,29	11,49
		251	0,26	0,52	30,20	5,76	1,32	3,40	768,60	9,38
		303	0,27	0,67	31,46	6,15	1,43	4,23	859,34	10,77
		400	0,28	0,84	30,59	6,22	1,55	5,14	882,56	10,60
		500	0,27	0,91	27,32	6,24	1,57	5,05	836,28	9,68
		599	0,27	0,80	26,22	6,39	1,73	5,40	834,32	9,42
		800	0,19	0,95	29,38	6,31	1,86	5,32	782,81	9,22
		1002	0,21	0,89	26,67	6,16	1,93	5,42	729,21	9,00
Maximum			0,31	0,95	33,21	6,39	1,93	5,42	882,56	11,49
Minimum			0,19	0,17	23,63	4,89	0,98	0,91	307,27	5,56
Surface (MLD)*			0,23	0,27	26,22	5,10	1,03	1,06	330,35	6,20
Sub-surface (500m)*			0,25	0,47	28,48	5,53	1,20	2,50	565,15	8,23
Inter (500-1700m)*			0,22	0,88	27,42	6,29	1,84	5,38	782,11	9,21

Table B4*-The multi-element, single sample aliquot, concentrations from the AAZ (DTM3) for the total (T) fraction. The data set reports concentrations with corrections for potentially contaminated samples. Data in red is considered anomalous. No std deviation is reported. The samples were collected unfiltered in PFA bottles. The ([a]) denotes units pmol/kg and ([b]) units in nmol/kg. The (*) denotes that results are an average of respective depths.*

Date: 15 January 2015

Domain (Station)	Latitude & Longitude	Depth (m)	Al[b]	TMn[b]	TFe[b]	TCo[a]	TNi[b]	TCu[b]	TZn[b]	TCd[a]	TPb[a]
AAZ (DTM3)	53°59,85'S 00°00.01'E	15	2,58	0,27	0,47	28,41	5,74	1,53	2,36	426,89	5,26
		23	1,48	0,31	0,55	31,36	5,71	1,52	5,87	533,96	5,26
		50	1,71	0,34	2,34	32,28	5,95	1,52	2,48	514,70	5,23
		75	1,75	0,32	1,08	29,60	5,39	1,44	2,74	406,89	7,34
		101	1,41	0,41	0,18	29,25	5,25	1,36	2,82	596,36	5,10
		151	1,67	0,53	0,32	36,54	6,02	1,63	4,98	848,85	6,99
		250	1,28	0,40	0,60	30,12	5,81	1,63	6,43	856,73	8,56
		298	1,48	0,68	2,19	35,36	6,76	1,95	6,37	927,65	8,72
		350	1,24	0,67	2,71	39,08	5,98	1,77	6,35	802,50	8,07
		398	1,29	0,50	1,63	30,46	6,34	1,92	6,07	848,66	8,49
		450	1,13	0,32	0,89	28,03	6,26	1,91	6,09	814,46	9,45
		500	1,14	0,29	0,26	22,98	6,18	0,57	6,73	838,34	7,52

Table B4 Continued.

Date: 15 January 2015

Domain (Station)	Latitude & Longitude	Depth (m)	TAl[b]	TMn[b]	TFe[b]	TCo[a]	TNi[b]	TCu[b]	TZn[b]	TCd[a]	TPb[a]
AAZ (DTM3)	53°59,85'S 00°00.01'E	549	1,36	0,38	2,00	31,45	6,86	2,20	6,79	812,36	7,06
		599	1,05	0,24	0,64	27,77	6,34	2,04	7,97	804,53	8,41
		650	1,04	0,26	0,78	30,24	7,05	2,29	7,33	830,68	7,61
		749	1,08	0,23	0,64	25,48	6,21	2,10	6,61	750,70	6,48
		1000	1,26	0,22	0,64	19,87	6,45	2,30	6,71	737,72	6,12
		1250	1,09	0,21	0,76	16,55	6,05	2,25	7,29	706,47	5,18
		1502	1,13	0,23	0,99	18,21	6,33	2,46	7,83	747,26	5,18
		1749	1,18	0,25	0,96	16,55	6,08	2,44	7,74	738,59	4,71
		2001	1,04	0,33	0,86	14,90	6,05	2,50	7,38	759,42	4,24
		2249	0,87	0,32	0,99	38,08	6,61	2,74	7,66	759,42	6,12
		2400	1,26	0,40	1,53	21,52	6,77	2,92	9,18	824,51	5,18
Maximum			1,75	0,68	2,71	39,08	7,05	2,92	9,18	927,65	9,45
Minimum			0,87	0,21	0,18	14,90	5,25	0,57	2,74	406,89	4,24
Surface (MLD)*			1,52	0,47	1,01	32,18	5,85	1,60	5,13	727,30	7,34
Sub-surface (500m)*			1,38	0,46	1,40	31,27	6,00	1,57	5,72	771,16	7,80
Inter (500-1700m)*			1,14	0,25	0,92	24,23	6,47	2,23	7,22	769,96	6,58
Deep (>1700m)*			1,09	0,33	1,08	22,76	6,38	2,65	7,99	770,48	5,06

***Table B5**-The multi-element, single sample aliquot, concentrations from the Weddell Gyre (TM2) for the total (T) fraction. The data set reports concentrations with corrections for potentially contaminated samples. Data in red is considered anomalous. No std deviation is reported. The samples were collected unfiltered in PFA bottles. The ([a]) denotes units pmol/kg and ([b]) units in nmol/kg. The (*) denotes that results are an average of respective depths.*

Date: 16 January 2015

Domain (Station)	Latitude & Longitude	Depth (m)	TMn[b]	TFe[b]	TCo[a]	TNi[b]	TCu[b]	TZn[b]	TCd[a]	TPb[a]
Weddell Gyre (TM2)	59°59,95'S 00°00.02'E	16	0,172	0,342	27,612	6,181	1,689	2,906	433,346	4,886
		41	0,166	0,251	22,364	5,636	1,587	3,591	546,346	4,916
		58	0,176	0,645	21,970	6,025	1,673	4,407	497,954	5,055
		60	0,311	2,017	34,090	6,335	2,112	4,500	684,076	6,085
		79	0,290	0,205	23,449	6,209	1,902	4,264	685,506	5,160
		100	0,310	0,261	22,357	6,351	1,997	5,877	739,673	5,905
		150	0,289	0,352	18,877	6,108	2,214	7,203	807,369	7,188
		199	0,284	0,442	19,765	6,919	2,571	7,619	897,462	7,039
		251	0,250	0,342	17,253	6,483	2,445	7,509	844,174	6,174
		300	0,261	0,311	19,792	6,793	2,607	8,163	904,004	6,287
		399	0,241	0,406	16,741	7,096	2,763	10,585	935,370	7,858
		500	0,204	0,332	16,170	6,710	2,764	7,883	869,654	5,777
		599	0,188	0,356	13,964	6,906	2,860	8,001	883,425	5,500
		800	0,178	0,469	12,830	7,003	2,929	8,034	869,037	6,066
		1001	0,148	0,452	10,888	6,508	2,758	7,572	776,731	5,621
Maximum			0,31	0,64	27,61	7,10	2,93	10,58	935,37	7,86
Minimum			0,15	0,20	10,89	5,64	1,59	2,91	433,35	4,89
Surface (MLD)*			0,17	0,30	24,99	5,91	1,64	3,25	489,85	4,90
Sub-surface (500m)*			0,25	0,35	20,58	6,40	2,19	6,21	737,08	6,03
Inter (500-1700m)*			0,17	0,43	12,56	6,81	2,85	7,87	843,06	5,73

***Table B6**-The multi-element, single sample aliquot, concentrations from the Eastern Weddell Gyre (DTM1) for the total (T) fraction. The data set reports concentrations with corrections for potentially contaminated samples. Data in red is considered anomalous. No std deviation is reported. The samples were collected unfiltered in PFA bottles. The ([a]) denotes units pmol/kg and ([b]) units in nmol/kg. The (*) denotes that results are an average of respective depths.*

Date: 18 January 2015

Domain (Station)	Latitude & Longitude	Depth (m)	TAl[b]	TV[b]	TMn[b]	TFe[b]	TCo[a]	TNi[b]	TCu[b]	TZn[b]	TMo[b]	TCd[a]	TPb[a]
Weddell Gyre (DTM1)	65˚ 00.15' S 00˚ 00.45' E	25	4,25	31,72	0,18	0,75	31,79	5,04	1,55	2,58	18,17	480,92	5,55
		39	3,19	33,24	0,23	0,45	28,96	5,30	1,67	3,66	21,91	700,56	6,87
		51	2,54	34,09	0,33	0,23	28,75	5,45	1,76	4,42	21,15	702,95	7,22
		70	2,35	33,02	0,38	0,26	29,88	5,68	1,90	5,33	21,56	761,33	7,62
		100	1,79	34,09	0,34	0,90	28,35	5,96	2,04	5,94	21,70	758,66	10,64
		151	1,65	32,64	0,29	0,73	27,95	5,63	1,92	4,93	20,78	674,98	7,58
		200	1,64	32,73	0,26	0,75	22,31	5,67	2,04	5,66	20,40	683,25	7,25
		400	1,09	29,52	0,21	0,59	72,38	5,19	2,05	5,10	22,73	616,51	5,39
		498	1,46	31,92	0,21	0,39	18,24	5,52	2,10	5,27	20,84	647,75	7,13
		749	1,41	33,55	0,18	0,88	30,24	5,68	2,36	5,44	22,33	657,33	8,11
		1001	1,85	34,01	0,20	1,29	20,97	6,17	2,57	5,82	22,49	702,53	7,65
		1251	1,20	31,98	0,16	1,41	15,06	5,41	2,33	5,30	22,57	660,92	6,25
		1501	3,00	31,20	0,17	1,13	13,82	5,35	2,31	5,69	21,70	637,99	5,02
		2002	1,03	28,61	0,14	0,79	16,76	4,88	2,18	4,88	20,35	576,54	4,44
		2501	1,40	32,43	0,18	1,22	29,33	5,59	2,55	6,13	24,21	650,61	6,91
		3001	1,08	31,61	0,19	1,40	18,85	5,25	2,45	5,09	23,28	635,00	7,53
		3650	1,06	29,85	0,25	2,70	36,83	5,23	2,52	5,25	22,05	577,32	8,55
Maximum			4,25	34,09	0,38	2,70	36,83	6,17	2,57	6,13	24,21	761,33	10,64
Minimum			1,03	28,61	0,14	0,23	13,82	4,88	1,55	2,58	18,17	480,92	4,44
Surface (MLD)*			3,33	33,02	0,25	0,48	29,84	5,26	1,66	3,55	20,41	628,14	6,55
Sub-surface (500m)*			2,22	32,55	0,27	0,56	27,03	5,49	1,89	4,76	21,03	669,66	7,25
Inter (500-1700m)*			1,78	32,53	0,19	1,02	19,67	5,63	2,33	5,50	21,99	661,31	6,83
Deep (>1700m)*			1,14	30,63	0,19	1,53	25,44	5,24	2,42	5,34	22,47	609,87	6,86

***Table B7**-The multi-element, single sample aliquot, concentrations from the South-Eastern Weddell Gyre (TM3) for the total (T) fraction. The data set reports concentrations with corrections for potentially contaminated samples. Data in red is considered anomalous. No std deviation is reported. The samples were collected unfiltered in PFA bottles. The ([a]) denotes units pmol/kg and ([b]) units in nmol/kg. The (*) denotes that results are an average of respective depths.*

Date: 19 January 2015

Domain (Station)	Latitude & Longitude	Depth (m)	TMn[b]	TFe[b]	TCo[a]	TNi[b]	TCu[b]	TZn[b]	TCd[a]	TPb[a]
Weddell Gyre (TM3)	67°58,04'S 00°01.12'E	15	0,300	0,980	45,166	6,477	2,106	5,327	744,365	6,119
		30	0,311	0,714	39,422	6,676	2,101	5,780	766,494	6,557
		40	0,304	0,209	67,484	6,513	2,043	5,149	770,065	7,301
		60	0,376	6,364	38,887	6,617	2,016	4,750	727,418	6,101
		80	0,286	0,320	33,874	6,547	1,968	4,649	714,565	6,418
		99	0,282	0,868	47,831	6,733	2,088	4,907	730,943	5,992
		150	0,286	0,928	33,659	6,597	2,302	6,377	810,731	6,359
		201	0,259	0,634	27,618	6,901	2,383	6,828	830,659	6,862
		250	0,253	0,745	23,828	6,884	2,517	6,636	835,748	6,046
		301	0,221	0,925	65,588	6,923	2,456	6,685	788,651	6,216
		400	0,208	0,414	19,506	6,676	2,526	6,881	790,992	5,750
		501	0,204	0,581	24,050	6,747	2,623	6,739	795,232	6,775
		600	0,190	0,681	47,475	6,688	2,695	7,063	799,710	7,110
		799	0,175	1,194	36,709	6,837	2,823	7,541	820,582	6,470
		1000	0,163	1,147	47,295	6,860	2,869	7,490	812,885	5,469
Maximum			0,38	6,36	47,83	6,92	2,87	7,54	835,75	7,30
Minimum			0,16	0,21	19,51	6,48	1,97	4,65	714,56	5,47
Surface (MLD)			0,32	1,72	39,34	6,57	2,05	5,13	744,58	6,50
Sub-surface (500m)			0,27	1,14	33,38	6,69	2,26	5,89	775,49	6,37
Inter (500-1700m)			0,18	0,90	38,88	6,78	2,75	7,21	807,10	6,46

***Table B8**-The multi-element, single sample aliquot, concentrations from the STZ (TM4) for the dissolved (D) fraction and the Cd/P ratio. One std deviation is reported for duplicate samples, values in red are deemed anomalous. The samples were filtered (0.2µm) and collected in LDPE's. The ([a]) denotes units pmol/kg and ([b]) units in nmol/kg. The (*) deontes that results are an average of respective depths.Std Dev values in blue have >10%RSD and are ommitted from calculations.*

Date: 05 February 2015

Domain (Station)	Latitude & Longitude	Depth (m)	DMn[b]	Std Dev.	DFe[b]	Std Dev.	DCo[a]	Std Dev.	DNi[b]	Std Dev.
STZ (TM4)	36˚ 00.00' S 13˚ 09.71' E	15	0,96	0,04	0,17	0,01	7,66	2,52	2,37	0,03
		30	0,95	0,00	0,27	0,09	6,69	1,40	2,39	0,02
		41	0,91	0,03	0,20	0,05	4,10	0,02	2,34	0,03
		60	0,79	0,03	0,18	0,00	7,00	0,76	2,36	0,05
		80	0,71	0,00	0,17	0,04	8,09	0,21	2,60	0,00
		100	0,63	0,03	0,13	0,01	11,33	1,30	2,45	0,03
		150	0,56	0,00	0,25	0,06	11,16	0,50	3,03	0,02
		250	0,28	0,00	0,35	0,01	18,43	0,16	3,25	0,08
		301	0,24	0,01	0,36	0,00	18,42	0,46	3,43	0,06
		400	0,27	0,00	0,39	0,00	22,15	0,11	3,81	0,06
		501	0,25	0,00	0,41	0,01	27,25	1,69	4,29	0,04
		600	0,25	0,00	0,59	0,01	31,06	0,01	4,79	0,02
		801	0,20	0,00	0,56	0,02	34,24	0,68	5,59	0,04
		1000	0,21	0,00	0,64	0,04	32,75	0,25	6,14	0,05
Maximum			0,96		0,64		34,24		6,14	
Minimum			0,20		0,13		4,10		2,34	
Surface (MLD)			0,94		0,21		6,15		2,37	
Sub-surface (500m)			0,59		0,26		12,93		2,94	
Inter (500-1700m)			0,23		0,55		31,32		5,20	

Table B8-(Continued)

Date: 05 February 2015

Domain (Station)	Latitude & Longitude	Depth (m)	DCu[b]	Std Dev.	DZn[b]	Std Dev.	DCd[a]	Std Dev.	DCd/P	DPb[a]	Std Dev.
STZ (TM4)	36˚ 00.00' S 13˚ 09.71' E	15	0,54	0,03	9,37	0,90	11,43	2,78	0,00	16,84	0,45
		30	0,56	0,01	13,98	4,50	8,68	0,09	0,00	17,92	0,06
		41	0,54	0,00	9,89	0,11	8,40	0,05	0,00	16,97	0,09
		60	0,45	0,00	10,22	0,42	8,62	0,02	50,73	16,43	0,29
		80	0,43	0,01	9,57	0,02	10,25	0,24	341,58	15,83	0,11
		100	0,46	0,02	9,04	0,41	21,47	0,38	178,93	17,03	0,41
		150	0,51	0,01	10,86	0,29	33,41	1,63	111,37	17,22	0,05
		250	0,58	0,02	9,44	0,22	106,50	2,87	247,66	19,49	0,28
		301	0,60	0,01	10,02	0,05	128,62	5,55	229,69	20,62	0,24
		400	0,63	0,01	10,65	0,05	181,83	3,21	279,74	17,91	0,17
		501	0,73	0,01	14,43	4,27	299,39	1,31	325,43	15,18	0,08
		600	0,83	0,00	10,26	0,21	445,76	6,28	362,41	15,16	0,08
		801	1,00	0,01	11,92	0,04	604,57	6,39	370,90	15,71	0,29
		1000	1,19	0,01	12,51	0,08	732,09	1,59	379,32	12,92	0,20
Maximum			1,19		14,43		732,09		379,32	20,62	
Minimum			0,43		9,04		8,40		0,00	12,92	
Surface (MLD)			0,55		11,08		9,50		0,00	17,24	
Sub-surface (500m)			0,55		10,68		74,42		160,47	17,40	
Inter (500-1700m)			0,94		12,28		520,45		359,51	14,74	

Table B9*-The multi-element, single sample aliquot, concentrations from the SAF (DTM2) for the dissolved (D) fraction and the Cd/P ratio. One std deviation is reported for duplicate samples, values in red are deemed anomalous. The samples were filtered (0.2µm) and collected in LDPE's. The ([a]) denotes units pmol/kg and ([b]) units in nmol/kg. The (*) deontes that results are an average of respective depths.Std Dev values in blue have >10%RSD and are ommitted from calculations.*

Date: 12 January 2015

Domain (Station)	Latitude & Longitude	Depth (m)	DAl[b]	Std Dev.	DV[b]	Std Dev.	DMn[b]	Std Dev.	DFe[b]	Std Dev.	DCd[a]	Std Dev.	DCd/P
SAF (DTM2)	46˚ 00.11' S 08˚ 00.00' E	14	13,38	0,45	32,12	0,35	0,23	0,00	0,38	0,03	249,01	0,57	145,62
		35	6,43	1,07	32,87	0,21	0,25	0,02	0,39	0,07	268,11	4,70	138,92
		75	4,84	1,23	33,06	0,45	0,28	0,02	0,61	0,24	269,61	13,40	142,65
		100	2,91	0,50	32,62	3,65	0,32	0,00	0,40	0,01	286,60	31,76	151,64
		150	2,93	0,03	35,44	0,05	0,31	0,00	0,47	0,07	431,72	0,84	208,56
		200	2,91	0,24	36,21	0,15	0,34	0,01	0,51	0,00	597,62	8,41	256,49
		400	3,14	0,21	38,12	1,58	0,27	0,02	0,68	0,02	727,69	30,50	270,52
		501	2,70	0,18	38,34	0,41	0,26	0,01	0,80	0,14	769,51	8,35	245,85
		622	2,34	0,01	34,96	2,24	0,24	0,02	0,61	0,03	760,55	46,08	224,35
		1000	2,85	0,19	37,18	0,17	0,29	0,01	0,87	0,05	836,17	6,13	287,34
		1501	2,77	0,02	38,17	1,81	0,25	0,01	1,04	0,10	722,64	37,87	283,39
		2000	2,94	0,16	36,74	0,73	0,25	0,00	0,98	0,03	629,05	12,17	238,28
		3000	2,68	0,05	36,39	0,92	0,18	0,00	0,95	0,10	667,70	14,40	233,46
		4002	3,22	0,16	36,34	0,89	0,17	0,00	0,86	0,06	708,84	19,89	220,14
		4302	2,70	0,14	38,44	0,00	0,18	0,01	0,84	0,08	787,23	0,87	223,01
Maximum			6,43		38,44		0,34		1,04		38,84		287,34
Minimum			2,34		32,12		0,17		0,38		13,27		138,92
Surface (MLD)*			5,64		32,68		0,26		0,46		262,24		142,39
Sub-surface (500m)*			3,70		34,85		0,28		0,53		36,01		195,03
Inter (500-1700m)*			2,65		36,77		0,26		0,84		32,11		265,03
Deep (>1700m)*			2,89		36,98		0,20		0,91		18,10		228,72

Table B9 *(Continued)*

Date: 12 January 2015												
Domain (Station)	**Latitude & Longitude**	**Depth (m)**	**DNi[b]**	**Std Dev.**	**DCu[b]**	**Std Dev.**	**DZn[b]**	**Std Dev.**	**DCo[a]**	**Std Dev.**	**DPb[a]**	**Std Dev.**
PFZ (DTM2)	46˚ 00.11' S 08˚ 00.00' E	14	5,07	0,02	1,00	0,03	1,46	0,61	33,34	0,94	11,34	0,80
		35	5,30	0,05	0,97	0,02	0,77	0,13	33,35	1,64	11,53	0,27
		75	5,36	0,01	1,04	0,12	3,42	2,85	35,47	2,21	16,82	5,71
		100	5,09	0,50	0,91	0,07	2,33	0,38	33,37	5,08	10,82	0,71
		150	5,51	0,01	1,02	0,02	1,32	0,07	37,59	0,59	12,31	0,14
		200	5,65	0,01	1,02	0,02	2,61	0,81	38,84	0,30	14,05	0,02
		400	6,30	0,29	1,23	0,05	2,85	0,36	37,73	1,15	15,50	1,28
		501	6,22	0,18	1,26	0,02	3,50	0,14	38,39	1,41	15,87	0,37
		622	6,11	0,44	1,32	0,09	3,39	0,11	33,05	1,55	13,43	0,75
		1000	6,77	0,03	1,74	0,03	4,82	0,00	32,42	0,36	13,55	0,81
		1501	6,63	0,34	1,90	0,12	5,01	0,13	30,87	1,90	13,00	1,06
		2000	6,27	0,09	1,97	0,02	5,15	0,56	27,52	1,14	11,70	0,21
		3000	6,47	0,17	2,44	0,05	5,22	0,08	18,34	0,79	8,37	0,05
		4002	6,68	0,24	2,82	0,09	6,14	0,08	13,29	0,73	9,87	0,00
		4302	7,26	0,03	3,15	0,01	6,96	0,35	13,27	0,46	7,46	0,28
Maximum			7,26		3,15		6,96		38,84		16,82	
Minimum			5,07		0,91		0,77		13,27		7,46	
Surface (MLD)*			5,24		1,00		1,11		34,05		13,23	
Sub-surface (500m)*			5,56		1,06		2,12		36,01		13,53	
Inter (500-1700m)*			6,43		1,55		4,18		33,68		13,96	
Deep (>1700m)*			6,67		2,59		5,87		18,10		9,35	

***Table B10**-The multi-element, single sample aliquot, concentrations from the PF (TM1) for the dissolved (D) fraction and the Cd/P ratio. One std deviation is reported for duplicate samples, values in red are deemed anomalous. The samples were filtered (0.2µm) and collected in LDPE's. The ([a]) denotes units pmol/kg and ([b]) units in nmol/kg. The (*) deontes that results are an average of respective depths.Std Dev values in blue have >10%RSD and are ommitted from calculations.*

Date: 14 January 2015

Domain (Station)	Latitude & Longitude	Depth (m)	DMn[b]	Std Dev.	DFe[b]	Std Dev.	DCo[a]	Std Dev.	DNi[b]	Std Dev.
PF (TM1)	50°26,99'S 02°00.12'E	16	0,13	0,01	0,23	0,01	20,30	0,83	4,98	0,23
		31	0,12	0,01	0,11	0,01	21,69	2,63	5,03	0,27
		40	0,13	0,00	0,11	0,01	22,64	0,40	5,11	0,09
		60	0,14	0,01	0,08	0,00	23,13	0,94	5,25	0,29
		78	0,14	0,00	0,15	0,07	23,01	0,59	5,21	0,06
		100	0,16	0,00	0,22	0,08	24,55	0,24	5,61	0,11
		150	0,29	0,00	0,21	0,02	32,51	0,24	5,65	0,03
		198	0,25	0,00	0,20	0,01	31,14	0,02	5,78	0,12
		251	0,25	0,00	0,34	0,10	31,73	0,38	6,07	0,00
		303	0,24	0,00	0,29	0,00	30,73	0,11	6,19	0,07
		400	0,24	0,00	0,34	0,01	27,74	1,06	6,12	0,26
		500	0,24	0,01	0,41	0,01	28,89	0,46	6,65	0,21
		599	0,20	0,00	0,38	0,01	28,96	0,34	6,33	0,02
		800	0,17	0,01	0,43	0,01	27,56	0,29	6,28	0,13
		1002	0,17	0,00	0,55	0,02	26,51	0,34	6,17	0,04
Maximum			0,29		0,55		32,51		6,65	
Minimum			0,12		0,08		20,30		4,98	
Surface (MLD)*			0,14		0,15		22,55		5,20	
Sub-surface (500m)*			0,19		0,23		26,50		5,64	
Inter (500-1700m)*			0,19		0,44		27,98		6,36	

***Table B10**-(Continued)*

Date: 14 January 2015

Domain (Station)	Latitude & Longitude	Depth (m)	DCu[b]	Std Dev.	DZn[b]	Std Dev.	DCd[a]	Std Dev.	DCd/P	DPb[a]	Std Dev.
PF (TM1)	50°26,99'S 02°00.12'E	16	0,94	0,05	1,27	0,31	245,60	11,16	132,76	5,32	0,23
		31	0,94	0,06	0,62	0,03	248,25	20,44	137,92	5,81	0,53
		40	0,95	0,03	0,62	0,00	247,15	3,44	140,42	5,86	0,00
		60	0,96	0,07	1,02	0,13	257,46	16,12	150,56	5,61	0,40
		78	0,96	0,01	0,61	0,01	253,52	1,21	137,04	5,96	0,10
		100	1,08	0,02	1,19	0,14	275,90	4,30	156,76	7,01	0,08
		150	1,09	0,00	2,53	0,02	698,59	4,03	268,69	9,43	0,00
		198	1,15	0,02	3,25	0,10	758,77	10,08	282,07	11,96	0,74
		251	1,33	0,01	3,51	0,02	831,51	2,83	262,31	10,33	0,08
		303	1,34	0,02	4,19	0,07	861,58	14,65	267,57	10,96	0,19
		400	1,41	0,05	4,81	0,18	859,94	28,78	259,80	10,17	0,22
		500	1,59	0,04	5,42	0,20	905,86	25,43	267,22	10,48	0,34
		599	1,63	0,03	6,28	0,84	830,61	1,39	238,68	8,53	0,08
		800	1,75	0,01	5,30	0,03	783,03	0,96	227,62	8,72	0,01
		1002	1,77	0,01	5,35	0,07	721,36	6,89	221,28	8,81	0,02
Maximum			1,77		6,28		905,86		282,07	11,96	
Minimum			0,94		0,61		245,60		132,76	5,32	
Surface (MLD)*			0,97		0,89		254,65		142,58	5,93	
Sub-surface (500m)*			1,14		2,42		537,01		205,26	8,24	
Inter (500-1700m)*			1,69		5,59		810,22		238,70	9,14	

***Table B11**-The multi-element, single sample aliquot, concentrations from the AAZ (DTM3) for the dissolved (D) fraction and the Cd/P ratio. One std deviation is reported for duplicate samples, values in red are deemed anomalous. The samples were filtered (0.2µm) and collected in LDPE's. The ([a]) denotes units pmol/kg and ([b]) units in nmol/kg. The (*) deontes that results are an average of respective depths.Std Dev values in blue have >10%RSD and are ommitted from calculations.*

Date: 15 January 2015

Domain (Station)	Latitude & Longitude	Depth (m)	DMn[b]	Std Dev.	DFe[b]	Std Dev.	DCo[a]	Std Dev.	DNi[b]	Std Dev.
AAZ (DTM3)	53°59,85' S 00°00.01' E	15	0,20	0,00	0,24	0,02	23,56	0,90	5,42	0,07
		23	0,21	0,00	0,12	0,01	25,68	0,28	5,78	0,06
		50	0,24	0,00	0,33	0,15	24,46	0,63	5,41	0,21
		75	0,24	0,02	0,30	0,08	24,43	0,79	5,23	0,02
		101	0,37	0,01	0,21	0,04	27,77	0,37	5,50	0,08
		151	0,49	0,02	0,27	0,05	32,47	0,05	5,68	0,04
		250	0,40	0,01	0,41	0,04	31,96	0,42	6,04	0,05
		298	0,58	0,02	1,22	0,00	31,77	1,20	6,31	0,27
		350	0,67	0,04	1,82	0,02	29,79	1,47	6,13	0,34
		398	0,45	0,02	0,92	0,01	28,51	0,64	6,10	0,02
		450	0,29	0,05	0,44	0,06	26,46	0,63	6,74	0,40
		500	0,30	0,02	3,43	2,98	28,87	1,10	6,59	0,17
		549	0,33	0,00	0,94	0,01	28,05	2,39	6,86	0,71
		599	0,23	0,02	0,45	0,05	26,72	1,82	6,55	0,14
		650	0,24	0,01	0,51	0,03	26,03	1,68	6,49	0,42
		749	0,25	0,01	0,46	0,00	23,60	1,37	6,35	0,38
		1000	0,19	0,01	0,39	0,00	18,67	0,07	6,19	0,06
		1250	0,19	0,00	0,43	0,01	17,76	0,19	6,24	0,00
		1502	0,18	0,01	0,49	0,08	16,26	0,40	6,18	0,14
		1749	0,19	0,00	0,48	0,01	15,64	0,41	6,10	0,15
		2001	0,25	0,01	0,57	0,01	15,14	0,31	6,06	0,04
		2249	0,26	0,01	0,56	0,02	14,42	0,34	6,29	0,21
		2400	0,29	0,02	0,59	0,01	14,69	0,25	6,27	0,14
Maximum			0,67		3,43		32,47		6,86	
Minimum			0,18		0,12		14,42		5,23	
Surface (MLD)*			0,25		0,24		25,18		5,47	
Sub-surface (500m)*			0,36		0,79		27,89		6,02	
Inter (500-1700m)*			0,21		0,46		20,47		6,29	
Deep (>1700m)*			0,25		0,55		14,97		6,18	

Table B11-(Continued)

Date: 15 January 2015

Domain (Station)	Latitude & Longitude	Depth (m)	DCu[b]	Std Dev.	DZn[b]	Std Dev.	DCd[a]	Std Dev.	DCd/P	DPb[a]	Std Dev.
AAZ (DTM3)	53°59,85' S 00°00.01' E	15	1,45	0,01	1,55	0,04	337,32	2,64	233,67	4,94	0,05
		23	1,42	0,00	3,01	0,07	364,28	2,15	254,84	5,14	0,08
		50	1,32	0,06	2,09	0,14	393,04	23,23	252,52	4,96	0,47
		75	1,35	0,03	2,55	0,13	375,99	3,22	239,40	7,27	0,10
		101	1,33	0,02	2,65	0,06	566,16	9,66	303,26	5,47	0,02
		151	1,41	0,01	4,44	0,01	778,08	11,97	366,85	6,70	0,16
		250	1,60	0,01	5,93	0,25	899,14	5,79	378,58	8,58	0,05
		298	1,72	0,07	6,22	0,25	903,99	46,65	373,96	8,22	0,40
		350	1,73	0,11	5,87	0,38	847,38	48,15	354,68	8,31	0,46
		398	1,70	0,01	6,18	0,00	822,10	1,40	338,11	8,33	0,03
		450	1,90	0,09	6,32	0,19	864,45	23,68	370,58	9,80	0,46
		500	1,95	0,06	6,61	0,13	851,31	20,41	374,00	7,64	0,60
		549	2,07	0,22	6,57	0,63	861,39	75,35	380,79	7,67	0,91
		599	2,04	0,03	7,27	0,34	840,60	15,91	378,69	6,68	0,49
		650	2,02	0,13	7,26	0,70	810,01	44,63	355,86	10,72	2,54
		749	2,03	0,16	7,06	0,72	770,50	39,06	342,75	6,90	0,36
		1000	2,14	0,02	6,26	0,01	706,04	3,04	332,89	5,44	0,04
		1250	2,17	0,01	6,95	0,00	726,00	7,38	320,94	5,11	0,02
		1502	2,28	0,06	7,15	0,05	746,40	17,36	336,25	4,44	0,15
		1749	2,30	0,05	7,45	0,28	738,15	19,53	320,32	4,22	0,12
		2001	2,34	0,01	7,51	0,13	741,19	6,08	331,80	4,84	0,59
		2249	2,55	0,06	7,66	0,20	772,87	18,66	321,60	5,60	0,27
		2400	2,46	0,04	7,96	0,10	765,49	7,81	334,23	4,52	0,00
Maximum			2,55		7,96		903,99		380,79	9,80	
Minimum			1,32		1,55		337,32		233,67	4,22	
Surface (MLD)*			1,38		2,37		407,36		256,74	5,56	
Sub-surface (500m)*			1,69		5,10		705,36		331,16	7,33	
Inter (500-1700m)*			2,16		6,85		737,23		333,21	5,47	
Deep (>1700m)*			2,41		7,65		754,42		326,98	4,79	

***Table B12**-The multi-element, single sample aliquot, concentrations from the South of the SB (TM2) for the dissolved (D) fraction and the Cd/P ratio. One std deviation is reported for duplicate samples, values in red are deemed anomalous. The samples were filtered (0.2µm) and collected in LDPE's. The ([a]) denotes units pmol/kg and ([b]) units in nmol/kg. The (*) deontes that results are an average of respective depths.Std Dev values in blue have >10%RSD and are ommitted from calculations.*

Date: 16 January 2015

Domain (Station)	Latitude & Longitude	Depth (m)	DMn[b]	Std Dev.	DFe[b]	Std Dev.	DCo[a]	Std Dev.	DNi[b]	Std Dev.
Weddell Gyre (SB) (TM2)	59°59,95'S 00°00.02'E	16	0,03	0,00	0,13	0,00	14,48	0,48	5,98	0,04
		41	0,10	0,00	0,46	0,01	20,48	0,20	6,09	0,08
		58	0,09	0,01	0,26	0,03	16,33	1,30	5,89	0,07
		60	0,23	0,00	0,19	0,00	24,12	0,07	6,17	0,01
		79	0,25	0,00	0,14	0,03	20,43	0,86	6,02	0,02
		100	0,29	0,01	0,33	0,02	23,27	0,50	6,16	0,18
		150	0,34	0,01	0,25	0,00	20,94	0,03	6,73	0,04
		199	0,28	0,01	0,24	0,01	19,24	0,63	6,83	0,20
		251	0,26	0,00	0,23	0,01	17,26	0,67	6,80	0,05
		300	0,27		0,28		17,22		6,97	
		399	0,23	0,00	0,33	0,02	14,97	0,13	6,73	0,10
		500	0,21	0,00	0,30	0,01	14,03	0,33	6,73	0,11
		599	0,19	0,00	0,30	0,01	14,12	1,21	6,71	0,08
		800	0,16	0,00	0,31	0,01	11,09	0,38	6,73	0,08
		1001	0,15	0,00	0,38	0,02	12,32	0,66	7,04	0,06
Maximum			0,34		0,46		24,12		7,04	
Minimum			0,03		0,13		11,09		5,89	
Surface (MLD)*			0,07		0,30		17,48		6,04	
Sub-surface (500m)*			0,21		0,26		18,69		6,38	
Inter (500-1700m)*			0,18		0,32		12,89		6,80	

Table B12-(Continued)

Date: 16 January 2015

Domain (Station)	Latitude & Longitude	Depth (m)	DCu[b]	Std Dev.	DZn[b]	Std Dev.	DCd[a]	Std Dev.	DCd/P	DPb[a]	Std Dev.
Weddell Gyre (SB) (TM2)	59°59,95'S 00°00.02'E	16	1,49	0,02	1,33	0,06	215,16	1,23	89,54	3,85	0,01
		41	1,60	0,03	3,22	0,29	473,32	5,55	153,48	4,85	0,10
		58	1,53	0,04	2,58	0,13	368,77	5,95	88,69	4,20	0,14
		60	1,77	0,04	3,89	0,04	641,89	5,47	164,87	5,53	0,01
		79	1,70	0,01	3,82	0,02	624,72	2,41	159,57	4,82	0,05
		100	1,90	0,08	4,97	0,15	719,12	18,61	159,52	5,67	0,05
		150	2,25	0,01	7,49	0,00	896,40	0,21	193,89	7,23	0,09
		199	2,38	0,06	7,38	0,18	884,64	25,79	196,76	6,58	0,13
		251	2,46	0,06	7,51	0,15	902,36	22,71	195,60	6,18	0,20
		300	2,51		7,83		918,23		180,24	6,21	
		399	2,51	0,06	7,93	0,11	886,59	7,69	173,13	6,17	0,18
		500	2,61	0,01	7,74	0,07	872,39	2,32	188,93	5,75	0,07
		599	2,63	0,04	7,82	0,16	862,76	12,91	192,31	5,27	0,15
		800	2,64	0,01	7,54	0,05	816,70	5,08	182,42	5,56	0,06
		1001	2,74	0,03	7,97	0,00	834,42	7,32	181,94	6,27	0,07
Maximum			2,74		7,97		918,23		196,76	7,23	
Minimum			1,49		1,33		215,16		88,69	3,85	
Surface (MLD)*			1,55		2,28		344,24		121,51	4,35	
Sub-surface (500m)*			2,02		5,26		680,49		160,36	5,53	
Inter (500-1700m)*			2,65		7,77		846,57		186,40	5,71	

***Table B13**-The multi-element, single sample aliquot, concentrations from the Eastern Weddell Gyre (DTM1) for the dissolved (D) fraction and the Cd/P ratio. One std deviation is reported for duplicate samples, values in red are deemed anomalous. The samples were filtered (0.2µm) and collected in LDPE's. The ([a]) denotes units pmol/kg and ([b]) units in nmol/kg. The (*) deontes that results are an average of respective depths.Std Dev values in blue have >10%RSD and are ommitted from calculations.*

Date: 18 January 2015

Domain (Station)	Latitude & Longitude	Depth (m)	DAl[b]	Std Dev.	DV[b]	Std Dev.	DMn[b]	Std Dev.	DFe[b]	Std Dev.	DCd[a]	Std Dev.	Cd/P
Weddell Gyre (DTM1)	65˚ 00.15' S 00˚ 00.45' E	25	2,82	0,18	28,93	0,03	0,03	0,00	0,21	0,02	124,69	3,79	80,43
		39	2,69	0,31	32,79	1,48	0,10	0,00	0,19	0,06	452,78	1,46	244,74
		51	1,92	0,12	30,51	1,54	0,24	0,01	0,23	0,05	619,91	19,97	306,89
		70	1,82	0,00	34,35	0,14	0,35	0,00	0,49	0,19	737,80	1,98	335,36
		100	2,17	0,04	33,19	1,55	0,33	0,01	0,29	0,01	731,83	26,79	319,58
		151	1,77	0,04	33,82	0,04	0,28	0,00	0,35	0,01	710,07	2,62	316,99
		200	1,98	0,23	32,27	0,19	0,25	0,00	0,36	0,06	684,35	0,48	311,07
		400	2,01	0,74	32,19	1,11	0,21	0,01	0,39	0,08	645,97	12,24	288,38
		498	1,69	0,41	33,44	0,49	0,19	0,00	0,40	0,08	657,97	3,62	304,62
		749	1,63	0,04	34,80	0,59	0,19	0,02	0,47	0,04	757,20	62,38	344,18
		1001	1,33	0,05	33,04	0,13	0,14	0,00	0,43	0,03	672,09	4,82	293,49
		1251	1,28	0,08	31,89	0,65	0,12	0,00	0,47	0,01	648,19	26,14	283,05
		1501	1,88	0,48	32,25	0,32	0,12	0,01	0,62	0,06	635,51	13,40	267,02
		2002	1,46	0,28	32,89	0,01	0,13	0,01	0,56	0,04	671,69	11,44	299,86
		2501	1,36	0,03	33,47	0,30	0,13	0,00	0,50	0,00	675,45	1,86	289,89
		3001	1,29	0,24	33,16	0,47	0,14	0,00	0,53	0,05	642,59	12,42	286,87
		3650	1,00	0,07	30,88	1,84	0,14	0,01	0,51	0,02	607,83	20,31	276,29
Maximum			2,82		34,80		0,35		0,62		26,09		344,18
Minimum			1,00		28,93		0,03		0,19		9,46		80,43
Surface (MLD)*			2,48		30,74		0,13				399,13		210,69
Sub-surface (500m)*			2,10		32,39		0,22		0,32		19,40		278,67
Inter (500-1700m)*			1,53		32,99		0,14		0,50		14,96		296,94
Deep (>1700m)*			1,28		32,60		0,14		0,53		13,85		288,23

Table B13-(Continued)

Date: 18 January 2015

Domain (Station)	Latitude & Longitude	Depth (m)	DNi[b]	Std Dev.	DCu[b]	Std Dev.	DZn[b]	Std Dev.	DMo[b]	Std Dev.	DCo[a]	Std Dev.	DPb[a]	Std Dev.
Weddell Gyre (DTM1)	65˚ 00.15' S 00˚ 00.45' E	25	4,65	0,01	1,29	0,01	1,02	0,03	19,71	0,22	9,46	0,12	3,80	0,16
		39	4,73	0,51	0,87	0,58	2,21	0,10	20,15	0,98	13,36	7,87	5,00	0,04
		51	4,96	0,20	1,48	0,05	3,68	0,12	19,71	1,06	24,01	0,95	6,08	0,30
		70	5,69	0,16	1,74	0,05	5,22	0,11	20,80	0,58	26,09	0,38	9,05	0,47
		100	5,76	0,25	1,89	0,09	5,78	0,01	21,40	0,39	24,12	0,70	8,95	0,29
		151	5,71	0,03	1,95	0,03	5,08	0,08	21,34	0,26	23,16	0,22	7,15	0,07
		200	5,55	0,02	1,87	0,01	5,05	0,04	21,45	0,10	20,87	0,16	6,25	0,27
		400	5,49	0,09	2,00	0,05	5,20	0,09	21,59	0,60	17,15	0,01	5,89	0,32
		498	5,56	0,03	2,03	0,00	5,33	0,00	21,19	0,66	16,40	0,03	6,67	0,10
		749	6,51	0,61	2,50	0,21	6,05	0,52	25,64	2,45	18,41	1,72	7,43	0,69
		1001	5,71	0,04	2,43	0,03	5,53	0,05	22,82	0,16	14,84	0,45	5,77	0,11
		1251	5,44	0,15	2,27	0,07	5,46	0,10	22,11	0,28	12,84	0,37	5,13	0,19
		1501	5,30	0,13	2,28	0,02	5,35	0,00	21,98	0,65	13,76	0,18	5,53	0,17
		2002	5,67	0,16	2,47	0,06	5,97	0,23	24,88	0,60	14,77	0,50	5,86	1,18
		2501	5,60	0,04	2,37	0,01	6,11	0,05	25,07	0,62	14,24	0,54	5,37	0,03
		3001	5,40	0,07	2,35	0,02	5,63	0,01	23,96	0,02	13,75	0,41	6,29	0,21
		3650	5,03	0,20	2,37	0,08	5,02	0,20	21,93	0,33	12,66	0,61	6,24	0,57
Maximum			6,51		2,50		6,11		25,64		757,20		9,05	
Minimum			4,65		0,87		1,02		19,71		124,69		3,80	
Surface (MLD)*			4,78		1,21		2,31		19,86		15,61		4,96	
Sub-surface (500m)*			5,35		1,68		4,29		20,82		596,15		6,54	
Inter (500-1700m)*			5,74		2,37		5,60		23,14		678,25		5,96	
Deep (>1700m)*			5,43		2,39		5,68		23,96		649,39		5,94	

***Table B14**-The multi-element, single sample aliquot, concentrations from the Southern Weddell Gyre (TM3) for the dissolved (D) fraction and the Cd/P ratio. One std deviation is reported for duplicate samples, values in red are deemed anomalous. The samples were filtered (0.2µm) and collected in LDPE's. The ([a]) denotes units pmol/kg and ([b]) units in nmol/kg. The (*) deontes that results are an average of respective depths.Std Dev values in blue have >10%RSD and are ommitted from calculations.*

Date: 19 January 2015

Domain (Station)	Latitude & Longitude	Depth (m)	DMn[b]	Std Dev.	DFe[b]	Std Dev.	DCo[a]	Std Dev.	DNi[b]	Std Dev.
Weddell Gyre (TM3)	67°58,04' S 00°01.12' E	15	0,26	0,01	0,11	0,00	30,05	1,65	6,02	0,30
		30	0,26	0,01	0,10	0,00	29,23	1,85	6,00	0,09
		40	0,28	0,00	0,10	0,01	28,20	0,53	6,31	0,08
		60	0,27	0,01	0,34	0,10	33,13	4,32	6,21	0,04
		80	0,26	0,00	0,10	0,01	27,79	0,49	6,23	0,09
		99	0,28	0,00	0,13	0,00	28,12	0,18	6,23	0,09
		150	0,30	0,01	0,24	0,00	25,65	0,21	6,57	0,16
		201	0,26	0,00	0,24	0,02	23,35	0,18	6,58	0,12
		250	0,24	0,00	0,28	0,01	21,73	0,11	6,61	0,00
		301	0,22	0,00	0,27	0,00	20,80	0,08	6,79	0,01
		400	0,25	0,05	0,35	0,01	22,20	2,57	6,75	0,13
		501	0,18	0,01	0,27	0,00	17,91	0,12	6,39	0,01
		600	0,16	0,00	0,31	0,00	17,96	0,52	6,40	0,08
		799	0,15	0,01	0,33	0,01	16,53	0,70	6,60	0,15
		1000	0,14	0,00	0,36	0,02	15,58	0,67	6,80	0,09
Maximum			0,30		0,36		33,13		6,80	
Minimum			0,14		0,10		15,58		6,00	
Surface (MLD)*			0,26		0,15		29,68		6,15	
Sub-surface (500m)*			0,25		0,21		26,12		6,35	
Inter (500-1700m)*			0,16		0,32		17,00		6,55	

Table B14-(Continued)

Date: 19 January 2015

Domain (Station)	Latitude & Longitude	Depth (m)	DCu[b]	Std Dev.	DZn[b]	Std Dev.	DCd[a]	Std Dev.	DCd/P	DPb[a]	Std Dev.
Weddell Gyre (TM3)	67°58,04' S 00°01.12' E	15	1,83	0,11	4,56	0,28	685,82	35,13	343,95	5,82	0,25
		30	1,81	0,05	4,61	0,12	701,32	15,37	337,40	5,78	0,14
		40	1,90	0,01	5,19	0,08	742,68	4,42	343,31	7,05	0,10
		60	1,86	0,02	17,12	12,45	732,23	5,30	345,23	5,93	0,08
		80	1,85	0,01	4,69	0,07	725,38	11,01	335,31	6,29	0,05
		99	1,89	0,02	4,88	0,08	744,93	10,48	337,74	6,17	0,09
		150	2,12	0,05	6,43	0,15	844,73	18,37	375,77	6,37	0,11
		201	2,19	0,04	6,77	0,04	831,88	13,74	350,26	7,12	0,01
		250	2,35	0,01	6,59	0,01	824,07	6,53	359,81	6,19	0,01
		301	2,34	0,01	6,79	0,03	826,52	5,00	354,32	6,56	0,01
		400	2,29	0,17	6,76	0,23	836,33	9,18	365,16	6,27	0,12
		501	2,38	0,03	6,68	0,13	787,07	14,89	394,73	5,51	0,21
		600	2,45	0,03	6,89	0,00	793,63	9,96	340,22	6,98	0,04
		799	2,55	0,04	7,44	0,15	807,59	18,61	359,25	6,37	0,23
		1000	2,58	0,01	7,28	0,03	809,61	0,33	340,89	5,26	0,06
Maximum			2,58		17,12		844,73		7,12	0,25	
Minimum			1,81		4,56		685,82		5,26	0,01	
Surface (MLD)*			1,85		7,23		717,49		341,04	6,17	
Sub-surface (500m)*			2,04		6,75		768,77		6,23	0,10	
Inter (500-1700m)*			2,49		7,07		799,47		6,03	0,13	